VOLUME IV

THE FINITE ANALYTIC METHOD

by

Ching-Jen Chen

and

Hamn-Ching Chen

IIHR Report No. 232-IV

Iowa Institute of Hydraulic Research
The University of Iowa
Iowa City, Iowa 52242

August 1982

FINAL REPORT
NASA NSG 3305

VOLUME 4

THE FINITE ANALYTIC METHOD

BY

CHING-JEN CHEN

HAMN-CHING CHEN

DIVISION OF ENERGY ENGINEERING AND
IOWA INSTITUTE OF HYDRAULIC RESEARCH

THE UNIVERSITY OF IOWA
IOWA CITY, IOWA

AUGUST 1982

THE FINITE ANALYTIC METHOD

CONTENTS OF VOLUMES 1-5

PREFACE

The Finite Analytic Method

This monograph contains the fundamental development of the new numerical method called the "Finite Analytic" method. The finite analytic method differs from the finite difference method and the finite element method. The basic idea of the finite analytic method is the incorporation of local analytic solutions in the numerical solution of linear or nonlinear partial differential equations. In the finite analytic method, the total problem is subdivided into a number of small elements. The local analytic solution is obtained for the small element in which the governing equation, if nonlinear, is linearized. The local analytic solutions are then expressed in algebraic form and are overlapped to cover the entire region of the problem. The assembly of these local analytic solutions, which still preserves the overall nonlinearity of the governing equation, results in a system of linear algebraic equations. The system of algebraic equations is then solved to provide the numerical solutions of the total problem.

Unlike the finite difference method, the finite analytic method does not tamper with the differentials or the derivatives of the governing equation, nor does the analytic method need the shape function which is made to satisfy the integral form of the governing equation, as in the finite element method. The finite analytic solution obtained from the finite analytic method is differentiable. As a result, the derivative of the solution obtained analytically is much more reliable. In this monograph the finite analytic solution is shown to be stable, even when the highest derivative term of the partial differential equation is multiplied by a small factor, such as one over Reynolds number. It is also shown that the finite analytic solution for Navier-Stokes equations at high Reynolds numbers automatically provides a gradual shift of the upwinding effect. Therefore the finite analytic solution accurately simulates the effect of convection and eliminates the false numerical diffusion that would occur in the upwinding difference or unidirection difference used in the finite difference or the finite element methods. The computational time for the finite anayltic solution is shown to be about equal to that of the finite difference method. In certain cases, due to the stability of the system of algebraic equations derived in the finite analytic method, the overall computational time can be even less. The finite analytic solution derived in

the present analytic mehtod is in its most elementary form in terms of accuracy. But it has already been shown to be sufficient for the problems under consideration. Further accurate finite analytic formulae can be derived and are indicated in the monograph.

The finite anlytic method was developed in early 1977, when Dr. Peter Li was then a graduate student working on his doctoral dissertation with me. He had been having difficulty in obtaining convergence of a system of finite difference algebraic equations derived from the Navier-Stokes equations for two-dimensional turbulent flow with a second-order turbulent model. I conceived the finite analytic method one night and solved the simple two-dimensional Laplace equation. Li then carried the finite analytic method to the unsteady diffusion equation and nonlinear ordinary differential equations and compited his Ph.D. dissertation in 1978. In 1982 Dr. Hann-Ching Chen developed the finite analytic method further by solving the unsteady three-dimensional Navier-Stokes equations. This bound volume contains the research results of Dr. Chen and myself.

ACKNOWLEDGEMENT

I would like to acknowledge Dr. Hamn-Ching Chen for taking the finite analytic method as his doctoral dissertation. Without him, the finite analytic method could not have been developed and understood as it is today.

I would also like to thank my colleagues, Professors V. C. Patel, David C. Chou, T. F. Smith, Allen Chwang, and K. Atkinson, for their encouragement and criticisms of the method. I would also like to thank Drs. William D. Mcnally, Peter M. Sockol, Gary Johnson, and J. J. Adamczyk of NASA Lewis Center for taking a keen interest in and supporting the continuation of the development of the finite analytic method. My thanks also go to Dr. Melvyn Ciment, of the Applied Mathematical Division, and Dr. Ronald W. Davis, of the Fluid Engineering Division, of the National Bureau of Standards, for their in-deep discussion of the method and to Drs. Oscar P. Manley of the U. S. Department of Energy and P.C. Lu of the University of Nebraska for their discussion and encouragement. This work is, in part, supported by NASA Grant No. N.S.G. 3305 and U. S. Department of Energy Grant No. DE-AC02-79ER-10515.A000. The support of the University of Iowa Computer Center and Division of Energy Engineering, The University of Iowa, is also acknowledged.

Ching-Jen Chen
Professor and Senior Research Scientist
Division of Energy Engineering and Iowa Institute of Hydraulic Research
The University of Iowa
Iowa City, Iowa 52240
(319) 353-4473

August 1982

THE FINITE ANALYTIC METHOD (IV)

Development of Finite Anaytic Method For Unsteady Three-Dimensional Navier-Stokes Equations

ABSTRACT

Unsteady 1D, 2D and 3D incompressible Navier-Stokes equations are numerically analyzed by a numerical scheme called the "Finite Analytic Method". The basic idea of the finite analytic method is the incorporation of a local analytic solution in the numerical solution of linear and nonlinear partial differential equations. In this study, the local analytic solutions for unsteady 1D, 2D and 3D convective transport equations are obtained from locally linearized governing equations by specifying suitable initial and boundary conditions for each local element. When the local analytic solution is evaluated at a given nodal point, it gives an analytic algebraic relationship between a nodal value in a local element to its neighboring nodal points. The solution of the problem is then achieved by solving the system of algebraic equations.

Depending on the boundary and initial functions chosen to represent the boundary and initial conditions for each local element, a number of local analytic solutions are derived. The results show that the boundary approximation based on the combination of exponential and linear function is the best one since the boundary function thus constructed

is the natural solution of the governing equation. The finite analytic coefficients thus obtained are shown to be relatively simple and do give the correct asymptotic behavior for both diffusion and convection dominated cases.

The finite analytic method is employed to solve several steady and unsteady fluid flow problems. In two-dimensional cases, the Navier-Stokes equations are formulated using both vorticity-streamfunction and primitive variables. The finite analytic numerical solution is first obtained for starting cavity flow of Reynolds numbers of 100, 400, 1000, 2000 and 5000. Then the finite analytic formula is used to obtain the numerical solutions for vortex shedding phenomenon behind a rectangular block for Reynolds numbers of 10, 50, 100, 200 and 500. In three dimensions, the 28-point finite analytic formula for unsteady convective transport equation is employed to study a three-dimensional cavity flow using primitive variable formulation. The results are obtained for Reynolds numbers of 100 and 400. In all test cases, the finite analytic solutions are shown to be converge rapidly, and to be stable and accurate.

TABLE OF CONTENTS

LIST OF TABLES

Table

Page

LIST OF FIGURES

LIST OF SYMBOLS

Alphabetical Symbols

A, B, C	Linearized convection coefficients in convective transport equation
A_n, A_{mn}	Fourier series coefficients in FA formulations
b_{nb}	FA coefficients for unsteady convective transport equations based on nonuniform grid spacing local elements (nb = EC, NE,...., ECT, NEB,.....)
C_{nb}	FA coefficients for steady convective transport equations based on uniform grid spacing local elements (nb = EC, NE,...., ECT, NEB,.....)
D, D^*, $\hat{D}$	Mass source terms defined in eq(V-13), eq(V-15a) and eq(V-17a) for velocities, starred velocities and pseudovelocities respectively.
F	Source function (Inhomogeneous term) in convective transport equations
f	A constant in a small local element to approximate the source function F
g	A constant in a local element to approximate the source function, higher order correction term and unsteady term.
h, k, l	Grid sizes in x, y and z direction respectively
L	Reference length scale
m, n, p, q, r	Indices in series summations
p	dimensionless pressure

p^*	Guessed (Imperfect) pressure field
p'	Pressure-correction = $p - p^*$
Pr	Prandtl number
R	Dimensionless parameter in convective transport equation
Re	Reynolds number
t	Dimensionless time
u, v, w	Dimensionless velocity components
U, V, W	Representative constant velocities over each local element
u', v', w'	Deviations of velocities in the small element with respect to U, V and W. (u' = u - U etc.)
u^*, v^*, w^*	Velocity field obtained from guessed pressure field p^*
$\hat{u}$, $\hat{v}$, $\hat{w}$	Pesudovelocities
U_0	Reference Velocity scale
x, y, z	Dimensionless Cartesian coordinate system
x_g, y_g, z_g	Global coordinate system

Greek Symbols

α	Dimensionless parameter in one-dimensional convective transport equation
γ_{pq} etc	Eigenvalues
δ_{pi}, δ_{qj} etc.	Kronecker deltas
ε	Convergence criterion used in numerical calculations
λ_m, λ'_m	Eigenvalues

μ_q, δ_r	Eigenvalues
ν	Kinematic vsicosity
ξ, η, ζ	Vorticity components
π	Pi = 3.141592654
ρ	Density
τ	Time increment
ϕ	Dependent variable of convective transport equations
$\tilde{\phi}$	Dependent variable of homogeneous convective transport equations
ϕ^*	Interpolated nodal values in nonuniform grid spacing local element
Φ	Scalar potential
ψ	Streamfunction
ψ_x, ψ_y, ψ_z	Components of vector potential $\vec{\psi}$
∇	Gradient
∇^2	Laplacian
$\nabla\cdot$	Divergence
$\nabla\times$	Curl
Δ	Difference

Subscripts

E, W, N, S, T, B	East, West, North, South, Top and Bottom boundaries
e, w, n, s, t, b	East, West, North, South, Top and Bottom control surfaces
EC	East Central (Similarly for WC, SE, NE etc.)

ECT	East-Center-Top (Similarly for NET etc.)
i, j, k	Nodal point location in the flow domain
nb	Neighboring nodal point
P	Interior point for two- and three-dimensional local elements
x, y, z, t	First derivatives with respect to x, y, z and t
xx, yy, zz	Second derivatives with respect to x, y and z

Superscripts

E, W, N, S, T, B	East, West, North, South, Top and Bottom boundaries
n, n-1	n^{th} and $(n-1)^{th}$ time steps

Abbreviations

FA	Finite Analytic
FAEL	Finite analytic formulation with exponential and linear boundary or initial functions
FAPL	Finite analytic formulation with piecewise-linear boundary approximations
FASP	Finite analytic formulation with second-order polynomial boundary or initial functions
FD	Finite Difference
FE	Finite Element
PDE	Partial differential equation
1D, 2D, 3D	one-, two-, and three-dimensional

CHAPTER I

INTRODUCTION

For the differential equations which can not be solved analytically, numerical methods are employed. Most of the numerical methods including the finite analytic (FA) method presented in this study, bear the following similarities. Firstly, all methods decompose the total region governed by differential equations into a number of small elements and grid points, and thus replace the continuous solution of differential equation with discrete values at a finite number of grid points or elements. Secondly, all methods derive an algebraic equation from the differential equation with suitable difference approximations or suitable profile functions of dependent variables between nodal points or in the whole local element. Thirdly, the resulting system of algebraic equations is solved with given boundary and/or initial conditions to obtain the numerical solutions for all of the grid points.

The numerical methods are distinguished from one another depending on how the corresponding algebraic representation of the differential equation is derived. Two commonly used methods in deriving the discrete

algebraic equation in the finite difference method are Taylor-series and control volume formulations. While for the finite element method, the variational formulations and the method of weighted residuals are often used.

In Taylor-series formulation, the finite difference algebraic equations are derived by approximating the derivatives in the differential equation via a truncated Taylor-series. Depending on the order of truncation, many alternate finite difference representations can be obtained. The validity of this formulation, however, greatly depends on how the truncation is made and how the difference is taken. For example, a truncated Taylor-series representation of an exponential profile often leads to unreasonable results since the truncated terms may be much larger than the terms retained when large exponents are encountered. Furthermore, since the Taylor-series formulation based on term by term difference approximation largely ignores the character of the partial differential equation, an accurate term by term finite difference analog for a partial differential equation does not necessarily lead to higher accuracy for the differential equation. (see Roache [1], for example). In fact, large errors usually called "Numerical diffusion" may result and instability of the solution of difference equation is often encountered.

A simple variant of Taylor-series formulation called

polynomial fitting [1] for obtaining the finite difference expression is to fit an analytic function with free parameters to the mesh-point values and then to differentiate the function analytically. When polynomials are used as the interpolation function, it is very similar to the Taylor-series formulation although not identical beyond the second-order polynomials. This method, however, has not been generally used because the higher order polynomial fits are sensitive to "noise" or small errors in the data.

In finite element methods, the two most commonly used formulations in obtaining the discretization (element) equations are the energy methods and the residual methods [2]. Use of the energy procedures requires knowledge of variational calculus. The calculus of variation shows that solving a differential equation is equivalent to minimizing a related quantity called the functional. This equivalence is known as variational principle. Depending on the functional considered, a number of variational formulation can be employed to derive the discretized element equations. For example, the principle of stationary potential and complementary energies and hybrid formulations are commonly used in finite element applications. The applicability of variational formulation in fluid flow problems is, however, very limited because a

variational principle does not always exist for differential equations governing the fluid flows.

The method of weighted residuals is based on minimization of the residual left after an approximate or trial solution is substituted into the differential equations governing a problem. The approximation function is constructed in terms of some chosen known functions and a number of undetermined parameters. The residual left is then minimized in some integral sense with suitable weighting functions to determine the unknown parameters. Depending on the weighting functions chosen to perform the integrations, many different versions of the method can be derived. Among them are collocation, subdomain, least square and Galerkin methods. The accuracy of these methods are, however, highly affected by the trial functions and weighting functions used. Unless the physically realistic shape functions and weighting functions are employed, the resulting discretization equations may lead to unacceptable solutions.

Another finite difference method of obtaining the algebraic equation is to express the conservation principle for dependent variable for a finite control volume, just as the differential equation expresses the conservation laws for an infinitesimal control volume. This can be done by integrating the differential equation

over each non-overlapping control volume surrounding each grid point. The control volume formulation can be regarded as a variant of subdomain method of the method of weighted residuals, but is more physical in its basis. The accuracy of this formulation is, however, still greatly dependent on the interpolation functions used between nodal points.

The finite analytic method presented by Chen et al. [3-8] invokes another means of deriving the algebraic equations. Unlike the finite difference or finite element method, the discretized algebraic equation is obtained from the analytic solution for each local element in the finite analytic formulation. Details of the principle and procedures in obtaining the finite analytic solution are presented in Chapter II.

In fluid flow and heat transfer problems, certain difficiculties such as numerical instability, false numerical diffusion and slow convergence are encountered in solving Navier-Stokes equations and similar convective transport equations when convective terms are significant. In finite difference formulations, the difficulty of the numerical instability has been overcome by considering a central difference approximation for the diffusion term and a backward (upwind) difference for the convective term [9,10]. Spadling [9] improved this result by utilizing the exact solution for steady one-dimensional

convective transport equation to derive an exponential scheme, and then further simplified to the hybrid scheme. Runchal [10] compared the numerical solution of a simple two-dimensional test problem obtained by hybrid scheme [9] with those obtained by upwind and central difference formulations, and concluded that based on accuracy and stability, the hybrid scheme is preferable. Patankar [11] gave a better approximation called "power-law scheme" to the exact solution, and used it extensively in the control volume formulations of 2D and 3D unsteady convective transport problems.

The all-positive coefficients for the resulting algebraic equation thus obtained lead to a stable solution because the resulting system of algebraic equations is diagonally-dominant. However, as shown in Patankar [11], the false numerical diffusion occurs when the flow is in a skew direction to the grid lines, and when there is a nonzero gradient of the dependent variables in the direction normal to the flow. The false numerical diffusion can be partially resolved by reducing the grid size or taking more nodal points into account in the formulation of discretization equations in each small local element. In two-dimensional problems, a number of finite difference formulas were proposed, in additional to regular four node formulation, to include part or all of the four corner

points so that the false numerical diffusion can be reduced. Works of Raithby [12] and Shay [13] which will be discussed in Chapter IV are some examples. They are, however, produced some undesirable negative coefficients in the algebraic equation representing the partial differential equation due to inadequate finite difference formulations. Furthermore, the extension of the above methods to three-dimensions to include 20 corner points is not obvious or straightforward.

In finite element formulation, a simple "upwind" scheme was derived in [14,15] by improving the weighting function of standard Galerkin formulation with modifying functions and a set of optimal parameters. The 9-point formula thus obtained provides a gradual shift to upwind when convective terms are significant. However, when examining both the diffusion and convection dominated cases, it is found that the resulting 9-point formula [15] does not give the physically realistic asymptotic behaviors. Besides, when nonuniform grid spacing is considered, the results may become increasing unreasonable.

In finite analytic formulation, the local analytic solution for steady two-dimensional convective transport equation in a small local element was obtained in Chen et al. [5,6] by locally linearized the governing equations. They adopted the second-order polynomial to approximate

the boundary condition for all boundaries in each local element. When the local analytic solution is evaluated at a given nodal point, a 9-point finite analytic algebraic equation is obtained. The 9-point FA formula exhibits a gradual, proper skew upwind shift, which is considerably better than those given in [12-15]. However, for convection dominated cases, i.e., at large cell Reynolds number or Peclet number, the finite analytic algebraic equation still produced some physically unrealistic, although small, negative FA coefficients. While the finite analytic solution given by Chen et al. [5,6] is stable and accurate, the complexity of the local analytic solution made it undesirable for extension to unsteady three-dimensional fluid flow problems. It now becomes clear that the appearance of small negative FA coefficients and the complexity of analytic solution originate from the polynomial approximation of boundary conditions made for each local element.

In this dissertation, the finite analytic solutions for unsteady 1D, 2D and 3D convective transport equations are derived in uniform and nonuniform grid spacing local elements. Significant improvements are reported in two-dimensional case when compared with the finite analytic solution obtained by Chen et al. [5,6]. In studying the unsteady one-dimensional convective transport equations,

a number of initial and boundary functions are used to derive finite solutions. Three of them are employed to solve some simple test problems. For two-dimensional cases, the finite analytic solution for steady two-dimensional Navier-Stokes equations derived by Chen et al. [5,6] is modified by considering the boundary approximation to be a combination of exponential and linear functions. Furthermore, an improved linearization scheme is proposed so that the higher order variation of convective terms in the local element can be properly accounted for. The finite analytic solution for nonuniform grid spacing local element is then derived so that the efficiency of computation is improved. As a result of present study, a reasonable set of FA coefficients is obtained and computational time is shortened because of the significant simplification of the FA formula. Extending the two-dimensional study, a 28-point finite analytic formula for unsteady three-dimensional convective transport equations is similarly derived in a general nonuniform grid spacing local element.

In Chapter II, the principle of finite analytic method is outlined. It follows in Chapter III with the finite analytic solutions for unsteady 1D, 2D and 3D convective transport equations. A number of initial and boundary functions are investigated in both uniform and

nonuniform grid spacing local elements. A linearization scheme associated with the higher order correction of convective terms is also outlined. Details of the derivations are given in Appendices A, B and C for 1D, 2D and 3D cases respectively.

The finite analytic numerical solutions of steady and unsteady convective transport equations for some typical examples are given in Chapter IV. The accuracy of the present FA method is demonstrated by a comparison of FA coefficients with those 9-point formulas obtained in finite difference, finite element and those obtained in the early study of finite analytic methods.

In Chapter V, the detailed numerical procedures associated with the finite analytic methods in solving fluid flow or heat transfer problems are outlined. In Chapter VI, simple test problems for one-dimensional convective transport equation are numerically analyzed. It follows in Chapter VII with two test problems of simple geometry for two-dimensional Navier-Stokes equations. The two-dimensional starting cavity flow is investigated first with a range of Reynolds numbers using both the vorticity-streamfunction and the primitive variable formulations. The vortex shedding phenomenon is then studied for uniform flows passing a rectangular block at several Reynolds numbers. In Chapter VIII, the

28-point FA formula for unsteady three-dimensional convective transport equations is employed to study the side wall effect for cubic cavity flow.

The last chapter of this dissertation summarizes the key findings and conclusions and suggests future researches.

CHAPTER II

PRINCIPLE OF FINITE ANALYTIC METHOD FOR UNSTEADY THREE-DIMENSIONAL CONVECTIVE TRANSPORT EQUATION

The basic idea of the finite analytic method is the incorporation of a local analytic solution into the numerical solution of the partial differential equations. The finite analytic method decomposes the total region of a problem governed by partial differential equations into a number of small elements in which local analytic solutions are obtained due to the simple geometry and to local linearization in the case of nonlinear problems. When the local analytic solution is evaluated at an interior node, it gives an algebraic equation relating the evaluated interior nodal value to its neighboring nodal values. The numerical solution of the total problem is then achieved by assembling and overlapping all local analytic solutions.

To illustrate the basic principle, a partial differential equation for unsteady three-dimensional flow $L_1(\phi) = F_1$ is considered as an example, where the operator L_1 can be linear or nonlinear, and F_1 is an inhomogeneous source term. Let x, y, z and t be the independent variables

in space and time, respectively. The PDE is to be solved in the region D shown in Fig. 1. Let the boundary and initial conditions be specified so that the problem is well-posed. In order to solve the problem with the FA method, the complex geometry of the problem is broken up into a number of small elements where analytic solutions can be obtained. Let the region D be subdivided into small elements shown in Fig. 1 by passing orthogonal planes through the region. A typical local element with the nodal point P(i,j,k,n) may be surrounded by the neighboring 26 points NET (northeast top), ECT (eastcenter top), EC (east center) etc. and those of previous time steps, which correspond to points (i+1, j+1,k+1,n), (i+1,j,k+1,n), (i+1,j,k,n) etc. and those at previous time steps n-1 and/or n-2 respectively.

Once the region D has been subdivided into small rectangular elements, the analytic solution in each local element may be obtained if the boundary and initial conditions for that element are properly specified. In the case when the PDE is nonlinear, the nonlinear equation may be locally linearized in the small element. In this fashion, the overall nonlinear effect can still be approximately presented by the assembling of local analytic solutions which constitute the numerical solution of the governing PDE over the whole region D.

Let $L(\phi) = F$ be linear or linearized governing

equation of $L_1(\phi) = F_1$ in a small local element shown in Fig. 1, so that an analytic solution can be obtained for the local element as a function of the boundary and initial conditions, i.e.,

$$\phi = f(f_T(x,y,t),\ f_B(x,y,t),\ f_E(y,z,t),\ f_W(y,z,t),\ f_N(x,z,t),\ f_S(x,z,t),\ f_I(x,y,z),\ h_T,\ h_B,\ h_E,\ h_W,\ h_N,\ h_s,\ \tau,\ x,\ y,\ z,\ t,\ F) \qquad \text{(II-1)}$$

where f_I is the initial condition and f_T, f_B, f_E, f_W, f_N and f_S are the top, bottom, eastern, western, northern and southern boundary conditions, respectively. h_T, h_B, h_E, h_W, h_N, h_S and τ are respectively the grid sizes in x, y, z direction and the step size in time domain. For numerical purpose, the boundary and initial conditions may be approximately expressed in terms of the nodal values along the boundary and also those values at the initial time step. For example,

$$f_T = f(\phi^n_{NET},\ \phi^n_{NWT},\ \phi^n_{SET},\ \phi^n_{SWT},\ \phi^n_{ECT},\ \phi^n_{WCT},\ \phi^n_{NCT},\ \phi^n_{SCT},\ \phi^n_{TC},\ \phi^{n-1}_{NET},\ \ldots\ \phi^{n-1}_{TC},\ x,\ y,\ t) \qquad \text{(II-2a)}$$

and

$$f_I = f(\phi^{n-1}_{NET},\ \ldots\ \phi^{n-1}_{TC},\ \phi^{n-1}_{NEB},\ \ldots\ \phi^{n-1}_{BC},\ \phi^{n-1}_{NEC},\ \ldots\ \phi^{n-1}_{P},\ x,\ y,\ z) \qquad \text{(II-2b)}$$

where ϕ's are the values of the dependent variables on nodal

points, and the superscripts n and n-1 denote those values at present and previous time steps respectively.

Substituting the boundary and initial conditions (II-2a) etc. and (II-2b) into eq(II-11), one has

$$\phi = f(\phi^n_{NET}, \ldots\ldots \phi^n_{TC}, \phi^n_{NEB}, \ldots\ldots \phi^n_{BC}, \phi^n_{NEC}, \ldots$$
$$\ldots \phi^n_{SC}, \phi^{n-1}_{NET}, \ldots\ldots \phi^{n-1}_{TC}, \phi^{n-1}_{NEB}, \ldots\ldots \phi^{n-1}_{BC},$$
$$\phi^{n-1}_{NEC}, \ldots\ldots \phi^{n-1}_{P}, h_T, h_B, h_E, h_W, h_N, h_S,$$
$$\tau, x, y, z, t, F) \qquad \text{(II-3)}$$

Evaluating eq(II-3) at an interior point P(0,0,0,τ), one has the one-time step 54 point finite analytic formula for the interior nodal value ϕ_P as

$$\phi^n_P = \sum_1^{26} C^n_{nb}\phi^n_{nb} + \sum_1^{27} C^{n-1}_{nb}\phi^{n-1}_{nb} + C'_P F_P \qquad \text{(II-4)}$$

where $C^{n'}$s and $C^{n-1'}$s are FA coefficients obtained from the local analytic solution, the subscript "nb" denotes a neighboring node to point P, and F_P is the value of the inhomogeneous term at the point P.

If steady 3D flow is considered, eq(II-4) reduces to a 27-point FA formula

$$\phi_P = \sum_1^{26} b_{nb}\phi_{nb} + b_P F_P \qquad \text{(II-5)}$$

In general, eq(II-4) may be derived for each unknown nodal point P(i,j,k,n) in internal small elements

$$\phi^{n}_{ijk} = \sum_{p=i-1}^{i+1}\sum_{q=j-1}^{j+1}\sum_{r=k-1}^{k+1}(1-\delta_{pi}\delta_{qj}\delta_{rk})C^{n}_{pqr}\phi^{n}_{pqr} + \sum_{p=i-1}^{i+1}\sum_{q=j-1}^{j+1}\sum_{r=k-1}^{k+1}C^{n-1}_{pqr}\phi^{n-1}_{pqr} + C'_{ijk}F_{ijk} \quad \text{(II-6)}$$

where δ_{pi}, δ_{qj} and δ_{rk} are Kronecker deltas defined as

$$\delta_{pi} = \begin{cases} 1, & \text{if } p=i \\ 0, & \text{if } p\neq i \end{cases} \qquad \text{etc.}$$

It should be remarked here that there are several possible ways other than the one presented here that may be employed to simulate the unsteady behavior of the problem. For example, the two-time step FA formulation or hybrid FA and FD formulation are possible alternatives. Because of the parabolic behavior in time domain, the approximations made on the unsteady may cause least problems. Thus, simpler approximate formulas can be used to reduce the complexity of unsteady flow problems, especially when the intermediate time steps serve as a numerical step in obtaining steady or large time solution. For simplicity and computational economics, the hybrid method, which approximates the unsteady term by a finite difference formula is adopted

in the present FA solution of unsteady two- and three-dimensional Navier-Stokes equations. For three-dimensional case, a 28-point FA formula instead of the 54-point formula (II-6) can be obtained for an internal node P(i,j,k,n), i.e,

$$\phi_P^n = \phi_{ijk}^n = \sum_{p=i-1}^{i+1} \sum_{q=j-1}^{j+1} \sum_{r=k-1}^{k+1} (1 - \delta_{pi}\delta_{qj}\delta_{rk}) C_{pqr}^n \phi_{pqr}^n + C_{ijk}^{n-1} \phi_{ijk}^{n-1} + C_{ijk}^{!} F_{ijk} \qquad \text{(II-7)}$$

The system of algebraic equations for all unknown nodes of i, j, k at a given time interval n can be solved to provide the finite analytic solution of the Navior-Stokes equations.

CHAPTER III

FINITE ANALYTIC SOLUTIONS FOR UNSTEADY CONVECTIVE TRANSPORT EQUATIONS

Fluid flow and heat transfer problems, in general, are described by a set of partial differential equations which are mathematical formulation of laws of conservation of mass, momentum and energy. For example, if the fluid is laminar, incompressible with a constant viscosity, the conservation of mass and momentum equations are decoupled from the conservation of energy equation, and can be written in dimensionless form as

(1) Equation of Continuity

$$u_x + v_y + w_z = 0 \qquad \text{(III-1)}$$

(2) Momentum (Navier-Stokes) Equations

$$u_t + uu_x + vu_y + wu_z = -p_x + \frac{1}{Re}(u_{xx} + u_{yy} + u_{zz}) \qquad \text{(III-2)}$$

$$v_t + uv_x + vv_y + wv_z = -p_y + \frac{1}{Re}(v_{xx} + v_{yy} + v_{zz}) \qquad \text{(III-3)}$$

$$w_t + uw_x + vw_y + ww_z = -p_z + \frac{1}{Re}(w_{xx} + w_{yy} + w_{zz}) \qquad \text{(III-4)}$$

where x, y and z are dimensionless Cartesian coordinates

normalized by a reference length L. u, v, w and p are dimensionless velocities and pressure normalized respectively by a reference velocity U and a reference pressure ρU^2, and t is the dimensionless time coordinate normalized by a reference time scale L/U. $Re=\frac{UL}{\nu}$ is the Reynolds number. The corresponding heat transfer in unsteady fluid flow can also be found from the dimensionless energy equation

(3) Energy Equation (constant thermal conductivity k)

$$T_t + uT_x + vT_y + wT_z = q + \frac{1}{Pe}(T_{xx} + T_{yy} + T_{zz}) \qquad \text{(III-5)}$$

where the Peclet number Pe is PrRe, and Pr is the Prandtl number, q is a heat source generated by radiation, viscous dissipation, etc.

In many engineering applications, the physical quantities considered may depend on one or two space coordinate only. For these cases, eqs(III-1) thru (III-5) can be further simplified, and the manipulation effort required to obtain the analytic or numerical solution is significantly reduced.

In this study, the FA method is first employed to obtain the finite analytic solutions of simple 1D problems. Alternatives for the boundary and initial functions are investigated in this simple case. The optimal one is then extended to derive the finite analytic solution for two and three dimensional fluid flow and heat transfer problems.

III-1 Finite Analytic Solutions for Unsteady One-Dimensional Convective Transport Equations

For some extremely simple or simplified fluid flow and heat transfer problems which depend on only one space coordinate, an unsteady one-dimensional convective transport equation of the form of

$$\phi_{xx} = R(\phi_t + u\phi_x) + F(x,t) \qquad \text{(III-6)}$$

is often encountered, where the convective velocity u may be a function of independent variables x, t and dependent variable ϕ. For example, the Burgers' equation which was introduced by Burgers [16] as a simple model for the one-dimensional fluid flow is the one with $u = \phi$ and $F = 0$.

Except for some simple cases, the analytic solution for eq(III-6) may not exist due to the nonlinearity, complicated convective velocity and source function, and/or complex initial and boundary conditions. Thus the finite analytic numerical method is employed in this study to formulate the discretization equations, so that an approximate numerical solution can be obtained.

Considered a domain D shown in Fig. 2. For numerical purposes, the region D is subdivided into many small elements, and the analytic solution is sought in each local element. A typical two-time step local element shown in Fig. 2(b) for point NC(i,n) is surrounded by

neighboring nodal points NW, NE and WC, EC, SW, SC ans SE of previous time steps, which correspond to (i-1,n), (i+1,n), (i-1,n-1), (i+1,n-1), (i-1,n-2), (i,n-2) and (i+1,n-2) respectively. On the other hand, an one-time step local element for point P(i,n) is surrounded by nodal points WC, EC, SW, SC, and SE as shown in Fig. 2(c).

After dividing the region D into small elements, complex initial and boundary conditions may be approximated by some simple initial and boundary functions, so that an analytic solution can be derived. However, even for such simple initial and boundary conditions, the analytic solution may still be difficult to obtain due to the complicated dependence of u and F on independent and/or dependent variables. In this situation, the convective transport equation (III-6) is further simplified by approximating the convective velocity as a constant over a small local element, i.e.,

$$\phi_{xx} = 2A\phi_x + B\phi_t + F(x,t) \qquad \text{(III-7)}$$

where $A = \frac{1}{2}KU$, $B = K$, and U is a representative constant velocity over the local element.

Equation (III-7) becomes a linear partial differential equation of constant coefficients. At this stage, the source term F(x,t) may be taken care of easily by a particular solution. Thus, only the homogeneous convective

transport equation

$$\phi_{xx} = 2A\phi_x + B\phi_t \qquad \text{(III-8)}$$

is considered in the following derivations.

Depending on the boundary and initial functions chosen to approximate the boundary and initial conditions for different local elements, three FA solutions are given to illustrate the basic principle of the finite analytic method. Three solutions of eq(III-8) are distinguished by the following formulations.

(1) FA formulation of eq(III-8) with second-order polynomial approximation for both initial and boundary functions.

(2) FA formulation of eq(III-8) with exponential and linear approximation for initial function and linear approximation for boundary functions.

(3) FA formulation of eq(III-8) with unsteady term approximated by a finite difference formula. This is a hybrid FA-FD method.

III-1-1 FA formulation of Unsteady One-Dimensional Convective Transport Equation with Second-Order Polynomial Initial and Boundary Functions

In this section, the linear or linearized unsteady one-dimensional convective transport equation (III-8) is

solved by finite analytic numerical method in a two-time step local element shown in Fig. 2(b). For the convective transport equation to be well-posed in the local element shown, an initial condition $\phi_I(x)$ and two boundary conditions $\phi_W(t)$ and $\phi_E(t)$ must be properly specified along the south, west and east sides of the local element respectively. Since each side, for numerical purpose, has three nodal values available, one may approximate the initial and boundary conditions by suitable initial and boundary functions which are expressed in terms of these nodal values. There are several initial and boundary functions which may be used to obtain the approximate initial and boundary conditions. In this case, a second-order polynomial is employed to approximate both the initial and boundary conditions as follows

$$\phi(x,0) = \phi_I(x) = a_S + b_S x + c_S x^2 \qquad \text{(III-9a)}$$

$$\phi(-h,t) = \phi_W(t) = a_W + b_W t + c_W t^2 \qquad \text{(III-9b)}$$

$$\phi(h,t) = \phi_E(t) = a_E + b_E t + c_E t^2 \qquad \text{(III-9c)}$$

where

$$a_S = \phi_{SC}, \quad b_S = \frac{1}{2h}(\phi_{SE} - \phi_{SW}),$$

$$c_S = \frac{1}{2h^2}(\phi_{SE} + \phi_{SW} - 2\phi_{SC})$$

$$a_W = \phi_{SW}, \quad b_W = \frac{1}{2\tau}(4\phi_{WC} - 3\phi_{SW} - \phi_{NW})$$

$$c_W = \frac{1}{2\tau^2}(\phi_{SW} + \phi_{NW} - 2\phi_{WC})$$

$$a_E = \phi_{SE}, \qquad b_E = \frac{1}{2\tau}(4\phi_{EC} - 3\phi_{SE} - \phi_{NE})$$

$$c_E = \frac{1}{2\tau^2}(\phi_{SE} + \phi_{NE} - 2\phi_{EC})$$

The linear partial differential equation (III-8) with initial condition (III-9a) and boundary conditions (III-9b) and (III-9c) can then be solved analytically by the method of separation of variables. Details of the derivation are given in Sec. A-1 of Appendix A. The local analytic solution when evaluated at the North-Center node $(0,2\tau)$ gives a finite analytic algebraic equation relating the interior nodal value ϕ_{NC} and its 7 neighboring nodal values as follows

$$\phi_{NC} = C_{NW}\phi_{NW} + C_{NE}\phi_{NE} + C_{WC}\phi_{WC} + C_{EC}\phi_{EC} + C_{SW}\phi_{SW} + C_{SE}\phi_{SE} + C_{SC}\phi_{SC} \qquad \text{(III-10)}$$

where

$$C_{NW} = e^{Ah}\left[Q_1 - \frac{Bh^2}{2\tau}(P_2 + Q_2) + 4\left(\frac{Bh^2}{2\tau}\right)^2(Q_3 - P_3)\right]$$

$$C_{NE} = e^{-2Ah}C_{NW}$$

$$C_{WC} = e^{Ah}\left[4\left(\frac{Bh^2}{2\tau}\right)(P_2 + Q_2) - 8\left(\frac{Bh^2}{2\tau}\right)^2(Q_3 - P_3)\right]$$

$$C_{EC} = e^{-2Ah}C_{WC}$$

$$C_{SW} = e^{Ah}\left[-P_2 - 3AhP_2 + 4(Ah)^2P_3 - \left(\frac{Bh^2}{2\tau}\right)(3P_2 + Q_2)\right.$$

$$\left. + 4\left(\frac{Bh^2}{2\tau}\right)^2(Q_3 - P_3)\right] + e^{-Ah}\left[-P_2 + AhP_2 + 4(Ah)^2P_3\right]$$

$$C_{SE} = e^{-Ah}\left[-P_2 + 3AhP_2 + 4(Ah)^2P_3 - \left(\frac{Bh^2}{2\tau}\right)(3P_2 + Q_2)\right.$$

$$\left. + 4\left(\frac{Bh^2}{2\tau}\right)^2(Q_3 - P_3)\right] + e^{Ah}\left[-P_2 - AhP_2 + 4(Ah)^2P_3\right]$$

$$C_{SC} = e^{Ah}\left[2P_2 + 4AhP_2 - 8(Ah)^2P_3\right] + e^{-Ah}\left[2P_2 - 4AhP_2\right.$$

$$\left. - 8(Ah)^2P_3\right]$$

where P_2, P_3, Q_1, Q_2 and Q_3 are defined by

$$P_i = \sum_{m=1}^{\infty} \frac{-(-1)^m \lambda_m h\, e^{-2F_m\tau}}{\left[(Ah)^2 + (\lambda_m h)^2\right]^i}, \qquad i = 2,3 \qquad \text{(III-11a)}$$

$$Q_i = \sum_{m=1}^{\infty} \frac{-(-1)^m \lambda_m h}{\left[(Ah)^2 + (\lambda_m h)^2\right]^i} \qquad i = 1,2,3 \qquad \text{(III-11b)}$$

with $2F_m\tau = \dfrac{(Ah)^2 + (\lambda_m h)^2}{Bh^2/2\tau}$ and $\lambda_m h = (m - \frac{1}{2})\pi$

Three of the five summation terms Q_1, Q_2 and Q_3 may be expressed analytically as those given in Appendix A to save some computational time, i.e.,

$$Q_1 = \frac{1}{2\cosh Ah} \qquad \text{(III-12a)}$$

$$Q_2 = \frac{\sinh Ah}{4(Ah)\cosh^2 Ah} \qquad \text{(III-12b)}$$

$$Q_3 = \frac{1}{16(Ah)^2\cosh Ah} + \frac{\sinh Ah}{16(Ah)^3\cosh^2 Ah} - \frac{1}{8(Ah)^2\cosh^3 Ah} \qquad \text{(III-12c)}$$

It is noted that the FA coefficients in eq(III-10) are functions of Ah and $\frac{Bh^2}{2\tau}$ only. The ratio of the parameters $\frac{2A\tau}{Bh} = \frac{U\tau}{h} = C_0$ is known to be the Courant number [1]. Thus, the FA coefficients can also be written as

$$C_{NW} = e^{Ah}\left[Q_1 - \frac{Ah}{C_0}(P_2 + 3Q_2) + 4\left(\frac{Ah}{C_0}\right)^2(Q_3 - P_3)\right]$$

$$C_{NE} = e^{-2Ah}C_{NW}$$

$$C_{WC} = e^{Ah}\left(\frac{4Ah}{C_0}\right)\left[P_2 + Q_2 - 2\left(\frac{Ah}{C_0}\right)(Q_3 - P_3)\right]$$

$$C_{EC} = e^{-2Ah}C_{WC}$$

$$C_{SW} = e^{Ah}\left[-(1+3Ah)P_2 + 4(Ah)^2P_3 - \left(\frac{Ah}{C_0}\right)(3P_2+Q_2) + 4\left(\frac{Ah}{C_0}\right)^2(Q_3-P_3)\right] + e^{-Ah}\left[(-1+Ah)P_2 + 4(Ah)^2P_3\right]$$

$$C_{SE} = e^{Ah}\left[(-1+3Ah)P_2 + 4(Ah)^2P_3 - \left(\frac{Ah}{C_0}\right)(3P_2+Q_2)\right.$$

$$\left. + 4\left(\frac{Ah}{C_0}\right)^2(Q_3-P_3)\right] + e^{Ah}\left[-(1+Ah)P_2 + 4(Ah)^2P_3\right]$$

$$C_{SC} = e^{Ah}\left[2(1+2Ah)P_2 - 8(Ah)^2P_3\right] + e^{-Ah}\left[2(1-2Ah)P_2\right.$$

$$\left. - 8(Ah)^2P_3\right] \qquad \text{(III-13)}$$

It should be remarked here that a simpler FA solution based on linear boundary conditions can be derived easily in an one-time step local element by letting $\phi_{WC} = 0.5(\phi_{NW} + \phi_{SW})$ and $\phi_{EC} = 0.5(\phi_{NE} + \phi_{SE})$ in eq(III-10). The one-time step FA formula thus obtained is used for initial time step of calculation with a time increment of 0.5τ. The two-time step FA formula is then employed to obtain the subsequent FA numerical solutions.

III-1-2 FA Formulation of Unsteady One-Dimensional Convective Transport Equation with Exponential and Linear Initial Function and Linear Boundary Functions

In the previous formulation, some of the FA coefficients in eq(III-10) may become negative for many combinations of Ah and Courant number C_0. The negative FA coefficients although small, may result in an unrealistic overshoot for some of the problems considered. In order to avoid these unrealistic negative FA coefficients, an exponential and linear function based on the natural solutions

$(e^{2Ax}, Bx-2At)$ of eq(III-8) is employed in this formulation to approximate the initial condition for the one-time step local element shown in Fig. 2(c). As to the boundary conditions, simple linear boundary functions are used in terms of two nodal variables available on each boundary.

$$\phi(x,0) = \phi_I(x) = a_S(e^{2Ax} - 1) + b_S x + c_S \qquad \text{(III-14a)}$$

$$\phi(-h,t) = \phi_W(t) = a_W + b_W t \qquad \text{(III-14b)}$$

$$\phi(h,t) = \phi_E(t) = a_E + b_E t \qquad \text{(III-14c)}$$

where

$$a_S = \frac{\phi_{SE} + \phi_{SW} - 2\phi_{SC}}{4\sinh^2 Ah}$$

$$b_S = \frac{\phi_{SE} - \phi_{SW} - \coth Ah(\phi_{SE} + \phi_{SW} - 2\phi_{SC})}{2h}$$

$$c_S = \phi_{SC}$$

$$a_W = \phi_{SW}, \qquad b_W = \frac{\phi_{WC} - \phi_{SW}}{\tau}$$

$$a_E = \phi_{SE}, \qquad b_E = \frac{\phi_{EC} - \phi_{SE}}{\tau}$$

After specifying the initial and boundary conditions (III-14a) - (III-14c) for the small local element shown in Fig. 2(c), the linear convective transport equation (III-8) is then solved analytically by the method of separation of variables. The local analytic solution when evaluated at

the interior point $P(0,\tau)$ will result in a finite analytic algebraic equation relating the interior nodal value ϕ_P to its 5 neighboring nodal values, i.e.,

$$\phi_P = C_{WC}\phi_{WC} + C_{EC}\phi_{EC} + C_{SW}\phi_{SW} + C_{SE}\phi_{SE} + C_{SC}\phi_{SC} \qquad \text{(III-15)}$$

where

$$C_{WC} = e^{Ah}\left[Q_1 + \frac{Bh^2}{\tau}(P_2 - Q_2)\right]$$

$$C_{EC} = e^{-2Ah}C_{WC}$$

$$C_{SW} = e^{Ah}\left[\frac{Bh^2}{\tau}(Q_2 - P_2) - 2Ah\ \text{coth}Ah\ P_2\right]$$

$$C_{SE} = e^{-2Ah}C_{SW}$$

$$C_{SC} = 4Ah\ \text{cosh}Ah\ \text{coth}Ah\ P_2$$

Details of the derivation are given in Sec. A-2 of Appendix A. Equation (III-15) can also be expressed in terms of the Courant number C_0 and the other parameter Ah as follows

$$C_{WC} = e^{Ah}S_1$$

$$C_{EC} = e^{-Ah}S_1$$

$$C_{SW} = e^{Ah}S_2 \qquad \text{(III-16)}$$

$$C_{SE} = e^{-Ah}S_2$$

$$C_{SC} = 4Ah\ \text{cosh}Ah\ \text{coth}Ah\ P_2$$

where

$$S_1 = \frac{2Ah}{C_0}(P_2 - Q_2) + Q_1$$

and

$$S_2 = \frac{2Ah}{C_0}(Q_2 - P_2) - 2Ah \coth Ah\ P_2$$

III-1-3 Hybrid FA Formulation of Unsteady One-Dimensional Convective Transport Equation

In order to reduce the manipulation effort and computational time, an alternative hybrid FA solution of one-dimensional convective transport equation (III-8) may be derived where an approximation for unsteady term may be used. For example, one may approximate the unsteady term by a simple finite difference formula.

$$B\phi_t = B\,\frac{\phi_P - \phi_{SC}}{\tau} = \text{constant} = g \qquad \text{(III-17)}$$

so that the unsteady convective transport equation (III-8) is reduced to be a steady-like convective transport equation with the unsteady term absorbed in a constant source term g for the local element as follows

$$\phi_{xx} = 2A\phi_x + g \qquad \text{(III-18)}$$

The finite analytic algebraic equation can be derived easily as that shown in Sec. A-3 of Appendix A.

$$\phi_P = \frac{e^{Ah}\phi_{WC} + e^{-Ah}\phi_{EC}}{e^{Ah} + e^{-Ah}} - \frac{\tanh Ah}{2Ah}\,gh^2 \qquad \text{(III-19)}$$

By substituting the expression of g into eq(III-19), a 4-point hybrid FA formula (see Fig. 1(c)) is obtained

$$\phi_P = C_{WC}\phi_{WC} + C_{EC}\phi_{EC} + C_{SC}\phi_{SC} \qquad \text{(III-20)}$$

$$= \frac{1}{1 + b_{SC}} (b_{WC}\phi_{WC} + b_{EC}\phi_{EC} + b_{SC}\phi_{SC}) \qquad \text{(III-20a)}$$

where

$$b_{SC} = \frac{Bh^2}{2\tau} \frac{\tanh Ah}{Ah} = \frac{1}{C_0} \tanh Ah$$

$$b_{WC} = \frac{e^{Ah}}{e^{Ah} + e^{-Ah}}$$

$$b_{EC} = \frac{e^{-Ah}}{e^{Ah} + e^{-Ah}}$$

It is noted that eq(III-17) is the only approximation made in the derivation of the hybrid FA formula (III-20), thus, the three-point steady state finite analytic solution can be obtained from eq(III-19) or (III-20) by simply letting g = 0 or B = 0. Which is

$$\phi_P = \frac{e^{Ah}\phi_{WC} + e^{-Ah}\phi_{EC}}{e^{Ah} + e^{-Ah}} \qquad \text{(III-21)}$$

By equating $\phi^n = \phi^{n-1}$ in equation (III-15), i.e., $\phi_P = \phi_{SC}$, $\phi_{SW} = \phi_{WC}$, $\phi_{SE} = \phi_{EC}$, the same steady-state solution (III-21) is recovered in the formulation using exponential and linear initial function and linear boundary functions.

III-2 Finite Analytic Solutions for Unsteady Two-Dimensional Convective Transport Equations

For unsteady fluid flow and heat transfer problems which depend on only two space variables, the dimensionless equation of continuity (III-1), momentum equation (III-2) thru (III-4) and energy equation (III-5) are simplified respectively to be

$$u_x + v_y = 0 \tag{III-22}$$

$$u_t + uu_x + vu_y = -p_x + \frac{1}{Re}(u_{xx} + u_{yy}) \tag{III-23}$$

$$v_t + uv_x + vv_y = -p_y + \frac{1}{Re}(v_{xx} + v_{yy}) \tag{III-24}$$

$$T_t + uT_x + vT_y = q + \frac{1}{Pe}(T_{xx} + T_{yy}) \tag{III-25}$$

If vorticity-streamfunction formulation is considered by eliminating the pressure term from eq(III-23) and (III-24), a vorticity transport equation can be obtained

$$\xi_t + u\xi_x + v\xi_y = \frac{1}{Re}(\xi_{xx} + \xi_{yy}) \tag{III-26}$$

where vorticity ξ is defined by

$$\xi = v_x - u_y = -(\psi_{xx} + \psi_{yy}) \tag{III-27}$$

$$\text{with } u = \psi_y \text{ and } v = -\psi_x \tag{III-28}$$

where the streamfunction ψ is defined by eq(III-28), so

that the equation of continuity (III-22) is automatically satisfied.

Either in vorticity-streamfunction (ψ,ξ,T) or in primitive variables (u,v,p,T) formulation, a convective transport equation of the form of

$$\phi_{xx} + \phi_{yy} = R\,(\phi_t + u\phi_x + v\phi_y) + \Gamma \qquad \text{(III-29)}$$

is often encountered in solving two-dimensional fluid flow or heat transfer problems. Where ϕ may represent velocities (R=Re), vorticity (R=Re), temperature (R=Pe) or streamfunction (R=0). The convective velocities u, v and the source term Γ, in general, are functions of independent variables x, y, t and dependent variables ϕ_j (e.g., u, v, p, T, ψ or ξ) including ϕ itself. Equation (III-29) may also be written in conservative form by applying the equation of continuity (III-22)

$$\phi_{xx} + \phi_{yy} = R\,[\phi_t + (u\phi)_x + (v\phi)_y] + \Gamma \qquad \text{(III-30)}$$

In most of the engineering applications, the analytic solution of eq(III-29) or (III-30) may not be available due to the complex geometry and boundary conditions, nonlinearity of the equation and also the coupling of the variables. Thus, the finite analytic numerical method is used to formulate the discretization equation for ϕ, so that an approximate numerical solution can be obtained.

III-2-1 Method of Linearization

To implement the FA method, the flow region as shown in Fig. 3 is subdivided into a number of small elements by passing orthogonal lines through the region. A typical local element with the interior nodal point P(i,j,n) may be surrounded by the neighboring points EC (East center), WC (West Center), NC (North Center), SC (South Center), NE (Northeast), NW (Northwest), SE (Southeast), SW (Southwest) and those of previous time step, which corresponding to (i+1,j,n), (i-1,j,n), (i,j+1,n), (i,j-1,n), (i+1,j+1,n), (i-1,j+1,n), (i+1,j-1,n), (i-1,j-1,n) and those at previous time step t_{n-1} respectively.

Even in the local element of such a simple geometry, the analytic solution for eq(III-8) or (III-9) may still be difficult to obtain due to the coupling of variables, nonlinearity of equation and the complicated source function. In this situation, a linearization scheme outlined in the following is employed to obtain the nominally linear convective transport equation, so that the analytic solution can be derived in each local element.

Considering the convective transport equation of conservation form (III-30) as an example, in order to solve eq(III-30) analytically in each local element, eq(III-30) is first rearranged to be

$$\phi_{xx} + \phi_{yy} = R\,(\phi_t + U\phi_x + V\phi_y) + F + R\,[(u'\phi)_x + (v'\phi)_y] \qquad \text{(III-31)}$$

with

$$u(x,y,t,\phi_j) = U + u'(x,y,t,\phi_j) \qquad \text{(III-31a)}$$

$$v(x,y,t,\phi_j) = V + v'(x,y,t,\phi_j) \qquad \text{(III-31b)}$$

where U and V are representative constant values in the local element, for example, the velocities at the interior point P or the area-averaged velocities over the local element. And ϕ_j may be any dependent variable including ϕ itself.

When the local element is small enough, the deviations u' and v' from U and V should be small also. Therefore, the term $R[(u'\phi)_x + (v'\phi)_y]$ may be considered as a higher order correction to the convective term in which the convection of ϕ variable in the element is carried by constant velocities U and V. Denoting two time steps t_{n-1} and t_n, one may locally linearize the convective transport equation (III-31) by approximating the source function and higher order correction term as a function known from previous time step t_{n-1} (or from the previous iteration in iterative steady-state method), i.e.,

$$(\phi_{xx} + \phi_{yy})^n = R\,(\phi_t + U\phi_x + V\phi_y)^n + f^{n-1}(x,y,\phi_j)$$

where (III-32)

$$f(x,y,t,\phi_j) = F(x,y,t,\phi_j) + R\,[(u'\phi)_x + (v'\phi)_y]$$

In this fashion, eq(III-30) is locally linearized to be a nominally linear partial differential equation of constant coefficients at n^{th} time step. Various solution methods as those described in Section III-1 for unsteady one-dimensional problems can thus be employed to derive the analytic solution for the linearized elliptic-parabolic partial differential equation (III-32). (elliptic in space and parabolic in time in space-time variables)

In previous formulations for one-dimensional problems, it is learned that different approximations to the unsteady term may result in different intermediate profile and speed of propagation, however, there is no direct effect on the steady-state solution profile. Furthermore, because of the parabolic nature in time domain and that the time derivative appears only in one term of eq(III-32), it is possible to adopt a simple approximation for unsteady term with a reasonable transient solution profile. Thus, the simple hybrid FA formula outlined in Sec. III-1-3 is used in this study to reduce the complexity of the derivation and to save the computational time. In the hybrid FA formulation, the unsteady term is then approximated by

$$R\phi_t = R\,\frac{\phi_P^n - \phi_P^{n-1}}{\tau} = \text{constant} \qquad \text{(III-33)}$$

where $\tau = t_n - t_{n-1}$ is the time increment, and the subscript P denotes the interior node P of the local element.

In addition, the nonhomogeneous part $f^{n-1}(x,y,\phi_j)$ of eq(III-32) can also be approximated by a representative constant value f_p in the local element, so that the manipulation effort and computational time required can be further reduced. Under these approximations, the unsteady two-dimensional convective transport equation (III-30) is simplified to be a nominally linear elliptic-like PDE with constant inhomogeneous term

$$\phi_{xx} + \phi_{yy} = 2A\phi_x + 2B\phi_y + g \qquad \text{(III-34)}$$

$$\text{where } A = \frac{1}{2} RU, \; B = \frac{1}{2} RV \qquad \text{(III-34a)}$$

$$\text{and} \quad g = \frac{R}{\tau} (\phi_p^n - \phi_p^{n-1}) + f_p = \text{constant} \qquad \text{(III-34b)}$$

It should be remarked here that the constants A, B and g may differ from one element to another, so that the overall nonlinearity is approximately preserved. And the coupling nature of variables can also be approximately preserved by solving the interlinked equations subsequently in each time step.

Since the initial condition has been taken care of by approximating the unsteady term by a finite difference, the equivalent elliptic PDE (III-34) can then be solved analytically if the boundary conditions are properly

specified. A typical local element for eq(III-34) at time step t_n (or at $t = \tau$ in Fig. 3) is enclosed by four boundaries (East, West, North and south), where each boundary for the numerical purpose has three nodes. Thus, the boundary conditions for linearized convective transport equation (III-34) may be approximately specified by these eight nodal values in the boundaries. In this study, three local analytic solutions for different local element and boundary approximations will be derived in the following

(1) Uniform grid spacing local element ($h_E=h_W=h$, $h_N=h_S=k$) with exponential and linear boundary approximations. (Fig. 4(a))

(2) Nonuniform grid spacing local element ($h_E \neq h_W$, $h_N \neq h_S$) with exponential and linear boundary approximations. (Fig. 4(b))

(3) Uniform grid spacing local element with piecewise-linear boundary approximations. (Fig. 4(a))

III-2-2 FA Formulation of Unsteady Two-Dimensional Convective Transport Equation for Uniform Grid Spacing Local Element with Exponential and Linear Boundary Approximations.

Chen et. al. [5,6] developed a FA solution to solve the steady vorticity transport equation

$$\xi_{xx} + \xi_{yy} = 2A\xi_x + 2B\xi_y \qquad \text{(III-35)}$$

in a uniform grid local element as shown in Fig. 4(a). In their formulation, eq(III-35), which is a special case of eq(III-34) with g = 0, is solved by using the second-order polynomial boundary approximations on each boundary. For example, the east boundary condition $\xi_E(x)$ is approximated by

$$\xi_E(x) = a_0 + a_1 y + a_2 y^2$$

where $a_0 = \xi_{EC}$, $a_1 = \frac{1}{2k}(\xi_{NE} - \xi_{SE})$

and $a_2 = \frac{1}{k^2}(\xi_{NE} + \xi_{SE} - 2\xi_{EC})$

The linear homogeneous vorticity transport equation (III-35) is then solved analytically by the method of separation of variables. The finite analytic solution when evaluated at the center node P gives

$$\xi_P = C_{EC}\xi_{EC} + C_{WC}\xi_{WC} + C_{NC}\xi_{NC} + C_{SC}\xi_{SC} + C_{NE}\xi_{NE} + C_{NW}\xi_{NW} + C_{SE}\xi_{SE} + C_{SW}\xi_{SW} \qquad \text{(III-36)}$$

The expressions of FA coefficients C_{EC}, C_{WC} etc. can be found in Chen et. al. [5,6]. It exhibits a gradual upwind shift, which is considerably better than those given by FD or FE methods [11 - 15]. However, the calculation of FA coefficients are rather time consuming, and some of the FA coefficients although small will become

negative when convective velocities are large. These negative FA coefficients are physically unrealistic [11], since the contribution from diffusion should be positive for all physical problems.

After further investigation, it now becomes clear that these negative FA coefficients originate from the boundary approximations. For example, let us consider the limiting case of negligible diffusion (i.e., $Re \to \infty$) where eq (III-35) is reduced to

$$2A\xi_x + 2B\xi_y = 0 \qquad \text{(III-37)}$$

The exact solution for this first-order hyperbolic equation is known to be

$$\xi = f(x - \frac{Ay}{B}) \qquad \text{(III-38)}$$

If second-order boundary approximation is used to approximate the south boundary condition (i.e., now the initial condition for eq(III-37)) for the case $0 \le Ak \le Bh$, the analytic solution evaluated at center node P will give

$$\xi_P = \frac{r}{2}(r+1)\xi_{SW} + (1-r^2)\xi_{SC} + \frac{r}{2}(r-1)\xi_{SE}$$

$$= C_{SW}\xi_{SW} + C_{SC}\xi_{SC} + C_{SE}\xi_{SE} \qquad \text{(III-39)}$$

where

$$r = \frac{Ak}{Bh}, \qquad 0 \le r \le 1$$

From eq(III-39) it is seen that the coefficient C_{SE} is always negative, and the maximum negative value, which occurs at r = 0.5, will be -0.125.

In order to construct a better boundary approximation for convective transport equation (III-34) or (III-35), the steady one-dimensional convective transport equation is investigated at first

$$\phi_{xx} = 2A\phi_x + g \qquad \text{(III-40)}$$

Equation (III-40) is exactly the same as equation (III-18) considered previously, the exact solution is given in Sec. A-3, and the derivative at point P can also be derived.

$$\phi_x\Big|_P = \frac{A}{\sinh 2Ah}\left(\phi_E - \phi_W + \frac{g}{A}h\right) - \frac{g}{2A} \qquad \text{(III-41)}$$

For the case g = 0, the solution (A-42) of eq(III-40) as a function of convective velocity U or parameter Ah, which has been discussed by Spadling [9], Patankar [11] and others, is plotted in Fig. 5.

It can be seen that when Ah changes from pure diffusion case (Ah = 0) to convective dominant cases ($|Ah| >> 1$), the exact solution at center point P (i.e., eq(III-21)) exhibits a gradual shift to upwind and the derivative at point P gradually decreases to zero. If second-order polynomial boundary approximation is used

to approximate the exact solution, negative or overshoot may occur at large Ah or convective velocity as that shown in Fig. 5. Furthermore, the derivative at point P is much larger than the true value. Thus, use of second-order polynomial as boundary functions may overestimate the diffusion effect at large convective velocities. On the other hand, use of the piecewise-linear boundary approximation shown in Fig. 5 will give a much better representation of upstream solution, however, the diffusion effect may be overestimated.

Extending the idea of using the exact solution for one-dimensional convective transport equation, one can construct a better approximation function of boundary conditions by utilizing the natural solution for two-dimensional convective transport equation (III-34). A natural solution for eq(III-34) may be written in x and y variables as

$$\phi = C_0 e^{2(Ax+By)} + C_1(Ay-Bx) + C_2 - \frac{g}{2(A^2+B^2)}(Ax+By) \qquad \text{(III-42)}$$

The last term in eq(III-42) is the particular solution of eq(III-34). The first three terms are solutions that satisfies the homogeneous part of eq(III-34). Writing

$$\phi = \tilde{\phi} - \frac{g}{2(A^2+B^2)}(Ax+By) \qquad \text{(III-43)}$$

and substituting ϕ in eq(III-43) into eq(III-34), then $\tilde{\phi}$ satisfies the homogeneous equation

$$\tilde{\phi}_{xx} + \tilde{\phi}_{yy} = 2A\tilde{\phi}_x + 2B\tilde{\phi}_y \qquad \text{(III-44)}$$

The natural solution (III-42) suggests that an exponential and linear function in terms of the three nodal values on each boundary may be employed to obtain the approximated boundary conditions for the local element considered. For example, the north boundary condition where y is fixed can be approximated by

$$\tilde{\phi}_N(x) = a_N(e^{2Ax}-1) + b_N x + c_N \qquad \text{(III-45a)}$$

where

$$a_N = \frac{\tilde{\phi}_{NE} + \tilde{\phi}_{NW} - 2\tilde{\phi}_{NC}}{4\sinh^2 Ah}$$

$$b_N = \frac{1}{2h}\left[\tilde{\phi}_{NE} - \tilde{\phi}_{NW} - \coth Ah(\tilde{\phi}_{NE} + \tilde{\phi}_{NW} - 2\tilde{\phi}_{NC})\right]$$

$$c_N = \tilde{\phi}_{NC}$$

The boundary conditions for south, east and west sides, i.e., $\tilde{\phi}_S(x)$, $\tilde{\phi}_E(y)$ and $\tilde{\phi}_W(y)$ can be similarly approximated by exponential and linear boundary functions as follows

$$\tilde{\phi}_S(x) = a_S(e^{2Ax}-1) + b_S x + c_S \qquad \text{(III-45b)}$$

$$\tilde{\phi}_E(y) = a_E(e^{2By}-1) + b_E y + c_E \qquad \text{(III-45c)}$$

$$\tilde{\phi}_W(y) = a_W(e^{2By}-1) + b_W y + c_W \qquad \text{(III-45d)}$$

where the coefficients a_S, b_S etc. are expressed in terms of the nodal values on each boundary in a way similar to that for a_N, b_N and c_N. The nominally linear convective transport equation (III-44) with boundary conditions $\tilde{\phi}_E(y)$, $\tilde{\phi}_W(y)$, $\tilde{\phi}_N(x)$ and $\tilde{\phi}_S(x)$ is then solved analytically by the method of separation of variables. The local analytic solution when evaluated at the interior point P of the rectangular local element gives a finite analytic algebraic equation relating the interior nodal value $\tilde{\phi}_P$ and its 8 neighboring nodal values as

$$\tilde{\phi}_P = C_{EC}\tilde{\phi}_{EC} + C_{WC}\tilde{\phi}_{WC} + C_{NC}\tilde{\phi}_{NC} + C_{SC}\tilde{\phi}_{SC} + C_{NE}\tilde{\phi}_{NE} + C_{NW}\tilde{\phi}_{NW} + C_{SE}\tilde{\phi}_{SE} + C_{SW}\tilde{\phi}_{SW} \qquad \text{(III-46)}$$

Here, the FA coefficients are

$$C_{EC} = e^{-Ah}(EB) \qquad C_{WC} = e^{Ah}(EB)$$

$$C_{NC} = e^{-Bk}(EA) \qquad C_{SC} = e^{Bk}(EA)$$

$$C_{NE} = e^{-Ah-Bk}E \qquad C_{NW} = e^{Ah-Bk}E \qquad \text{(III-47)}$$

$$C_{SE} = e^{-Ah+Bk}E \qquad C_{SW} = e^{Ah+Bk}E$$

where

$$E = \frac{1}{4\cosh Ah \cosh Bk} - Ah \coth Ah\, E_2 - Bk \coth Bk\, E_2' \qquad \text{(III-48a)}$$

$$EA = 2Ah \cosh Ah \coth Ah \; E_2 \qquad \text{(III-48b)}$$

$$EB = 2Bk \cosh Bk \coth Bk \; E_2' \qquad \text{(III-48c)}$$

and

$$E_2 = \sum_{m=1}^{\infty} \frac{-(-1)^m(\lambda_m h)}{[(Ah)^2+(\lambda_m h)^2]^2 \cosh \sqrt{A^2+B^2+\lambda_m^2}\, k} \qquad \text{(III-48d)}$$

$$E_2' = \sum_{m=1}^{\infty} \frac{-(-1)^m(\lambda_m' k)}{[(Bk)^2+(\lambda_m' k)^2]^2 \cosh \sqrt{A^2+B^2+\lambda_m'^2}\, h} \qquad \text{(III-48e)}$$

$$= \frac{h^2}{k^2} E_2 + \frac{Ak \tanh Bk - Bh \tanh Ah}{4ABk^2 \cosh Ah \cosh Bk} \qquad \text{(III-48f)}$$

with

$$\lambda_m h = (m - \tfrac{1}{2})\pi \quad , \quad \lambda_m' k = (m - \tfrac{1}{2})\pi$$

Details of the solution procedures are given in Sec. B-1 of Appendix B. It should be noted that in the finite analytic solution (III-46), there is only one series summation term needed to be calculated numerically. That is E_2, and it may be replaced by suitable approximation functions to further reduce the computational time.

For the unsteady inhomogeneous convective transport equation (III-34) with higher order correction term, i.e., $g \neq 0$, the local analytic solution can be obtained by substituting $\tilde{\phi}$ of eq(III-43) at 9 nodal points into eq(III-46) for ϕ, which gives

$$\phi_P = C_{NE}\phi_{NE} + C_{NW}\phi_{NW} + C_{SE}\phi_{SE} + C_{SW}\phi_{SW} + C_{EC}\phi_{EC} + C_{WC}\phi_{WC} + C_{NC}\phi_{NC} + C_{SC}\phi_{SC} - C_P g \qquad \text{(III-49)}$$

where

$$C_P = \frac{1}{2(A^2+B^2)}\{ Ah\ \tanh Ah + Bk\ \tanh Bk - 4\ \cosh Ah * \cosh Bk\ [\ (Ah)^2 E_2 + (Bk)^2 E_2'\ ]\ \} \qquad \text{(III-50)}$$

By substituting g of eq(III-34b) into eq(III-49), a 10-point FA formula for unsteady two-dimensional convective transport equation can be obtained

$$\phi_P = \frac{1}{1 + \frac{R}{\tau} C_P} (C_{NE}\phi_{NE} + C_{NW}\phi_{NW} + C_{SE}\phi_{SE} + C_{SW}\phi_{SW} + C_{EC}\phi_{EC} + C_{WC}\phi_{WC} + C_{NC}\phi_{NC} + C_{SC}\phi_{SC} + \frac{R}{\tau} C_P \phi_P^{n-1} - C_P f_P) \qquad \text{(III-51)}$$

where

$$f_P = f^{n-1}(x,y,\phi_j)\Big|_P = \{ F(x,y,t,\phi_j) + R\ [\ (u'\phi)_x + (v'\phi)_y\ ]\ \}\Big|_{P(0,0,0)} \qquad \text{(III-51a)}$$

and the nodal values without superscript denote those values evaluated at n^{th} time step, while ϕ_P^{n-1} denotes the known nodal value of interior point at $(n-1)^{th}$ time step.

It is noted that the FA coefficients C_{NE}, C_{NW} etc. and the parameter C_p/h^2 are functions of Ah, Bk and the ratio h/k only. For local element of uniform grid sizes

($h_E = h_W = h_N = h_S = h$), they will depend on Ah and Bh only. And the parameter Rh^2/τ, in this case, is often used to determine the optimal time step τ.

In the limiting case $Rh^2/\tau \to 0$, the steady state solution (III-48) is recovered. The same steady state solution can also be obtained by equating $\phi_P^n = \phi_P^{n-1}$ in eq(III-51).

The derivatives of ϕ, i.e., ϕ_x and ϕ_y, may be obtained analytically by differentiating the local analytic solution directly [5,6], or by a simple formula described below.

Assume an analytic function along the x-axis

$$\phi(x,0) = a_0(e^{2Ax}-1) + b_0x + c_0$$

which passing through 3 nodal points WC, P and EC in the local element (see Fig. 4), so that

$$a_0 = \frac{\phi_{EC} + \phi_{WC} - 2\phi_P}{4\sinh^2 Ah}$$

$$b_0 = \frac{1}{2h}[\phi_{EC} - \phi_{WC} - \coth Ah(\phi_{EC} + \phi_{WC} - 2\phi_P)]$$

$$c_0 = \phi_P$$

then the derivative at any point along the x-axis can be easily obtained

$$\phi_x(x,0) = 2Aa_0e^{2Ax} + b_0 \qquad \text{(III-52)}$$

Evaluating eq(III-52) at $x = 0$, then the derivative of ϕ with respect to x at nodal point P will be

$$\phi_x\Big|_P = \frac{\phi_{EC} - \phi_{WC}}{2h} + \frac{Ah - \sinh Ah \cosh Ah}{2h \sinh^2 Ah}(\phi_{EC} + \phi_{WC} - 2\phi_P) \qquad \text{(III-52a)}$$

Derivative of ϕ with respect to y at point P can also be derived in a similar way. It can be seen that eq(III-52a) provides a gradual shift from central difference at the pure diffusion case ($Ah = 0$) to upward difference at convection dominant cases ($|Ah| >> 1$). Furthermore, the derivatives at points WC, EC etc. can also be obtained from eq(III-52) whenever needed.

III-2-3 Finite Analytic Formulation of Unsteady 2D Convective Transport Equation for Nonuniform Grid Spacing Local Element with Exponontial and Linear Boundary Approximation

In previous formulation, the local analytic solution for the nominally linear two-dimensional convective transport equation (III-34) is derived in terms of the 8 boundary nodes which are equally spaced on the boundary of the rectangular local element with grid spacing h and k respectively. A finite analytic discretization equation is then obtained by evaluating the local analytic solution at the center of the local element. The resulting FA formulas (III-49) - (III-51) are applicable to fluid flow

or heat transfer problems with uniform rectangular or square elements over the whole domain of calculation. Although a freedom of employing different uniform grid spacing in x and y direction is offered, it may still be impractical for problems where extremely fine grids are needed in a small portion of domain of calculation only. For this kind of problems, the use of nonuniform grid spacing in a local element as that shown in Fig. 3 or Fig. 4(b) is often desirable, since it enables us to obtain physically meaningful solutions more effectively.

By using the same exponential and linear boundary function (III-45a) - (III-45d), but expressed in terms of the unequally spaced nodal values, a finite analytic solution for nonuniform grid spacing local element may also be obtained by the method of separation of variables as that outlined in Sec. B-2 of Appendix B. However, the derivations are much more complicated than those for uniform rectangular local elements, and the computational time required for numerical calculations of FA coefficients will increase significantly. This additional complexity may totally offset the advantages gained by using the nonuniform grid local element. Thus, in present study, instead of using this general formulation, a simple interpolation formula utilizing the local analytic solution (III-50) or (III-51) for uniform rectangular

element is employed to derive the finite analytic algebraic equation for local element of nonuniform grid spacing.

Consider the case $h_E < h_W$ and $h_N < h_S$ shown in Fig. 4(b) as an example. A smaller rectangular element of width $2h_E$, height $2h_N$ and with the interior point P located at the center is drawn as shown. The FA formula (III-49) derived previously for ϕ_P can then be written in terms of nodal values ϕ^*_{NW}, ϕ^*_{WC} etc. on smaller rectangular element as follows

$$\phi_P = C_{NE}\phi_{NE} + C_{NW}\phi^*_{NW} + C_{SE}\phi^*_{SE} + C_{SW}\phi^*_{SW} + C_{EC}\phi_{EC} + C_{WC}\phi^*_{WC} + C_{NC}\phi_{NC} + C_{SC}\phi^*_{SC} - C_P g \qquad \text{(III-53)}$$

where the FA coefficients C_{NE}, C_{NW} etc. are defined previously in eq(III-49) with grid sizes $h = h_E$ and $k = h_N$.

If suitable interpolation functions are employed to approximate the unknown nodal values ϕ^*_{NW}, ϕ^*_{SE} etc. in terms of the known values ϕ_{NW}, ϕ_{SE} etc. at 9 nodes which are unequally spaced on the larger element, a FA formula for nonuniform grid spacing local element can then be obtained by substituting the interpolated nodal values ϕ^*_{NW}, ϕ^*_{SE} etc. into eq(III-53).

Although there are several interpolation functions may be used to approximate the nodal values ϕ^*_{NW}, ϕ^*_{WC} etc. the same exponential and linear boundary function (III-45a) - (III-45d) is employed as the interpolation function to

obtain the unknown nodal values on smaller rectangular element, so that the error introduced by interpolation will be minimized. For example, the north boundary condition can be approximated by the boundary function

$$\phi_N(x) = a_N(e^{2Ax}-1) + b_N x + c_N \qquad \text{(III-54)}$$

where

$$a_N = \frac{h_W\phi_{NE} + h_E\phi_{NW} - (h_E+h_W)\phi_{NC}}{h_W(e^{2Ah_E}-1) + h_E(e^{-2Ah_W}-1)}$$

$$b_N = \frac{(e^{-2Ah_W}-1)(\phi_{NE}-\phi_{NC}) - (e^{2Ah_E}-1)(\phi_{NW}-\phi_{NC})}{h_W(e^{2Ah_E}-1) + h_E(e^{-2Ah_W}-1)}$$

$$c_N = \phi_{NC}$$

in terms of the unequally spaced nodal values ϕ_{NE}, ϕ_{NC} and ϕ_{NW} on north boundary.

The interpolated nodal value ϕ^*_{NW} can then be obtained by simply evaluating the boundary function (III-54) at $x = -h_E$, which gives

$$\phi^*_{NW} = (s-1)\phi_{NE} + \bar{s}\phi_{NW} + (2-s-\bar{s})\phi_{NC} \qquad \text{(III-55)}$$

where

$$s = \frac{h_W(e^{2Ah_E} + e^{-2Ah_E} - 2)}{h_W(e^{2Ah_E}-1) + h_E(e^{-2Ah_W}-1)}, \qquad \bar{s} = s\,\frac{h_E}{h_W}$$

Similar exponential and linear boundary functions can also be employed to obtain other nodal values ϕ^*_{WC}, ϕ^*_{SC}, ϕ^*_{SE} and ϕ^*_{SW} as those shown in (B-33b) - (B-33e) of Appendix B. By substituting interpolated nodal values ϕ^*_{NW}, ϕ^*_{WC} etc. into eq(III-53), a 9-point FA formula for local element of nonuniform grid spacing is obtained.

$$\phi_P = \frac{1}{G}\left(b_{NE}\phi_{NE} + b_{NW}\phi_{NW} + b_{SE}\phi_{SE} + b_{SW}\phi_{SW} + b_{EC}\phi_{EC} + b_{WC}\phi_{WC} + b_{NC}\phi_{NC} + b_{SC}\phi_{SC} - b_P g\right) \qquad \text{(III-56)}$$

where

$$G = 1 - (2-s-\bar{s})C_{WC} - (2-t-\bar{t})C_{SC} - (2-s-\bar{s})(2-t-\bar{t})C_{SW}$$

$$b_{NE} = C_{NE} + (s-1)C_{NW} + (t-1)C_{SE} + (s-1)(t-1)C_{SW}$$

$$b_{NW} = \bar{s}C_{NW} + \bar{s}(t-1)C_{SW}$$

$$b_{SE} = \bar{t}C_{SE} + \bar{t}(s-1)C_{SW}$$

$$b_{SW} = \bar{s}\bar{t}C_{SW}$$

$$b_{EC} = C_{EC} + (s-1)C_{WC} + (2-t-\bar{t})C_{SE} + (s-1)(2-t-\bar{t})C_{SW}$$

$$b_{WC} = \bar{s}C_{WC} + \bar{s}(2-t-\bar{t})C_{SW}$$

$$b_{NC} = C_{NC} + (t-1)C_{SC} + (2-s-\bar{s})C_{NW} + (t-1)(2-s-\bar{s})C_{SW}$$

$$b_{SC} = \bar{t}C_{SC} + \bar{t}(2-s-\bar{s})C_{SW}$$

$$b_P = C_P$$

and

$$t = \frac{h_S(e^{2Bh_N} + e^{-2Bh_N} - 2)}{h_S(e^{2Bh_N} - 1) + h_N(e^{-2Bh_S} - 1)}, \qquad \bar{t} = t\,\frac{h_N}{h_S}$$

For the unsteady two-dimensional convective transport equation with nonzero source function, a 10-point FA formula similar to eq(III-51) can also be obtained for the nonuniform grid spacing local element considered.

$$\phi_P = \frac{1}{G + \frac{R}{\tau} b_P} (b_{NE}\phi_{NE} + b_{NW}\phi_{NW} + b_{SE}\phi_{SE} + b_{SW}\phi_{SW} + b_{EC}\phi_{EC} + b_{WC}\phi_{WC} + b_{NC}\phi_{NC} + b_{SC}\phi_{SC} + \frac{R}{\tau} b_P \phi_P^{n-1} - b_P f_P) \qquad \text{(III-57)}$$

Where the nodal values without superscript denote those values evaluated at n^{th} time step, while ϕ_P^{n-1} denotes the nodal value of interior point P at $(n-1)^{th}$ time step.

For the cases $h_E > h_W$ and/or $h_N > h_S$, the finite analytic algebraic equation (III-57) can still be applied by simply reversing the flow direction and renaming the nodal points. It can be carried out easily through the change of signs and indices in numerical calculation. Details are given in the subroutine COEFF2 of Appendix D.

III-2-4 Finite Analytic Formulation of Unsteady 2D Convective Transport Equation for Uniform Grid Spacing Local Element with Piecewise-linear Boundary Approximation

Another possible boundary approximation which may give all-positive FA coefficients is the piecewise-linear boundary function mentioned in Section III-2-2. Thus, instead of using the exponential and linear boundary function (III-45a), one may approximate the boundary condition on the north boundary by a piecewise-linear profile as

$$\tilde{\phi}_N(x) = \begin{cases} \tilde{\phi}_{NC} + (\tilde{\phi}_{NE} - \tilde{\phi}_{NC}) \frac{x}{h} & , \quad 0 < x < h \\ \tilde{\phi}_{NC} - (\tilde{\phi}_{NW} - \tilde{\phi}_{NC}) \frac{x}{h} & , \quad -h < x < 0 \end{cases} \tag{III-58}$$

and $\tilde{\phi}_S(x)$, $\tilde{\phi}_E(y)$ and $\tilde{\phi}_W(y)$ can be similarly formulated.

The linearized homogeneous convective transport equation (III-44) with piecewise-linear boundary conditions $\tilde{\phi}_N(x)$, $\tilde{\phi}_S(x)$, $\tilde{\phi}_E(y)$ and $\tilde{\phi}_W(y)$ is then solved by the method of separation of variables. A finite analytic algebraic equation can then be obtained by evaluating the local analytic solution at the interior point P of the local element. i.e.,

$$\tilde{\phi}_P = C_{NE}\tilde{\phi}_{NE} + C_{NW}\tilde{\phi}_{NW} + C_{SE}\tilde{\phi}_{SE} + C_{SW}\tilde{\phi}_{SW} + C_{EC}\tilde{\phi}_{EC} + C_{WC}\tilde{\phi}_{WC} + C_{NC}\tilde{\phi}_{NC} + C_{SC}\tilde{\phi}_{SC} \tag{III-59}$$

where

$$C_{NE} = \frac{1}{2}\left(e^{-Bk}F_2 + e^{-Ah}F_2'\right) + e^{-Ah-Bk}[E^* + (Ah)E_2 + (Bk)E_2']$$

$$C_{NW} = \frac{1}{2}\left(e^{-Bk}F_2 + e^{Ah}F_2'\right) + e^{Ah-Bk}[E^* - (Ah)E_2 + (Bk)E_2']$$

$$C_{SE} = \frac{1}{2}\left(e^{Bk}F_2 + e^{-Ah}F_2'\right) + e^{-Ah+Bk}[E^* + (Ah)E_2 - (Bk)E_2']$$

$$C_{SW} = \frac{1}{2}\left(e^{Bk}F_2 + e^{Ah}F_2'\right) + e^{Ah+Bk}[E^* - (Ah)E_2 - (Bk)E_2']$$

$$C_{EC} = e^{-Ah}(2Bk\ \sinh Bk\ E_2' - F_2')$$

$$C_{WC} = e^{Ah}(2Bk\ \sinh Bk\ E_2' - F_2')$$

$$C_{NC} = e^{-Bk}(2Ah\ \sinh Ah\ E_2 - F_2)$$

$$C_{SC} = e^{Bk}(2Ah\ \sinh Ah\ E_2 - F_2)$$

and

$$E^* = \frac{1}{2}(E_1 + E_1') = \frac{1}{4\cosh Ah\ \cosh Bk}$$

$$F_2 = \sum_{m=1}^{\infty} \frac{(Ah)^2 - (\lambda_m h)^2}{[(Ah)^2+(\lambda_m h)^2]^2\ \cosh \mu_m k}$$

with $\lambda_m h = (m - \frac{1}{2})\pi$, $\mu_m = \sqrt{A^2+B^2+\lambda_m^2}$

$$F_2' = \sum_{m=1}^{\infty} \frac{(Bk)^2 - (\lambda_m' k)^2}{[(Bk)^2+(\lambda_m' k)^2]^2\ \cosh \mu_m' h}$$

with $\lambda_m' k = (m - \frac{1}{2})\pi$, $\mu_m' = \sqrt{A^2+B^2+\lambda_m'^2}$

And E_1 ,E_1', E_2 and E_2' are the same series summations as those given in eq(III-48) and Sec. B-1.

When unsteady two-dimensional convective transport equation is considered, a 10-point FA formula exactly the same as eq(III-51) and (III-51a) will be obtained except that the FA coefficients in eq(III-47) are replaced by those defined in eq(III-59).

III-3 Finite Analytic Solutions for Unsteady Three-Dimensional Convective Transport Equations

The unsteady three-dimensional incompressible flow problem in Cartesian coordinate is governed by the equation of continuity (III-1) and Navier-Stokes equations (III-2) - (III-4) given previously. One may take the curl of the Navier-Stokes equations to eliminate the pressure term, so that three vorticity transport equations are obtained.

$$\xi_t + u\xi_x + v\xi_y + w\xi_z = \frac{1}{Re}(\xi_{xx} + \xi_{yy} + \xi_{zz}) + \xi u_x + \eta u_y + \zeta u_z \qquad \text{(III-60)}$$

$$\eta_t + u\eta_x + v\eta_y + w\eta_z = \frac{1}{Re}(\eta_{xx} + \eta_{yy} + \eta_{zz}) + \xi v_x + \eta v_y + \zeta v_z \qquad \text{(III-61)}$$

$$\zeta_t + u\zeta_x + v\zeta_y + w\zeta_z = \frac{1}{Re}(\zeta_{xx} + \zeta_{yy} + \zeta_{zz}) + \xi w_x + \eta w_y + \zeta w_z \qquad \text{(III-62)}$$

where ξ, η and ζ are the vorticity components given by

$$\xi = w_y - v_z \,, \quad \eta = u_z - w_x \,, \quad \zeta = v_x - u_y \qquad \text{(III-63)}$$

By the use of equation of continuity (III-1), eq(III-63) may also be written as

$$u_{xx} + u_{yy} + u_{zz} = \eta_z - \zeta_y \qquad \text{(III-64)}$$

$$v_{xx} + v_{yy} + v_{zz} = \zeta_x - \xi_z \qquad \text{(III-65)}$$

$$w_{xx} + w_{yy} + w_{zz} = \xi_y - \eta_x \qquad \text{(III-66)}$$

for velocity components u, v and w.

Instead of solving u, v and w in eq(III-64) - (III-66), another commonly used vorticity-based formulation did introduce a scalar potential Φ, and a vector potential $\vec{\psi} = \psi_x \vec{i} + \psi_y \vec{j} + \psi_z \vec{k}$, such that

$$\vec{V} = u \vec{i} + v \vec{j} + w \vec{k} = \nabla\Phi + \nabla\times\vec{\psi} \qquad \text{(III-67a)}$$

$$\nabla\cdot\vec{\psi} = 0 \qquad \text{(III-67b)}$$

then eq(III-64) - (III-66) may be replaced by

$$\nabla^2\Phi = 0 \qquad \text{(III-68)}$$

$$\nabla^2\psi_x = -\xi \qquad \text{(III-69)}$$

$$\nabla^2\psi_y = -\eta \qquad \text{(III-70)}$$

$$\nabla^2\psi_z = -\zeta \qquad \text{(III-71)}$$

Either in primitive variable (u,v,w,p) or in vorticity-based (ξ,η,ζ,u,v,w or $\xi,\eta,\zeta,\Phi,\psi_x,\psi_y,\psi_z$)

formulations, a convective transport equation of the form of

$$\phi_{xx} + \phi_{yy} + \phi_{zz} = R(\phi_t + u\phi_x + v\phi_y + w\phi_z) + F \qquad \text{(III-72)}$$

is often encountered, where ϕ may represent any one of the convective transport quantities, ϕ_j, such as velocities u, v, w (R = Re), vorticities ξ, η, ζ (R = Re), scalar potential Φ (R = 0), components of vector potential ψ_x, ψ_y, ψ_z (R = 0) or temperature (R = Pe). The convective velocities u, v, w and the source function F, in general, are functions of independent variables x, y, z, t and dependent variables ϕ_j including ϕ itself. By utilizing the equation of continuity (III-1), eq(III-72) may also be written in conservative form as

$$\phi_{xx} + \phi_{yy} + \phi_{zz} = R[\phi_t + (u\phi)_x + (v\phi)_y + (w\phi)_z] + F \qquad \text{(III-73)}$$

Due to the coupling of variables, nonlinearity of governing equation and/or complex geometry and boundary conditions, the analytic solution of eq(III-72) or (III-73) may be very difficult, if not impossible, to obtain. Thus, the FA numerical method is used to formulate the discretization equation for ϕ, so that an approximate numerical solution can be obtained.

III-3-1 Method of Linearization

To implement the FA method, the flow region as shown in Fig. 1 is subdivided into a number of small elements with variable grid spacing h_E, h_W, h_N, h_S, h_T and h_B in x, y and z direction respectively, so that the difficulties of complex geometry and boundary conditions can be approximately resolved. For coupled nonlinear convective transport equations, a linearization scheme similar to that described in Section III-2-1 for two-dimensional case may be employed to obtain a nominally linear convective transport equation, so that the analytic solution can be derived in each local element.

Consider the convective transport equation of conservative form (III-73) as an example, even in a simple rectangular local element shown in Fig. 1, the analytic solution of eq(III-73) may still be difficult to obtain due to the complex nonlinearity of the equation and also the coupling of variables. In this situation, a linearization scheme outlined in Sec. III-2-1 ($u = U + u'$, $v = V + v'$, $w = W + w'$) is employed to approximate the convective transport equation as

$$\phi_{xx} + \phi_{yy} + \phi_{zz} = R(\phi_t + U\phi_x + V\phi_y + W\phi_z) + f(x,y,z,t,\phi_j) \qquad \text{(III-74)}$$

with

$$f = F(x,y,z,t,\phi_j) + R[(u'\phi)_x + (v'\phi)_y + (w'\phi)_z]$$

where U, V and W are representative constant values in the local element, for example, the velocities at the interior point P or the area-averaged velocities over the local element. And ϕ_j may be any dependent variable including ϕ itself. The source function f in eq(III-74) which includes the original source term $F(x,y,z,t,\phi_j)$ of eq(III-73) and the higher order correction term $R[(u'\phi)_x+(v'\phi)_y+(w'\phi)_z]$, is approximated by a function known either from previous time step t_{n-1} or from previous iteration in iterative steady-state formulation.

The linear convective transport equation (III-74) may be solved analytically in each local element as long as the initial and boundary conditions are properly specified. However, we would like to reduce the complexity encountered in deriving the analytic solution for eq(III-74). If a simple finite difference formula (III-33) is employed to approximate the unsteady term and the nonhomogeneous term (III-74a) is approximated by a representative constant f_p ($=f^{n-1}(x,y,z,\phi_j)\big|_p$, for example) in the local element, eq(III-73) is simplified to a linear elliptic PDE with constant inhomogeneous term

$$\phi_{xx} + \phi_{yy} + \phi_{zz} = 2A\phi_x + 2B\phi_y + 2C\phi_z + g \qquad \text{(III-75)}$$

where

$$A = \tfrac{1}{2}RU\ ,\ B = \tfrac{1}{2}RV \text{ and } C = \tfrac{1}{2}RW$$

$$g = \frac{R}{\tau}(\phi_P^n - \phi_P^{n-1}) + f_P = \text{constant}$$

And the constant A, B, C and g may differ from one element to another, so that the overall nonlinearity is approximately preserved. Furthermore, the coupling nature of variables which appears in convection coefficients A, B, C and source term g may also be preserved by solving the interlinked equations subsequently in each time step.

For convenience, a change of variable can be made to absorb the inhomogeneous term in eq(III-75)

$$\tilde{\phi} = \phi + \frac{g}{2(A^2+B^2+C^2)}(Ax+By+Cz) \qquad \text{(III-76)}$$

so that $\tilde{\phi}$ satisfies the homogeneous convective transport equation

$$\tilde{\phi}_{xx} + \tilde{\phi}_{yy} + \tilde{\phi}_{zz} = 2A\tilde{\phi}_x + 2B\tilde{\phi}_y + 2C\tilde{\phi}_z \qquad \text{(III-77)}$$

in the local element.

With the boundary conditions properly specified, the homogeneous convective transport equation (III-77) can be solved analytically by the method of separation of variables to provide the local analytic solution for each small local element. In what follows, eq(III-77) is first solved for a rectangular local element of $h_E = h_W = h$, $h_N = h_S = k$ and $h_T = h_B = l$ as shown in Fig. 6(a), and is then extended to that for the nonuniform grid spacing local element shown in Fig. 6(b).

III-3-2 Finite Analytic Formulation of Unsteady Three-Dimensional Convective Transport Equation for Uniform Grid Spacing Local Element

In the FA formulation of one- and two-dimensional problems, several boundary approximations are investigated. Among them, the exponential and linear boundary function is shown to be relatively simple and does give the correct asymptotic behavior for both diffusion and convection dominated cases. Thus, in the FA formulation of unsteady three-dimensional problems, a generalized exponential and linear boundary function will be employed to approximate all of the six boundary conditions in terms of 26 boundary nodes which are equally spaced on the local element shown in Fig. 6(a). As an example, the boundary function on the top surface can be written as

$$\tilde{\phi}_T(x,y) = a_{T1} + a_{T2}(e^{2Ax}-1)(e^{2By}-1) + a_{T3}(e^{2Ax}-1)y + a_{T4}(e^{2By}-1)x + a_{T5}(e^{2Ax}-1) + a_{T6}(e^{2By}-1) + a_{T7}x + a_{T8}y + a_{T9}xy \qquad \text{(III-78)}$$

where the coefficients a_{T1}, a_{T2} etc. are related to the nine boundary nodes on the top boundary surface and are given in eq(C-9) of Appendix C.

The boundary conditions for bottom, east, west, north

and south sides, i.e., $\tilde{\phi}_B(x,y)$, $\tilde{\phi}_E(y,z)$, $\tilde{\phi}_W(y,z)$, $\tilde{\phi}_N(x,z)$ and $\tilde{\phi}_S(x,z)$ can be similarly approximated by exponential and linear functions in terms of the nine nodal points available on each boundary.

The linearized convective transport equation (III-77) with boundary conditions $\tilde{\phi}_T(x,y)$, $\tilde{\phi}_B(x,y)$, $\tilde{\phi}_E(y,z)$, $\tilde{\phi}_W(y,z)$, $\tilde{\phi}_N(x,z)$ and $\tilde{\phi}_S(x,z)$ can be solved analytically by the method of separation of variables. A finite analytic algebraic equation is then obtained by evaluating the local analytic solution at the interior point P, which will give a 27-point FA formula

$$\tilde{\phi}_P = \sum_{1}^{26} C_{nb}\tilde{\phi}_{nb} \qquad \text{(III-79)}$$

where the subscript "nb" denotes the neighboring nodal points to interior point P, and the FA coefficients C_{nb} are given in the following

$$C_{NET} = e^{-Ah-Bk-Cl}\,P \quad , \quad C_{NWT} = e^{Ah-Bk-Cl}\,P \quad ,$$

$$C_{SET} = e^{-Ah+Bk-Cl}\,P \quad , \quad C_{SWT} = e^{Ah+Bk-Cl}\,P \quad ,$$

$$C_{NEB} = e^{-Ah-Bk+Cl}\,P \quad , \quad C_{NWB} = e^{Ah-Bk+Cl}\,P \quad ,$$

$$C_{SEB} = e^{-Ah+Bk+Cl}\,P \quad , \quad C_{SWB} = e^{Ah+Bk+Cl}\,P \quad ,$$

$$C_{NCT} = e^{-Bk-Cl}\,(QA) \quad , \quad C_{SCT} = e^{Bk-Cl}\,(QA) \quad ,$$

$$C_{NCB} = e^{-Bk+Cl}\ (QA)\ , \qquad C_{SCB} = e^{Bk+Cl}\ (QA)\ ,$$

$$C_{ECT} = e^{-Ah-Cl}\ (QB)\ , \qquad C_{WCT} = e^{Ah-Cl}\ (QB)\ ,$$

$$C_{ECB} = e^{-Ah+Cl}\ (QB)\ , \qquad C_{WCB} = e^{Ah+Cl}\ (QB)\ ,$$

$$C_{NEC} = e^{-Ah-Bk}\ (QC)\ , \qquad C_{NWC} = e^{Ah-Bk}\ (QC)\ ,$$

$$C_{SEC} = e^{-Ah+Bk}\ (QC)\ , \qquad C_{SWC} = e^{Ah+Bk}\ (QC)\ ,$$

$$C_{EC} = e^{-Ah}\ (RA)\ , \qquad C_{WC} = e^{Ah}\ (RA)\ ,$$

$$C_{NC} = e^{-Bk}\ (RB)\ , \qquad C_{SC} = e^{Bk}\ (RB)\ ,$$

$$C_{TC} = e^{-Cl}\ (RC)\ , \qquad C_{BC} = e^{Cl}\ (RC)\ ,$$

where

$$P = \frac{1}{8\,\mathrm{coshAh\ coshBk\ coshCl}} - FA - FB - FC + GA + GB + GC$$

$$QA = 2\,\mathrm{coshAh}\ (FA - GB - GC)$$

$$QB = 2\,\mathrm{coshBk}\ (FB - GA - GC)$$

$$QC = 2\,\mathrm{coshCl}\ (FC - GA - GB)$$

$$RA = 4\,\mathrm{coshBk\ coshCl}\ (GA)$$

$$RB = 4\,\mathrm{coshAh\ coshCl}\ (GB)$$

$$RC = 4\,\mathrm{coshAh\ coshBk}\ (GC)$$

and FA, FB, FC, GA, GB and GC are defined by

$$FA = 2Ah\ \mathrm{cothAh}\ (EA)$$

$$FB = 2Bk\ \mathrm{cothBk}\ (EB)$$

$$FC = 2Cl\ \mathrm{cothCl}\ (EC)$$

with

$$EA = E_{12}^{y} + E_{21}^{z}$$

$$EB = E_{21}^{x} + E_{12}^{z} = \left(\frac{h}{k}\right)^2 (EA) + \frac{1}{16\,\mathrm{coshAh\ coshBk\ coshCl}} \left[\frac{\mathrm{tanhBk}}{\mathrm{Bk}} - \left(\frac{h}{k}\right)^2 \frac{\mathrm{tanhAh}}{\mathrm{Ah}} \right]$$

$$EC = E_{12}^{x} + E_{21}^{y} = \left(\frac{h}{l}\right)^2 (EA) + \frac{1}{16\,\mathrm{coshAh\ coshBk\ coshCl}} \left[\frac{\mathrm{tanhCl}}{\mathrm{Cl}} - \left(\frac{h}{l}\right)^2 \frac{\mathrm{tanhAh}}{\mathrm{Ah}} \right]$$

and

$$GA = 4\mathrm{BkCl\ cothBk\ cothCl}\ E_{22}^{x}$$

$$GB = 4\mathrm{AhCl\ cothAh\ cothCl}\ E_{22}^{y}$$

$$GC = 4\mathrm{AhBk\ cothAh\ cothBk}\ E_{22}^{z}$$

where E_{ij}^{x}, E_{ij}^{y} and E_{ij}^{z} are double series summations of the form of

$$E_{ij}^{x} = \sum_{q=1}^{\infty} \sum_{r=1}^{\infty} \frac{(-1)^{q+r}(\mu_q k)(\delta_r l)}{2[(Bk)^2+(\mu_q k)^2]^i[(Cl)^2+(\delta_r l)^2]^j \cosh\gamma_{qr} h}$$

$$E_{ij}^{y} = \sum_{p=1}^{\infty} \sum_{r=1}^{\infty} \frac{(-1)^{p+r}(\lambda_p h)(\delta_r l)}{2[(Cl)^2+(\delta_r l)^2]^i[(Ah)^2+(\lambda_p h)^2]^j \cosh\gamma_{pr} k}$$

$$E_{ij}^{z} = \sum_{p=1}^{\infty} \sum_{q=1}^{\infty} \frac{(-1)^{p+q}(\lambda_p h)(\mu_q k)}{2[(Ah)^2+(\lambda_p h)^2]^i[(Bk)^2+(\mu_q k)^2]^j \cosh\gamma_{pq} l}$$

$$i, j = 1, 2.$$

$$\lambda_p h = (p - \tfrac{1}{2})\pi \quad , \quad \mu_q k = (q - \tfrac{1}{2})\pi \quad , \quad \delta_r l = (r - \tfrac{1}{2})\pi$$

$$\gamma_{pr} = \sqrt{A^2+B^2+C^2+\lambda_p^2+\delta_r^2}$$

$$\gamma_{qr} = \sqrt{A^2+B^2+C^2+\mu_q^2+\delta_r^2}$$

$$\gamma_{pq} = \sqrt{A^2+B^2+C^2+\lambda_p^2+\mu_q^2}$$

Details of the derivations are given in Sec. C-1 of Appendix C. Numerical results of FA coefficients for some typical cases will be given in Chapter IV.

The local analytic ϕ_p of unsteady nonhomogeneous convective transport equation (III-75) can be obtained by substituting eq(III-76) into eq(III-79) at 27 nodal points

$$\phi_P = \tilde{\phi}_P = \sum_1^{26} C_{nb} \left[\phi_{nb} + \frac{g}{2(A^2+B^2+C^2)} (Ax_{nb} + By_{nb} + Cz_{nb}) \right] \qquad \text{(III-80)}$$

where (x_{nb}, y_{nb}, z_{nb}) is the position of each neighboring nodal point at Cartesian coordinate, and g may including the unsteady term, source function and the higher order correction term used to compensate the assumption of constant convective velocities for local element.

By substituting g of eq(III-75b) into eq(III-80), a 28-point FA formula of unsteady three-dimensional convective transport equation can be obtained for the local element of uniform grid spacing as follows

$$\phi_P = \frac{1}{1+\frac{R}{\tau}C_P}\left(\sum_1^{26} C_{nb}\phi_{nb} + \frac{R}{\tau}C_P\,\phi_P^{n-1} - C_P f_P\right) \quad \text{(III-81)}$$

where

$$C_P = -\sum_1^{26}\frac{(Ax_{nb}+By_{nb}+Cz_{nb})\,C_{nb}}{2(A^2+B^2+C^2)} \quad \text{(III-82a)}$$

$$= \frac{1}{2(A^2+B^2+C^2)}\{Ah\ \tanh Ah + Bk\ \tanh Bk + Cl\ \tanh Cl -$$

$$16\cosh Ah\ \cosh Bk\ \cosh Cl\,[(Ah)^2(EA) + (Bk)^2(EB) +$$

$$(Cl)^2(EC)\} \quad \text{(III-82b)}$$

$$f_P = \{F(x,y,z,t,\phi_j) + R[(u'\phi)_x + (v'\phi)_y + (w'\phi)_z]\}\Big|_P$$

and the nodal values without superscript denote those values evaluated at n^{th} time step, while ϕ_P^{n-1} and f_P are nodal value and source function (including the higher order correction term) of interior point P evaluated at $(n-1)^{th}$ time step.

In the limiting case $Rh^2/\tau \to 0$, the steady-state solution, i.e., eq(III-80) with $g=f_P$ will be recovered It can also be written as

$$\phi_P = \sum_1^{26} C_{nb}\phi_{nb} - C_P f_P \quad \text{(III-83)}$$

The same steady-state solution can also be obtained by equating $\phi_P^{n-1} = \phi_P^n$ in eq(III-81).

III-3-3 Finite Analytic Formulation of Unsteady Three-Dimensional Convective Transport Equation for Nonuniform Grid Spacing Local Element

In many engineering applications, the use of nonuniform grid spacing local element is often desirable because inevitablly fine grids or nonuniform grid spacing are needed in some region of the domain of calculation to capture the physical phenomenon or to save computational time. Thus, a local analytic solution for the local element of nonuniform grid spacing h_E, h_W, h_N, h_S, h_T and h_B as shown in Fig. 1 is derived in this section, so that one may obtain physically meaningful solutions with minimum computation.

Consider the case $h_E < h_W$, $h_N < h_S$ and $h_T < h_B$ shown in Fig. 6(b) as an example. Following the idea described in Section III-2-3, one may apply the FA formula (III-81) to a smaller uniform grid spacing rectangular element of width $2h_E$, depth $2h_N$ and height $2h_T$ as shown in Fig. 6(b) as follows

$$\phi_P = \phi_P^* = \frac{1}{1 + \frac{R}{\tau} C_P} \left(\sum_1^{26} C_{nb} \phi_{nb}^* + \frac{R}{\tau} C_P \phi_P^{n-1} - C_P f_P \right) \tag{III-84}$$

where the unknown nodal values ϕ_{nb}^* on the boundaries of the smaller rectangular element may be approximated by

simple interpolation formula in terms of the known nodal values ϕ_{nb} on the larger nonuniform grid spacing local element. In this formulation, the same exponential and linear interpolation function given in previous section III-2-3 will be employed to obtain the interpolated nodal values ϕ^{*}_{nb}, so that the error introduced by interpolation will be minimized. For example, the unknown nodal value ϕ^{*}_{NWT} may be approximated by exponential and linear boundary function in terms of ϕ_{NWT}, ϕ_{NCT} and ϕ_{NET} on the boundary of larger nonuniform grid local element.

$$\phi^{*}_{NWT} = (s-1)\phi_{NET} + \bar{s}\phi_{NWT} + (2-s-\bar{s})\phi_{NCT} \qquad \text{(III-85)}$$

where

$$s = \frac{h_W(e^{2Ah_E} + e^{-2Ah_E} - 2)}{h_W(e^{2Ah_E} - 1) + h_E(e^{-2Ah_W} - 1)}, \quad \bar{s} = s\frac{h_E}{h_W} \qquad \text{(III-85a)}$$

Similar exponential and linear interpolation formulas can also be employed to obtain other interpolated nodal values as those shown in eq(C-35) of Appendix C, while $\phi^{*}_{nb} = \phi_{nb}$ at nodal points NET, NEC, ECT, EC, NCT, NC and TC are encountered. By substituting these interpolated nodal values into eq(III-84), a 28-point FA formula for unsteady three-dimensional convective transport equation can be obtained in the local element of nonuniform grid spacing h_E, h_W, h_N, h_S, h_T and h_B as follows

$$\phi_P = \frac{1}{G + \frac{R}{\tau} b_P} \left(\sum_{1}^{26} b_{nb}\phi_{nb} + \frac{R}{\tau} b_P \phi_P^{n-1} - b_P f_P \right) \quad \text{(III-86)}$$

where

$$G = 1 - (2-s-\bar{s})C_{WC} - (2-t-\bar{t})C_{SC} - (2-r-\bar{r})C_{BC} - (2-s-\bar{s})(2-t-\bar{t})C_{SWC} - (2-s-\bar{s})(2-r-\bar{r})C_{WCB} - (2-t-\bar{t})(2-r-\bar{r})C_{SCB} - (2-s-\bar{s})(2-t-\bar{t})(2-r-\bar{r})C_{SWB}$$

$$b_{NET} = C_{NET} + (s-1)C_{NWT} + (t-1)C_{SET} + (r-1)C_{NEB} + (s-1)(t-1)C_{SWT} + (t-1)(r-1)C_{SEB} + (s-1)(r-1)* C_{NWB} + (s-1)(t-1)(r-1)C_{SWB}$$

$$b_{ECT} = C_{ECT} + (s-1)C_{WCT} + (2-t-\bar{t})C_{SET} + (r-1)C_{ECB} + (s-1)(r-1)C_{WCB} + (2-t-\bar{t})(r-1)C_{SEB} + (s-1)(2-t-\bar{t})C_{SWT} + (s-1)(2-t-\bar{t})(r-1)C_{SWB}$$

$$b_{NCT} = C_{NCT} + (2-s-\bar{s})C_{NWT} + (t-1)C_{SCT} + (r-1)C_{NCB} + (2-s-\bar{s})(t-1)C_{SWT} + (2-s-\bar{s})(r-1)C_{NWB} + (t-1)(r-1)C_{SCB} + (2-s-\bar{s})(t-1)(r-1)C_{SWB}$$

$$b_{NEC} = C_{NEC} + (s-1)C_{NWC} + (t-1)C_{SEC} + (2-r-\bar{r})C_{NEB} + (s-1)(t-1)C_{SWC} + (s-1)(2-r-\bar{r})C_{NWB} + (t-1)(2-r-\bar{r})C_{SEB} + (s-1)(t-1)(2-r-\bar{r})C_{SWB}$$

$$b_{EC} = C_{EC} + (s-1)C_{WC} + (2-t-\bar{t})C_{SEC} + (2-r-\bar{r})C_{ECB} + (s-1)(2-t-\bar{t})C_{SWC} + (s-1)(2-r-\bar{r})C_{WCB} + (2-t-\bar{t})*$$

$$(2-r-\bar{r})C_{SEB} + (s-1)(2-t-\bar{t})(2-r-\bar{r})C_{SWB}$$

$$b_{NC} = C_{NC} + (t-1)C_{SC} + (2-s-\bar{s})C_{NWC} + (2-r-\bar{r})C_{NCB} +$$

$$(2-s-\bar{s})(t-1)C_{SWC} + (t-1)(2-r-\bar{r})C_{SCB} + (2-s-\bar{s})(2-$$

$$r-\bar{r})C_{NWB} + (2-s-\bar{s})(t-1)(2-r-\bar{r})C_{SWB}$$

$$b_{TC} = C_{TC} + (r-1)C_{BC} + (2-s-\bar{s})C_{WCT} + (2-t-\bar{t})C_{SCT} +$$

$$(2-s-\bar{s})(r-1)C_{WCB} + (2-t-\bar{t})(r-1)C_{SCB} + (2-s-\bar{s})(2-$$

$$t-\bar{t})C_{SWT} + (2-s-\bar{s})(2-t-\bar{t})(r-1)C_{SWB}$$

$$b_{NWT} = \bar{s}\,[\,C_{NWT} + (t-1)C_{SWT} + (r-1)C_{NWB} + (t-1)(r-1)*$$

$$C_{SWB}\,]$$

$$b_{NWC} = \bar{s}\,[\,C_{NWC} + (t-1)C_{SWC} + (2-r-\bar{r})C_{NWB} + (t-1)(2-r-\bar{r})$$

$$C_{SWB}\,]$$

$$b_{WCT} = \bar{s}\,[\,C_{WCT} + (2-t-\bar{t})C_{SWT} + (r-1)C_{WCB} + (2-t-\bar{t})(r-1)$$

$$C_{SWB}\,]$$

$$b_{WC} = \bar{s}\,[\,C_{WC} + (2-t-\bar{t})C_{SWC} + (2-r-\bar{r})C_{WCB} + (2-t-\bar{t})(2-$$

$$r-\bar{r})C_{SWB}\,]$$

$$b_{SET} = \bar{t}\,[\,C_{SET} + (s-1)C_{SWT} + (r-1)C_{SEB} + (s-1)(r-1)*$$

$$C_{SWB}\,]$$

$$b_{SEC} = \bar{t}\,[\,C_{SEC} + (s-1)C_{SWC} + (2-r-\bar{r})C_{SEB} + (s-1)(2-r-\bar{r})$$

$$C_{SWB}\,]$$

$$b_{SCT} = \bar{t}\,[\,C_{SCT} + (2-s-\bar{s})C_{SWT} + (r-1)C_{SCB} + (2-s-\bar{s})(r-1)C_{SWB}]$$

$$b_{SC} = \bar{t}\,[\,C_{SC} + (2-s-\bar{s})C_{SWC} + (2-r-\bar{r})C_{SCB} + (2-s-\bar{s})(2-r-\bar{r})C_{SWB}]$$

$$b_{NEB} = \bar{r}\,[\,C_{NEB} + (s-1)C_{NWB} + (t-1)C_{SEB} + (s-1)(t-1)^{*} C_{SWB}]$$

$$b_{ECB} = \bar{r}\,[\,C_{ECB} + (s-1)C_{WCB} + (2-t-\bar{t})C_{SEB} + (s-1)(2-t-\bar{t})C_{SWB}]$$

$$b_{NCB} = \bar{r}\,[\,C_{NCB} + (2-s-\bar{s})C_{NWB} + (t-1)C_{SCB} + (2-s-\bar{s})(t-1)C_{SWB}]$$

$$b_{BC} = \bar{r}\,[\,C_{BC} + (2-s-\bar{s})C_{WCB} + (2-t-\bar{t})C_{SCB} + (2-s-\bar{s})(2-t-\bar{t})C_{SWB}]$$

$$b_{SEB} = \bar{t}\bar{r}\,[\,C_{SEB} + (s-1)C_{SWB}]$$

$$b_{SCB} = \bar{t}\bar{r}\,[\,C_{SCB} + (2-s-\bar{s})C_{SWB}]$$

$$b_{NWB} = \bar{s}\bar{r}\,[\,C_{NWB} + (t-1)C_{SWB}]$$

$$b_{WCB} = \bar{s}\bar{r}\,[\,C_{WCB} + (2-t-\bar{t})C_{SWB}]$$

$$b_{SWT} = \bar{s}\bar{t}\,[\,C_{SWT} + (r-1)C_{SWB}]$$

$$b_{SWC} = \bar{s}\bar{t}\,[\,C_{SWC} + (2-r-\bar{r})C_{SWB}]$$

$$b_{SWB} = \bar{s}\bar{t}\bar{r}\,C_{SWB}$$

$$b_{P} = C_{P}$$

where s and $\bar{s}$ are defined in eq(III-85a), and t, $\bar{t}$, r and $\bar{r}$ are similarly defined as

$$t = \frac{h_S(e^{2Bh_N} + e^{-2Bh_N} - 2)}{h_S(e^{2Bh_N} - 1) + h_N(e^{-2Bh_S} - 1)}, \qquad \bar{t} = t\,\frac{h_N}{h_S}$$

$$r = \frac{h_B(e^{2Ch_T} + e^{-2Ch_T} - 2)}{h_B(e^{2Ch_T} - 1) + h_T(e^{2Ch_B} - 1)}, \qquad \bar{r} = r\,\frac{h_T}{h_B}$$

The coefficients C_{nb} are given in eq(III-79) with $h = h_E$, $k = h_N$ and $l = h_T$. For the cases $h_E > h_W$, $h_N > h_S$ etc., the FA solution (III-86) can still be used by opposite the flow directions and rename the indices of neighboring nodal points. Details are given in the subroutine COEFF3 of Appendix D.

CHAPTER IV

RESULTS AND DISCUSSION OF FINITE ANALYTIC COEFFICIENTS

In Chapter III, several kinds of discretization algebraic equations for multidimensional convective transport equations were derived with different initial and boundary approximation functions in each local element considered. In general, these finite analytic solutions are functions of convective velocities (or convection coefficients A = RU/2, B = RV/2 etc.), grid sizes and time increment. In order to illustrate the functional behavior of these analytic solutions, examples of FA coefficients are given in this chapter. A comparison with the 9-point FA formula derived previously by Chen et. al. [5,6] is made for the case of steady two-dimensional convective transport equation.

IV-1 Finite Analytic Coefficients for Unsteady One-Dimensional Convective Transport Equation

In Section III-1, three sets of FA coefficients for FA solution of eq(III-7) were derived as shown in (III-13), (III-15) and (III-20) for two-time and one-time step local

elements respectively. For the two-time step local element considered, second-order polynomials were employed to approximate the initial and boundary conditions. The resulting 8-point FA formula (III-13) then relates the nodal value ϕ_{NC} to its 7 neighboring nodal values with two parameters Ah and $Bh^2/2\tau$ (or Ah and Courant number $C_0 = 2A\tau/Bh$). The 7 FA coefficients are tabulated in Table (1) and (2) for a range of Ah and Courant number, C_0, of 1. Physically, the dependent variable ϕ may be considered as a temperature variable carried by fluid moving at a constant velocity U or a cell Reynolds number of 2Ah in an element. A Courant number of 1 means that a fluid particle will travel a distance of h from WC to NC in a time interval τ. However, the temperature of the particle may not remain the same in this transport process, since , in additional to convection, the fluid particle also diffuses its energy to the surrounding fluid particles. For convection dominant cases (i.e., $|Ah| >> 1$), the diffusion effect is so small that the temperature field is practically frozen with fluid flowing at the velocity of U in a time interval of τ. The influence of strong convective motion on the dependent variable ϕ can be seen easily from Table (1) that $C_{WC} \to 1$ for $Ah \geq 10^3$. That is the upstream value of ϕ_{WC} without diffusion is carried to the node NC or $\phi_{NC} = \phi_{WC}$. On the other hand, if the diffusive transport

process is much stronger than the convective heat transport carried by fluid velocity (i.e., $Ah \to 0$), the influence from upstream and downstream should be nearly the same, since the diffusive transport is driven by the temperature difference and not by the convective velocity U. Again, this can be seen from Table (1) that $C_{NW} = C_{NE} = 0.5$ as $Ah \to 0$, or $\phi_{NC} = 0.5(\phi_{NE} + \phi_{NW})$.

In Table (2), the influence of convective velocity is studied for the case of $Bh^2/2\tau = 1$ by varying the Ah value. Physically, this is the case with given time increment τ and grid spacing h, and the parameter Ah is proportional to convective velocity U. Thus, a large value of Ah may be interpreted as a large velocity. It can be seen from Table (2) that the FA coefficients gradually shift upward when the convective transport becomes dominant. However, the negative FA coefficients although small are encountered, these negative FA soefficients may translate into locally unrealistic numerical result of overshoot as shown in Sec. III-2. Instead of second-order polynomials, an exponential and linear approximation for initial function is employed to derive a 6-point FA formula (III-15) or (III-16) in a one-time step local element. This results in all-positive FA coefficients as shown in Table (3) and (4) because the exponential and linear approximation does not overshoot the three nodal values

used for the initial condition. On the other hand, the results in Table (3) still properly exhibit an upward shift of the influence of FA coefficients on ϕ_P value. In Table (4), the influence of Courant number C_0 is investigated for a convective dominated case of Ah = 50. The FA coefficients indicate that when diffusion effect is small, the nodal value at point P is largely determined by the information from upstream boundary. Since linear boundary approximation is used along the west boundary, the weight of C_{WC} and C_{SW} should be linear also when $C_0 > 1$, because characteristic line issued from the node P intercept the west boundary. On the other hand, if $0 \leq C_0 \leq 1$, the characteristic line now intercept with the initial line, and the nodal value ϕ_P is determined by the exponential and linear initial approximation function along the south side.

In order to reduce the effort of manipulation and computational time, an alternative, hybrid FA solution (III-20) for eq(III-7) is derived in Section III-1-3, in which the time derivative is approximated by finite difference. The values of FA coefficients thus obtained are tabulated in Table (5) for comparison. For large or small Courant number C_0, there is little difference between the hybrid approach and general FA formulation (III-15) in the one-time step local element considered.

However, the discrepancy between FA coefficients for eq(III-15) and (III-20) becomes significant when the Courant number is of the order of 1. This is because when the Courant number is near one, the nodal value at point P is mainly determined by ϕ_{SW}, yet the hybrid FA solution does not take the nodal value ϕ_{SW} into account. As a consequence, a numerical diffusion is then introduced in the hybrid formulation when the nodal value ϕ_{SW} is approximated by the neighboring nodal values ϕ_{WC} and ϕ_{SC}.

From this study, one may conclude that, when the same boundary functions are used, the FA formulation using the exponential and linear initial function always gives the physically realistic results and requires less computational time. On the other hand, if the same initial function is employed, the use of two-time step element and higher order boundary functions reduces the false numerical diffusion, but the effort of manipulation and computational time increase significantly.

IV-2 Finite Analytic Coefficients for Unsteady Two-Dimensional Convective Transport Equation

In Section III-2, the 9-point FA formula derived by Chen et. al. [5,6] for steady two-dimensional homogeneous vorticity transport equation was first improved by using exponential and linear boundary approximation instead of

the second-order polynomial originally proposed. A 10-point FA formula (III-57) for unsteady two-dimensional convective transport equation in a nonuniform grid spacing local element is then derived while the best available boundary approximation is employed. The FA coefficients thus derived for nonuniform grid spacing element are, in general, functions of A, B, R, h_E, h_W, h_N, h_S and τ. If a local element of uniform grid spacing, $h_E = h_W = h_N = h_S = h$, is considered, the FA coefficients become functions of Ah, Bh and Rh^2/τ only. In this section, the effect of three different boundary approximations, namely, second-order polynomial (FASP), exponential and linear (FAEL) and piecewise-linear (FAPL) boundary approximations, on FA coefficients is investigated at first for the steady two-dimensional convective transport equation (III-35) on a local element of uniform grid spacing. Several examples are then given to show the functional dependence of FA coefficients on convective velocities (or A and B), grid sizes h and k , and also the time increment τ. After that, a brief comparison with some 9-point formulas derived from finite difference or finite element formulations will be made. Thereafter, the FA formula is employed to solve some practical test problems.

(A) Comparison of FA coefficients for Laplace Equation

($A=B=0$, $h_E = h_W = h_N = h_S = h$)

Table (6) shows a comparison of FA coefficients for FASP, FAEL and FAPL formulations when $Ah = Bh = 0$ is considered for an element of equal grid spacing. One observes that the FAEL and FASP formulations give the same values since the second-order polynomial boundary profile is recovered in FAEL formulation when A and B approach zero. The resulting FA coefficients are close to the fourth-order accurate Greenspan formula [17]. (i.e., $C_{EC} = C_{WC} = C_{NC} = C_{SC} = 0.2$, $C_{NE} = C_{NW} = C_{SE} = C_{SW} = 0.05$). On the other hand, the FAPL formulation apparently overestimates the diffusion influence at four corner points due to the less accurate piecewise-linear boundary approximation used.

(B) Comparison of FA coefficients for steady 2D convective transport equation ($h_E = h_W = h_N = h_S = h$)

In Table (7), (8) and (9), three different convection dominated cases of (i) $Ah = Bh = 5$, (ii) $Ah = 50$, $Bh = 0$ and (iii) $Ah = 50$, $Bh = 25$ are considered in a local element of equal grid spacing. It can be seen that all three FA formulations exhibit a gradual upwind shift when the convective velocities becomes large. The FAEL and FAPL formulations give all-positive FA coefficients for all range of convective velocities , while negative FA coefficients are encountered in FASP formulation if

either Ah or Bh becomes large. These negative FA coefficients although small are physically unrealistic [11]. On the other hand, the FAPL formulation still overestimates the diffusion effect at the corner points NW and SW in Case (ii). As mentioned earlier, this false numerical diffusion is caused by the less accurate piecewise-linear boundary approximation although the physical diffusion should be much smaller. From the comparisons made above, one may conclude that the finite analytic solution derived from the exponential and linear boundary approximation is the most accurate one among the three FA solutions considered. Furthermore, FAEL formulation needs only one series summation term in the numerical calculation of FA coefficients (see Appendix B), while three summation terms are needed in FASP and FAPL formulations. When unsteady three-dimensional convective transport equation is considered (see Appendix C), the manipulation effort and computational time for FAEL formulation can thus be substantially reduced. This additional advantage makes the FAEL formulation parctical and attractive in solving unsteady three-dimensional convective transport equations which is presented in Section III-3. It is concluded that FAEL formulation is the most accurate and most economic FA formulation among the three boundary approximations considered.

Since the FAEL formulation gives the most accurate result for both diffusion and convection dominant cases, and requires least computational time among the three FA formulations, in what follows, only the FA coefficients obtained from FAEL formulation will be considered for unsteady two-dimensional convective transport equations in unequal grid spacing local elements.

In Table (10), the FA coefficients for Laplace equation are calculated in a local element of $h_E = h_W = h$ and $h_N = h_S = k$ for different aspect ratio h/k. It can be seen that when h/k becomes larger and larger, the influence from two nearest nodal points NC and SC becomes more and more significant, and a correct asymptotic behavior is obtained when $h/k \to \infty$.

Table (11) shows the FA coefficients for steady 2D convective transport equation of A = B = 20 in a local element of k = 0.1 and different aspect ratio of h/k = 1, 2, 5 and 10. The results indicate that when the aspect ratio is increased, the influence from SW decreases while the influence from the nearest upstream nodal point SC gradually increases. It should be remarked that the FA coefficients remain positive for all range of the convective velocities considered, a physically realistic solution is thus insured even if unequal grid spacing local element is considered. Such a positiveness of

coefficients must be guaranteed for any numerical method, FA, FD or FA, if a physically realistic solution is expected.

When unsteady two-dimensional convective transport equation (III-32) is considered, a 10-point FA formula (III-51) which contains the information from interior point P at previous time step is obtained. If small time increment is considered, the influence of ϕ_P^{n-1} from previous time step would be dominant as those shown in Table (12). On the other hand, the influence of ϕ_P^{n-1} becomes vanishingly small when the time increment becomes large (i.e., $Rh^2/\tau \to 0$). In fact, the influence from interior point P at previous time step may be written explicitly from eq(III-51) as

$$C_P' = \frac{\frac{R}{\tau} C_P}{1 + \frac{R}{\tau} C_P}$$

while the FA coefficients at the present time step are reduced at the same rate of $1/(1 + \frac{R}{\tau} C_P)$. Thus, the unsteady effect is equivalent to an under-relaxation factor of the magnitude of $1/(1 + \frac{R}{\tau} C_P)$ when the iterative procedure is adopted to obtain a steady-state solution. Since C_P is a function of A, B, h_E, h_W, h_N and h_S, the under-relaxation factor may vary from one element to another. It is thus expected that the solution obtained

by marching in time will perform better than that obtained by the steady-state iterative method.

Before applying the finite analytic algebraic equation (III-51) to solve any practical engineering problems, it is helpful to compare the FA coefficients with some of the 9-point formulas derived from finite difference or finite element formulations in obtaining algebraic representation of partial differential equations.

In most of the finite difference formulations, the convective term in convective transport equation is often approximated by central difference, upward difference or exponential schemes to obtain a 5-point discretization equation (i.e., interior node P and four neighboring nodes EC, WC, NC and SC) for steady two-dimensional convective transport equation (III-35). Raithby [12,18] investigated these commonly used finite difference formulas and concluded that more neighboring nodal points should be considered if the false numerical diffusion is to be reduced. A skew upstream difference scheme (SUDS) and a skew upstream weighted difference scheme (SUWDS) are then proposed [12] to brought in the corner points in the control volume formulation of convective transport equation. In the SUDS formulation, simple extrapolation formulas were used to evaluate the convective and diffusive fluxes through the control surfaces in terms of the two upstream

nodal points. However, the resulting 9-point formula does have some negative coefficients as long as nonzero convective velocities are considered. In the SUWDS formulation, an exponential and linear profile in terms of two upstream and one downstream nodal points is employed to estimate the convective and diffusive fluxes through the control surfaces, so that a 6-point formula including only one upstream corner point is resulted. The 6-point formula thus obtained is rather complicated and is not free from overshooting when applied to a simple step flow problem where the main stream coming from a skew direction. This physically unrealistic overshoot indicates that some of the coefficients are still negative. Recently, Stubley et al. [9] independently proposed a method similar to the FA method developed by Chen et al. [5,6] to obtain the discretization equation for the steady 2D convective transport equation. Instead of using the method of separation of variables, the method of Green's function is used to obtain the analytic solution by employing either second order polynomial or piecewise-linear boundary approximations. The result for second-order polynomial boundary approximation is exactly the same as FASP formulation described before, and the solution using piecewise-linear boundary approximation is also given in FAPL formulation of the present study by the method of separation of variables.

Shay [13] developed a finite difference method to approximate the convective term in vorticity transport equation in terms of the 9 nodal points in a square local element, where the 9 coefficients are chosen based on a Taylor-series expansion. With the diffusion term approximated by the usual central difference formulation, a 9-point finite difference discretization equation for steady two-dimensional vorticity transport equation is obtained. The resulting 9-point FD formula gives equal weight for four center nodes, i.e., EC, WC, NC and SC, for all range of convective velocities while the FD coefficients at four corner points NE, NW, SE and SW are always negative. Since no upward shift on four center points is exhibited and physically unrealistic negative coefficients are always encountered at corner points when convective velocities are not zero, it is expected that the solution obtained by this FA formulation will become increasing unreasonable when convective term becomes large. In fact, physically unrealistic two major eddies flow pattern were encountered even when a fine mesh of 0.0125 was used to solve a driven cavity flow problem at Reynolds numbers of 2000 and 5000.

In finite element formulation, an "upwind scheme" similar to those used in finite difference formulation was derived in [14,15] by improving the weighting function

of standard Galerkin formulation with modifying functions and a set of optimal parameters. The exact solution for one-dimensional case is recovered in this formulation when the optimal parameter is used. The same optimal parameter is then employed to derive a 9-point formula for two-dimensional convective transport equation. The 9-point FE formula thus obtained provides a gradual shift to upwind when convective terms are significant. However, large negative coefficients are often encountered in convective dominated cases. Furthermore, when pure diffusion case (A = B = 0) is considered, equal weight of 1/8 are resulted for all of the eight neighboring nodal points. Thus, physically unrealistic solutions may be resulted when applying this FE formula to multidimensional fluid flow and heat transfer problems.

All of the comparison made above are based on a square local element of equal grid spacing $h_E = h_W = h_N = h_S = h$. When unequal grid spacing are considered, the results obtained by finite difference and finite element formulations may become even more unreasonable, while the FAEL formulation still gives all-positive coefficients and correct upward shift although some numerical diffusion are encountered due to the use of interpolations. Thus, it is concluded that the FAEL formulation is by far the most accurate 9-point formula with a reasonable computational expense.

IV-3 Finite Analytic Coefficients for Unsteady Three-Dimensional Convective Transport Equation

In Section III-3, the most accurate and economic exponential and linear boundary profile is employed to derive the unsteady three-dimensional convective transport equation (III-75) in both equal and unequal grid spacing local elements. The FA coefficients (III-79) for some typical cases are shown numerically in the following to illustrate the relative importance of each coefficient, so that the physical significance of the upward shift can be more easily understood.

In order to examine the effect of convective velocities on the FA coefficients, several different convective velocities come from different directions are considered in Table (13) thru (15) for an equal grid spacing local element of $h_E = h_W = h_N = h_S = h_T = h_B = h$. For the case $A = B = C = 0$, the convective transport equation (III-75) reduces to the simple Laplace equation. In this case, the FA coefficients are symmetric to the interior point P, and the influence from eight corner points are quite small, while the influence from the center of each boundary surface is much more significant because they are much closer to the interior point P. When the convective velocity is gradually increases along the z-direction, the

influence from upstream nodal points becomes more and more profound as shown in Table (13). For example, the FA coefficient C_{BC} for the upstream node increases gradually from 0.113631 at Ch = 0 to 0.980101 at Ch = 100, while those nodal values at downstream decrease gradually to zero.

In Table (14), a resultant convective velocity comes from SCB (South, Center, Bottom) edge is considered, the influence from the upstream nodal point SCB gradually increases from 0.023943 at Bh = Ch = 0 to 0.824620 at Bh = Ch = 50. It can be seen that when the convective velocities become large, the interior nodal value ϕ_p is mainly determined by the three upstream nodal points SCB, BC and SC. If the resultant velocity is come from one of the corner point SWB as those shown in Table (15), then the influence from the four upstream nodal points SWB, SCB, WCB and SWC will increase when convective velocities become large. On the other hand, the FA coefficients for downstream nodal points become negligibly small when large convective velocities are encountered.

It can be seen from Table (14) and (15) that when the resultant velocity is not aligned with the grid lines, the 7-point formulas (i.e., EC, WC, NC, SC, TC, BC and the interior point P) which are adopted in many finite difference methods may suffer from false numerical diffusion, because the information contained at upstream

corner points is not accounted for. On the other hand, the 27-point FA formula can take care of the convective velocity from any skew direction, thus, much accurate solutions should be obtained when the 27-point FA formula is used to solve any fully elliptic fluid flow and heat transfer problems.

When unsteady three-dimensional convective transport equation (III-74) is considered, the influence from nodal value ϕ_P^{n-1} at previous time step can be written from eq(III-81) as

$$C_P' = \frac{\frac{R}{\tau} C_P}{1 + \frac{R}{\tau} C_P}$$

while the FA coefficients at the present time step are reduced at the same rate of $1/(1 + \frac{R}{\tau} C_P)$. Since C_P is a function of A, B, C, h_E, h_W, h_N, h_S, h_T and h_B, this equivalent under-relaxation factor may vary from one element to another. It is therefore expected that stable steady-state solution may be easily obtained when the unsteady approach instead of the steady-state iterative method is used.

CHAPTER V

METHODS OF NUMERICAL CALCULATIONS

In Chapter III, the finite analytic solutions for unsteady multi-dimensional convective transport equations were obtained. These FA formulas can be employed directly to solve the general convective transport equations for ϕ (e.g., temperature, vorticities, concentration etc.) in the presence of a given flow field. However, except in some extremely simple circumstances, it is not possible to specify the flow field or to solve it analytically. In general, one must calculate the velocity field numerically from appropriate governing equations. For incompressible fluid flows, the velocity components are governed by the equation of continuity and Navier-Stokes equations as equations (III-1) thru (III-4) shown in Chapter III. Although Navier-Stokes equations are complicated due to the nonlinearity and coupling of variables, they are just special cases of general convective transport equation (III-72) to describe the transport processes of momentum. As mentioned before, the problem of the nonlinearity can be resolved by employing a local linearization scheme in marching or iterative processes. And the difficulty of the

coupling in several variables may also be handled by solving sequently the system of algebraic equations for each variable one at a time. In primitive variables (u,v, w,p) formulation, the finite analytic numerical solution of the velocity field can be obtained from three momentum equations when the pressure field is made to satisfy the equation of continuity. However, the pressure-velocity coupling via equation of continuity happens to be a particular troublesome source in solving incompressible fluid flow problems for many years (see Patankar [11] and Raithby and Schneider [20]). For compressible flow problems, one may extract pressure from density via equation of state by considering the density as the dependent variable of equation of continuity. [20]. But such a compressible flow formulation is inappropriate to constant density or incompressible fluid flows. For incompressible fluid flows, the equation of continuity is reduced to a constraint of velocity field to be satisfied indirectly through the correct choice of pressure. This indirect specification of pressure field, however, is not very useful unless a direct method is employed to solve the whole set of discretization equations for momentum and continuity equations simultaneously. In order to avoid large storage and time expense associated with direct methods, several other formulations which will be discussed

later have been employed to eliminate the pressure or to convert the indirect information in equation of continuity into a direct algorithm for the calculation of pressure, so that iterative methods may be used to solve the set of discretization equations much more economically.

V-1 Vorticity-based Formulations

In order to avoid the difficulties associated with the pressure-velocity coupling for incompressible fluid flows, one may simply eliminate the pressure by taking the curl of the Navier-Stokes equations. For two-dimensional fluid flow problems, the elimination of pressure from the momentum equations (III-23) and (III-24) leads to a vorticity transport equation (III-26). Furthermore, the velocity components u and v can also be defined in terms of a streamfunction (i.e., eq(III-28)) which satisfies the equation of continuity (III-22). Thus, instead of dealing with three variables u, v and p in continuity and two momentum equations, one need to solve only two equations to obtain the vorticity and streamfunction. The velocity components u and v, which also presented as the convection coefficients of vorticity transport equation, are obtained from the definition of streamfunction (III-28). The troublesome third variable, namely pressure, can be solved afterwards.

There are, however, some disadvantages to this well-known vorticity-streamfunction formulation. Firstly, the vorticity boundary condition at the wall is not easy to specify and is often the source of difficulties such as inaccurate solution and instability. Secondly, it cannot be easily extended to solve turbulent fluid flow problems. Thirdly, the extension to three-dimensional flows where a streamfunction does not exist is rather difficult, and the complexity of this formulation becomes even greater than that of solving directly the continuity and the three momentum equations.

For three-dimensional incompressible fluid flows, the elimination of pressure from Navier-Stokes results in three vorticity transport equations (III-60) thru (III-62) for three vorticity components. A streamfunction , however, does not exist. Thus, one need to solve six equations (III-60) - (III-62) and (III-64) - (III-66) for three vorticity and three velocity components. (see Dennis et al. [21], for example). On the other hand, a scalar potential Φ in additional to three vector potential components ψ_x, ψ_y and ψ_z similar to streamfunction ψ for two-dimensional case may be introduced, so that simpler governing equations (III-68) - (III-71) can be obtained. In both formulations, the complexity is actually greater than that of solving continuity and three momentum equations for u, v, w and p

directly. Furthermore, the vorticity and vector-potential components are hard to visualize and interpret in three dimensions, while complicated vorticity boundary conditions are often encountered. Thus, a formulation using the so called primitive variables, namely, the velocity components and pressure, becomes more attractive in solving three-dimensional fluid flow and heat transfer problems.

Since the governing equation for all of the vorticity, velocity and scalar/vector potential (a streamfunction in 2D problems) components are special cases of convective transport equation described in Chapter III with R = Re or R = 0, the finite analytic solution can be employed directly to obtain the vorticity and vector-potential or velocity field in vorticity-based formulations. Consider the two-dimensional case as an example, the only nonzero vorticity and vector-potential component, i.e., ξ and ψ are governed by

$$\xi_{xx} + \xi_{yy} = Re(\xi_t + u\xi_x + v\xi_y) \qquad (V-1)$$

$$\psi_{xx} + \psi_{yy} = -\xi \qquad (V-2)$$

Application of the FA method described in Section III-2 to equations (V-1) and (V-2) leads to the finite analytic algebraic equation in a small element as shown in Fig. 7 as

$$\xi_P = \frac{1}{G + \frac{Re}{\tau} b_P} \left(\sum_1^8 b_{nb}\xi_{nb} + \frac{Re}{\tau} b_P \xi_P^{n-1} - b_P f_P \right) \quad (V-3)$$

and

$$\psi_P = \frac{1}{G'} \left(\sum_1^8 b'_{nb}\psi_{nb} + b'_P \xi_P \right) \quad (V-4)$$

where $f = Re\,[(u'\xi)_x + (v'\xi)_y]$ is the higher order correction term defined previously. b_{nb}, b_P and G are FA coefficients defined in eq(III-56) with $A = Re\,u_P/2$, $B = Re\,v_P/2$. b'_{nb}, b'_P and G' are FA coefficients defined by the same equation (III-56) but with A = B = R = 0.

The higher order correction term in eq(V-1) is approximated by a representative constant value f_P at node P in this study. For example, among other possibilities, one may approximate the higher order correction term as

$$f_P = Re\left[\frac{(u'\xi)_e - (u'\xi)_w}{0.5(\Delta x_e + \Delta x_w)} + \frac{(v'\xi)_n - (v'\xi)_s}{0.5(\Delta y_n + \Delta y_s)} \right] \quad (V-5)$$

where $u'_e = u_e - u_P$ and velocity u_e and vorticity ξ_e across the east control surface denoted by the dashed line in Fig. 7 can be obtained by suitable interpolations between nodal points P and EC. Other variables in eq(V-5) are defined in a similar way.

When the initial and boundary conditions for ξ and ψ are properly specified in the whole domain of calculation,

the numerical solution for equations (V-1) and (V-2) can be easily obtained by solving the system of algebraic equations resulted from assembly of equations (V-3) and (V-4). Details of the numerical procedures, which can be easily extended to three dimensions, are outlined in the following.

(1) Divided the domain of calculation into a suitable number of small elements.

(2) Specify the initial condition for vorticity at all grid points at $t = 0$.

(3) Calculate the FA coefficients b'_{nb}, b'_p and G' for streamfunction ψ using eq(III-56) with $R = A = B = 0$. Since these coefficients are functions of mesh sizes only, it needed to be calculated only once for all.

(4) Solve the Possion equation (V-2) for streamfunction at all field points by the 9-point FA formula (V-4). The system of algebraic equations is solved by tridiagonal algorithm (line by line method) until converged. Over-relaxation factor is often used to save the computational time.

(5) Specify the vorticity boundary conditions in terms of streamfunctions on or near the boundary.

(6) Calculate the velocity field $u = \psi_y$ and $v = -\psi_x$.

(7) Calculate the FA coefficients b_{nb}, b_p and G for vorticity using eq(III-56) with R = Re, $A_{ij} = \frac{1}{2} Re\, u_{ij}$ and $B_{ij} = \frac{1}{2} Re\, v_{ij}$ at all field points.

(8) Calculate the higher order correction term $f_{ij} = Re\,[(u'\xi)_x + (v'\xi)_y]$ at all field points using eq(V-5) whenever needed.

(9) Solve the unsteady vorticity transport equation (V-1) at all field points by the 10-point FA formula (V-3). The system of algebraic equation is solved by a tridiagonal algorithm until convergence is achieved.

(10) Stop if the steady-state criterion is achieved or the time t exceeds the maximum time period assigned.

(11) If not, return to step (4) for $(n+1)^{th}$ time step calculation.

It should be remarked here that when large time step is used, but the calculation of higher order correction term is based on the previous time step t_{n-1}, error may increase in the transient solutions although the steady state solution is unaffected. In this circumstance, one may use the updated vorticity ξ^n_{ij} at n^{th} time step to calculate the higher order correction term at each internal iteration. In other word, instead of performing internal iterations at step (9) only, one may update f_{ij} by repeating steps (6) - (9) until converged ξ^n_{ij} is obtained.

V-2 Primitive Variable Formulations

As mentioned before, the real difficulty in obtaining the velocity field in the primitive variable formulation lies in the unknown pressure field. The pressure field influences the velocity field through the pressure gradient terms in momentum equations. Yet, there is no obvious equation for solving pressure. If the velocity components u and v are thought to be governed by the two momentum equations (III-23) and (III-24), then the pressure field should be, though indirectly, specified by the equation of continuity. It should be noted that when the correct pressure gradient is used in momentum equations, the resulting velocity field from two momentum equations automatically satisfies the equation of continuity. Since there is no particular difficulty in solving momemtum equations by the FA method, the main task in using primitive variable formulation thus is to translate the equation of continuity into a direct algorithm for the calculation of pressure, so that the correct pressure field can be employed in solving the momentum equations.

In order to extract the pressure from the equation of continuity, one may derive a Possion equation for pressure by taking the divergence of Navier-Stokes equations. In two-dimensions, this leads to

$$P_{xx} + P_{yy} = 2\,(u_x v_y + u_x^2 + v_y^2) + \frac{1}{Re}\,(D_{xx} + D_{yy}) - (uD_x + vD_y) \qquad (V\text{-}6)$$

where

$$D = u_x + v_y \qquad (V\text{-}6a)$$

From equation of continuity $D = 0$, hence, equation (V-6) reduced to

$$P_{xx} + P_{yy} = 2(u_x v_y - v_x u_y) \qquad (V\text{-}7)$$

Thus, one may solve the Possion equation (V-7) and two momentum equations (III-23) and (III-24) for the variables u, v and p. However, since the velocity components u, v computed from equations (III-23) and (III-24) do not necessarily satisfy the continuity equation, erroneous pressure solution might result from solving the Possion equation (V-7). Consequently, nonlinear instability may arise in solving iteratively between the momentum equations and the pressure equation (see Roache [1], for example). Many investigators included part or all of the "mass source" term D_{ij} presented in eq(V-1) and forcing $D_{ij}^{n+1} = 0$ at $(n+1)^{th}$ time step, so that a converged solution can be achieved. However, slow convergence of the solution usually results. Recently, Singh [22] solved the continuity, momentum and Possion equation (V-7) alternatively using a momentum

dominated or momentum averaging scheme. The major disadvantage of these formulations is that iterative scheme is explicit in solving u, v and p. For 3D problems, the additional dimension makes the iterative scheme converge very slow. Thus, a method that requires explicit iteration among velocity components and pressure variables is likely to suffer slow convergence.

Chorin [23,24] proposed an iterative scheme based on Helmoholtz's decomposition theorem to resolve the pressure-velocity coupling problem encountered in two- and three-dimensional fluid flows. The Navier-Stokes equations are arranged in a suitable form such that the pressure gradient and unsteady term are respectively the irrotational and solenoidal part of a defined vector field. An auxillary velocity field obtained by omitting the pressure term in momentum equations is introduced in performing the decomposition. The pressure field is then extracted from the auxillary velocity field by requiring the equation of continuity to be satisfied at $(n+1)^{th}$ time step. Goda [25] employed a simple variant of Chorin's method to solve the two- and three-dimensional driven cavity flow problems. In his study, the same splitting fractional-step method used in Chorin [23] is employed to calculate the auxillary velocity field, but the pressure field is solved by a triple sweep iteration

technique. In both cases, complicated boundary conditions are needed to keep the numerical accuracy. Takami & Kuwahara [26] modified Chorin's method by considering the acceleration rather than the velocity field as the dependent variables, the velocity field is then obtained by integration of acceleration field with respect to time. Due to the explicit nature in time for these numerical schemes, the time increment is restricted to $\Delta t < \Delta x/|u_{max}|$ for stability consideration.

Several other methods of handling the pressure-velocity coupling problems used the velocity correction formulas and pressure correction equations to extract the pressure from the equation of continuity (Raithby et al. [20]). These methods are somewhat related to Chorin's method, but are equally applicable to steady and unsteady numerical schemes. The basic idea of these approaches is to express the velocity-correction in terms of the pressure-correction in an imperfect flow field, so that the pressure may be updated by requiring the corrected velocity field to satisfy the equation of continuity. Depending on the approximations made in updating pressure, different governing equations for pressure may be obtained. Detailed discussions and comparisons of several pressure update schemes can be found in Raithby et al. [20]. Among them, the pressure-update-Patankar (PUP) scheme combined

with Patankar-Spadling p' equation gives the best result. In PUP scheme (see also Patankar [11]), instead of updating pressure gradually from the pressure correction equation, a pseudovelocity field obtained by omitting the pressure gradient term in Navier-Stokes equations is introduced so that the pressure field can be obtained directly from a guessed velocity field. It is noted that the pseudovelocity field is somewhat similar to the auxillary velocity field used by Chorin [23] and Goda [25], however, no approximation is made in obtaining pseudovelocities, and the complicated boundary conditions for auxillary velocities are not encountered at all.

In the present study, a staggered grid for velocity components which was first introduced by Harlow & Welch [27] in their MAC method is adopted to avoid the possible unrealistic pressure and velocity fields resulted from the finite difference representation of pressure gradient term in momentum equations and also the equation of continuity [11]. Fig. 8 shows the locations of staggered grid formation for u, v and p in xy-plane. Where "•", "→" and "↑" respectively denote the node location for p, u and v. The location of w can be similarly constructed. The dashed lines represent the control volume faces, and the pressure is calculated at the center of the control volume. For convenience, with e, n, t respectively denoting

east, north and top; u_e, v_n, w_t and p_P are assigned the same index as u_{ijk}, v_{ijk}, w_{ijk} and p_{ijk} respectively. In such a staggered grid system, the 28-point FA formula for unsteady three-dimensional momentum equation (III-4) in x-direction becomes

$$u_e = \frac{1}{G^u + \frac{Re}{\tau} b_e^u} \left(\sum_1^{26} b_{nb}^u u_{nb} + \frac{Re}{\tau} b_e^u u_e^{n-1} - b_e^u (Re\, p_x + f_e^u) \right) \tag{V-8}$$

where the pressure gradient term p_x is approximated by

$$p_x = \frac{p_{EC} - p_P}{0.5(\Delta x_E + \Delta x_P)} \tag{V-8a}$$

and the higher order correction term $f_e^u = Re[(u'u)_x + (v'u)_y + (w'u)_z]\Big|_e$ is a representative constant value evaluated in a similar way as f_p in eq(V-5).

In order to resolve the pressure-velocity coupling problem described before, one may introduce a pseudovelocity field [11] for u_e, or $\hat{u}_e$, based on eq(V-8) or

$$\hat{u}_e = \frac{1}{G^u + \frac{Re}{\tau} b_e^u} \left(\sum_1^{26} b_{nb}^u u_{nb} + \frac{Re}{\tau} b_e^u u_e^{n-1} - b_e^u f_e^u \right) \tag{V-9}$$

Eq(V-9) defines the pseudovelocity and is essentially eq(V-8) without the pressure. Therefore, the discretized momentum equation (V-8) can be written as

$$u_e = \hat{u}_e - d_e(p_{EC} - p_P) \tag{V-10a}$$

where

$$d_e = \frac{Re\ b_e^u}{0.5(\Delta x_E + \Delta x_P)(G^u + \frac{Re}{\tau} b_e^u)}$$

and the FA coefficients b_{nb}^u, b_e^u and G^u are defined in eq(III-86). Similarly, the other two momentum equations in y and z directions can be written as

$$v_n = \hat{v}_n - d_n(p_{NC} - p_P) \tag{V-10b}$$

$$w_t = \hat{w}_t - d_t(p_{TC} - p_P) \tag{V-10c}$$

where $\hat{v}_n$, $\hat{w}_t$, d_n and d_t are defined in a similar way as $\hat{u}_e$ and d_e.

The momentum equations (V-10a) thru (V-10c) can be solved for u, v and w as long as the pressure field is somewhat estimated. However, unless the correct pressure field is employed, the resulting velocity field u_e, v_n etc. will not satisfy the equation of continuity. Let the imperfect velocity field based on a guessed pressure field p^* be u^*, v^* and w^* or

$$u_e^* = \hat{u}_e^* - d_e(p_{EC}^* - p_P^*) \tag{V-11a}$$

$$v_n^* = \hat{v}_n^* - d_n(p_{NC}^* - p_P^*) \tag{V-11b}$$

$$w_t^* = \hat{w}_t^* - d_t(p_{TC}^* - p_P^*) \tag{V-11c}$$

In order to obtain an improved estimation of pressure field, such that the resulting starred velocity field u^*, v^* and w^*, after each iterative calculation for momentum equations, will approach the true velocity field and satisfy the discretized equation of continuity, one needs to know how the velocity components respond to a change in pressure field. By substracting eq(V-10) from eq(V-11), three velocity correction formulas relating the velocity-corrections $u_e - u_e^*$ etc. to the pressure-correction $p' = p - p^*$ can be obtained as follows

$$u_e - u_e^* = (\hat{u}_e - \hat{u}_e^*) - d_e(p'_{EC} - p'_P) \qquad \text{(V-12a)}$$

$$v_n - v_n^* = (\hat{v}_n - \hat{v}_n^*) - d_n(p'_{NC} - p'_P) \qquad \text{(V-12b)}$$

$$w_t - w_t^* = (\hat{w}_t - \hat{w}_t^*) - d_t(p'_{TC} - p'_P) \qquad \text{(V-12c)}$$

If we required the velocity field to satisfy the discretized equation of continuity of the form of

$$D = u_x + v_y + w_z = 0$$

or

$$D = \frac{u_e - u_w}{\Delta x_p} + \frac{v_n - v_s}{\Delta y_p} + \frac{w_t - w_b}{\Delta z_p} = 0 \qquad \text{(V-13)}$$

an equation for p' in terms of u^*, v^* and w^* can be derived. However, due to the implicit nature of velocity correction terms $u - u^*$, $v - v^*$ and $w - w^*$, where u^*, v^* and

w^* are function of p^* in eq(V-11), the resulting pressure equation for p' by substituting eq(V-12) into (V-13) would involve pressure correction p' at all grid points in the calculation domain, and ultimately becomes unmanageable. Since the velocity and pressure correction formulas become trivial in the final converged solution where both the velocity and pressure corrections, i.e., $u - u^*$, $v - v^*$, $w - w^*$ and $p' = p - p^*$, are exactly zero, the pressure correction equation for p' can be considered as an intermediate algorithm that leads to the correct pressure field p and have no direct effect on the final solution [11]. Thus, it is possible to simplify or to omit part of the velocity-corrections in eq(V-12a) - (v-12c), so that a simpler pressure correction formula for p' can be obtained. The final converged solution should not depend on the approximation made on velocity and pressure correction formulas during intermediate calculations, although the rate of convergence will depend on the approximate formulation of p'. The simplest approximation as that used in SIMPLE [11,28] or SIMPLER [11] algorithm, is to omit the indirect influence $\hat{u} - \hat{u}^*$, $\hat{v} - \hat{v}^*$ etc. in eq(V-12a) - (v-12c), such that the velocity-corrections can be expressed explicitly in terms of the pressure correction p' as

$$u_e - u_e^* = d_e(p'_P - p'_{EC}) \tag{V-14a}$$

$$v_n - v_n^* = d_n(p'_P - p'_{NC}) \tag{V-14b}$$

$$w_t - w_t^* = d_t(p'_P - p'_{TC}) \tag{V-14c}$$

If we required the approximate velocity correction formulas (V-14a) - (V-14c) to satisfy the discretized equation of continuity (V-13), then a Poission equation for pressure-correction p' can be derived.

$$a_P p'_P = a_e p'_{EC} + a_w p'_{WC} + a_n p'_{NC} + a_s p'_{SC} + a_t p'_{TC} + a_b p'_{BC} - D^* \tag{V-15}$$

where

$$a_e = \frac{d_e}{\Delta x_p}\ ,\ a_w = \frac{d_w}{\Delta x_p}\ ,\ a_n = \frac{d_n}{\Delta y_p}\ ,\ a_s = \frac{d_s}{\Delta y_p}$$

$$a_t = \frac{d_t}{\Delta z_p}\ ,\ a_B = \frac{d_b}{\Delta z_p}$$

$$a_P = a_e + a_w + a_n + a_s + a_t + a_b$$

and

$$D^* = \frac{u_e - u_w}{\Delta x_p} + \frac{v_n - v_s}{\Delta y_p} + \frac{w_t - w_b}{\Delta z_p} \tag{V-15a}$$

The boundary condition for p' can be easily specified in the following manner. If the pressure is given at a boundary, i.e., $P^* = P_{given}$, then the pressure-correction

p' at the boundary will be zero. On the other hand, if the normal velocity is given at a boundary, e.g., $u_e^* = u_e$, then there is no need to consider the velocity correction equation (V-14a). Hence, no information for p'_{EC} will be needed [11]. In both cases, $p' = 0$ everywhere at the final stage of convergence when $D^* = 0$ in the whole domain of calculation. Thus, the velocity-correction formulas (V-14a) - (V-14c) becomes trivial as mentioned before.

After obtaining the pressure-correction p' from eq(V-15), one may update the pressure by letting

$$p = p^* + \alpha p' \qquad \text{(V-16)}$$

with an under-relaxation parameter α. However, extremely small under-relaxation factor α may be needed for some problems [20]. Furthermore, due to the approximation made on velocity-correction formulas, many iterations are needed to obtain a converged solution even if the correct pressure field p^* is used as an initial guess. Since the pressure-correction equation does a fair job in correcting the velocities, but a rather poor job in updating the pressure [11], a number of alternatives for updating the pressure were proposed [20] to avoid this shortcoming. In the present study, the SIMPLER [11] algorithm (i.e., PUP scheme in Raithby et al. [20]) is adopted to update the pressure field. By requiring equations (V-10a) - (V-10c)

to satisfy the discretized equation of continuity (V-13), one obtains a Possion equation for pressure as

$$a_P p_P = a_e p_{EC} + a_w p_{WC} + a_n p_{NC} + a_s p_{SC} + a_t p_{TC} + a_b p_{BC} - \hat{D} \qquad \text{(V-17)}$$

where

$$\hat{D} = \frac{\hat{u}_e - \hat{u}_w}{\Delta x_P} + \frac{\hat{v}_n - \hat{v}_s}{\Delta y_P} + \frac{\hat{w}_t - \hat{w}_b}{\Delta z_P} \qquad \text{(V-17a)}$$

and a_p, a_e , a_w etc. are defined in eq(V-15). It is noted that eq(V-17) is similar to eq(V-15), and the boundary condition for pressure is the same as that for pressure-correction p' also. But there is no approximation made in obtaining eq(V-17). Thus, if a correct velocity field is employed as the initial guess, eq(V-17) would at once give the correct pressure field. In this fashion, one can extract the pressure directly from an estimated velocity field, and thus avoid the slow convergence resulted from the approximated velocity-correction formulas (V-14a) - (V-14c). The pressure-correction (V-15) is used to correct only the velocity field, so that a better estimated velocity field can be obtained.

For unsteady fluid flow problems, the flow field is required to satisfy the equation of continuity at each time step. Unless a correct initial field which satisfy the

equation of continuity is given, it is not possible to obtain a physically meaningful transient flow field. For problems where the initial and boundary conditions are properly specified, the transient numerical solution can be obtained in the following manner.

(1) Discretize the domain of calculation into suitable number of small local elements.

(2) Specify the initial condition for velocity field, or generally at $(n-1)^{th}$ step.

(3) The velocity field at $(n-1)^{th}$ time step is employed as the initial guess for the velocity field at n^{th} time step.

(4) Calculate the FA coefficients b^u_{nb}, b^v_{nb}, b^w_{nb} etc., and also the FA coefficients for pressure and pressure-correction equations, i.e., a_e, a_w etc.

(5) Calculate the higher order correction terms f^u, f^v and f^w if needed.

(6) Calculate the pseudovelocities $\hat{u}$, $\hat{v}$, $\hat{w}$ from eq(V-9) etc. in terms of velocity field of $(n-1)^{th}$ time step.

(7) Calculate $\hat{D}$ from eq(V-17a) and solve the pressure equation (V-17) by tridiagonal algorithm to obtain the pressure field; p.

(8) Treating this pressure field, p, as guessed pressure field p^*, solve the momentum equations (V-11a) -

(V-11c) to obtain the starred velocity field u^*, v^* and w^*. The system of algebraic equations is solved by tridiagonal algorithm.

(9) Calculate the mass source term D^* in eq(V-15a), and hence solve the pressure-correction equation (V-15) to obtain p'. The system of algebraic equations is solved by the tridiagonal algorithm also.

(10) Correct the velocity field using velocity-correction formulas (V-14a) thru (V-14c), but do not correct the pressure. The velocity field u, v and w thus obtained should satisfy the equation of continuity (V-13).

(11) Return to step (4) and repeated the steps (4) to (10) until convergence criterion is achieved. i.e., $\max|D^*_{ijk}| < \varepsilon$.

(12) Stop if the steady-state criterion is achieved (i.e., $\max|u^n_{ijk} - u^{n-1}_{ijk}| < \varepsilon$ etc.), or the time t exceeds the maximum time period assigned.

(13) If not, return to step (3) for $(n+1)^{th}$ time step calculation.

For problems where only the steady-state solution is sought, one may relax the convergence criterion and use a larger time increment for intermediate velocity field calculations in this time marching procedure as long as during the computations the variables become stationary.

It should be remarked here that if uniform grids are employed to construct the staggered grid coordinate system, then the no-slip conditions cannot be satisfied exactly on the moving and stationary walls. Thus, fictitious boundary conditions outside the solution domain are used for velocities parallel to the walls. [20], [25]. On the other hand, if nonuniform grids are employed, then the no-slip conditions can be exactly satisfied by choosing control volumes of zero thickness along the moving and stationary walls [11]. In this study, the FA solution is formulated in a general nonuniform grid local element and control volumes of zero thickness are chosen (see Fig. 8) along the walls for the numerical calculations of two- and three-dimensional fluid flow problems.

CHAPTER VI

EXAMPLES OF ONE-DIMENSIONAL FLUID FLOW PROBLEMS

In this chapter, the unsteady FA formulas derived in Section III-1 are tested for several unsteady linear and nonlinear one-dimensional convective transport equations. They are

(1) Large time (steady-state) solutions of linear convective transport equation

$$u_t + cu_x = \alpha u_{xx} \qquad 0 \le x \le 1 \qquad \text{(VI-1)}$$

$$u(x,0) = 0 , \qquad 0 \le x \le 1$$

$$u(0,t) = 1 , \quad u(1,t) = 0 , \qquad t > 0$$

where the convective velocity c, in general, is a function of space and time.

Exact solutions for $t \to \infty$ are respectively

(a) $c = 0$, $\quad u = 1 - x$ (VI-1a)

(b) $c = 1$, $\quad u = \dfrac{e^{cx/\alpha} - e^{c/\alpha}}{1 - e^{c/\alpha}}$ (VI-1b)

(c) $c = \dfrac{\alpha(n-1)}{(x+0.01)}$, $\quad u = \dfrac{(1.01)^n - (x+0.01)^n}{(1.01)^n - (0.01)^n}$ (VI-1c)

(2) Large time (steady-state) solution of nonlinear convective transport equation

$$u_t + uu_x = \alpha u_{xx} \qquad 0 \le x \le 1 \qquad \text{(VI-2)}$$

$$u(x,0) = 0 , \qquad 0 \le x \le 1$$

$$u(0,t) = 1 , \quad u(1,t) = 0 \qquad t > 0$$

Exact solution for $t \to \infty$ is

$$u = c' \frac{1 - e^{\frac{c'}{\alpha}(x-1)}}{1 + e^{\frac{c'}{\alpha}(x-1)}} , \qquad c' = \coth \frac{c'}{2\alpha} \qquad \text{(VI-2a)}$$

(3) Transient solution of nonlinear convective transport equation (Burgers equation)

$$u_t + uu_x = \alpha u_{xx} \qquad -\infty < x < \infty \qquad \text{(VI-3)}$$

$$u(x,0) = \begin{cases} 1 , & x \le 0 \\ 0 , & x > 0 \end{cases}$$

$$u(-\infty,t) = 1, \quad u(\infty,t) = 0 \qquad t > 0$$

Exact solution for eq(VI-3) is given in [29] as

$$u(x,t) = \frac{1}{1 + \exp[\frac{1}{2\alpha}(x - \frac{1}{2}t)] \dfrac{\operatorname{erfc}(-x/2\sqrt{\alpha t})}{\operatorname{erfc}[(x-t)/2\sqrt{\alpha t}]}} \qquad \text{(VI-3a)}$$

VI-1 Linear Burgers Equation

In case (1), the finite analytic solution for the linear convective transport equation (VI-1) is examined for its large time behavior at several prescribed

convective velocities (a) c = 0, (i.e., heat equation) (b) c = 1 with α varying from 0.001 to 0.1 and (c) c = α(n-1)/(x+0.01) (variable c(x)) with n ranging from 2 to 20. Different mesh sizes ranging from 0.025 to 0.2 and time increments of O(h) to $O(10^4 h)$ are employed to study the stability and the accuracy of three FA formulations described in Section III-1. In obtaining the large time solution with small time increments, many time steps are needed which is not necessary unless instability occurs. On the other hand, if the numerical solution is stable, very large time increment can be used, then the steady-state solution can be obtained in one or two time steps, although the transient solutions may not be accurate. Since the three FA formulations (III-10), (III-15) and (III-20) considered here are all implicit in time, no stability problem is encountered even if very large time steps are used. It is therefore always possible to obtain the steady state FA solution of eq(VI-1) efficiently by using large time increments in equations (III-10), (III-15) and (III-20). These steady-state results are shown in Tables (16) thru (19). It is seen that the steady-state FA solution for heat equation (c = 0) approaches the exact solution (VI-1a) in two or three time steps with time increment τ = 1000 and grid size h = 0.2 for all of

the three FA formulations considered. Similarly, the steady-state FA solution for linear convective transport equation of unity convective velocity (c = 1) converges to the exact solution (VI-1b) in 2 to 4 time steps for each formulation as those shown in Tables (17) & (18). However, small error although negligibly small are encountered when second-order polynomial initial function (FASP) is employed in the FA formulation, while the exact convergence is achieved in FAEL and hybrid FA formulations.

Since the construction of exponential and linear initial function is based on the analytic solution of steady one-dimensional convective transport equation of constant convective velocity c, the exact solutions should be recovered in FAEL and hybrid FA formulations as shown in Tables (16) thru (18). It is therefore desirable to choose some test cases with variable convective velocities to rigorously test the accuracy of three FA formulations. In this study, a rapid-varying velocity field of $c/a = (n-1)/(x+0.01)$ is chosen for this purpose. It is found that the results for different values of n ranging from 2 to 20 agree very well with the exact solutions (VI-1c). For example, even for the case n = 20 using a coarse grid of 0.1, the maximum error is still less than 0.5% for all of the three FA formulations as shown in Table (19).

It should be remarked here that the FAEL and hybrid FA formulations give the same transient solutions for each case tabulated in Tables (16) thru (19) due to the use of large time increments. In these cases, the influence from previous time step becomes vanishingly small, thus results in the same FA coefficients and same transient solutions. This is, however, not necessary true when small time increments are used. It should be remarked here also that the 9-point FA formula (III-10) obtained by FASP formulation can not be applied directly to the initial step of calculation since there is only 5 neighboring nodal points available. In this study, for the first time step of calculation, a 6-point FA formula derived from the 9-point FA formula (III-10) by replacing τ by $\frac{1}{2}$, u_P by $\frac{1}{2}(u_{NE}+u_{SE})$ and u_W by $\frac{1}{2}(u_{NW}+u_{SW})$ is used. The FA formula thus obtained should be exactly the same as the one derived in terms of second-order polynomial initial function and linear boundary functions.

VI-2 Nonlinear Burgers Equation

For the linear convective transport equation (VI-1) considered in case (1), the convection coefficient is a prescribed function of space and time, thus, there is little problem in determining the coefficients A and B. However, nonlinear problems are often encountered in

many engineering applications. It is therefore desirable to study the nonlinearity and linearization schemes adopted in FA formulations for solving nonlinear convective transport equations. In cases (2) and (3), the nonlinear convective transport equation of convective velocity u (i.e., Burgers equation) is tested in a bounded and an infinite domain to obtain the steady-state or transient solutions. In case (2), different mesh sizes ranging from 0.025 to 0.1 and time increments of order of h to 10^5h are used to study the accuracy and stability of three FA formulations. The convection coefficient in each local element is approximated by a representative constant (area-averaged $A = \frac{1}{2} \alpha \bar{u}$ in this study) known from previous time steps, so that a marching process can be used without iteration at each time step. It is found that although the steady-state solution can be obtained much more efficiently by using larger time increments, there is, however, little saving in computational time when time increment exceeds 10^3h. This phenomenon, which differs very much from that for linear problems, is due to the approximation made on the convection coefficient. When large time increment is used, the convection coefficient A based on previous time steps is far from accurate. Consequently, approximately same number of time steps is needed for $\tau > 10^3$h in order to achieve

the same accurate large time solution. If transient solution is desired, one may either use a small time increment or a somewhat larger time increment but with internal iterations at each time step to update the convection coefficients.

In Figs. 9(a) and 9(b), the transient solutions of Burgers equation for $\alpha = 0.1$ and 0.01 are shown at $t = \tau$, 2τ, 3τ, 4τ and 10τ for FAEL (or hybrid FA) and FASP formulations. As mentioned before, the transient FA solutions are not accurate in these figures due to large time increments used. But it shows that the steady-state solution can always be obtained economically in a few time steps and yet no stability problem is encountered. It can be seen that the results obtained by FAEL and FASP formulations are almost identical, while the results obtained by hybrid FA formulation are exactly the same as those obtained by FAEL formulation due to the large time increment and the same exponential and linear initial function employed. It can also be seen that the steady-state solution at $t = 10\tau$ obtained by FA formulations agree very well with exact solutions represented by solid lines. This demonstrates the accuracy of the FA method. In order to compare the dependence of FA solution on the grid sizes, the FA solution for the case $\alpha = 0.01$ is also calculated using coarser grid of 0.1 and 0.05. Even in

such a coarse grid, the agreements between the exact solution and FA solution are still very good. For example, if h = 0.05 is used, the steady-state velocity u at x = 0.95 is 0.983788 for FAEL or hybrid FA formulations, and is 0.983791 for FASP formulation. The errors are less than 0.3% when compared with the exact solution of 0.986614.

In cases (1) and (2), the stability and accuracy of three FA formulations for one-dimensional linear or nonlinear convective transport equations are tested using several different time increments and mesh sizes. No instability problem is encountered even when very large time increments of $O(10^4)$ are used. Besides, the steady-state solutions agree very well with exact solutions even if large mesh sizes of 0.1 or 0.2 are employed. For case (3), a wave propagation problem [30] defined by eq(VI-3) is invoked in the test for the accuracy of the FA transient solutions. The problem is solved for $\alpha = 0.01$ and 0.001, where a step function is used as the initial condition. After a long time, the exact solutions should be propagating with a constant speed V = 0.5 and preserve the large time solution profile. In the present FA calculation, a mesh size of 0.01 and a time increment of 0.002 are used for both cases. After 200 time steps of calculation, no more changes in wave shapes are observed in FA solutions, thus the long time solutions

can be assumed. The results are shown in Figs. 10(a) and 10(b) for $\alpha = 0.01$ and 0.001 respectively. For the case of $\alpha = 0.01$, the wave shapes obtained by three different FA formulations agree very well with the exact solution. However, small phase errors of about 1% are encountered in time domain for FASP and hybrid FA formulations. The FA solutions are propagate at $V = 0.505$, 0.500 and 0.493 for FASP, FAEL and hybrid FA formulations, which differ slightly from $V = 0.5$ for the exact solution. These phase errors are partly due to the approximation on boundary conditions and partly due to the linearization of convection coefficient. It is possible to reduce these phase errors by employing a better estimated convection coefficient based on two or more time steps interpolation so that the nonlinearity of the governing equation can be more accurately simulated. However, the internal iterations needed may make the procedure very time-consuming. Thus, in the present study, the convection coefficient is simply approximated by a constant known from previous time step t_{n-1}, so that a non-iterative marching process can be employed.

For the case $\alpha = 0.001$ where very sharp gradient is encountered, three FA formulations begins to differ from the exact solution not only in the speed of propagation but also in the wave shape. It can be seen that the phase

error is small in FASP formulation since a second-order polynomial boundary approximation is used. However, unrealistic overshoots and oscillations which come from the inadequate second-order polynomial initial function are seen in the downstream. On the other hand, physically realistic solutions are obtained in FAEL and hybrid FA formulations although ths phase errors and the discrepancy in wave shape are somewhat larger due to the coarse grid and also the simple linearization of convection coefficient employed.

It is noted that the wave shapes obtained by FAEL and hybrid FA formulations are not exactly the same even though same exponential and linear function is employed. This indicates that an improvement in the boundary approximation in time domain may improve the accuracy in space domain also. Hence, a FA formulation using exponential and linear initial function and higher order boundary approximations should reduce the phase error and also gives a better agreement in wave shape with exact solution. The derivation based on higher order boundary approximations is, however, not given in the present study because the extension to multi-dimensional problems is quite complicate. Furthermore, the steady-state solution is completely unaffected by this improvement.

CHAPTER VII

EXAMPLES OF TWO-DIMENSIONAL FLUID FLOW PROBLEMS

In previous chapters, it is concluded that the FA formulations using exponential and linear boundary approximations give most accurate results and require least computational time among several FA formulations considered. Thus, in studying two-dimensional fluid flow problems, the FA formula based on exponential and linear boundary approximations is employed to solve two fluid flow problems where comparison with experimental measurements or other theoretical or numerical calculations are available. The two problems are

(1) Incompressible flow in a square cavity driven by a moving wall.

(2) Development of vortex street behind a rectangular block.

The two-dimensional driven cavity flow is often chosen for the purpose of examining the numerical solutions of Navier-Stokes equations [5,6,13,25,26,31-48]. This ideal prototype nonlinear problem is of fundamental importance because it is a part of the large steady and unsteady separated flow. In addition, it is a flow where

the fluid is set into motion by the viscous shear on the moving plate and the viscosity and nonlinear convection affect the entire flow region. Their geometry simplicity make them by far the best model problem for testing new numerical schemes.

The numerical methods presented in the literature for the driven cavity flow differ not only in problem formulations, discretization schemes, boundary approximations for vorticity and pressure on the no-slip walls, but also in the method used to solve the resulting system of algebraic equations. Detailed reviews of previous works and the comparison of their numerical results in the two-dimensional driven cavity flow are given by, among others, Vahl Davis & Mallinson [32], Tuann & Olson [33], Gupta & Manohar [35] and Chen et al. [6].

In this study, the improved 10-point FA formula is employed to solve the two-dimensional driven cavity flow problem in both the vorticity-streamfunction and the primitive variable formulations. The unsteady approach is used to obtain both the transient and steady-state solutions. If only the steady-state solution is sought, a good initial guess (for example, if known, a flow profile at lower Reynolds number) and large time increments can be used to obtain the steady-state solution much more economically. Furthermore, the convergence

criterion for intermediate time steps can be relaxed to reduce further the computational time.

Although there are several experimental works [49,50] and numerical solutions available for the steady two-dimensional driven cavity flow problems, the detailed results for the transient behavior of the starting cavity flow are, however, very limited. It is thus somewhat difficult to judge the accuracy of the transient solutions obtained by the present FA method in the starting cavity flow test problem. In order to test the applicability of the 10-point FA formula for unsteady two-dimensional convective transport equation more rigorously, it is desirable to choose an unsteady flow problem with unique feature and comparable solutions. In this study, the development of vortex street behind a rectangular block is chosen for this purpose.

Numerically, the vortex street prediction behind a rectangular block was first investigated by Fromm & Harlow [51]. In their study, the upstream and downstream boundary conditions were assumed to be periodic. Artificial perturbations in vorticity field were introduced to trigger the vortex shedding process. Numerical results for streamlines, stationary streamlines and streaklines patterns are presented for Re = 50, 100, 200, 300 and 6000. Smith & Berbbia [52] employed a finite element formulation

to solve a similar problem for Reynolds number of 20, 50 and 100. Due to the relatively long obstacle (0.4m long by 0.166m wide) they used, the vortices are rather weak and were not observed for Reynolds numbers under 100. In both cases, rather small time increments are needed to obtain accurate transient solutions. As to the experimental works, the Strouhal numbers for several similar shaped blocks were given in [53]. For flat plate obstacle with sharp edges, the Strouhal number reaches a maximum value of 0.16 around Re=100, and then gradually decreases to 0.13 for very large Reynolds numbers. Although experimental measurement of transition from laminar to turbulent vortex shedding is not known for rectangular block, however, it is observed for cylindrical obstacle to occur around Reynolds number of 150 [53]. In Prandtl & Tietjens [54], streamlines of flow past a flat plate were shown for Re = 0.25, 10 and 250. Vortex street flow pattern was observed at Re = 250, while symmetric flow patterns were observed at lower Reynolds numbers of 0.25 and 10.

Since it is not easy to specify an initial velocity field that satisfies the continuity requirement for vortex street problems formulated in terms of primitive variables, the vorticity-streamfunction formulation is employed in the present study. Relatively coarse nonuniform grid

are used to obtain the physically meaningful solutions economically. In addition, large time increments are employed to further reduce the computational time needed.

VII-1 Two-Dimensional Starting Cavity Flow in Vorticity-Streamfunction Formulation

Consider a square cavity as shown in Fig. 11, where the cavity with depth and width of length L is initially filled with incompressible fluid at rest. The bottom wall is then set to move with a constant speed U_0 in the positive x direction when $t > 0$. The other walls are kept at rest. The flow is assumed to be two-dimensional with constant transport properties and laminar.

Introducing the dimensionless variables

$$x = \frac{X}{L} , \quad y = \frac{Y}{L} , \quad u = \frac{U}{U_0} , \quad v = \frac{V}{U_0} \text{ and } \quad t = \frac{\hat{t}U_0}{L}$$

the dimensionless Navier-Stokes equations in vorticity-streamfunction form can then be written as

$$\xi_{xx} + \xi_{yy} = Re\ (\xi_t + u\xi_x + v\xi_y) \qquad \text{(VII-1)}$$

where the vorticity ξ is defined by

$$\xi = v_x - u_y = -(\psi_{xx} + \psi_{yy}) \qquad \text{(VII-2)}$$

and $u = \psi_y , \quad v = -\psi_x$ (VII-2a)

The Reynolds number $Re = U_0 L/\nu$ is based on the velocity of the moving wall U_0 and the cavity depth L. The no-slip and impermeable conditions are specified on the four boundaries of the cavity as follows

(1) On the bottom wall $\psi = 0, \quad \psi_y = 1$ (VII-3a)

(2) On the top wall $\psi = 0, \quad \psi_y = 0$ (VII-3b)

(3) On the left wall $\psi = 0, \quad \psi_x = 0$ (VII-3c)

(4) On the right wall $\psi = 0, \quad \psi_x = 0$ (VII-3d)

The vorticity boundary conditions for eq(VII-1) may be approximately derived from the above boundary conditions using Taylor-series expansions of the streamfunction from the wall to interior points normal to the wall. Many alternatives of boundary conditions were investigated by, among others, Vahl Davis & Mallinson [32], Gupta & Manohar [35], Benjamin & Denny [37], Quartapelle [38] and Gupta, Manohar & Noble [36]. In this study, the simple first-order and second-order boundary conditions are adopted. They are

(1) First-order vorticity boundary conditions

$$\xi_w = -\frac{2\psi_{w-1}}{h_w^2} - \frac{2}{h_w}\left(\frac{\partial \psi}{\partial n}\right)_w \qquad \text{(VII-4a)}$$

(2) Second-order vorticity boundary conditions

$$\xi_w = -\frac{8\psi_{w-1} - \psi_{w-2}}{2h_w^2} - \frac{3}{h_w}\left(\frac{\partial\psi}{\partial n}\right)_w \qquad \text{(VII-4b)}$$

where the subscripts w, w-1 and w-2 denote nodal points on the wall, and one or two points in from the wall. n is the outward normal measured from the center of the cavity, h_w is the first grid size from the wall. In eq(VII-4b), the first two mesh sizes near the wall are chosen to be equal (both equal to h_w).

As to the initial condition, a zero initial vorticity field is given at t = 0 to simulate the initial development of starting cavity flow.

$$\xi(x,y,0) = 0 \qquad \text{(VII-5)}$$

Following the numerical procedures described in Section V-1, the governing equations (VII-1) and (VII-2) with boundary conditions (VII-3), (VII-4) and initial condition (VII-5) can be easily solved to provide the numerical solutions for starting cavity flow. In this study, the starting cavity flow is tested for Reynolds numbers of 100, 400, 1000, 2000 and 5000 in several uniform or nonuniform grids ranging from 11×11 to 51×51 and time increments from 0.05 to 2.0. The transient solutions for Re = 1000, 2000 and 5000 are studied in details using both the first- and second-order vorticity

boundary conditions. The convergence criterions between two iterations at each time step are 10^{-7} for streamfunction and 10^{-5} (Re = 1000 and 2000) or 10^{-6} (Re = 5000) for vorticity respectively. An over-relaxation factor of 1.6 for the internal iterations of streamfunction is used to reduce the computational time needed. For steady flow calculation of Re = 100 and 400, a nonzero initial condition and large time increments are used to obtain the FA solutions in order to save computational time. The convergence criterion for internal iterations of streamfunction and vorticity are also relaxed to reduce the computational time.

A typical transient solution of starting cavity flow based on the second-order vorticity boundary condition (VII-46) is shown in Figs. 12 and 13 for Re = 1000. A 41×41 nonuniform grid system is used with mesh sizes arranging as 0.015 (4 nodes), 0.025 (8 nodes), 0.03 (16 nodes), 0.025 (8 nodes) and 0.015 (4 nodes) in x and y directions. A time increment of 0.1 is used for the first 40 time steps, after that a time increment of 0.15 is employed. The steady-state solution is achieved at t = 40 with $\Delta\psi < 10^{-11}$ and $\Delta\zeta < 10^{-11}$ between two time steps. It can be seen from Fig. 12 that the vortex center moves from the lower left corner at the early time of t = 1 toward the center of the cavity at later time of t = 40,

while the vorticity generated by the moving wall is convected and diffused gradually to the downstream and the center of the cavity as shown in Fig. 13. A careful study shows that a separation bulb first occurs near the middle section of the right wall around t = 3. This separation bulb continues to grow and moves downstream while another separation bulb appears at the upper-right corner. As time increases, the separation bulb at right wall is convected further upward and eventually emerges with the enlarged upper-right corner separation region around t = 5 as shown in Fig. 12(c). As the strength of the primary vortex continues to grow during transient state, the upper-right corner separation bulb reaches a maximum size and then begins to shrink around t = 10. After t = 10, the upper-right secondary vortex continues to shrink due to the further increase in the strength of the primary vortex, but the upper-left secondary vortex enlarges gradually to its maximum size. When the steady-state solution is achieved around t = 40, the strength of the primary vortex reaches its maximum value of 0.103053. On the other hand, the upper-right secondary vortex reduces to about half of its maximum size. The steady-state solution obtained in the present calculation agrees fairly well with those obtained by Takemitsu [39] and Benjamin & Denny [7], where both works employed a

large number (101×101) of uniform grid in obtaining the numerical solutions.

In Fig. 13, the development of vorticity exhibits a boundary layer like behavior near the wall. At the initial stage of development, the high velocity gradient along the moving wall generated a strong vorticity field near the moving wall and the lower-right corner. This highly concentrated vorticity field is then convected downstream by the fluid driven by the moving wall. At the same time, a negative vorticity field starts to generate near the right wall via the increased velocity gradient along the right wall. Eventually, the positive vorticity field generated by the moving wall and the negative vorticity field generated by the stationary right wall are transported downstream and simultaneously diffused into the center of the cavity. When the flow approaches steady-state, the vorticity field generated by the moving and stationary walls is then balanced by the viscous dissipation of vorticity field. Thus, even at the steady-state, the vorticity is continuously generated by the moving and stationary walls and diffused into the cavity creating a boundary layer phenomenon near the walls with a nearly uniform vorticity core surrounded the vortex center.

Quartapelle [38] investigated the starting cavity flow for Re = 1000 using a time increment of 0.05 for 300 time steps. The transient streamlines and vorticity contours exhibit similar patterns as those obtained in the present study. However, detailed comparison can not be meaningfully made because secondary vortices were not shown in his study. Furthermore, physically unrealistic oscillations were encountered in Quartapelle's calculation of vorticity field. It is suspected that these oscillations would be amplified gradually by the instability of his scheme, and his solution may become unstable if the calculation is carried beyond t = 15. On the other hand, smooth results are obtained in the present study for a large time even if coarse meshs of 21×21 and 31×31 are used.

The numerical solutions obtained in coarser nonuniform grids of 21×21 and 31×31 exhibit the similar transient behavior as those shown in Figs. 12 and 13 for finer grid of 41×41. However, the strength of the primary vortex is somewhat lower and the sizes of secondary vortices are somewhat larger. Figures 12 thru 15 compare the steady state solutions of Re = 1000 in 41×41 grid with those using nonuniform meshs of 21×21 and 31×31. It can be seen that there is not much difference between results obtained by 31×31 and 41×41 nonuniform grids. Thus, one may

conclude that the transient solution obtained with 41×41 grid is sufficiently grid independent and accurate.

In this study, both the first- and second-order vorticity boundary conditions are tested for selected cases. The result shows that the second-order vorticity boundary condition gives better performance for all of the cases considered. For example, when a nonuniform grid of 21×21 with mesh size ranging from 0.03 to 0.07 is used to obtain the streamlines and vorticity contours shown in Fig. 14 for Re = 1000, there is a 3% improvement in the maximum value of streamfunction (i.e., 0.0768 vs 0.0792). But the solution employing the first-order vorticity boundary condition gives the solution of maximum streamfunction to within 1% (0.0989 vs 0.0998) of that employing the second-order vorticity boundary condition when a finer mesh of 37×37 is used. Benjamin & Denny [37] reported a much larger improvement in their study of Re = 1000 using an equal grid of 41×41 with the second- and third-order vorticity boundary conditions. The fact that the present study gives more consistent results may be due to that better numerical scheme and finer mesh sizes near the wall are adopted.

It should be remarked here that the vorticity boundary condition happens to be a particular troublesome source of causing divergent or unrealistic solutions for

many numerical schemes. Thus, many sophisticated treatment of boundary conditions were proposed to obtain reasonable solutions. For example, Greenspan [40] updated the streamfunctions on an "inner boundary" located one mesh point in from the boundary by a formula different from those for other field points to calculate the steady-state cavity flow up to Reynolds numbers of 10^5. Nallasamy & Prasad [41,42] used the similar type of vorticity boundary condition as that of Greenspan [40] to obtain the numerical solutions for steady driven cavity flow over a wide range of Reynolds numbers from 0 to 50000. Nallasamy & Prasad [42] reported that two major eddies flow pattern would be encountered in numerical solution if the additional formula for streamfunction on the inner boundary was not employed. Vahl Davis & Mallinson [32] studied this type of boundary condition in both uniform and nonuniform meshs and concluded that the overspecification of streamfunction on the "inner boundary" would force the boundary layer to adhere closely to the wall. For high Reynolds numbers, this could compensate the effect of the false numerical diffusion by increasing the size of the core region. Thus, unless very fine meshs are used, the results obtained in this way are not reliable for Reynolds numbers higher than 1000. Another commonly used higher order vorticity boundary condition

is obtained in the following form by modifying the first truncated term in eq(VII-4a)

$$\xi_w = -\frac{3\psi_{w-1}}{h_w^2} - \frac{3}{h_w}\left(\frac{\partial\psi}{\partial n}\right)_w - \frac{\xi_{w-1}}{2} \qquad \text{(VII-6)}$$

This second-order accurate boundary function was used by, among others, Gosman et al. [43], Bozeman & Dalton [44] and Vahl Davis & Mallinson [32]. Vahl Davis & Mallinson [32] reported that the central difference numerical scheme can be stabilized for Reynolds numbers higher than 1000 if the second-order vorticity boundary condition (VII-6) is employed. Their attempt for Re = 5000 was, however, not succeeded due to a similar numerical instability encountered in Re = 1000 when the first-order vorticity boundary condition (VII-4a) is used. Recently, more sophisticated vorticity boundary conditions based on fourth-order governing equation for streamfunction were derived in Quartapelle [38] and Gupta et al [36]. However, the performance of these schemes in predicting high Reynolds number flows has not been rigorously tested. It can be seen from these discussions that the convergence properties for various numerical schemes depend strongly on the treatment which is adopted to approximate the vorticity boundary conditions. Moreover, even when

converged solutions are obtained, there are still large discrepancies of local and global quantities between apparently comparable calculations. Most of the researchers tend to believe that the discrepancies come from the approximations made on vorticity boundary conditions. It is, however, in view from the present study, more likely that numerical scheme itself and not the vorticity boundary condition which is responsible for these discrepancies and instability phenomenon. In the present study, even the simplest first-order vorticity boundary condition still gives reasonable solutions for all cases considered. Furthermore, the use of higher order vorticity boundary condition does not significantly change the global or local features of the numerical solutions. Thus, the stability of the present FA method is demonstrated. The all-positive FA coefficients and desired upwind shift on FA solutions gurantee a physically realistic and stable solution with minimum false numerical diffusion as long as vorticity boundary conditions are properly posed. However, it is found that smaller time increments are needed to obtain satisfactory solutions if higher order boundary conditions are used. For example, when the second-order vorticity boundary condition (VII-4b) is employed for Re = 1000 with 41×41 nonuniform mesh, the attempt to use a time increment larger than 0.2 is not

succeeded, while, if the first-order vorticity boundary condition (VII-4a) is used for Re = 2000 in the same nonuniform grid, time increments as large as 0.4 can be used without difficulty and larger time increment is still possible for the calculation if one needs only the steady-state solution. Similar situations are observed in other test cases. Thus, it is suggested from the present study that finer mesh sizes near the wall in company with lower order boundary approximation is preferred in obtaining the approximated boundary vorticity values.

For the starting cavity flow of Re = 2000, the same 41×41 nonuniform grid is used to obtain the transient streamlines and vorticity contours as those shown in Figs. 16 and 17 respectively. The simplest first-order vorticity boundary condition (VII-4a) is employed to update the boundary vorticity values in every iteration. Time increments from 0.1 to 0.4 are used for 240 time steps until the steady-state solution is reached at t = 60 (t = 0.1×40 (steps) + 0.2×80 + 0.3×80 + 0.4×40) with $\Delta\psi < 10^{-11}$ and $\Delta\xi < 10^{-11}$ between last two steps. After that, the second-order vorticity boundary condition (VII-4b) is employed for 50 time steps to obtain an improved steady state solution at t = 65. The transient solution for Re = 2000 exhibits similar behavior as those for Re = 1000 before

t = 20, except that the separation bulb on the right wall appears earlier around t = 2 at a lower position as shown in Fig. 16(b). After t = 20, the upper-right and upper-left secondary vortices almost reach their stationary sizes, while a third secondary vortex comes to exist near the lower-left corner around t = 21. The steady-state solutions mostly agree with those obtained by Vahl Davis & Mallinson [32], Pepper & Cooper [45] and Chen et al. [5,6] where the existence of a similar third secondary vortex is reported. The appearance of the third secondary vortex is also predicted in Olson & Tuann [34] and Bejamin & Denny [37] for comparable Reynolds numbers. However, the shrinking of the upper-right secondary vortex was not predicted in their study. In Figs. 16(i) and 17(i), the steady-state streamlines and vorticity contours based on second-order vorticity boundary conditions are given for comparison. It can be seen that the use of the higher order vorticity boundary conditions does not significantly improve the global or local features over those obtained with the first-order vorticity boundary conditions. This is because small mesh size of 0.015 is used near the wall, in the present calculation, the strength of the primary vortex obtained by the second-order vorticity boundary conditions increases only for about 1% (0.0934 vs 0.0943) over that by the first-order vorticity boundary conditions.

The FA solution of starting cavity flow for Re = 5000 is also calculated using a 51×51 nonuniform grid with mesh sizes ranging from 0.01 to 0.025. A time increment of 0.1 is used for the first 200 time steps, after that a time increment of 0.15 is used. The numerical solutions shown in Figs. 18 and 19 are obtained using first-order vorticity boundary condition (VII-4a) until t = 47. The second-order vorticity boundary condition (VII-4b) is then used to obtain the steady-state solution at t = 52. Comparison of solutions for different Reynolds numbers shows that the separation bulb on the right wall occurs earlier and closer to the lower-right corner as Reynolds number increases. Furthermore, the third secondary vortex enlarged considerably while tertiary vortex comes to exist at upper-right corner. These features agree well with the study of Benjamin & Denny [37] where the numerical solution for Re = 10000 was obtained in an 151×151 nonuniform grid. Due to the relatively coarse grid used in the present study, the strength of the primary vortex for Re = 5000 is somewhat lower when compared with those obtained by Benjamin & Denny [37] for Reynolds numbers of 3200 and 10000. If sufficiently fine grids are used, it is expected that the strength of the primary vortex will increase and the sizes of upper-right and upper-left secondary vortices will decrease. Besides,

the tertiary vortex driven by the upper-right secondary vortex may disappear or at least shrink in size. One may conclude that with increasing Reynolds number, the upper-right secondary vortex starts to shrink around Re = 2000, while the upper-left secondary vortex begins to shrink at a higher Reynolds number around 5000. It is also expected that the size of the lower-left secondary vortex will decrease for much higher Reynolds numbers. Benjamin & Denny [37] made a different conclusion that the sizes of secondary vortices will continue to increase with increasing Reynolds number with a series of counterrotating vortices occupied the two upper corners. This conclusion seems to be unreasonable because the continuous enlarging of secondary vortices eventually would result in a large separation bulb near the top wall.

It is noted that the movement of vortex center for Re = 5000 during starting phase is somewhat different from those for Re = 1000 and 2000. Unlike the solutions for Re = 1000 and 2000, the locus of the vortex center for Re = 5000 makes a curl figure "๑" motion. The vortex center begins to move from lower-right corner to a position higher than the geometric center around t = 10 (Fig. 18(e)) and continue to move leftward. After passing a peak, the vortex center is convected downward to approximately at mid-height of the cavity as that shown at t = 20 before

it reaches the steady-state position slightly below the cavity center. For Re = 1000 and 2000, the locus of the vortex center simply moves from the lower-right corner to the steady and peak position below the cavity center. This difference in movement of vortex center may be due to the fact that at the initial stage of development for high Reynolds number flows, the top and left walls have little effect on the development of primary vortex. It is expected that this behavior would persist at higher Reynolds numbers.

As mentioned before, the steady-state solution can be obtained much more efficiently by relaxing the convergence criterion at each time step and by employing larger time increments in the numerical calculation. On the other hand, a better-estimated initial profile can reduce the computational time needed for calculating steady-state solutions. A series of steady-state solutions thus obtained are shown in Figures 20 thru 23 for Re = 100, 400, 1000 and 2000 respectively. In all cases, the first-order vorticity boundary condition (VII-4a) and uniform meshs are used. A higher order correction term of non-conservative form of

$$f_p = \frac{5}{9} Re \sum_{i=1}^{8} C_i \{(u_i - u_p)\xi_x\Big|_i + (v_i - v_p)\xi_y\Big|_i\} \quad \text{(VII-7)}$$

is employed in these calculations. C_i are FA coefficients for steady convective transport equations. Considerable saving in computational time are resulted in each case. For example, the steady-state solution for Re = 1000 can be obtained with a time increment of 0.4 for first 50 time steps and a time increment of 0.5 for another 40 time steps. The optimal time increment for fast, convergent result can be determined easily by running the program for a few time steps. It is noted that the shape of the upper-right secondary vortex given in Fig. 23 for Re = 2000 differs slightly from those (see Fig. 16(i)) obtained with a higher order correction term tabulated in conservative form (V-5). This small discrepancy may be due to the relatively coarse grid near the wall and non-conservative higher order correction term used in Fig. 23. Nevertheless, the global features of the numerical results obtained by these two approachs (V-5) and (VII-7) are still in good agreements for both Re = 1000 and 2000.

VII-2 Development of Vortex Street Behind a Rectangular Block

In previous section, the 10-point FA formula for unsteady two-dimensional convective transport equation is employed to solve the starting cavity flow problems for Reynolds numbers from 100 to 5000. The steady-state

solutions agree well with most of the calculations obtained by other researchers while the transient solutions are also provided. Due to the lack of the reliable experimental and other numerical or theoretical works, the accuracy of the transient solutions can not be rigorously verified. It is thus desired to test the present FA formulation for some other problems with comparable transient behaviors. In this section, the development of vortex street behind a rectangular block is chosen for this purpose.

For easy comparison with the results obtained by Fromm & Harlow [51], a rectangular block of height L and width L/4 as shown in Fig. 24 is chosen for the test. A calculation domain of 26L×6L is used to simulate the infinite extent of the region. The Reynolds number is defined by $U_0 L/\nu$, where U_0 is the uniform oncoming velocity. The block is located at a distance 2L from upstream. A nonuniform grid of 0.5 (3 nodes), 0.25 (14 nodes), 0.5 (10 nodes) and 0.8 (20 nodes) is used in the x-direction for the cases considered, while uniform grid of 0.25 is used in the y-direction for Re = 10, 50, 100 and 200, and a nonuniform grid of 0.5 (2 nodes), 0.125 (32 nodes) and 0.5 (2 nodes) is used for Re = 500.

From the experience obtained in solving the starting cavity flow problems, first-order vorticity boundary condition (VII-4a) derived from impermeable and no-slip

boundary conditions is used along the boundary of the rectangular block while the streamfunction is set zero on the walls. As to the outer boundary, the boundary conditions are specified as $\xi = 0$, $\psi = -3$; $\xi = 0$, $\psi = 3$ and $\xi = 0$, $\psi = y$ on bottom, top and upstream boundary, while downstream boundary conditions are specified as $\xi_x = 0$ and $\psi_x = 0$. For all calculations, a zero initial vorticity field is specified at t=0, a time increment of 0.5 is used for the first 40 (Re = 100, 200 and 500) or 60 (Re = 10 and 50) time steps, after that the time increment is reduced to 0.2 to obtain accurate transient solutions. The convergence criterion at each time step is specified as $\Delta\psi < 10^{-5}$ and $\Delta\xi < 10^{-5}$ for all field points between two internal iterations.

From the present FA calculation, both steady and unsteady separation flows behind the rectangular block are predicted. It should be remarked that the boundary conditions posed for the problem do not stipulate the symmetry condition at the plane of geometric symmetry, therefore the prediction does produce the asymmetric flow pattern such as vortex shedding phenomenon. It is found that the flow pattern at the initial phase of flow is symmetric, however, except for Re = 10, the flow pattern becomes asymmetric and oscillatory. For example, at Re = 500, the separation bulb (see Fig. 25) which is initially

symmetric begins to show asymmetric pattern around t = 20 and eventually the FA calculation predicts vortex shedding. This behavior is quite different from the calculations made by Fromm & Harlow [51]. They reported that an artificial perturbation on vorticity at 3 mesh points just in front of the rectangular block is needed to start the vortex shedding process. In order to clarify this point, a stringent criterion of $\Delta\psi < 10^{-6}$ and $\Delta\xi < 10^{-6}$ is used to calculate the FA numerical solution for Re = 500 for first 40 time steps to see if the vortex shedding can be surpressed in the present calculation. However, asymmetric flow pattern still occurs as that shown in Fig. 25 at t = 20 although the symmetric pattern persists a little longer. It is thus expected that even if a very strict convergence criterion is used, the computer round-off error would still be sufficient to trigger the vortex shedding after a certain time and destroy the initially developed symmetric pattern. In this study, the effect of artificial perturbation is also investigated for two selected cases of Re = 10 and 500 to examine the difference it may bring. In the case of Re = 500, the vorticities at two points upstream of the rectangular block are artificially increased by about 20% of its value at t = 20. In the subsequent time of calculation, this vorticity disturbance convected

downstream while simltaneously diffused away. However, the influence diminishes very rapidly. After 20 time increment of 0.2 at t = 24, the flow pattern as shown in Fig. 26 is almost the same as the one obtained without artificial disturbance. On the other hand, for the case of Re = 10 (Fig. 27), even if a large artificial vorticity perturbation of about 80% of its value is introduced at the same upstream nodes at t = 30, the steady-state pattern recovered very soon in about 10 time steps or at t = 35. In both cases, the artificial perturbation dies out in less than 20 time steps. Thus, the stability of the finite analytic transient numerical solutions is demonstrated. It is concluded that the unsteady flow pattern of vortex street is an expected pattern for high Reynolds numbers of $O(10^2)$ to $O(10^3)$, while the symmetric flow pattern is only stable for low Reynolds numbers.

A typical streamline pattern for vortex shedding process can be seen clearly in Fig. 28 for Re = 100 where the flow patterns are shown for every quarter period. At t = 43.6, the upper eddy has accumulated sufficient vorticity generated by the flow over the block and is about to leave the rectangular block while the lower eddy just begins to absorb the voeticity generated by the flow over the lower side of the block. Quarter

period later, the upper eddy leaves the block because the eddy has grown sufficiently large in size to block the flow on top of the rectangular block. As the upper eddy moves downstream, the lower eddy continues to grow and eventually forms a closed bulb. Around t = 46.8, the upper eddy has already shedded downstream and the lower eddy grows to its maximum strength and starts to leave the block. In the meantime, the accumulation of vorticity at the upper corner leads to the birth of a second upper eddy. The second upper eddy then continues to grow as that shown in Fig. 28(d). At a later time of t = 50, the second upper eddy reaches its maximum strength and begins the next cycle of vortex shedding process. The time period for this vortex shedding process is about 6.4. The corresponding Strouhal number is 0.156, which agrees favorably with the experimental measurement [53] of 0.165 based on a similar block with sharp edges. Furthermore, the streamlines pattern at t = 45.2 and 48.4 (lagged by half period) exhibit a very similar pattern as the experimental result shown in Prandtl & Tietjens [54] for Re = 250. Thus, the adequateness of the present unsteady 10-point FA formula in predicting the unsteady two-dimensional fluid flow problems is demonstrated. It is noted that, due to the convection, the eddies are carried downstream. Therefore, eddies other than relatively

stationary one such as those immediately behind the block can not be visualized on plot of streamlines. For example, in streamline plots, there are only two closed separation bulbs in Fig. 28(b) for t = 45.2, and even less closed streamlines in Fig. 28(h) for t = 56.8 are observed. In order to visualize the eddies that are convected downstream, one may subtract the free stream velocity from the streamlines configuration. The rest streamlines thus obtained are equivalent to the stream pattern observed by an observer on the rest ambient fluid when a rectangular block moves with uniform velocity through it. In Fig. 29, the downstream eddies can be easily seen in the rest streamlines configurations after the vortex shedding process occurs. The corresponding vorticity contours are shown in Fig. 29 for comparison. It is seen that at each time step, the regions of high vorticity concentration coincide with the center of eddies shown in the corresponding rest streamlines patterns. One thus may conclude that in the vortex shedding process, the vorticity produced by the block is first accumulated in the eddies formed behind the block and then carried downstream by the eddies when they are shedded. The vorticity is then diffused away rapidly. Similar vortex shedding processes are also predicted in the cases of Re = 50 and 200. The streamlines, rest streamlines and

vorticity contours are plotted in Figures 30 and 31 for Re = 50 and 200 respectively. The corresponding Strouhal numbers are 0.14 and 0.135, which also follow the correct trend of the experiment [53] that gives approximately 0.140 and 0.155 for Re = 50 and 200 respectively.

For a higher Reynolds number of 500, the FA solution of streamlines is shown in Fig. 32. Which shows that vortex are shedded alternatively. However, eddies are not easy to observe from Fig. 32. Thus, the rest streamlines are plotted in Fig. 33 to capture the vortex shedding process. The vorticity contours shown in Fig. 34 exhibit a higher concentration and a slimer shape than those obtained at lower Reynolds numbers. Experiments of Blevins [53] show that the Strouhal numbers for various non-circular section obstacles at high Reynolds numbers lie between 0.12 and 0.16. In the present study, the Strouhal number for Re = 500 is estimated to be about 0.13, which agrees quite well with the experimental data [53] although at higher Reynolds number of 500, the flow may be in the transition region.

It should be remarked here that all of the calculations performed in this section are based on relatively coarse nonuniform grids (48×25 for Re = 10, 50, 100, 200 and 48×37 for Re = 500) with fairly large time increments of 0.2 and 0.5. Yet accurate and stable solutions are

obtained. On the other hand, the dimensionless time increment used by Fromm & Harlow [51] is restricted to a much smaller increment of about 0.03. Smith & Berbbia [52] also used a small time increment of 0.03 for Re = 100, and even smaller time increments are needed for higher Reynolds numbers. It should be remarked here also that coarser grids may indeed be used in predicting FA solution for Re = 500 if the calculation of FA coefficients for large grid sizes that requires the summation of large exponential functions can be made by the present computer facility. As mentioned before, there is only one series summation term E_2 (or E_2') needed to be evaluated numerically. In most of the cases considered in Sections VII-1 and VII-2, accurate FA coefficients can be obtained with 10 to 15 terms summation of Fourier series containing exponential function, exp(s), of order $s \leq 100$. However, for some combinations of A, B, h and k, accurate series summation of E_2 (or E_2') can not be obtained (i.e., $s > 100$) with present generation of computer due to the computer round-off error. Thus, large mesh sizes are not employed in the present calculation, so that the difficulty of evaluating FA coefficients is avoided. It is possible to replace E_2 or E_2' by some approximate analytic expression, so that all calculations of series summation can be eliminated and the limitation in numerical evaluation of

FA coefficients for large Ah, Bk etc. can then be removed. In the preliminary study, an approximated expression of eq(III-51) based on a collocation formulation is given in Chen & Chen [55] for an equal grid spacing local element of $h_E = h_W = h_N = h_S = h$ as

$$\phi_P = \frac{1}{1 + \frac{R}{\tau} C_P} [\, G_1 (e^{-Ah}\phi_{EC} + e^{Ah}\phi_{WC} + e^{-Bh}\phi_{NC} + e^{Bh}\phi_{SC}) +$$

$$G_2 (e^{-Ah-Bh}\phi_{NE} + e^{Ah-Bh}\phi_{NW} + e^{-Ah+Bh}\phi_{SE} + e^{Ah+Bh}\phi_{SW})$$

$$+ \frac{R}{\tau} C_P \phi_P^{n-1} - C_P f_P] \qquad \text{(VII-8)}$$

where

$$G_1 = \frac{Bh\ \sinh Ah\ \cosh Bh - Ah\ \sinh Ah\ \cosh Bh}{2(Bh\ \cosh^2 Bh\ \sinh Ah - Ah\ \cosh^2 Ah\ \sinh Bh)}$$

$$G_2 = \frac{Ah\ \sinh Bh - Bh\ \sinh Ah}{4(Bh\ \cosh^2 Bh\ \sinh Ah - Ah\ \cosh^2 Ah\ \sinh Bh)}$$

and

$$C_P = \frac{\cosh Ah - \cosh Bh}{2(Ah\ \cosh Ah\ \coth Ah - Bh\ \cosh Bh\ \coth Bh)}$$

It should be remarked that even though eq(VII-8) is only an approximate expression, the FA coefficients based on eq(VII-8) will recover the Greenspan formula [17] in pure diffusion case (A = B = 0) and approach the same asymptotic values as those given in FA formula (III-51) for the convective dominated cases. If eq(VII-8) is used in

the calculation for FA coefficients of equal grid spacing, the difficulty and restriction in evaluating E_2 (or E_2') is then resolved.

At the time of writing this thesis, Cheng [56] has proposed another approximation formula for the summation term E_2 as

$$E_2 = \frac{1}{4ABh^2 \sinh Bk \cosh Ah}\left[A\left(1 - \frac{Bk\cosh Bk}{\sinh Bk}\right) + \frac{B^2 h \sinh Ah}{\cosh Ah}\right] * \frac{\sinh \mu_1 k}{\mu_1 \cosh \mu_1 k} \qquad \text{(VII-9)}$$

where

$$\mu_1 = \sqrt{A^2 + B^2 + \left(\frac{\pi}{2h}\right)^2}$$

Therefore, the difficuly and restriction in evaluating E_2 for uniform and nonuniform grid spacing local elements can be approximately circumvented. Currently, further study in evaluating E_2 without a series summation applicable to nonuniform grid spacing local element is under investigation.

VII-3 Two-Dimensional Starting Cavity Flow in Primitive Variable Formulation

As mentioned earlier in Chapter V, the vorticity-streamfunction formulation suffers from some disadvantages when applied to turbulent or 3D fluid

flow problems. Thus, a formulation using the so-called primitive variables, i.e., velocities and pressure becomes attractive for these complicate fluid flow problems. However, additional efforts should be devoted to resolve the pressure-velocity coupling one way or another. In past two decades, several numerical schemes [22-28], which are capable of solving the pressure-velocity coupling problem were developed. Again, the driven cavity flow problem is often chosen to test these numerical schemes.

Ghia, Hankey & Hodge [47] employed a totally central difference scheme to solve the driven cavity flow in primitive variable formulation. In order to avoid the nonlinear instability resulted from the pressure-velocity coupling, the dilatation term in Possion equation (V-6) for pressure is kept. The numerical solutions for Re = 100, 400 and 1000 were obtained by both uniform and nonuniform grids ranging from 15×15 to 57×57. Goda [25] employed a numerical algorithm based on a simple variant of Chorin method [23] to solve the two-dimensional driven cavity flow in terms of primitive variables. The central difference scheme was used to discretize the governing equations in a staggered grid coordinate system. An auxillary velocity field introduced by Chorin [23] was invoked to resolve the pressure-velocity coupling problem. Rather complicate boundary conditions for pressure and

auxillary velocity field are needed to keep the numerical accuracy. Bercovier & Engleman [48] used a finite element method of penalization type to solve the two-dimensional cavity flow problem. In their calculations, rather coarse grid were used to obtain the numerical solution for Re = 0, 100, 400 and 1000. The results exhibit the same features as those obtained by Ghia et al. [47] and Goda [25]. However, oscillations in velocity field were encountered near the wall. Singh [22] employed the finite analytic method developed by Chen et al. [5,6] to solve the same problem for Re = 100, 400 and 800. A momentum-averaging scheme is used to resolve the pressure-velocity coupling, so that a continuity-satisfied velocity field can be obtained.

In the present calculation of FA solution, the starting cavity flows for Re = 100, 400 and 1000 are solved in a staggered grid coordinate system using uniform meshs ranging from 21×21 to 41×41. In order to apply the no-slip boundary conditions exactly on the moving and stationary walls, control volumes of zero thickness are chosen along the wall (see Fig. 8). The 10-point FA formula for unsteady two-dimensional convective transport equation based on nonuniform grid local element is employed to discretize the momentum equations. A pseudovelocity field described in eq(V-9) of Section V-2 is then introduced

so that the pressure field can be obtained via the equation of continuity. The guessed flow field is corrected by velocity-correction formulas (V-14a) - (V-14c) to obtain a continuity-satisfied flow field [11]. Detailed numerical procedures are given previously in Section V-2.

In order to obtain the steady-state solutions more rapidly, the convergence criterion for intermediate time steps are relaxed. Furthermore, the convection coefficients 2A and 2B are evaluated in terms of the velocities of previous time steps, so that the computational time needed can be minimized. In all calculations, zero initial velocity field is specified at the beginning, time increments ranging from 0.1 to 0.6 are used to obtain the steady-state solutions.

In the present algorithm, the velocity field governed by equations (III-23) and (III-24) satisfies the equation of continuity (III-22) at each iteration or each time step after employing the velocity-correction formulas (V-14a) - (V-14c). Thus, the corresponding streamfunction can be easily obtained by simple integration of the velocity field along suitable paths. In this study, the streamfunction at any field point is obtained by integrating the horizontal velocity u along constant x lines. The steady streamfunctions thus obtained are shown in Fig. 35 for Re = 100, 400 and 1000 respectively. The results shown in

Figs. 35(a) thru 35(d) agree well with those FA solutions obtained by the vorticity-streamfunction formluation given in Figures 12, 14, 20 and 21. The magnitude and direction of the velocity field are shown in Figs 36(a) thru 36(d) in terms of flow vectors for Re = 100, 400 and 1000 respectively. It can be seen that the vortex center moves gradually toward the geometric center as Reynolds number increases. Moreover, the velocity field obtained in the 21×21 or 41×41 uniform grids for Re = 1000 in Figs. 36(c) or 36(d) shows a boundary layer phenomenon near the top wall. It is also noted that, unlike the vorticity-streamfunction formulation, the sizes of the secondary vortices are relatively insensitive to the mesh size used in the primitive variable formulation. This is due to the fact that the no-slip and impermeable boundary conditions are exactly satisfied in the primitive variable formulation, while the vorticity boundary conditions are strongly dependent on the grid sizes employed near the wall. In additional to the streamlines and flow vector profiles, the pressure field which is not calculated in vorticity-streamfunction formulation is given in Fig. 37. The results are also in good agreement with those obtained by Burggraf [31], Singh [22] and Ghia et al. [47].

In this study, the FA numerical solutions based on nonuniform grids are also obtained for Re = 400 and 1000. In general, some improvement of numerical results are anticipated when computed in nonuniform grids. However, negligible improvement is found in using nonuniform grids when same numbers of total grid points are employed. One may wonder why the calculation with nonuniform grids does not differ from that with uniform grids; one possible reason may be due to the loss of accuracy in the evaluation of pressure gradient terms which should be encountered for all numerical schemes formulated in staggered grids when nonuniform grids are used. It can be seen from eq(V-8a) that the pressure gradient term is only first-order accurate if the point e is not located at the midway of point EC and point P. The attempt to obtain a second-order accurate representation of pressure gradient term would lead to more complicate governing equation for pressure and thus offset the advantages gained in using nonuniform grids. In future study, it is proposed, when situations allow, to use the regular grid instead of the staggered grid coordinate system, so that the pressure gradient which forms a part of the source term for a momentum equation can be accurately evaluated.

CHAPTER VIII

EXAMPLES OF THREE-DIMENSIONAL FLUID FLOW PROBLEMS

In this chapter, the 28-point FA formula for unsteady three-dimensional convective transport equation is employed to solve a simple three-dimensional cavity flow driven by a moving wall. Due to its simple geometry and boundary conditions, the three-dimensional cavity flow is often chosen to test the new numerical schemes for steady or unsteady Navier-Stokes equations. Takami & Kuwahara [26] employed a modified Chorin method [23] but using the acceleration instead of velocity field as the dependent variable to solve the three-dimensional cavity flow problem for Re = 0, 100 and 400. All of the results are calculated in a staggered grid coordinate system using mesh size of 0.05. Small time increment of 0.025 is used for Re = 100 and 400 while a smaller time increment of 0.02 is used for Re = 0. Goda [25] used a technique which is also based on a simple variant of Chorin's method to solve the same cavity flow problem for Re = 100 and 400. The numerical solutions are obtained in a staggered grid coordinate system of equal grid size of 0.05. The results in general agree with those reported by Takami &

Kuwahara [26]. In both cases, the pressure field is solved directly via the equation of continuity, thus only four equations are needed to obtain the velocity and pressure fields. On the other hand, the vorticity-based formulations may also be employed. For example, Vahl Davis & Mallinson [32] used the vorticity-vector potential formulation to solve the three-dimensional cavity flow problem at Re = 100 and 400 for aspect ratio ranging from 1 to 5 to study the effect of three-dimensionality on the two-dimensional model. Dennis et. al [21] employed a vorticity-velocity formulation to study the cubic cavity flow problem up to Reynolds number of 100, but the attempt for Re = 400 was not succeeded. Agarawal [57] used the same vorticity-velocity formulation, but instead of diagonal dominated second-order finite difference scheme, a third-order accurate upwind scheme is employed to solve the steady cavity flow problem for Re = 0, 100 and 400. Three different mesh sizes of 0.1, 0.0625 and 0.05 were used to obtain the numerical solutions. The results agree quite well with those reported by Takami & Kuwahara [26] and Goda [25].

In the present study, the primitive variable formulation described in Section V-2 is adopted to formulate the three-dimensional starting cavity flow problems in terms of u, v, w and p. The cubic cavity of

unit length shown in Fig. 38 is driven by the bottom wall with unit normalized velocity in the positive x-direction. Because of the symmetry with respect to the plane $y = 0.5$, only half of the flow domain needed to be considered. The flow domain is divided into many rectangular control volumes and a staggered grid arrangement described in Section V-2 is employed. In other word, the pressure is calculated at the center of the control volume, while the velocities u, v and w are calculated at staggered locations across the control surfaces. Furthermore, control volumes of zero thickness are chosen along the wall, so that the no-slip condition can also be applied exactly on the moving and stationary walls. Symmetric boundary conditions at $y = 0.5$ are satisfied by equating the velocities u and w at plane $y = \frac{1}{2}(1 + \Delta y)$ to those at plane $y = \frac{1}{2}(1 - \Delta y)$. The boundary condition for pressure is not needed since pressure is needed only to compute velocity but the impermeable boundary conditions prescribe the zero normal velocities already on the boundaries.

Following the numerical procedures described in Sec. V-2, the starting cavity flows of Reynolds numbers of 100 and 400 are solved using uniform mesh sizes of $\Delta x = \Delta y = \Delta z = 0.1$ and $\Delta x = \Delta z = 0.0625$, $\Delta y = 0.125$ respectively. Due to the limited computer storage available, no attempt was made to calculate the results in finer mesh sizes

or higher Reynolds numbers. A time increment of 0.3 is used in both cases, while the steady-state solutions are achieved in 50 time steps.

The steady-state x-component velocity profiles on the plane x = 0.5 are shown in Figs. 39(a) and 39(b) for Re = 100 and 400. The results in general agree well with those obtained by Goda [25], Takami & Kuwahara [26] and Agarwal [57], even though coarser grids of 0.1 and 0.0625 are used in the present study. For the case of Re = 100, the x-component velocity profile at central part y = 0.45 is almost two-dimensional. However, the maximum velocity in y-direction, which occurs near the vortex center in xz plane, still has a magnitude of 0.025. As the Reynolds number increases to 400, the magnitude of the secondary flow increases, and the x-component velocity profile at y = 0.4375 differs significantly from that at y = 0.3125. It indicates that the effect of the side walls at y = 0 and y = 1 on the total flow becomes important, and the flow pattern at y = 0.5 thus differs significantly from the two-dimensional pattern at the same Reynolds number. The finite analytic solution also agrees well with the study of Vahl Davis & Mallinson [32], where the effect of side walls at different aspect ratio is reported.

Since the scalar streamfunction does not exist in three-dimensional flows, it is better to examine the

flow structure in the xz plane by means of the flow vectors so that a comparison with two-dimensional cavity flow can be meaningfully made. Figs. 40 and 41 show the profiles of flow vectors in the plane $y = \frac{1}{2}\Delta y$ and $y = \frac{1}{2}(1 - \Delta y)$ for Reynolds numbers of 100 and 400 respectively. It can be seen that the magnitude of the flow vectors at $y = \frac{1}{2}\Delta y$ is greatly affected by the presence of the side walls in y-direction and the locations of the vortex centers are closer to the moving wall than those at $y = \frac{1}{2}(1 - \Delta y)$. In additional to the profiles of flow vectors, the corresponding magnitude of the velocity components u and w at $y = \frac{1}{2}\Delta y$ and $\frac{1}{2}(1 - \Delta y)$ for Reynolds number 400 are shown in Figures 42 and 43 respectively. However, the flow direction and magnitude can only be completely described until the velocity normal to xz plane is prescribed. Thus, the secondary flow for Re = 400 in y-direction is given in Figs. 44(a) thru 44(c). It can be seen that there is a tendency for the flow around the vortex center to go toward the center of the cubic cavity. On the other hand, except for part of the right wall, the flow near the boundaries goes toward the side walls at y = 0 and y = 1. All of the velocity contours agree fairly well with those obtained by Agarwal [57] and Goda [25].

Due to the limited computer storage presently available at the University of Iowa computer center, no attempt was made to calculate the numerical results for Reynolds numbers higher than 400. However, from the finite analytic numerical solutions for Re = 100 and 400, it may still be concluded that the pressure gradient in y-direction and the secondary flow increase with increasing Reynolds number. Thus results in a significant reduction of the strength of primary vortex when compared with two-dimensional cases. Therefore, if one desire to obtain an approximately two-dimensional cavity flow experimentally or numerically from a three-dimensional set up, it is suggested that the aspect ratio of the three-dimensional cavity should increase with increasing Reynold numbers so that the two-dimensional assumption can be insured. However, viscous effect of the side walls may decrease for very large Reynolds numbers.

It should be remarked here that in cited previous works, relatively small time increments were needed for most of the unsteady numerical schemes so that stable numerical solutions can be obtained. For example, the time increment used by Goda [25] is restricted by $\tau < h/|u_{max}|$. Even smaller time increments of 0.02 and 0.025 are used in Takami & Kuwahara [26] in solving three-dimensional cavity flow problems. On the other hand,

a large time increment of 0.3 was used in the finite analytic method, while even larger time increment is still possible. Thus, the stability of the present FA method is also established in the three-dimensional calculation. Moreover, the fact that the 28-point FA formula provides all-positive coefficients and desired upwind shift gurantees that physical realistic numerical solution with minimum false numerical diffusion can be obtained as long as the problem is well-posed. There is, however, some improvements can still be made in the present FA method. It is noted that the use of staggered grid coordinate requires three sets of FA coefficients for u, v and w respectively and the evaluation of pressure gradient is only of first-order accuracy when nonuniform mesh is employed. The use of regular grid instead of staggered can not only reduce the computer storage and computational time needed but also provide accurate higher order evaluation of pressure gradient terms. It is also noted that there are four series summation terms needed to be evaluated numerically. For high Reynolds numbers, the evaluation of these summation terms could be very time-consuming or even diverged due to the round-off error in the present day computers. If the series summation terms are replaced by some approximation functions, then the limitation in evaluating

FA coefficients can be removed. Also, the computational time is significantly reduced.

CHAPTER IX

CONCLUSIONS

The finite analytic solutions for unsteady 1D, 2D and 3D convective transport equations are derived in both uniform and nonuniform grid spacing local elements. When the present finite analytic solution is compared with the finite analytic solution obtained by Chen et al. [5,6] for steady two-dimensional case, significant improvements are seen due to the better boundary approximations and the better linearization scheme for convective terms. The improved 10-point FA formula for unsteady two-dimensional convective transport equation is employed to study the two-dimensional starting cavity flows and vortex shedding processes behind a rectangular block. The finite analytic numerical solutions for the driven cavity flow are obtained using both vorticity-streamfunction and primitive variable formulations. In vorticity-streamfunction formulation, contour plots of streamfunction and vorticity at steady-state are provided for Reynolds number of 100, 400, 1000, 2000 and 5000. Transient solutions of the starting cavity flow are also given in the cases of Re = 1000, 2000 and 5000. In primitive variable formulation, the

streamlines, pressure contours and flow vector profiles are plotted for Re = 100, 400 and 1000. The results agree well with those obtained in vorticity-streamfunction formulation. The vortex shedding phenomenon is then studied by investigating the transient solutions of uniform flow passing a rectangular block of height L and width L/4. The numerical solutions for streamlines and vorticity contours are given for Reynolds numbers of 10, 50, 100, 200 and 500. Except for Re = 10, vortex street developments are observed. The flow patterns and the corresponding Strouhal numbers obtained from finite analytic method are consistent with theoretical and experimental studies.

In three-dimensional case, the 28-point FA formula formulated in terms of the primitive variables is employed to solve a three-dimensional cubic cavity flow problem. Flow vector profiles and contour plots of velocities at several cross-sections are given. The numerical solutions show that the presence of the side walls reduce the strength of the primary vortex when compared with the two-dimensional square cavity flow. Furthermore, this effect becomes significant for Reynolds number of 400.

In all of the test problems considered, the finite analytic numerical solutions are shown to be accurate and stable. Significant results are summarized in the following.

(1) In steady two-dimensional case, the FA solution based on exponential and linear boundary approximations does give all-positive FA coefficients, which is more reasonable and requires less computational time than those obtained by Chen etal. [5,6]. Thus, the extension to unsteady three-dimensional cases becomes practical.

(2) The 28-point FA formula for unsteady 3D convective transport equation derived in a nonuniform grid spacing local element gives physically realistic all-positive coefficients and exhibits a desired upwind shift. Furthermore, the false numerical diffusion is minimized because of the inclusion of all corner points.

(3) Higher order corrections for the convective terms in Navier-Stokes equations are considered in this dissertation. It significantly improves the linearization scheme and the accuracy of the FA solutions.

(4) The equivalent under-relaxation factor for steady-state iterative method can be derived from the FA solution for unsteady flow. It is found that the under-relaxation factor for steady Navier-Stokes equations varies from element to element, and make the FA numerical solution more stable than the

solution obtained with constant under-relaxation factor in the steady-state iterative method.

(5) For unsteady fluid flow problems, large time increment that is several times of mesh size can be often used to obtain the FA solution for transient problems. Even larger time increments can be employed in the FA method to calculate steady problems. Thus, the stability and computational efficiency of the present FA method is demonstrated.

There are, however, still some improvements in the present FA method that can be made in future study. Firstly, the series summation terms required in evaluating the FA coefficients can be replaced by some approximation functions so that the limitation in numerical evaluation of FA coefficients can be removed, and the computational time can be further reduced. Secondly, for convection dominated cases where the downstream FA coefficients are practically zero, it is possible to improve the accuracy in these cases by taking more upstream nodal points into account in deriving the FA coefficients. Thirdly, for problems where recirculating flows occur in only part of the domain, it is instructive to incorporate the simple exponential scheme or power-law scheme [11] in the finite analytic formulation, so that the accurate solutions can be obtained more economically.

Ah	10^{-7}	10^{-2}	10^{-1}	1	10	10^{2}	10^{8}
C_{NW}	0.5000	0.4975	0.4722	0.2566	0.0488	0.0050	10^{-8}
C_{NE}	0.5000	0.4876	0.3866	0.0347	10^{-10}	10^{-87}	0
C_{WC}	10^{-7}	0.0100	0.1005	0.5997	0.9040	0.9900	1.000
C_{EC}	10^{-7}	0.0098	0.0823	0.0812	10^{-9}	10^{-87}	0
C_{SW}	-10^{-8}	-0.0025	-0.0229	-0.0053	0.0449	0.0050	10^{-8}
C_{SE}	-10^{-8}	-0.0024	-0.0187	-0.0013	-0.0006	-10^{-14}	0
C_{SC}	0	10^{-17}	10^{-11}	0.0345	0.0028	10^{-14}	0

Table (1) FA coefficients for unsteady 1D convective transport equation with second-order polynomial initial and boundary approximation for Courant number $C_0 = 1$

Ah	10^{-7}	10^{-2}	10^{-1}	1	10	10^{2}	10^{8}
C_{NW}	0.1093	0.1104	0.1206	0.2566	0.8555	0.9851	1.000
C_{NE}	0.1093	0.1082	0.0988	0.0347	10^{-9}	10^{-87}	0
C_{WC}	0.3251	0.3284	0.3579	0.5997	0.1890	0.0199	10^{-8}
C_{EC}	0.3251	0.3219	0.2930	0.0812	10^{-10}	10^{-89}	0
C_{SW}	0.0218	0.0220	0.0237	-0.0053	-0.0445	-0.0495	10^{-8}
C_{SE}	0.0218	0.0216	0.0194	-0.0013	-10^{-10}	-10^{-89}	0
C_{SC}	0.0875	0.0875	0.0867	0.0345	10^{-43}	0	0

Table (2) FA coefficients for unsteady 1D convective transport equation with second-order polynomial initial and boundary approximation for $Bh^2/2\tau=1$

Ah	0.001	0.01	0.1	1	10	100
C_{WC}	0.27215	0.27461	0.29958	0.55647	0.95000	0.99500
C_{EC}	0.27160	0.26917	0.24527	0.07531	10^{-9}	10^{-87}
C_{SW}	0.18454	0.18620	0.20260	0.29523	0.05000	0.00500
C_{SC}	0.08752	0.08751	0.08667	0.03303	10^{-43}	0
C_{SE}	0.18417	0.18251	0.16588	0.03996	10^{-10}	10^{-89}

Table (3) FA coefficients for unsteady 1D convective transport equation with exponential and linear initial approximation and linear boundary approximations for $Bh^2/2\tau = 0.5$

$Bh^2/2\tau$	C_{WC}	C_{EC}	C_{SW}	C_{SC}	C_{SE}
0	1.000000	10^{-44}	10^{-8}	0	10^{-52}
10	0.800000	10^{-44}	0.200000	10^{-38}	10^{-44}
20	0.600000	10^{-44}	0.400000	10^{-13}	10^{-44}
30	0.400003	10^{-44}	0.599991	0.000005	10^{-44}
40	0.203003	10^{-44}	0.793244	0.003754	10^{-44}
50	0.056150	10^{-45}	0.887717	0.056141	10^{-44}
60	0.007097	10^{-46}	0.820323	0.172581	10^{-44}
70	0.003887	10^{-46}	0.707623	0.288491	10^{-44}

Table (4) FA coefficients for unsteady 1D convective transport equation with exponential and linear initial approximation and linear boundary approximations for Ah = 50

$Bh^2/2\tau$	C_{WC}	C_{EC}	C_{SC}
0	1.000000	10^{-44}	0
10	0.833333	10^{-44}	0.166667
20	0.714286	10^{-44}	0.285714
30	0.625000	10^{-44}	0.375000
40	0.555556	10^{-44}	0.444444
50	0.500000	10^{-44}	0.500000
60	0.454545	10^{-44}	0.545455
70	0.416667	10^{-44}	0.583333

Table (5) FA coefficients for unsteady 1D convective transport equation with hybrid FA formulation for Ah = 50

	FAEL	FASP	FAPL
$C_{EC}=C_{WC}=C_{NC}=C_{SC}$	0.20531	0.20531	0.16234
$C_{NE}=C_{NW}=C_{SE}=C_{SW}$	0.04469	0.04469	0.08766

Table (6) Comparison of FA coefficients for Laplace equation (A = B = 0) in an equal grid spacing local element of $h_E = h_W = h_N = h_S = h$

	FAEL	FASP	FAPL
C_{SW}	0.52286	0.43650	0.52927
$C_{WC} = C_{SC}$	0.23854	0.32490	0.23212
$C_{NW} = C_{SE}$	0.00323	0.00002	0.00323
$C_{EC} = C_{NC}$	0.00001	-0.04316	0.00001
C_{NE}	10^{-9}	-10^{-6}	10^{-7}

Table (7) Comparison of FA coefficients for steady 2D convective transport equation in an equal grid spacing local element of $h_E = h_W = h_N = h_S = h$ for Ah = Bh = 5

	FAEL	FASP	FAPL
C_{WC}	0.9800	0.9800	0.8874
$C_{NW} = C_{SW}$	0.0100	0.0100	0.0563
$C_{NC} = C_{SC}$	10^{-11}	0	10^{-11}
$C_{NE} = C_{SE}$	10^{-48}	0	10^{-25}
C_{EC}	10^{-44}	0	10^{-44}

Table (8) Comparison of FA coefficients for steady 2D convective transport equation in an equal grid spacing local element of $h_E = h_W = h_N = h_S = h$ for Ah = 50, Bh = 0

	FAEL	FASP	FAPL
C_{SW}	0.49969	0.38704	0.49950
C_{SC}	0.00020	0.00038	0.00035
C_{SE}	10^{-44}	10^{-4}	10^{-35}
C_{WC}	0.50010	0.72522	0.50013
C_{EC}	10^{-44}	10^{-43}	10^{-40}
C_{NW}	10^{-22}	-0.11256	0.00001
C_{NC}	10^{-26}	10^{-25}	10^{-23}
C_{NE}	10^{-66}	10^{-25}	10^{-35}

Table (9) Comparison of FA coefficients for steady 2D convective transport equation in a local element of $h_E = h_W = h_N = h_S = h$ for $Ah = 50$, $Bh = 25$

h/k	1	2	5	∞
$C_{EC} = C_{WC}$	0.20531	0.04451	0.00040	0
$C_{NC} = C_{SC}$	0.20531	0.38613	0.48002	0.5
$C_{NE} = C_{NW}$	0.04469	0.03468	0.00979	0
$C_{SE} = C_{SW}$	0.04469	0.03468	0.00979	0

Table (10) FA coefficients for Laplace equation (A = B = 0) in a local element of $h_E = h_W = h$ and $h_N = h_S = k$

h/k	1	2	5	10
C_{SW}	0.30845	0.32953	0.18648	0.09466
C_{SC}	0.33396	0.55522	0.79314	0.88735
C_{SE}	0.00565	0.00011	10^{-10}	10^{-18}
C_{WC}	0.33396	0.09891	0.00244	10^{-6}
C_{EC}	0.00612	0.00003	10^{-11}	10^{-22}
C_{NW}	0.00565	0.00604	0.00342	0.00173
C_{NC}	0.00612	0.01017	0.01453	0.01625
C_{NE}	0.00010	10^{-6}	10^{-11}	10^{-20}

Table (11) FA coefficients for steady 2D convective transport equation with exponential and linear boundary approximation in a local element of $h_E = h_W = h$, $h_N = h_S = k = 0.1$ and $A = B = 20$

Rh^2/τ	0.00001	0.1	1	10	1000
C'_{SW}	0.52282	0.52246	0.48587	0.29685	0.00678
$C'_{WC} = C'_{SC}$	0.23853	0.23673	0.22166	0.13543	0.00309
$C'_{NW} = C'_{SE}$	0.00002	0.00002	0.00002	0.00002	10^{-7}
$C'_{NC} = C'_{EC}$	0.00001	0.00001	0.00001	0.00001	10^{-7}
C'_{NE}	10^{-9}	10^{-9}	10^{-9}	10^{-9}	10^{-11}
C'_P	0.00001	0.00756	0.07075	0.43226	0.98704

Table (12) FA coefficients for unsteady 2D convective transport equation with exponential and linear boundary approximations ($h = k$, $Ah = Bh = 5$)

Ch	0	.1	10	100
C_{BC}	0.11363	0.25008	0.81127	0.98010
$C_{ECB}=C_{WCB}=C_{SCB}=C_{NCB}$	0.02394	0.04966	0.04380	0.00495
$C_{SEB}=C_{SWB}=C_{NEB}=C_{NWB}$	0.00386	0.00780	0.00257	0.00003
$C_{EC} = C_{WC} = C_{NC} = C_{SC}$	0.11363	0.09419	0.00072	10^{-16}
$C_{NEC}=C_{NWC}=C_{SEC}=C_{SWC}$	0.02394	0.01960	0.00008	10^{-17}
$C_{ECT}=C_{WCT}=C_{NCT}=C_{SCT}$	0.02394	0.00672	10^{-10}	10^{-89}
$C_{NET}=C_{NWT}=C_{SET}=C_{SWT}$	0.00386	0.00106	10^{-11}	10^{-92}
C_{TC}	0.11363	0.03384	10^{-9}	10^{-87}

Table (13) FA coefficients for steady 3D convective transport equation in a local element of equal grid spacing $h_E = h_W = h_N = h_S = h_T = h_B = h$ with Ah = Bh = 0

Bh = Ch	0	1	10	20	50
C_{SCB}	0.0239	0.1044	0.5981	0.7181	0.8246
C_{NCT}	0.0239	0.0019	10^{-18}	10^{-35}	10^{-87}
$C_{BC} = C_{SC}$	0.1136	0.2106	0.1596	0.1191	0.0785
$C_{NC} = C_{TC}$	0.1136	0.0285	10^{-10}	10^{-18}	10^{-45}
$C_{EC} = C_{WC}$	0.1136	0.0793	0.0001	10^{-7}	10^{-8}
$C_{NCB}=C_{SET}$	0.0239	0.0141	10^{-9}	10^{-18}	10^{-44}
$C_{SEB}=C_{SWB}$	0.0039	0.0160	0.0275	0.0167	0.0080
$C_{NET}=C_{NWT}$	0.0039	0.0003	10^{-19}	10^{-37}	10^{-89}
$C_{ECB}=C_{WCB}=C_{SEC}=C_{SWC}$	0.0239	0.0413	0.0069	0.0026	0.0006
$C_{NEB}=C_{NWB}=C_{SET}=C_{SWT}$	0.0039	0.0022	10^{-10}	10^{-19}	10^{-46}
$C_{NEC}=C_{ECT}=C_{NWC}=C_{WCT}$	0.0239	0.0056	10^{-11}	10^{-20}	10^{-47}

Table (14) FA coefficients for steady 3D convective transport equation in an equal grid spacing local element with Ah = 0

Ah = Bh = Ch	0	5	30
C_{SWB}	0.003862	0.255536	0.539682
$C_{SCB}=C_{WCB}=C_{SWC}$	0.023943	0.163256	0.127785
$C_{SEB}=C_{NWB}=C_{SWT}$	0.003862	0.000012	10^{-18}
$C_{SC}=C_{WC}=C_{BC}$	0.113631	0.084868	0.025654
$C_{SEC}=C_{NWC}=C_{SCT}$	0.023943	0.000007	10^{-18}
$C_{WCT}=C_{ECB}=C_{NCB}$	0.023943	0.000007	10^{-18}
$C_{NEB}=C_{SET}=C_{NWT}$	0.003862	10^{-9}	10^{-35}
$C_{EC}=C_{BC}=C_{TC}$	0.113631	0.000004	10^{-19}
$C_{NEC}=C_{ECT}=C_{NCT}$	0.023943	10^{-10}	10^{-36}
C_{NET}	0.003862	10^{-14}	10^{-53}

Table (15) FA coefficients for steady 3D convective transport equation in an equal grid spacing local element of $h_E = h_W = h_N = h_S = h_T = h_B = h$

x		0	0.2	0.4	0.6	0.8	1
Exact	$t \to \infty$	1	0.800000	0.600000	0.400000	0.200000	0
FASP	$t = \tau$	1	0.799968	0.599948	0.399952	0.199972	0
	$t = 2\tau$	1	0.800016	0.600026	0.400024	0.200014	0
	$t \geq 3\tau$	1	0.800000	0.600000	0.400000	0.200000	0
FAEL & Hybrid FA	$t = \tau$	1	0.799953	0.599937	0.399945	0.199969	0
	$t \geq 2\tau$	1	0.800000	0.600000	0.400000	0.200000	0

Table (16) Large time solutions for linear 1D convective transport equation. $c = 0$ (heat equation), $\alpha = 0.01$ and $\tau = 1000$

x		0	0.2	0.4	0.6	0.8	1
Exact	$t \to \infty$	1	1.000000	1.000000	1.000000	1.000000	0
FASP	$t = \tau$	1	1.000000	0.999900	0.999800	0.999700	0
	$t = 2\tau$	1	1.000000	1.000050	1.000100	1.000149	0
	$t \geq 3\tau$	1	1.000000	1.000000	1.000000	1.000000	0
FAEL & Hybrid FA	$t = \tau$	1	1.000000	0.999900	0.999800	0.999600	0
	$t \geq 2\tau$	1	1.000000	1.000000	1.000000	1.000000	0

Table (17) Large time solutions for linear 1D convective transport equation. $c = 1$, $\alpha = 0.001$, $h = 0.2$ and $\tau = 2000$

x		0	0.2	0.4	0.6	0.8	1
Exact	$t \to \infty$	1	0.999710	0.997567	0.981729	0.864704	0
FASP	$t = \tau$	1	0,999686	0.997444	0.981516	0.864451	0
	$t = 2\tau$	1	0.999721	0.997624	0.981835	0.864830	0
	$t = 3\tau$	1	0.999710	0.997566	0,981729	0.864704	0
	$t \geq 4\tau$	1	0.999710	0.997566	0,981728	0.864704	0
FAEL & Hybrid FA	$t = \tau$	1	0.999610	0.997368	0.981442	0.864385	0
	$t \geq 2\tau$	1	0.999710	0.997567	0.981729	0.864704	0

Table (18) Large time solutions for linear 1D convective transport equation. $c = 1$, $\alpha = 0.01$, $h = 0.2$ and $\tau = 2000$

x		0	0.4	0.6	0.8	0.9	1
c/α		1900	46.34	31.15	23.46	20.88	18.8
Exact	$t \to \infty$	1	0.999992	0.999798	0.987886	0.875720	0
FASP	$t = \tau$	1	0.999996	0.999957	0.988787	0.879743	0
	$t = 2\tau$	1	1.000002	0.999973	0.988814	0.879772	0
	$t \geq 3\tau$	1	1.000000	0.999968	0.988804	0.879762	0
FAEL & Hybrid FA	$t = \tau$	1	0.999995	0.999956	0.988785	0.879741	0
	$t \geq 2\tau$	1	1.000000	0.999967	0.988804	0.879761	0

Table (19) Large time solutions for linear 1D convective transport equation. $c/\alpha = 19/(x + 0.01)$, $h = 0.1$ and $\tau = 1000$

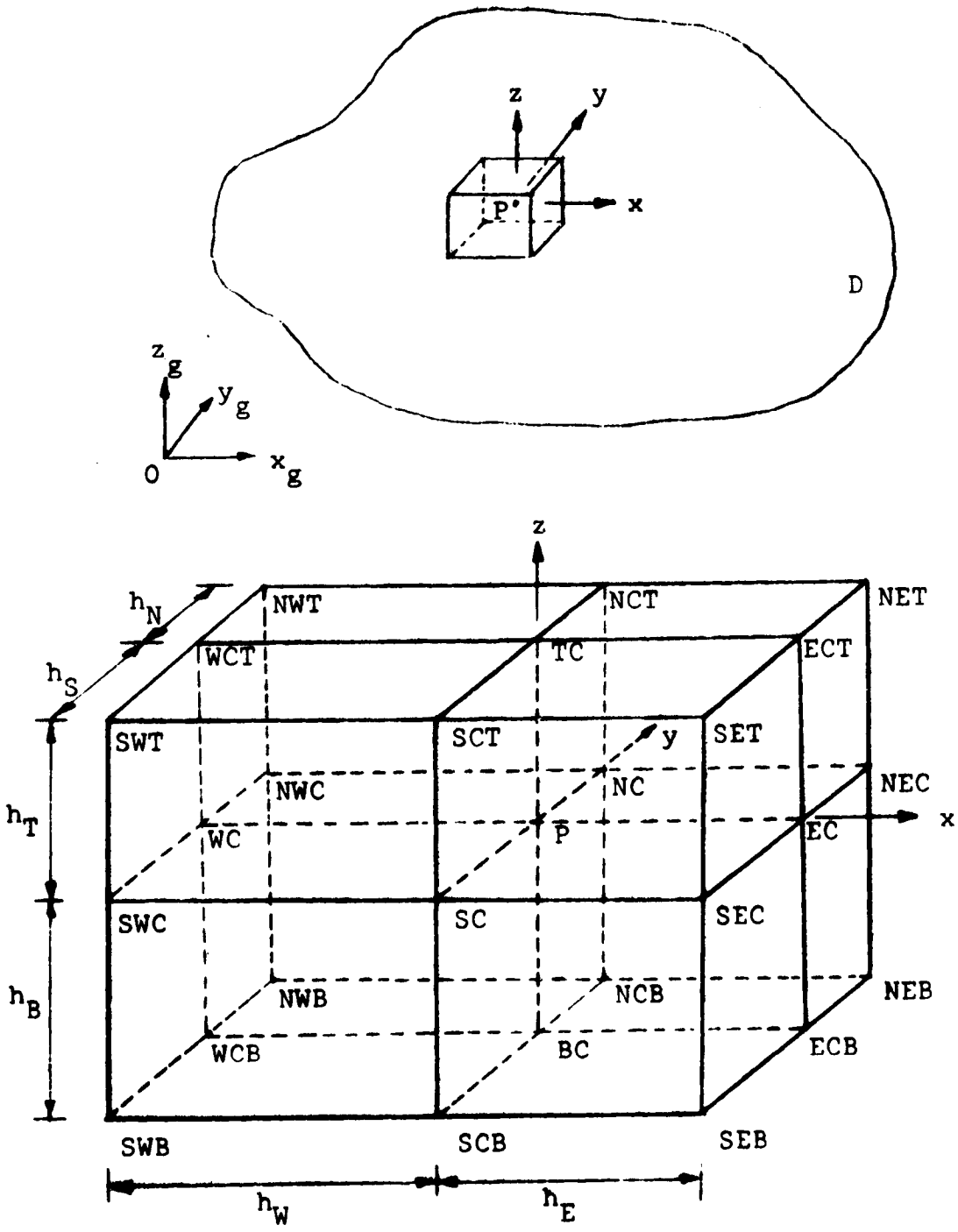

Figure 1 : Domain and local element for finite analytic formulations of unsteady three-dimensional convective transport equation.

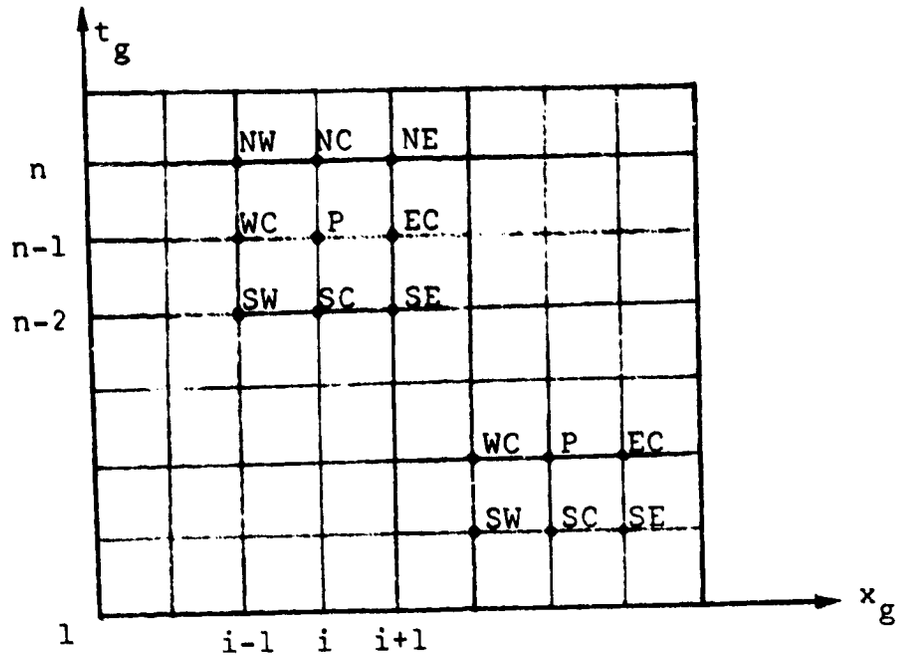

(a) Domain

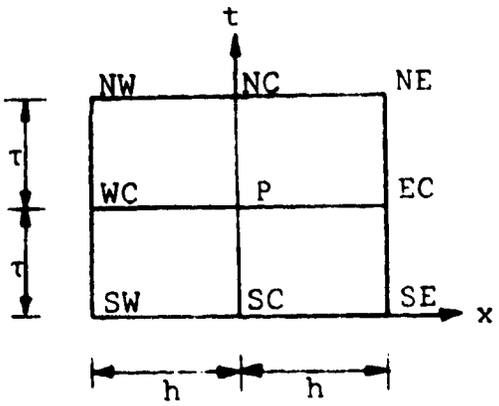

(b) Two-time step local element

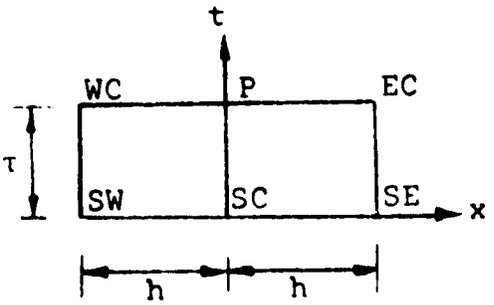

(c) One-time step local element

Figure 2 : Domain and local elements for finite analytic formulations of unsteady one-dimensional convective transport equation.

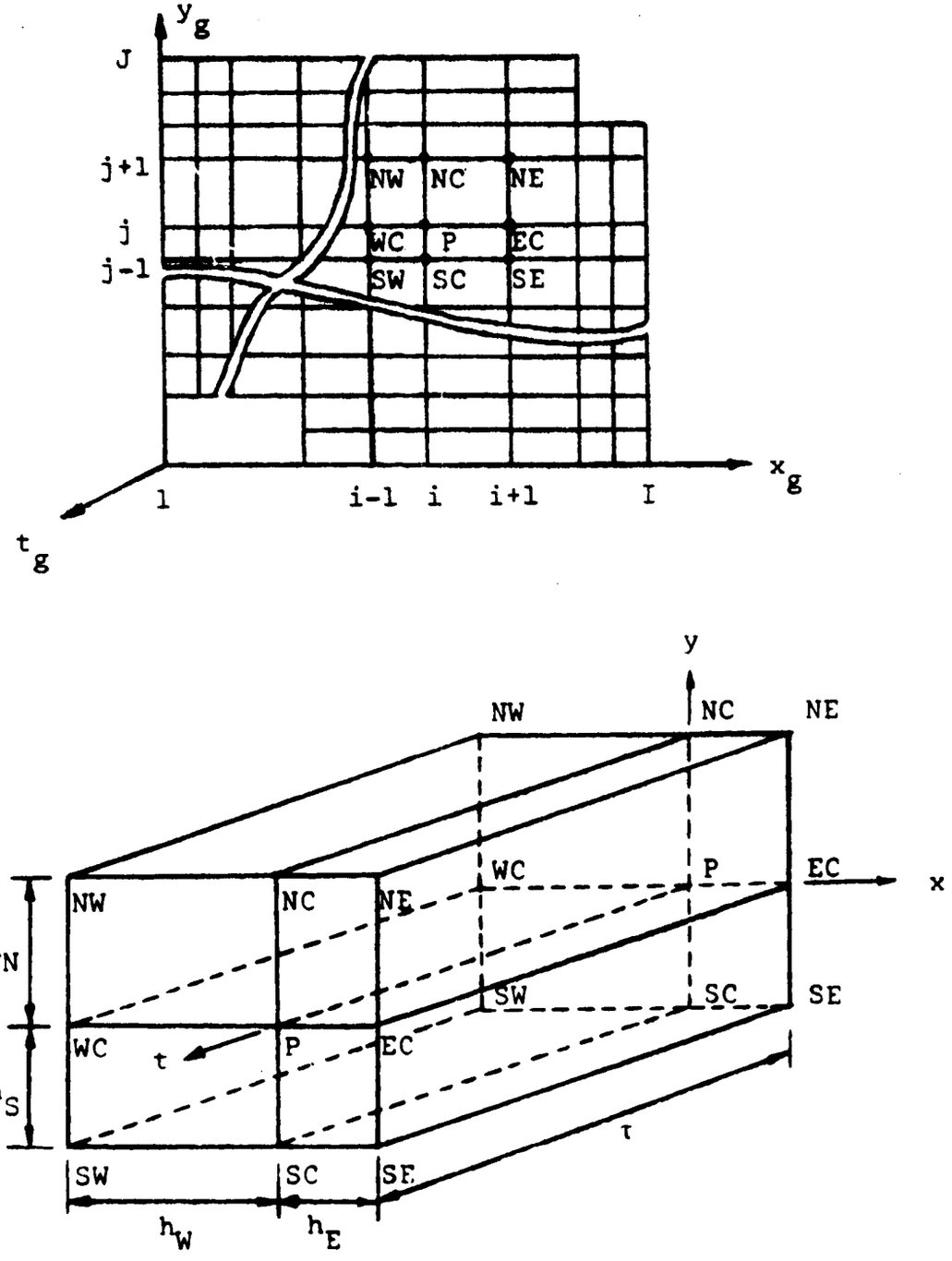

Figure 3 : Domain and local element for finite analytic formulations of unsteady two-dimensional convective transport equation.

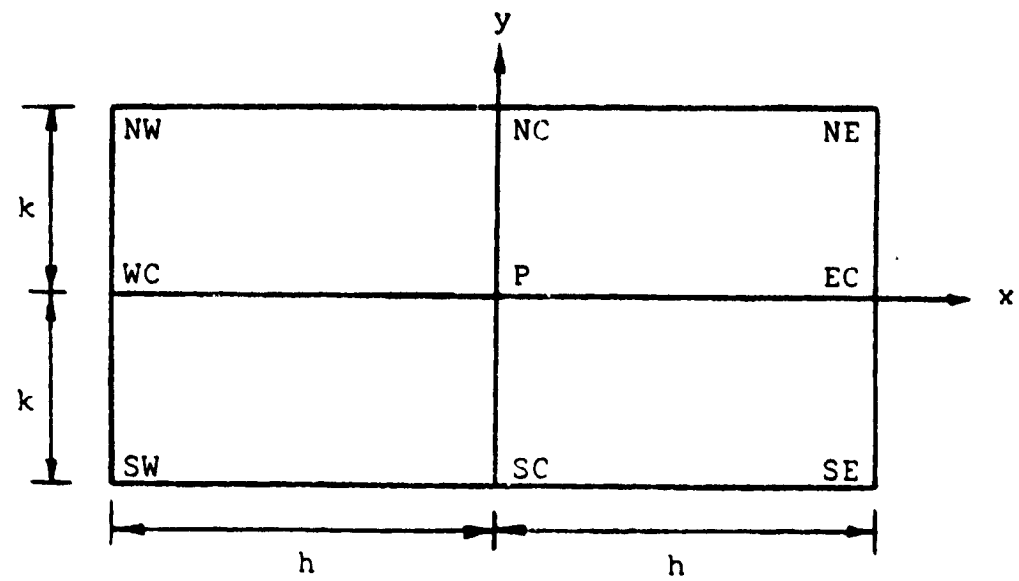

(a) Local element of uniform grid spacing

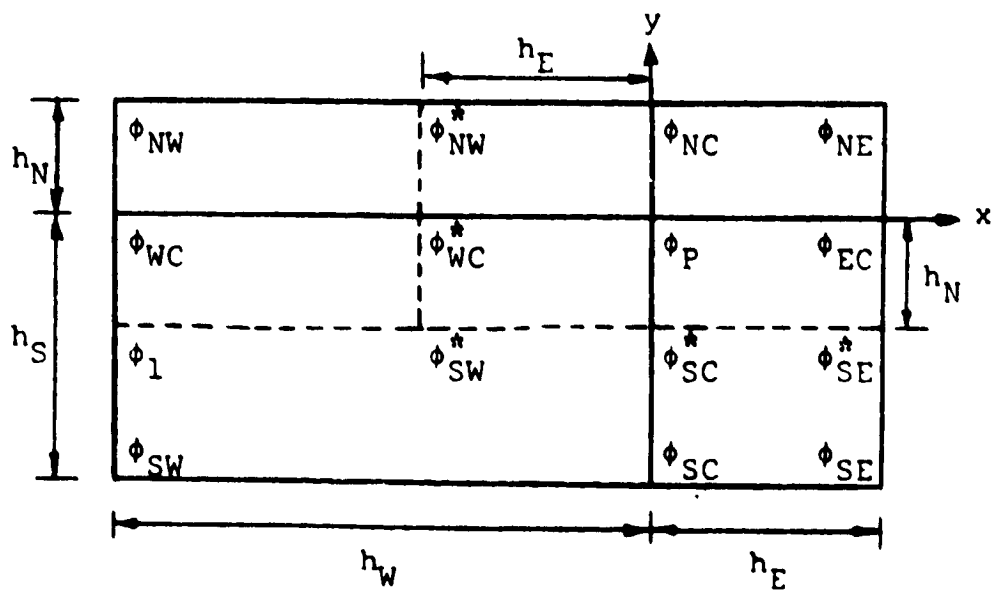

(b) Local element of nonuniform grid spacing

Figure 4 : Local elements of uniform and nonuniform grid spacing for two-dimensional convective transport equation.

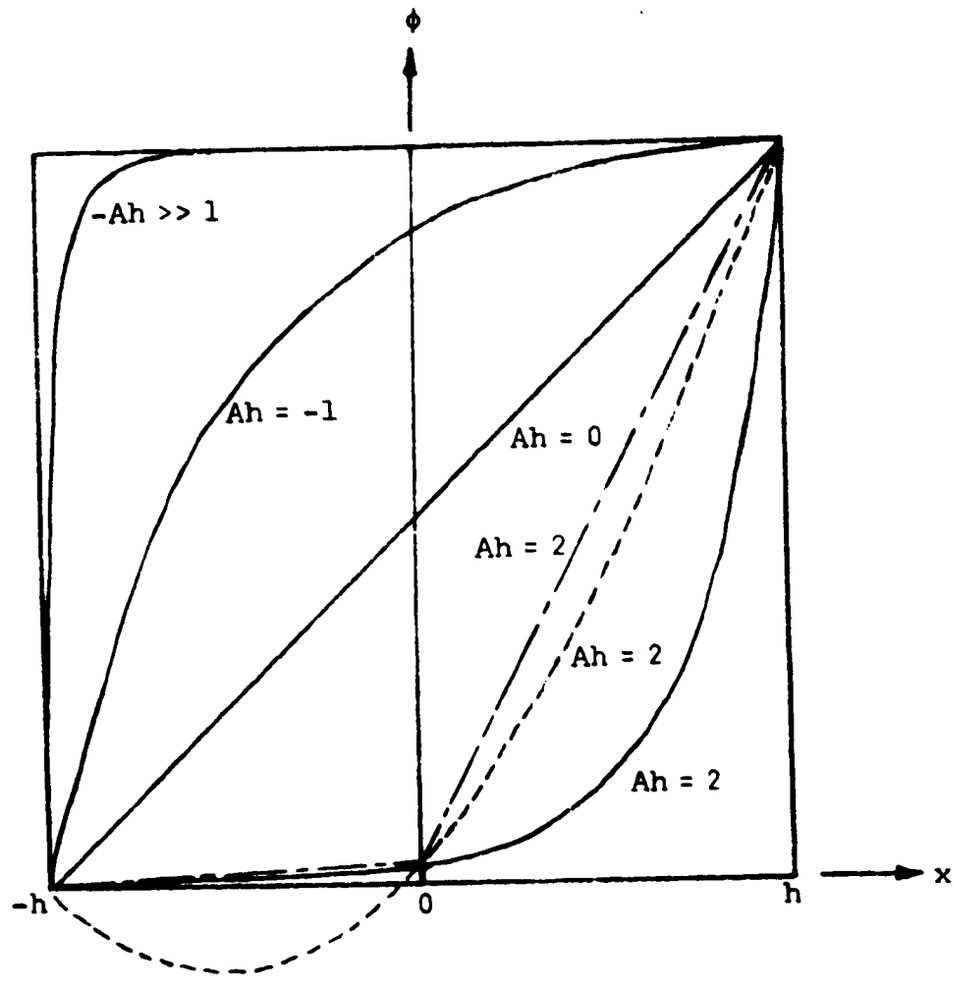

Figure 5 : Exact solution and approximation functions for one-dimensional convective transport equation. ———— exact solution, ----- second-order polynomial approximation, —·— piecewise-linear approximation.

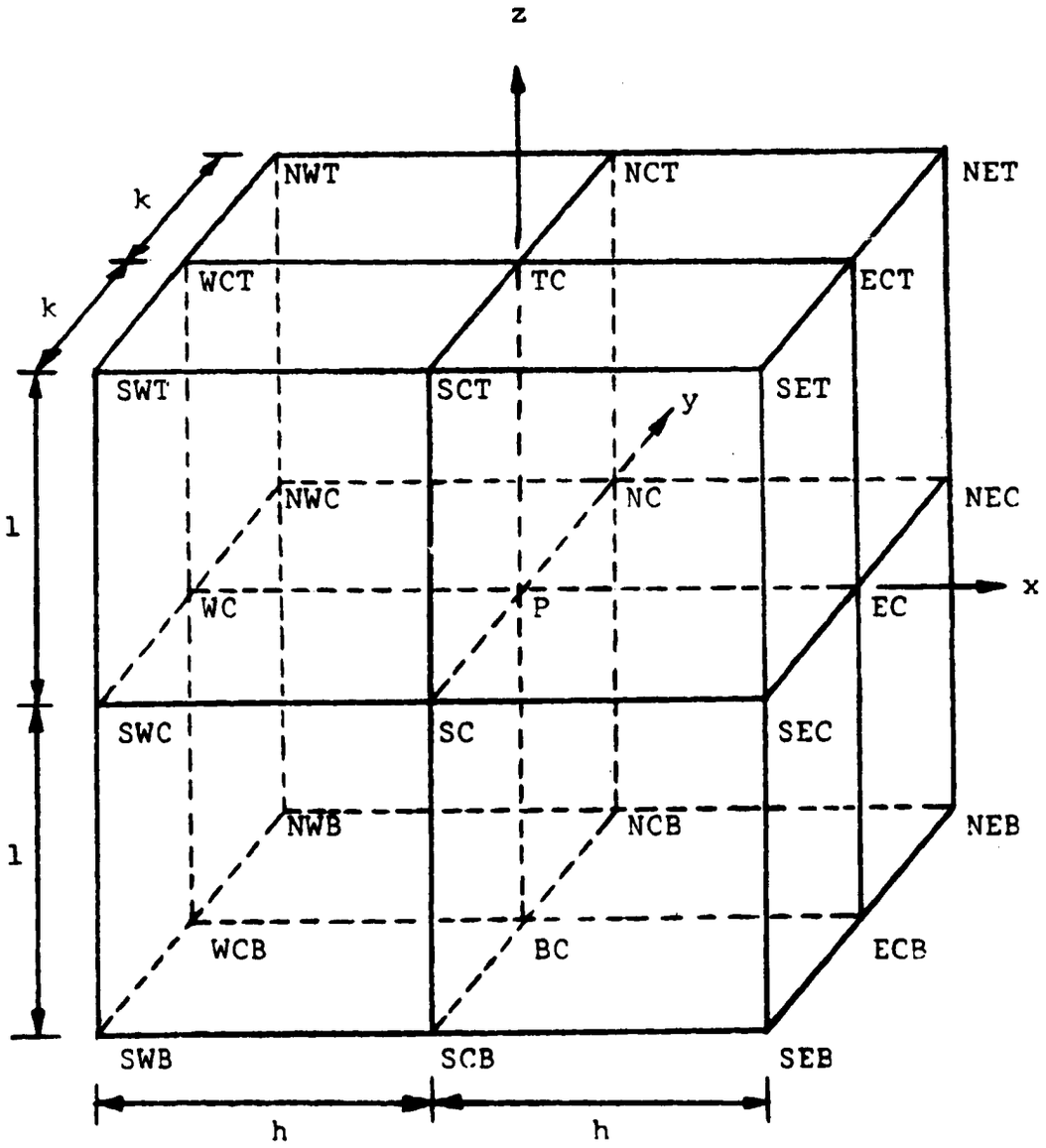

(a) Local element of uniform grid spacing

Figure 6 : Local elements of uniform and nonuniform grid spacing for three-dimensional convective transport equation.

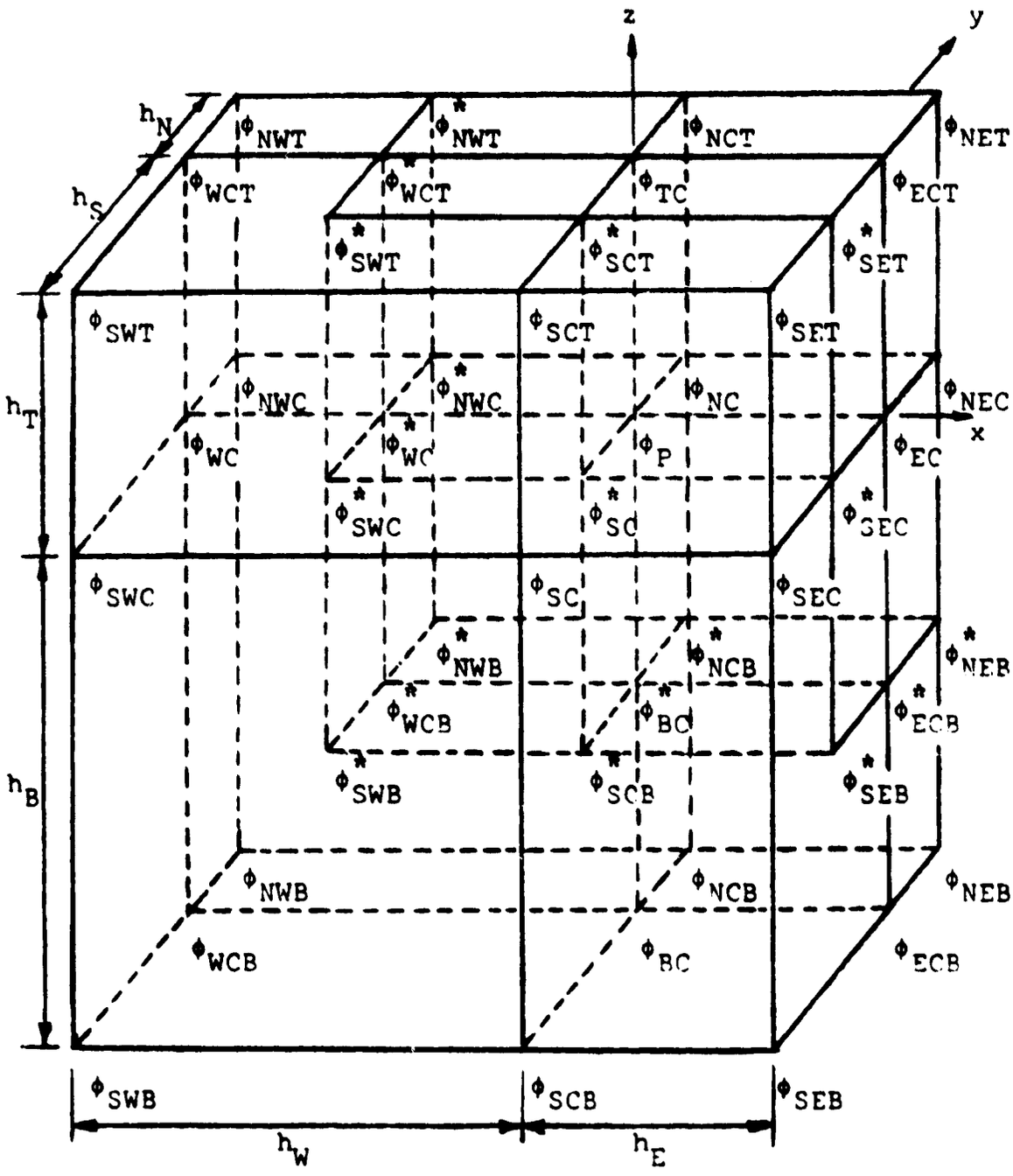

(b) Local element of nonuniform grid spacing

Figure 6(cont'd)

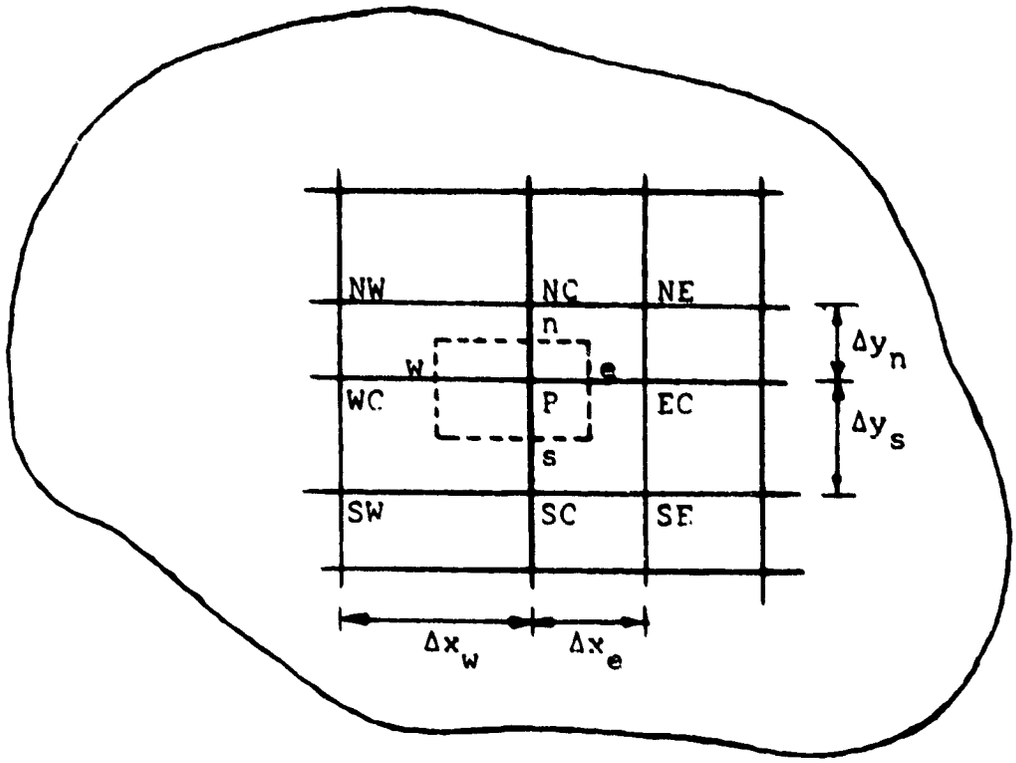

Figure 7 : Local element and control volume surrounding nodal point P.

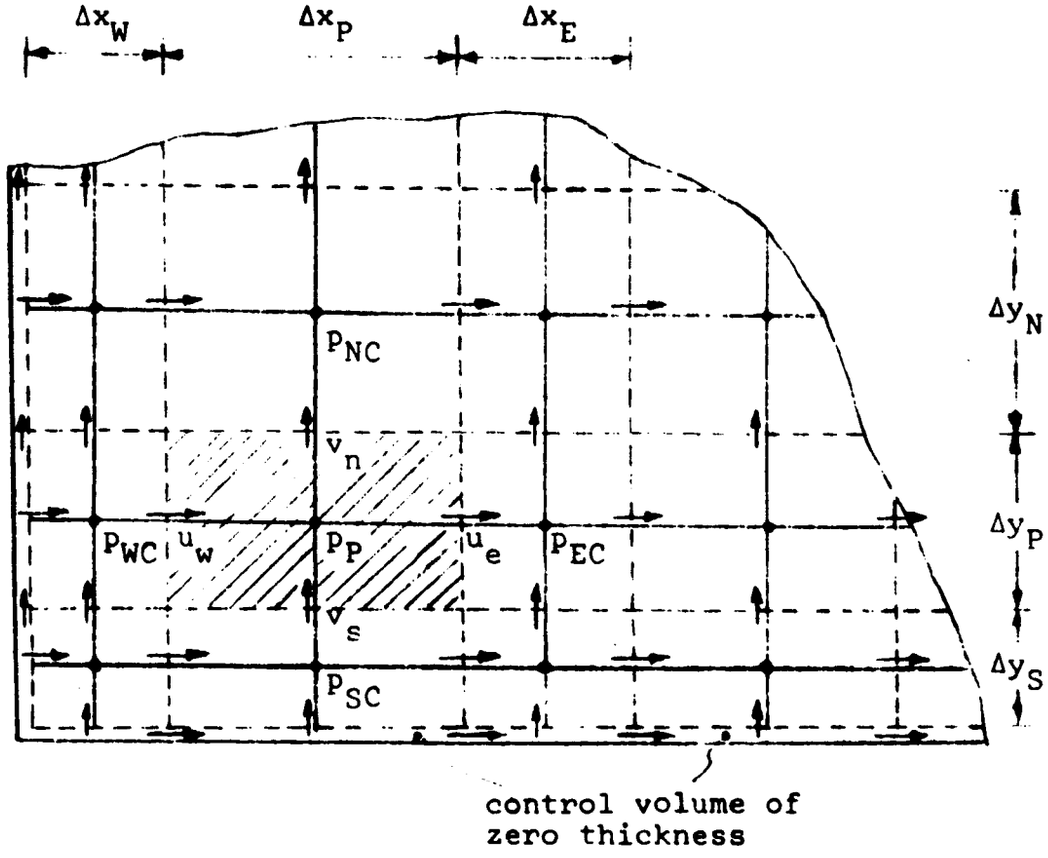

Figure 8 : Staggered grid coordinate system.
"•" pressure, "→" u, "↑" v.

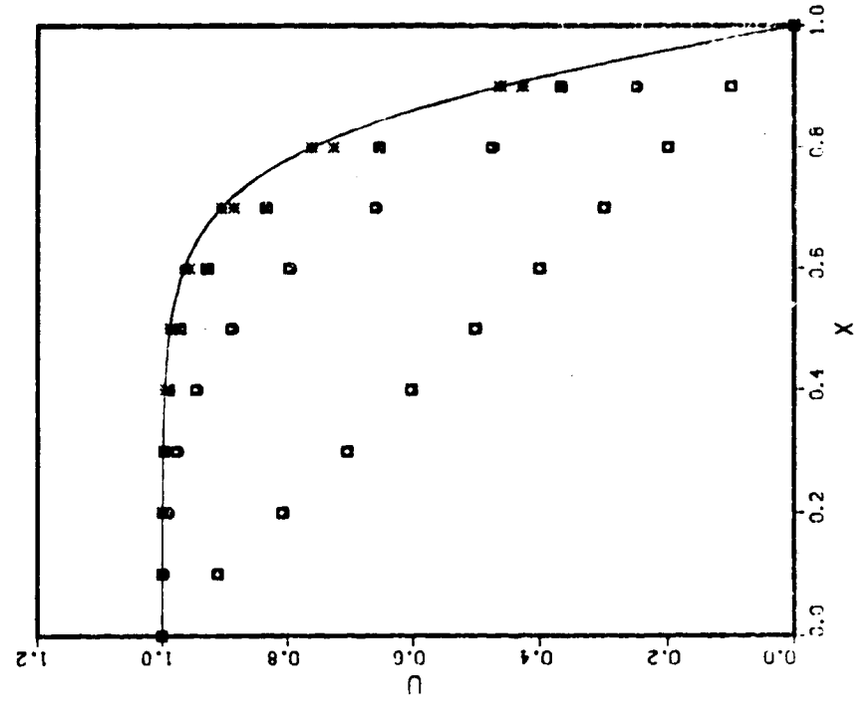

(b) $\alpha = 0.01$, $h = 0.025$, $\tau = 100$.

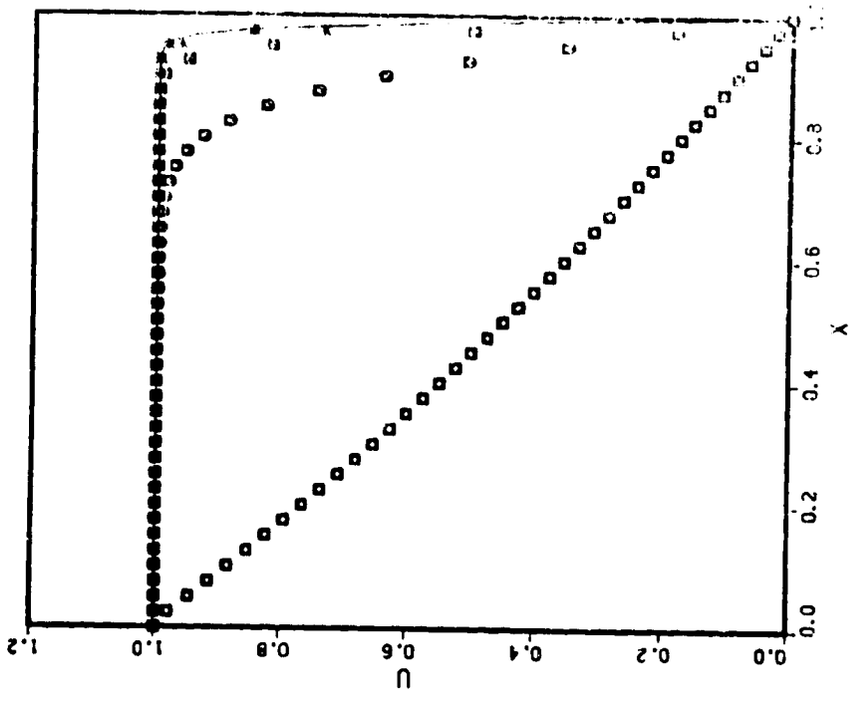

(a) $\alpha = 0.1$, $h = 0.1$, $\tau = 100$.

Figure 9 : Large time solutions for Burgers equation. —— exact solutions.
FASP : "◇" $t = \tau$, "▽" $t = 2\tau$, "■" $t = 3\tau$, "✱" $t = 4\tau$, "◆" $t = 10\tau$.
FAEL & Hybrid FA : "□" $t = \tau$, "○" $t = 2\tau$, "△" $t = 3\tau$, "+" $t = 4\tau$,
"×" $t = 10\tau$.

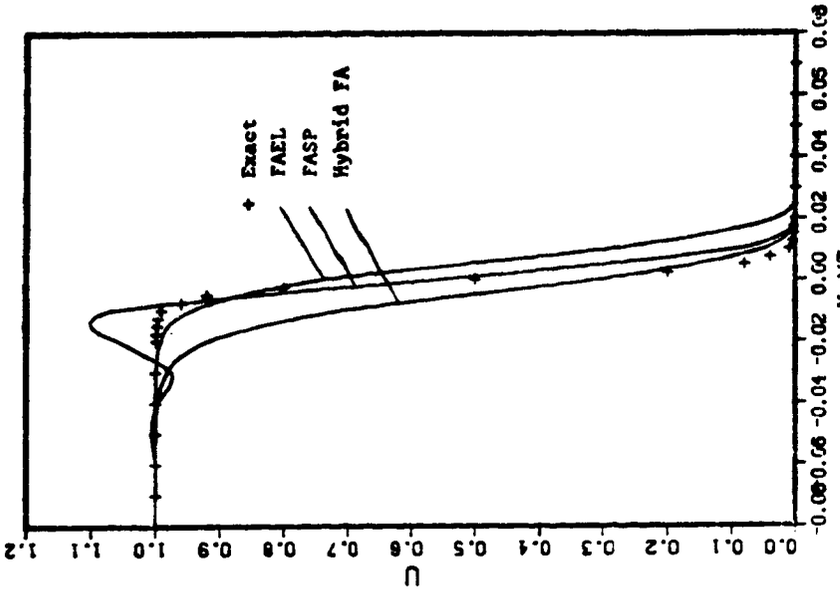

(b) α=0.001

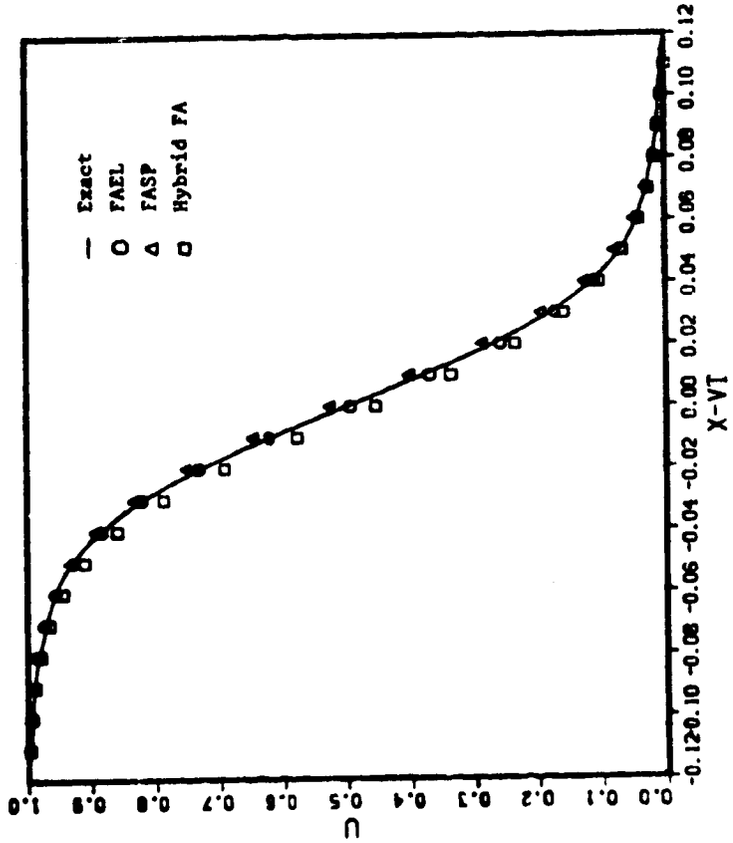

(a) α = 0.01

Figure 10 : Transient solutions at t = 0.4 for Burgers equation. h = 0.01, τ = 0.002.

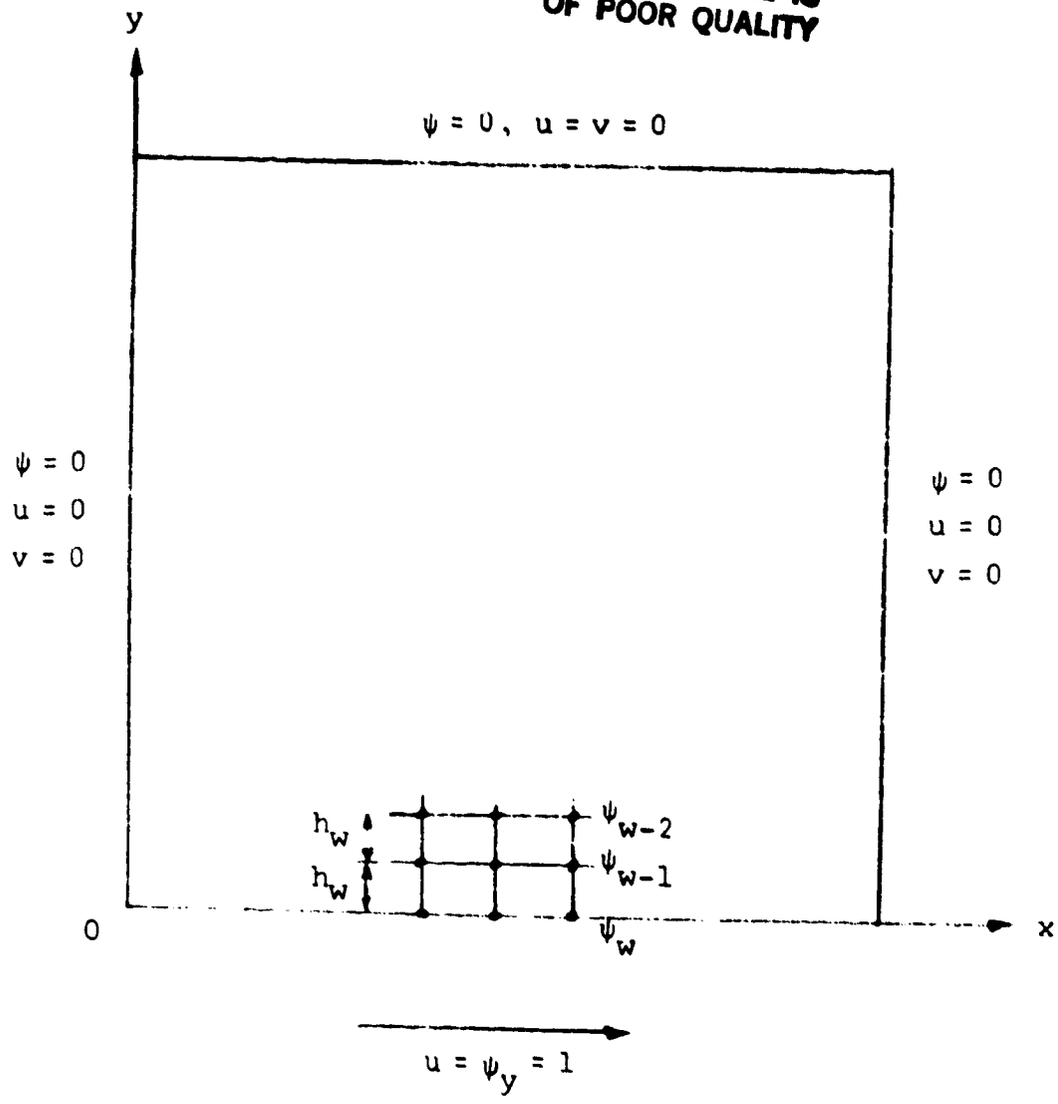

Figure 11 : Coordinates and boundary conditions for two-dimensional starting cavity flow.

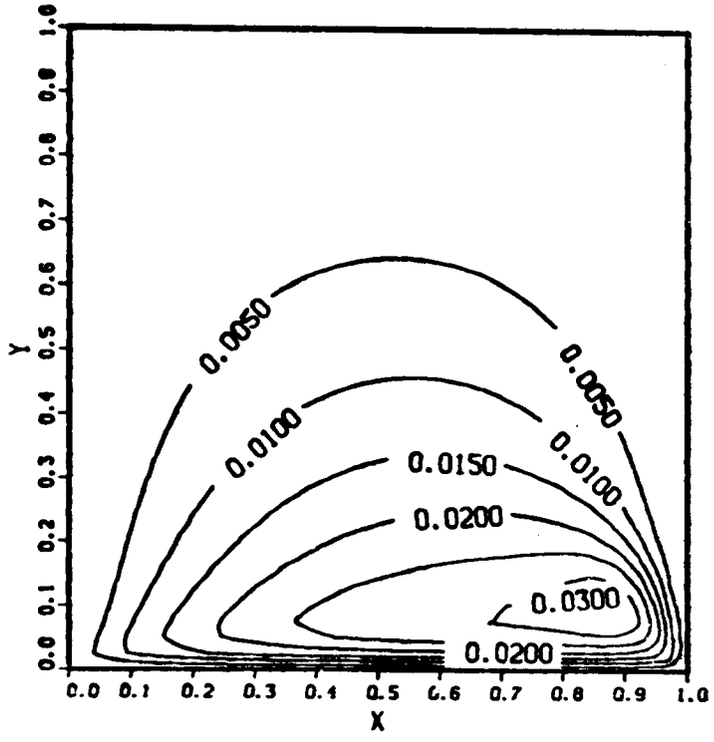

(a) t = 1

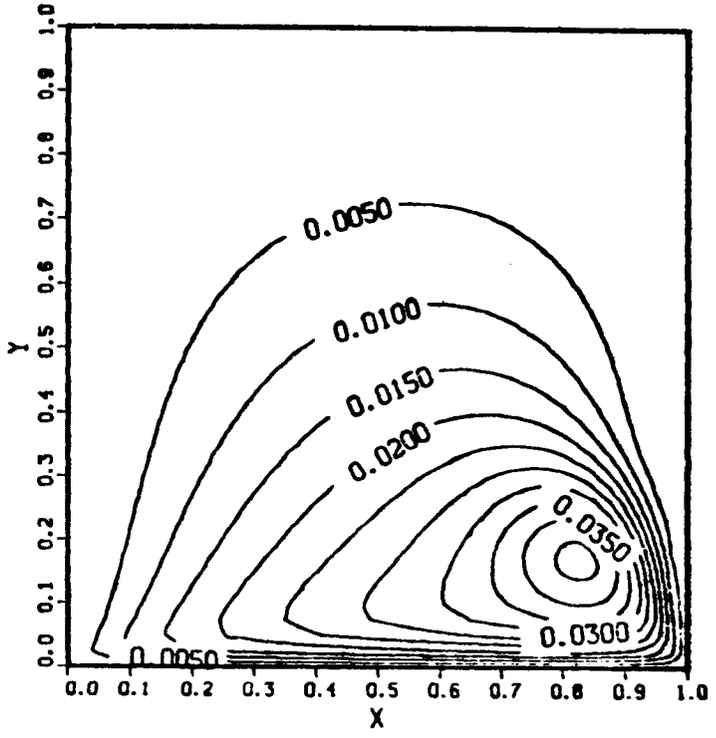

(b) t = 2

Figure 12 : Streamlines for 2D starting cavity flow of Re = 1000, 41 × 41 nonuniform grid.

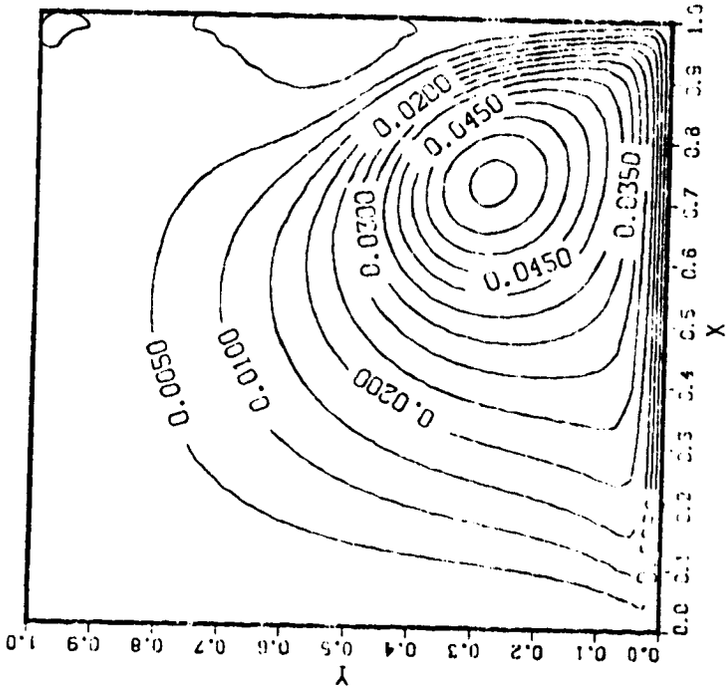

(d) t = 4

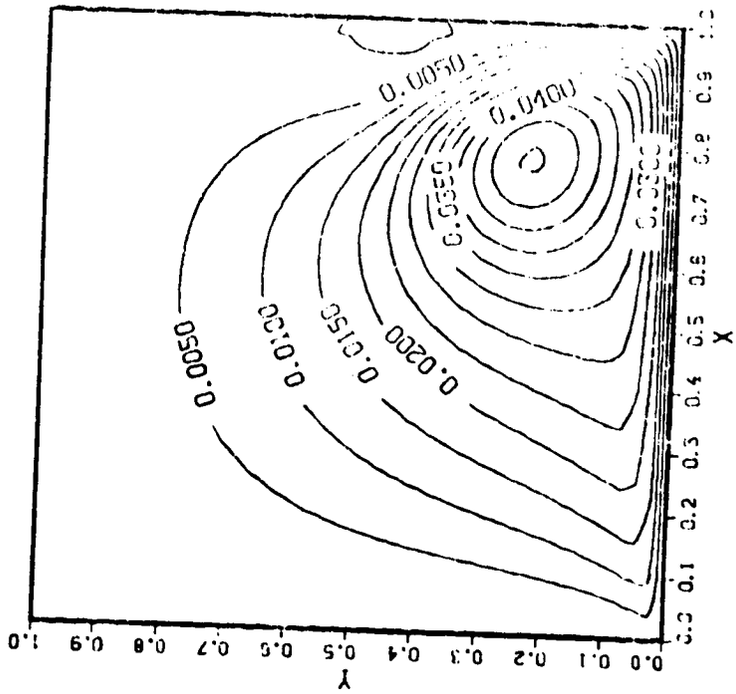

(c) t = 3

Figure 12 (cont'd)

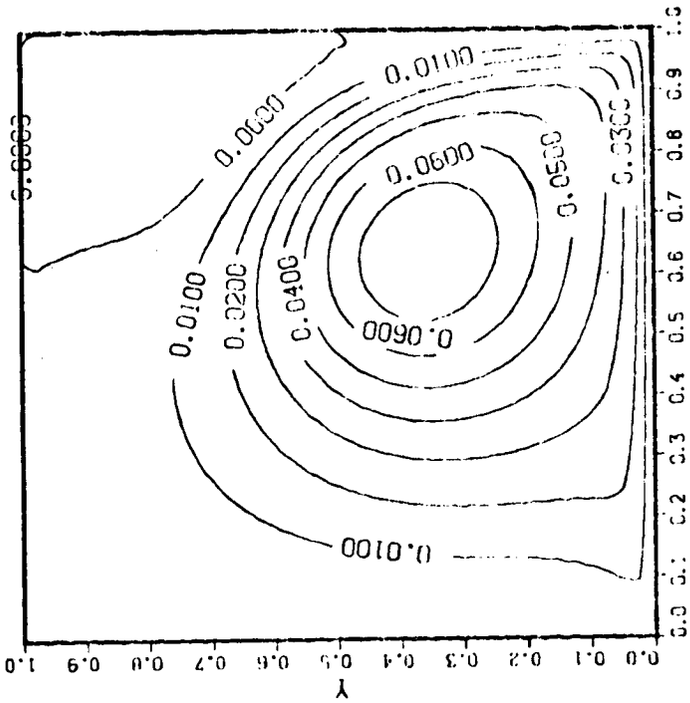

(f) t = 7

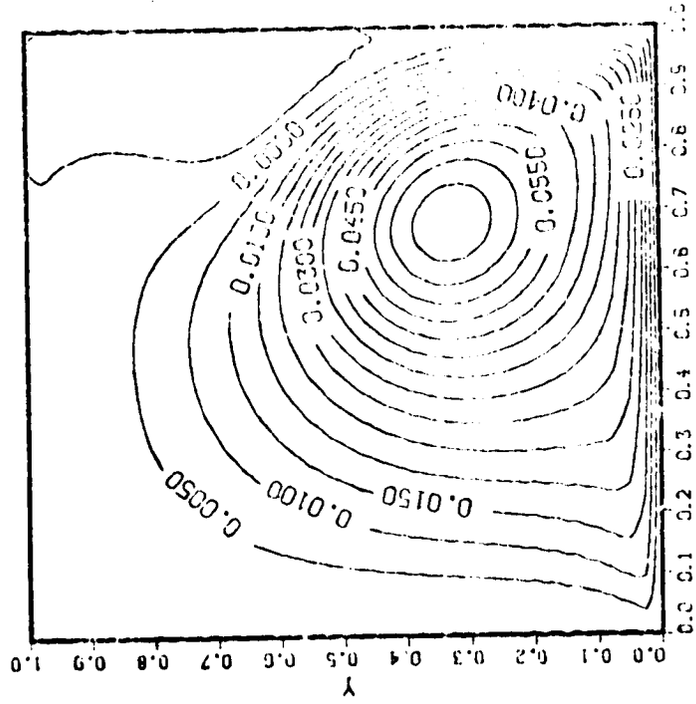

(e) t = 5.5

Figure 12 (cont'd)

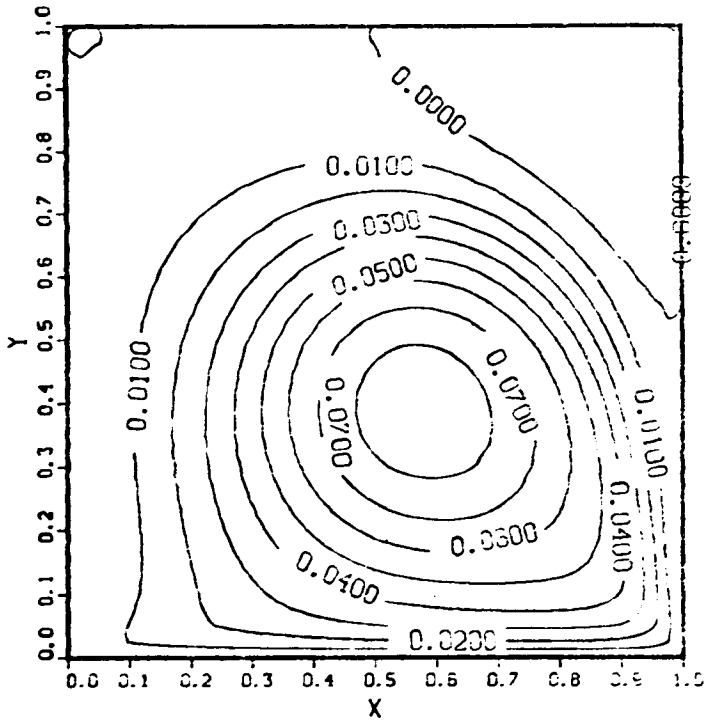

(g) t = 10

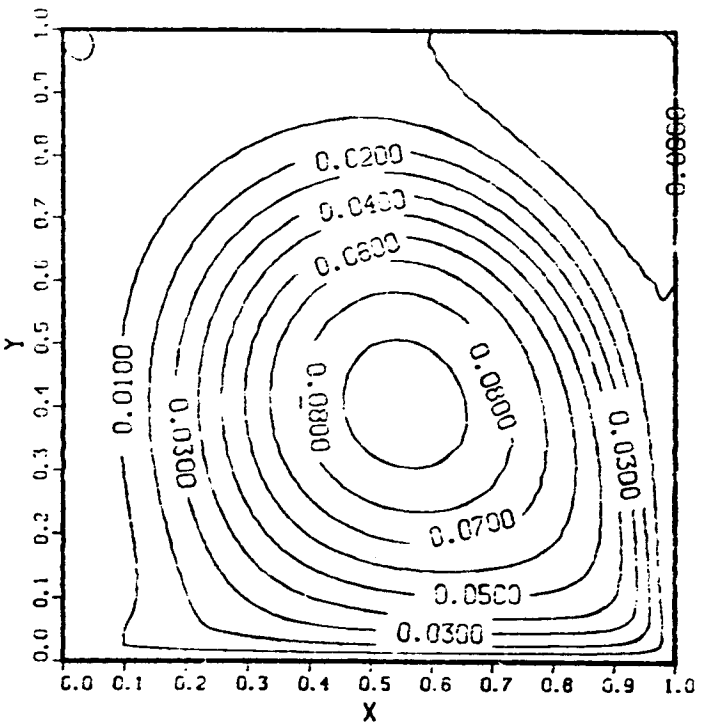

(h) t = 14.5

Figure 12 (cont'd)

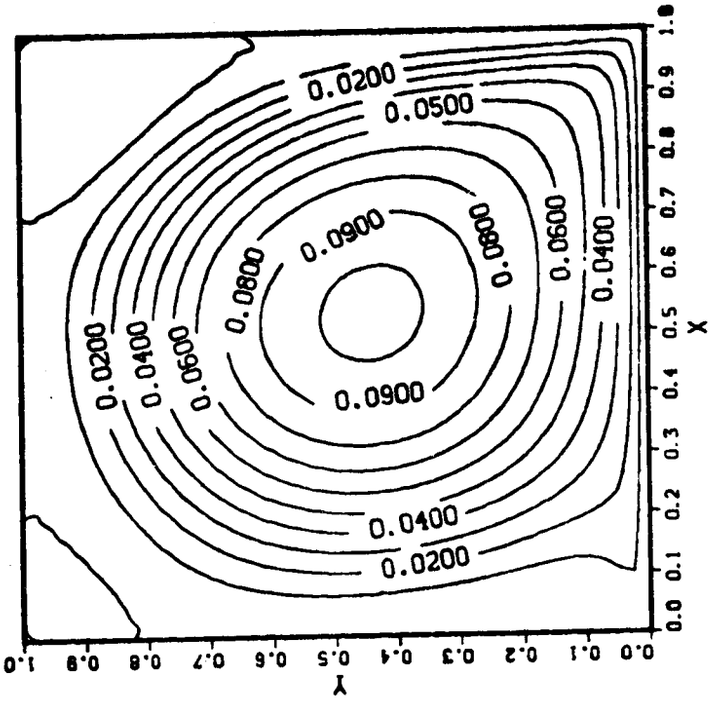

(j) t = 40

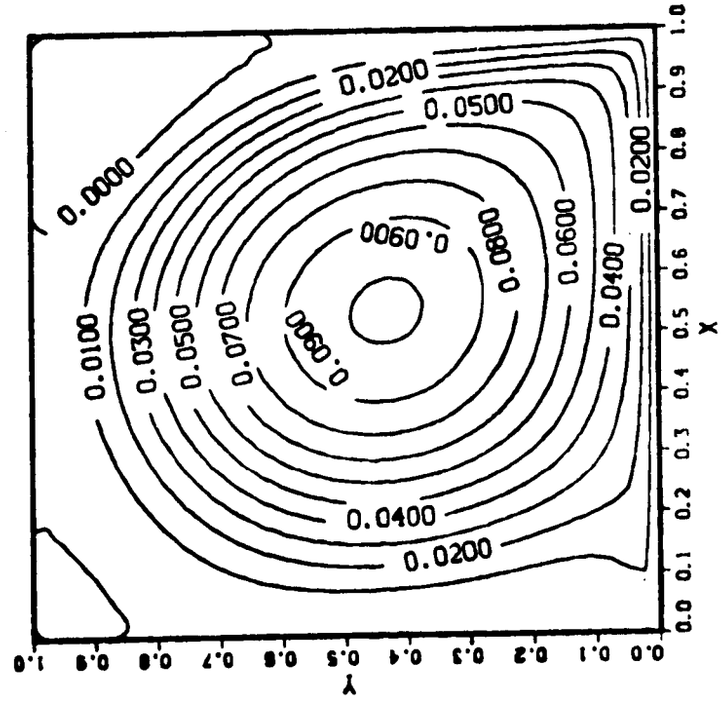

(i) t = 22

Figure 12(cont'd)

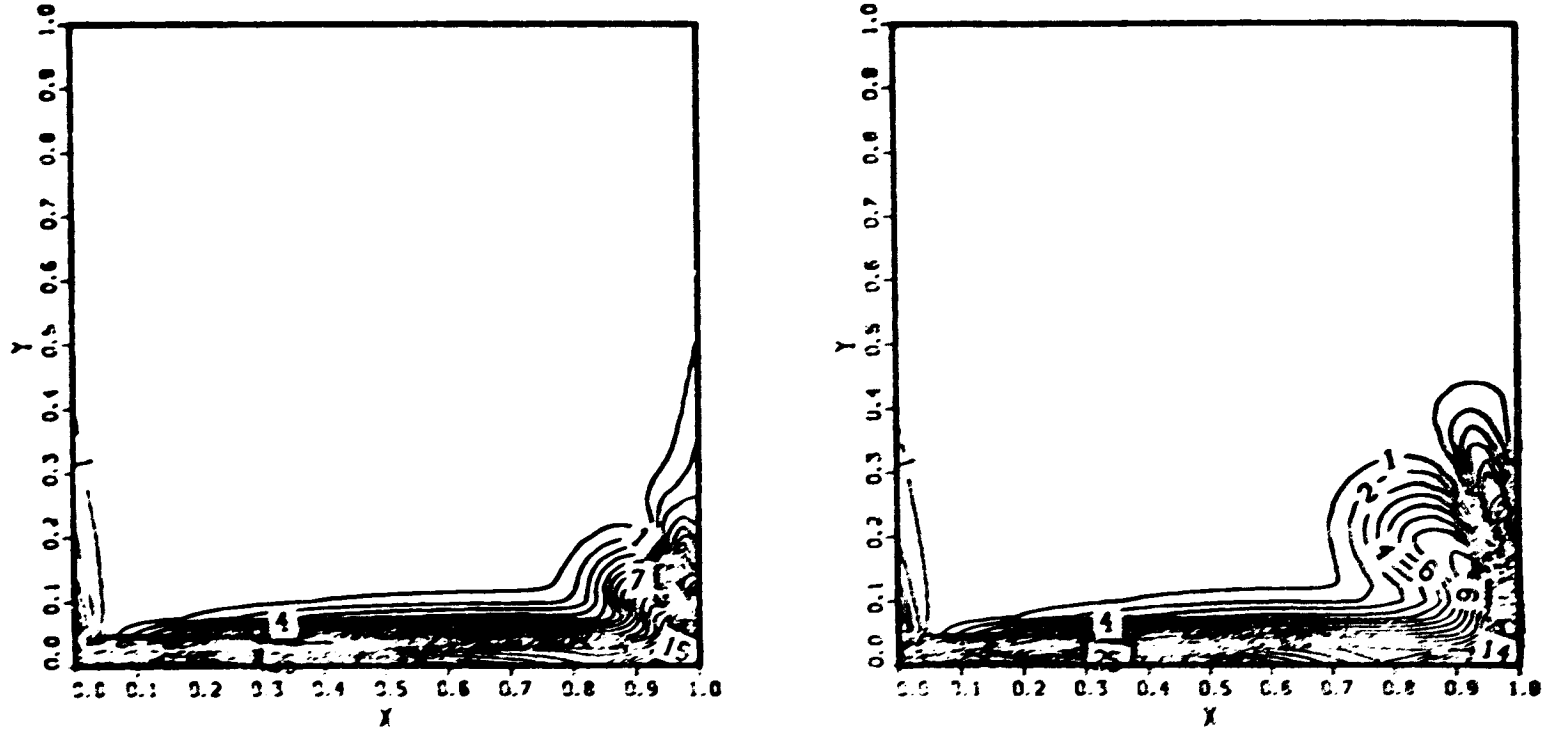

(a) t = 1

(b) t = 2

ORIGINAL PAGE IS
OF POOR QUALITY

Figure 11 : Vorticity contours for 2D starting cavity flow of Re = 1000, 41 x 41 nonuniform grid.

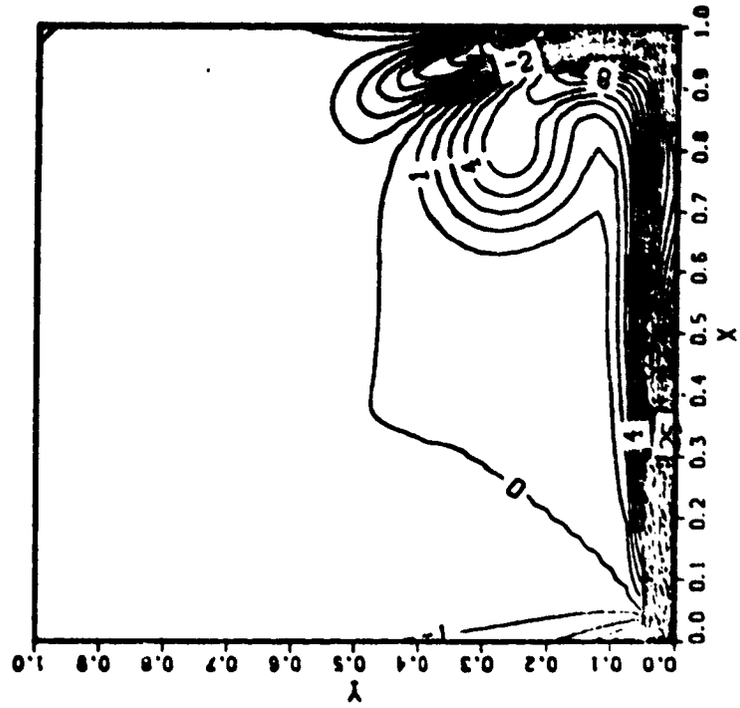

(d) t = 4

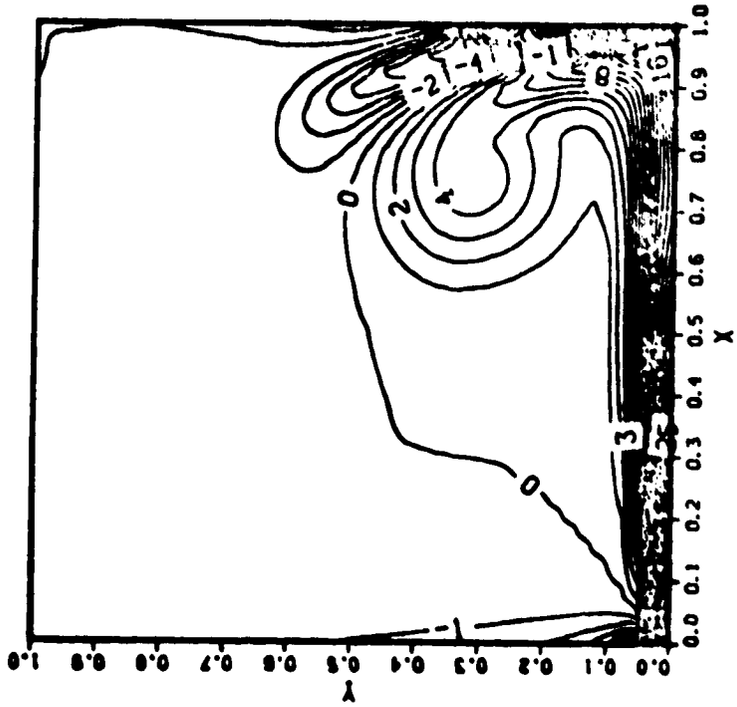

(c) t = 3

Figure 13(cont'd)

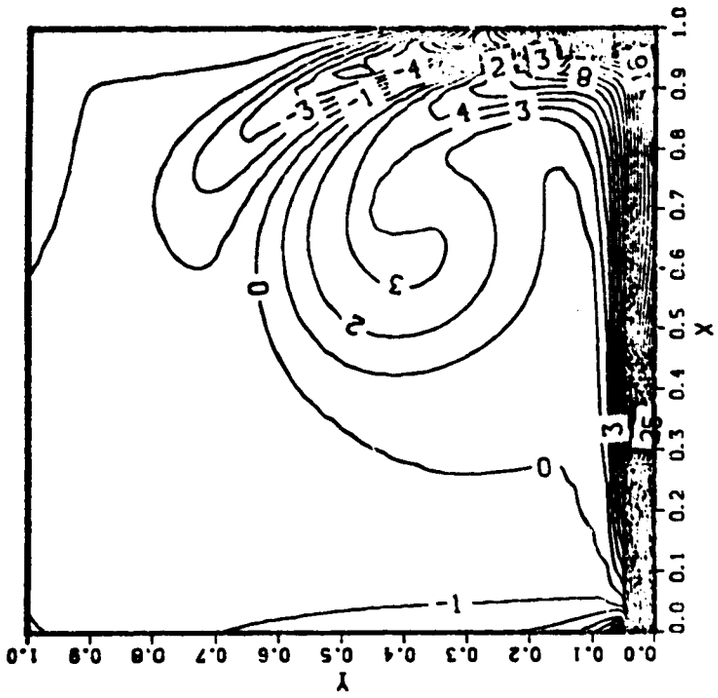

(f) t = 7

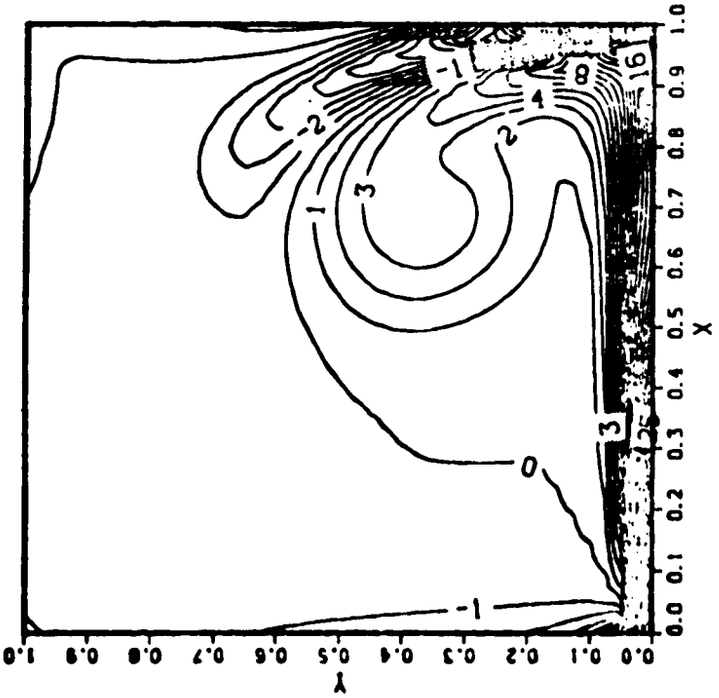

(e) t = 5.5

Figure 13(cont'd)

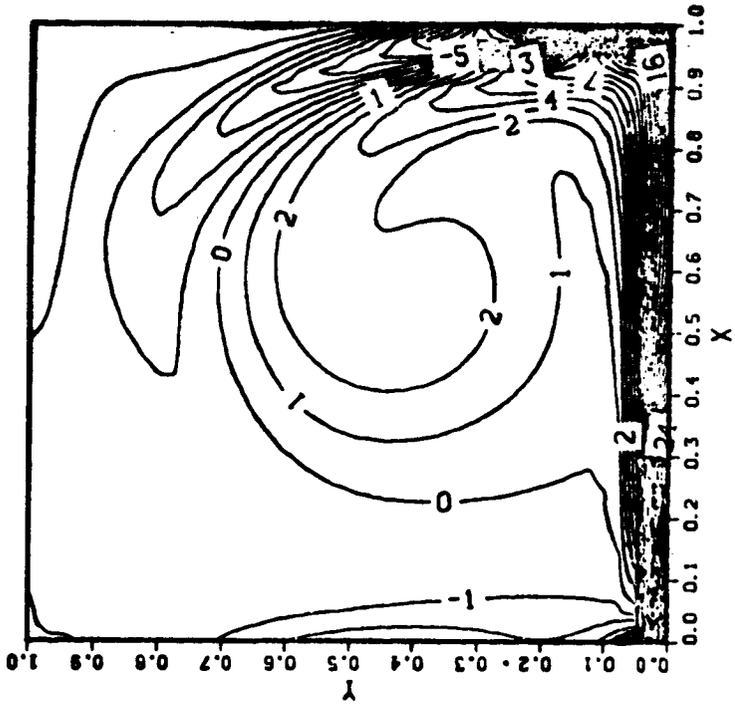

(h) t = 14.5

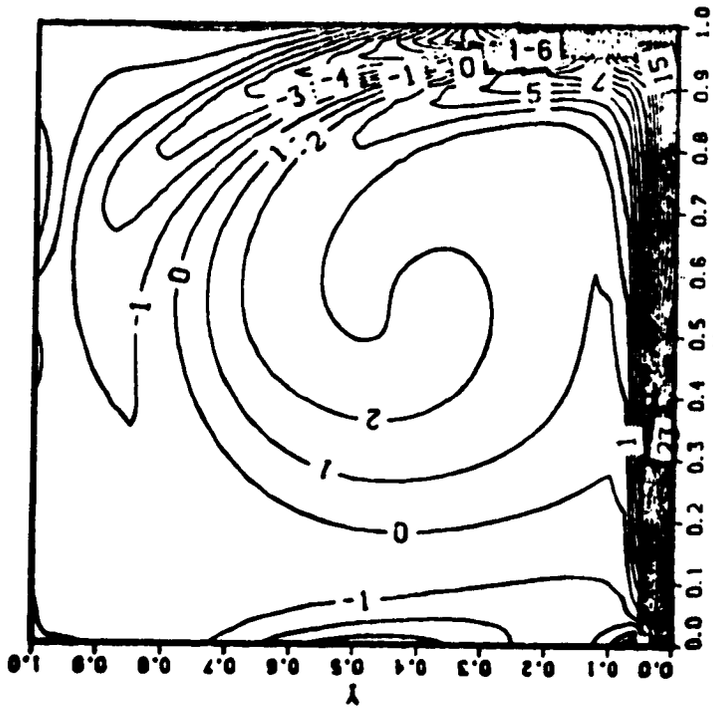

(g) t = 10

Figure 13 (cont'd)

(i) t = 22

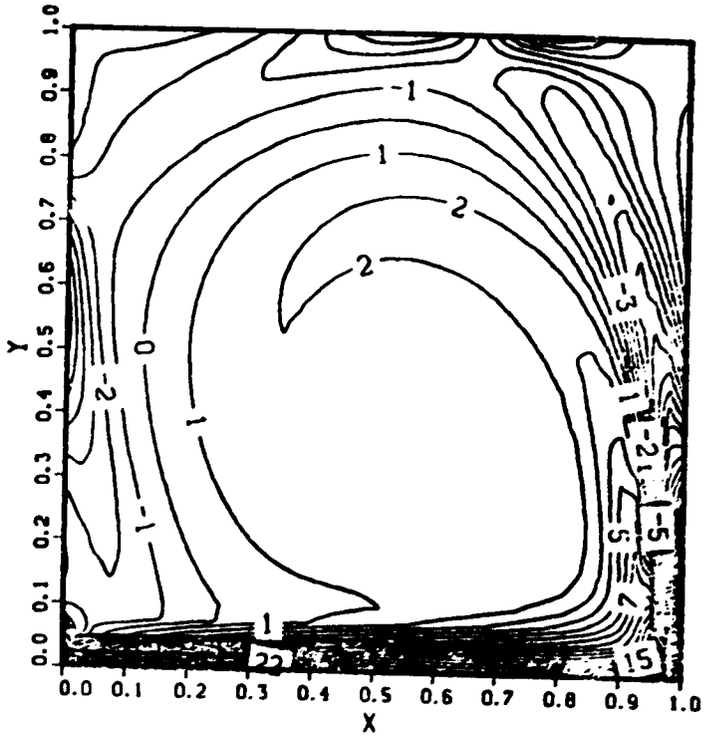

(j) t = 40

Figure 13 (cont'd)

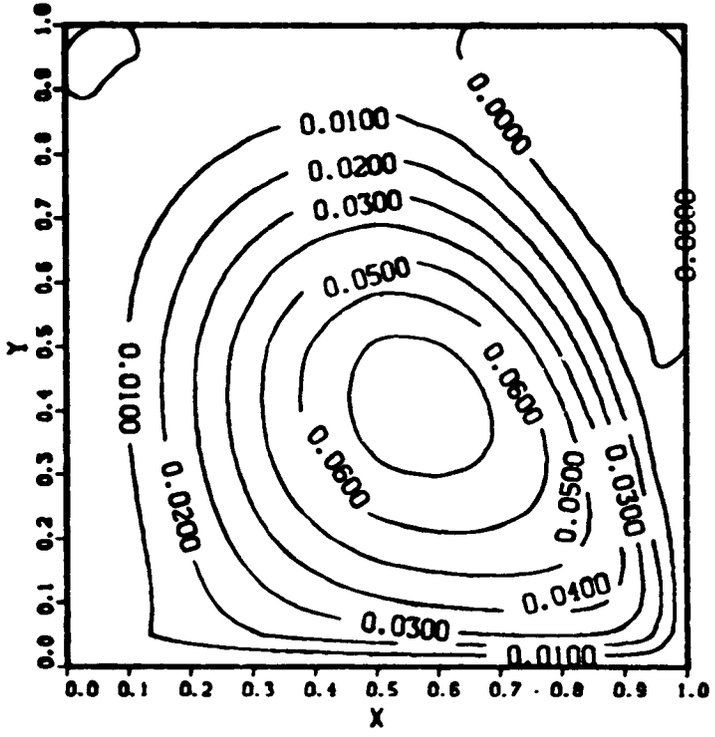

(a) Streamlines (first-order vorticity boundary conditions)

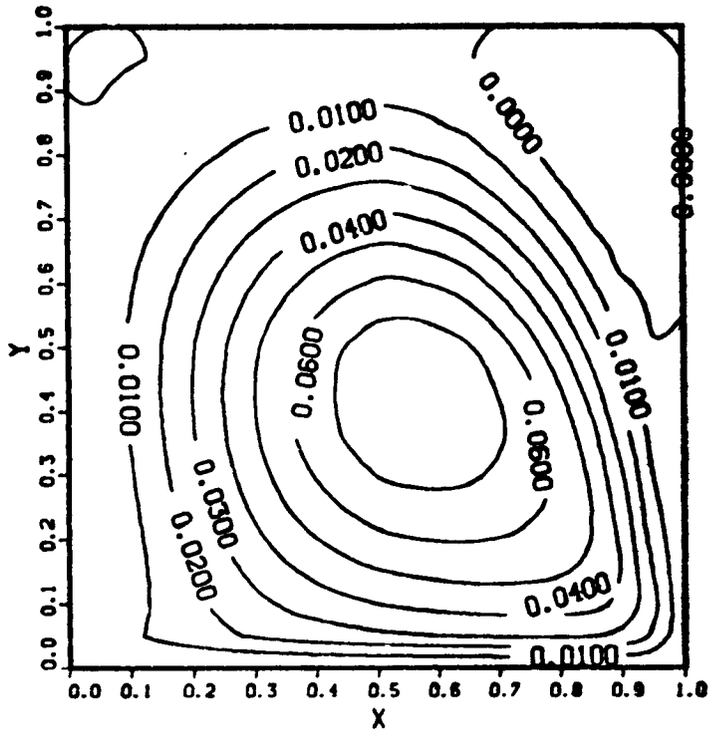

(b) Streamlines (second-order vorticity boundary conditions)

Figure 14 : Comparison of steady streamlines and vorticity contours for 2D starting cavity flow of Re = 1000, 21 × 21 nonuniform grid.

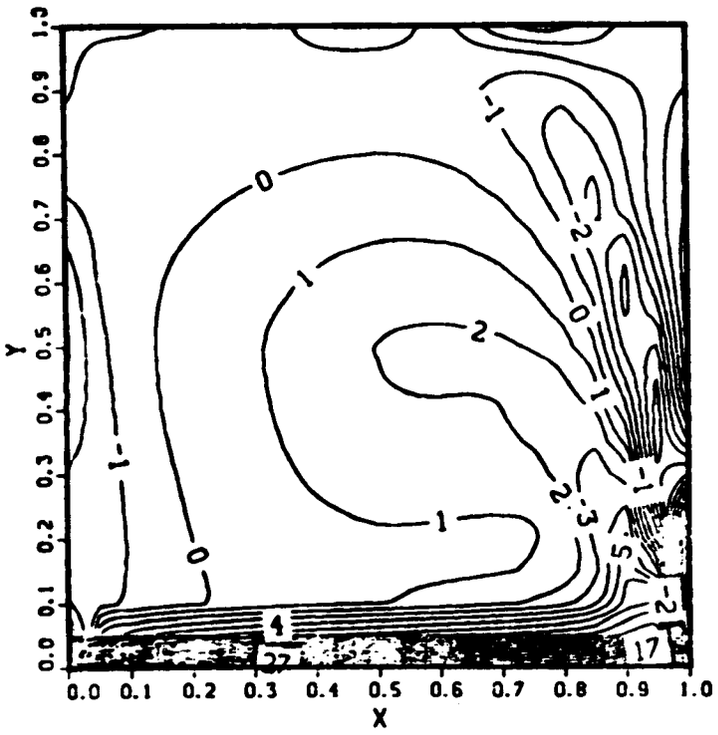

(c) Vorticity contours (first-order vorticity boundary conditions)

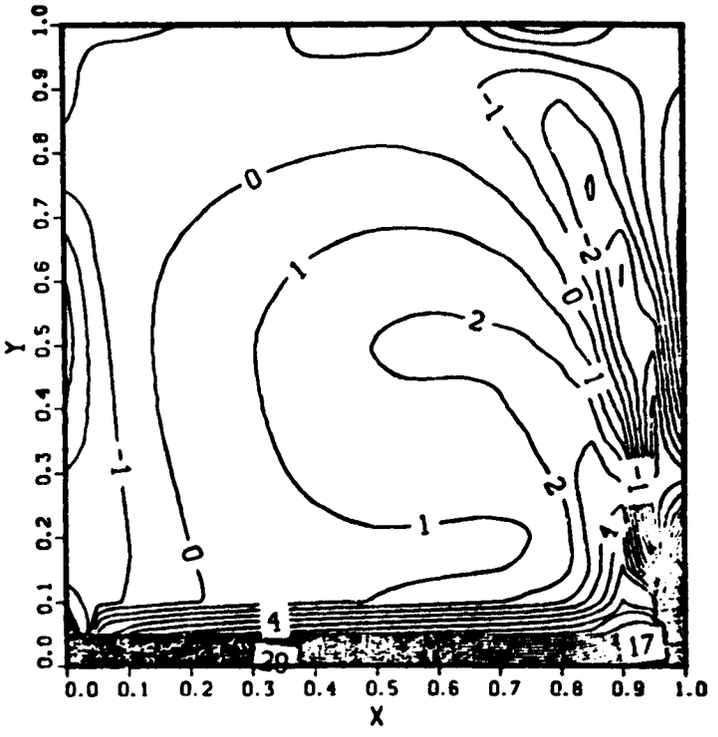

(d) Vorticity contours (second-order vorticity boundary conditions)

Figure 14 (cont'd)

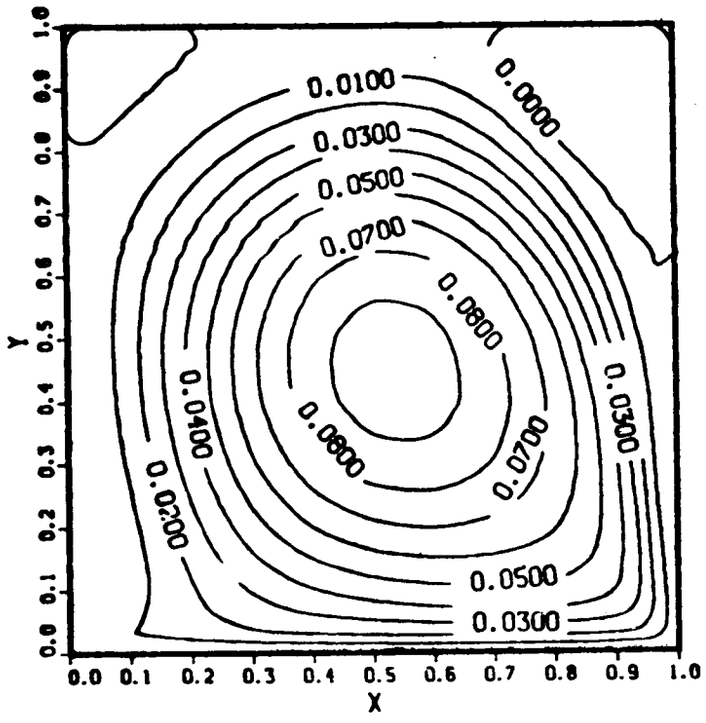

(a) Streamlines

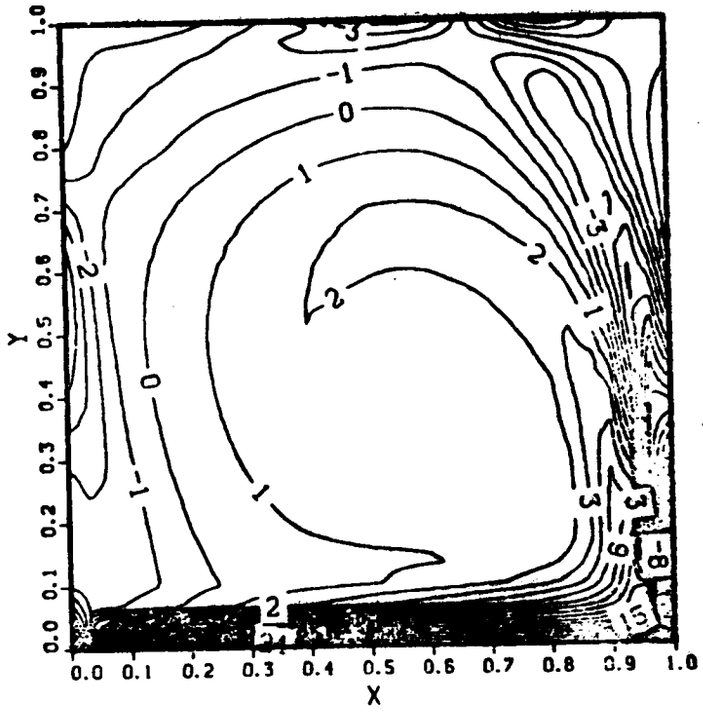

(b) Vorticity contours

Figure 15 : Steady streamlines and vorticity contours for 2D starting cavity flow of Re = 1000, 31 × 31 nonuniform grid (first-order vorticity boundary conditions).

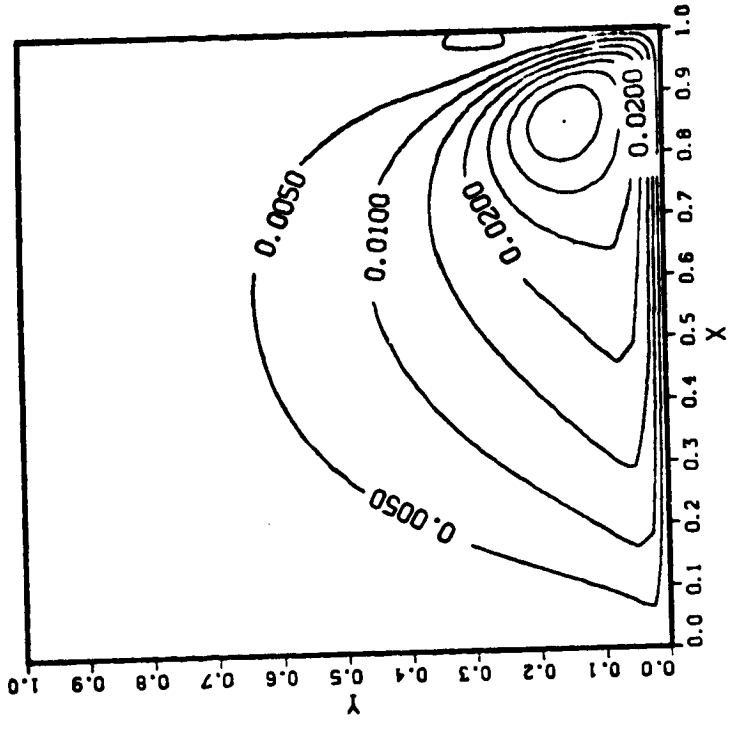

(b) t = 2

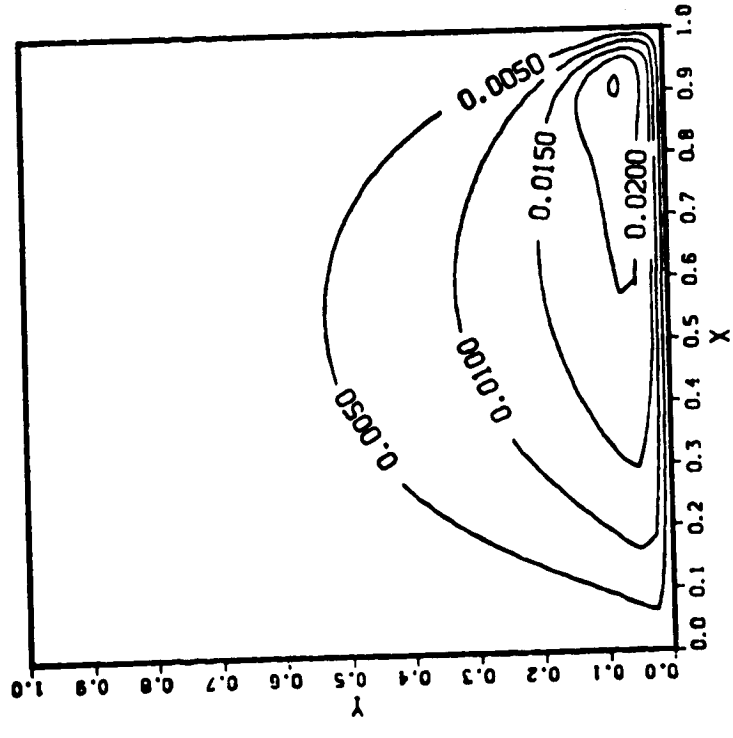

(a) t = 1

Figure 16 : Streamlines for 2D starting cavity flow of Re = 2000, 41 × 41 nonuniform grid.

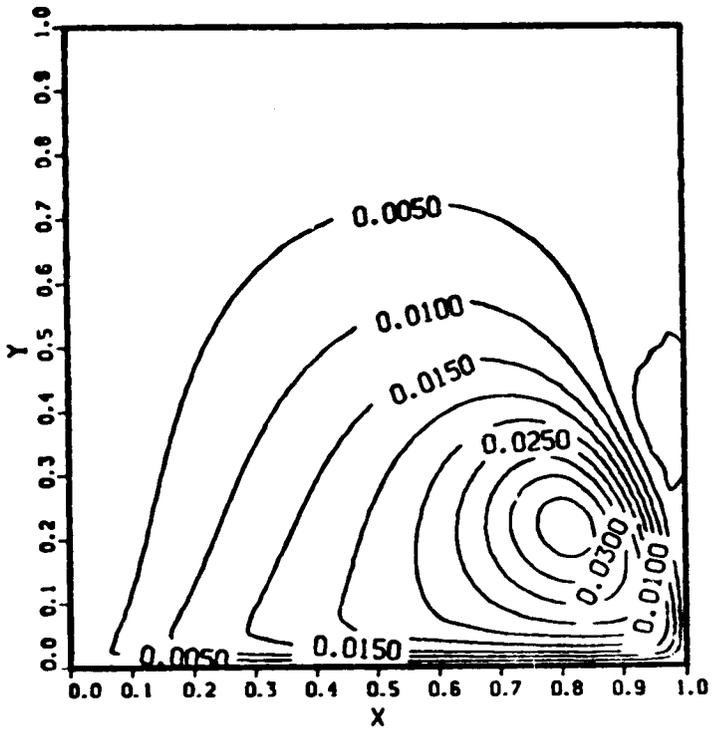

(c) t = 3

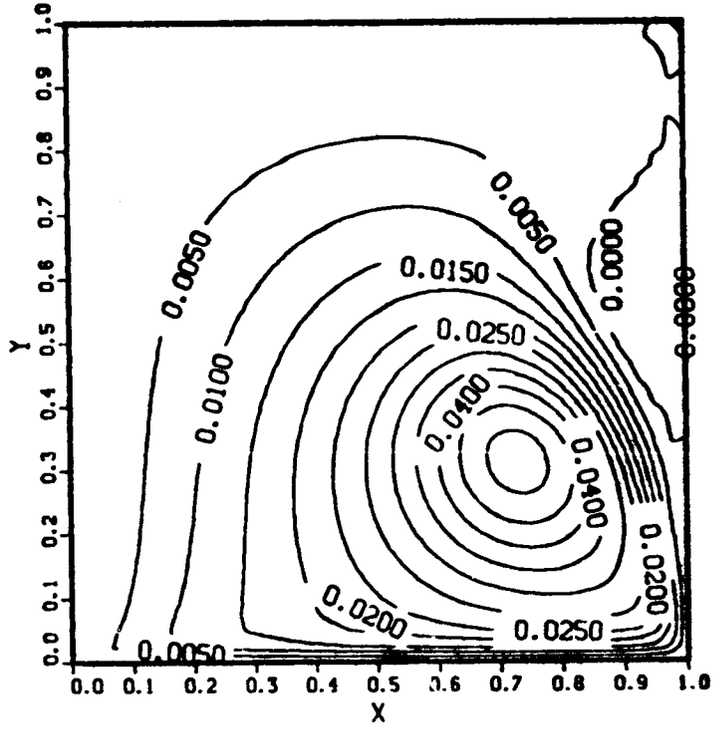

(d) t = 5

Figure 16 (cont'd)

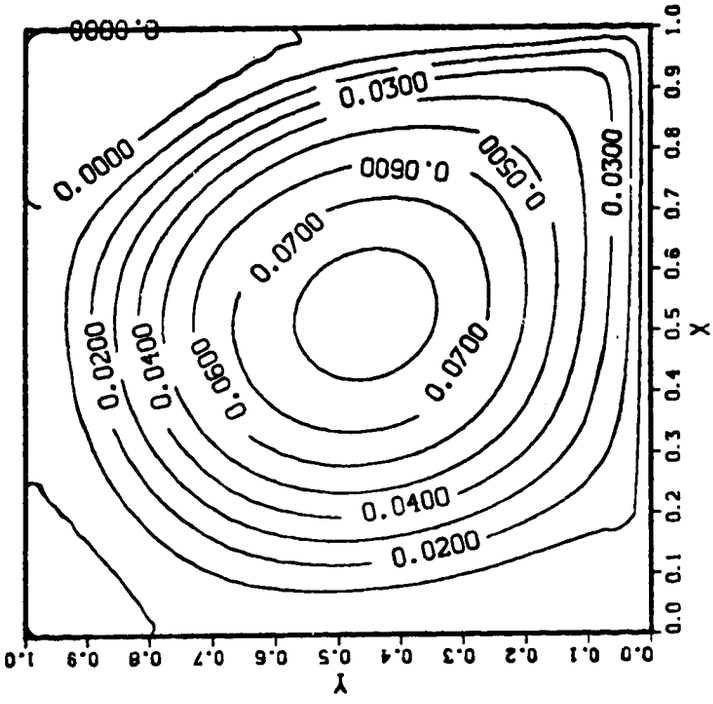

(f) t = 20

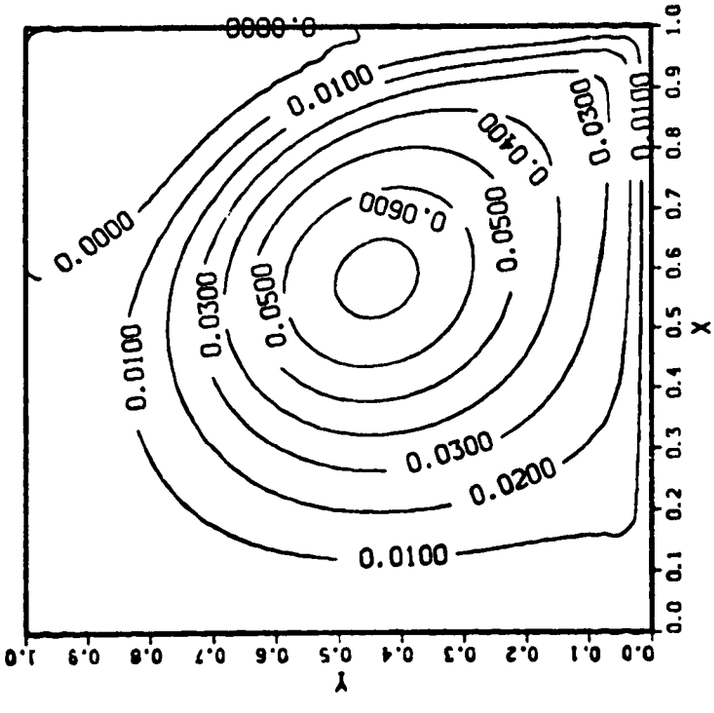

(e) t = 10

Figure 16 (cont'd)

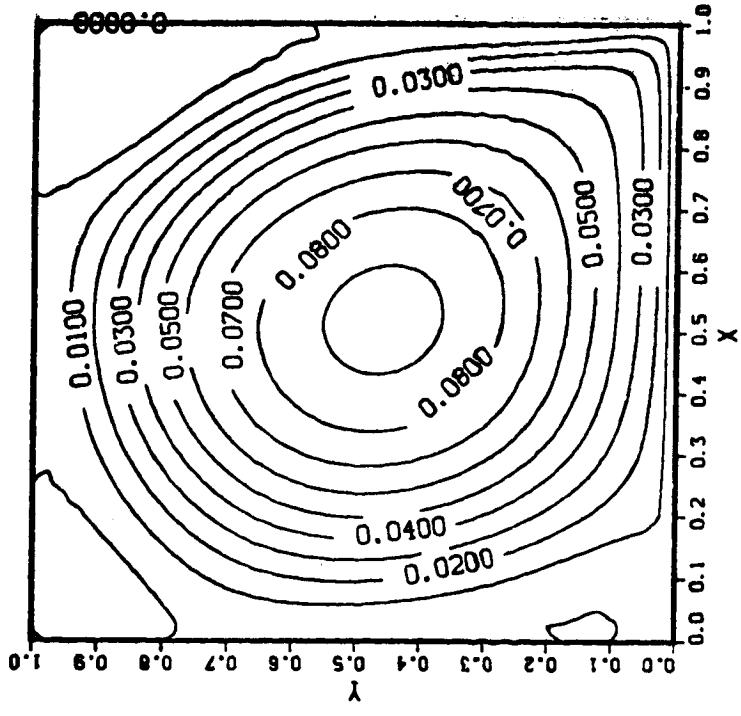

(h) t = 60

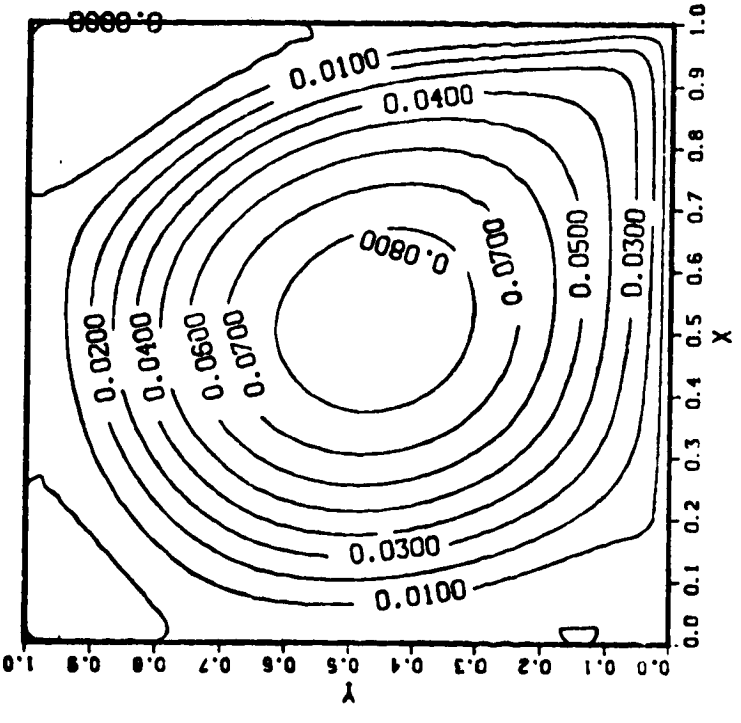

(g) t = 26

Figure 16 (cont'd)

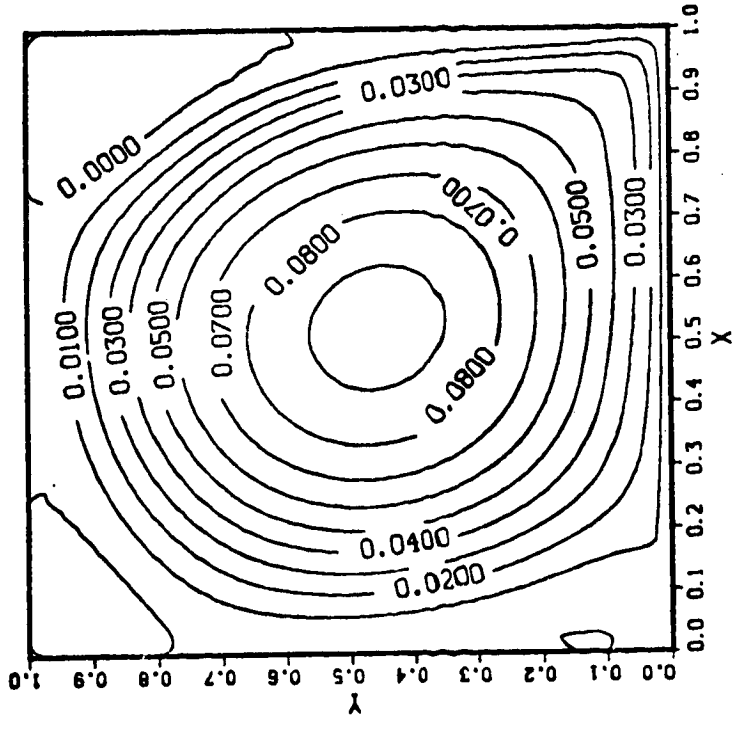

(i) t = 65

Second-order vorticity boundary conditions

Figure 16 (cont'd)

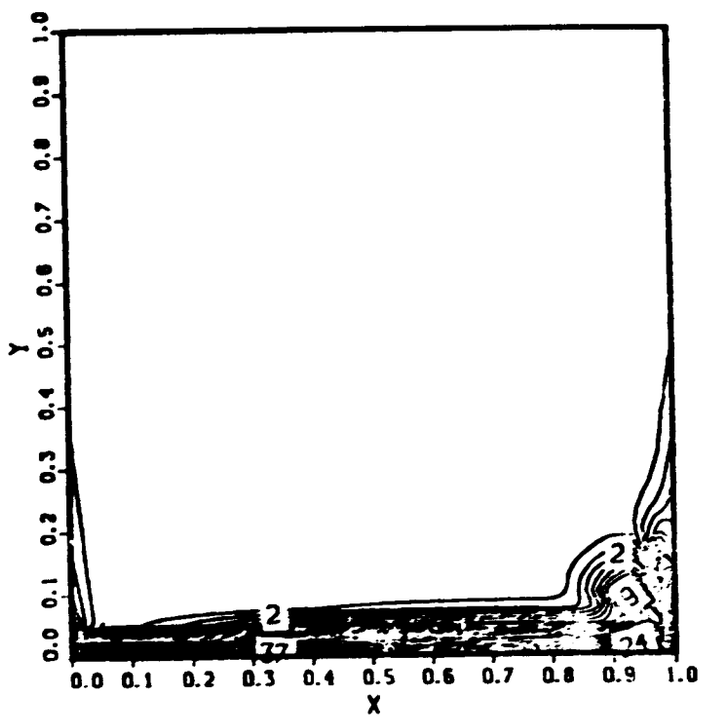

(a) t = 1

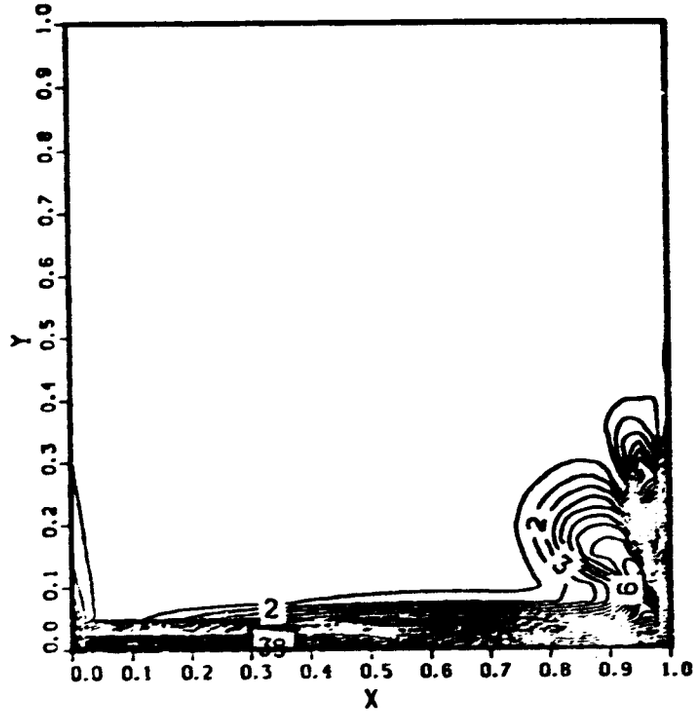

(b) t = 2

Figure 17 : Vorticity contours for 2D starting cavity flow of Re = 2000, 41 x 41 nonuniform grid.

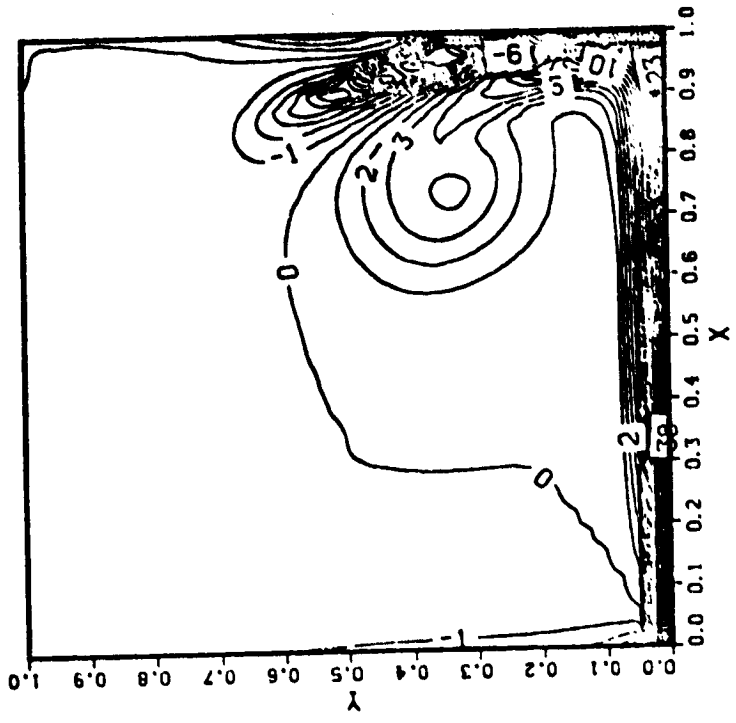

(d) t = 5

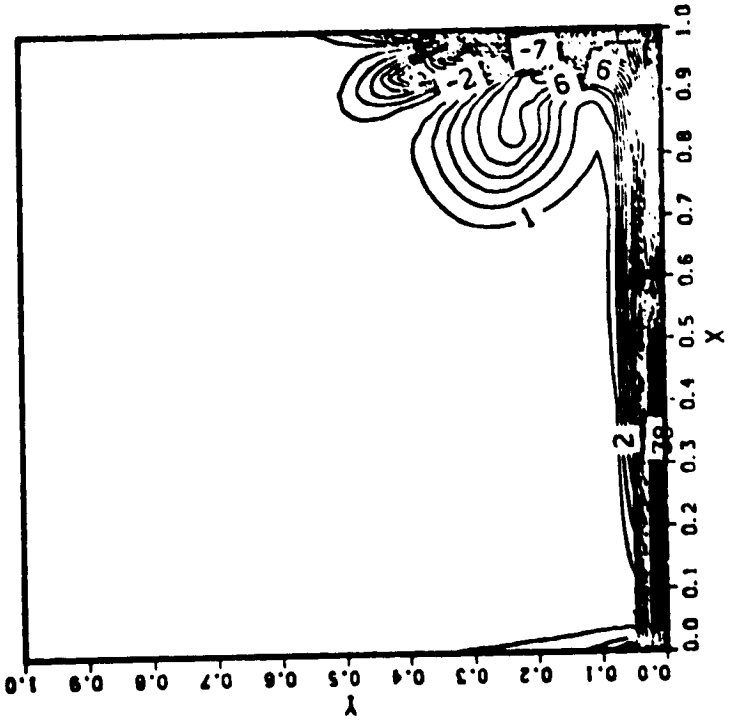

(c) t = 3

Figure 17 (cont'd)

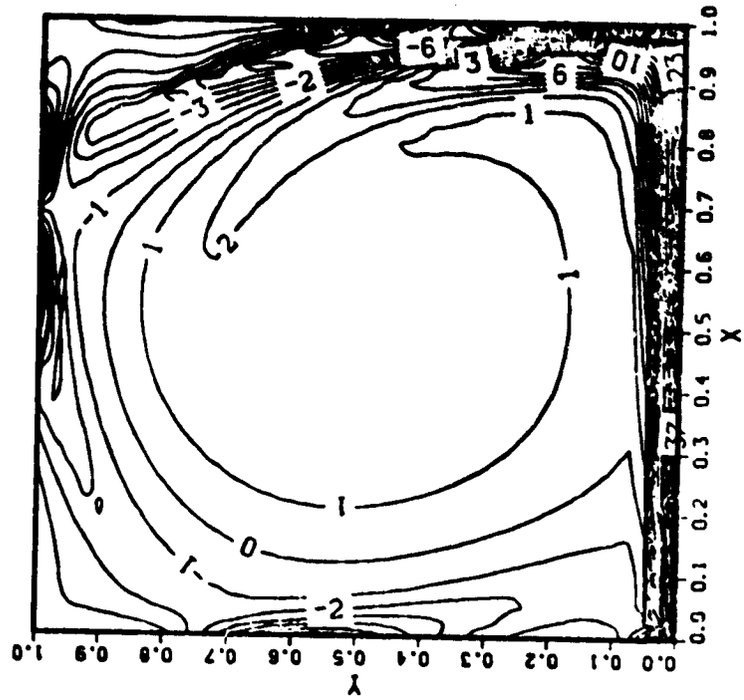

(f) t = 20

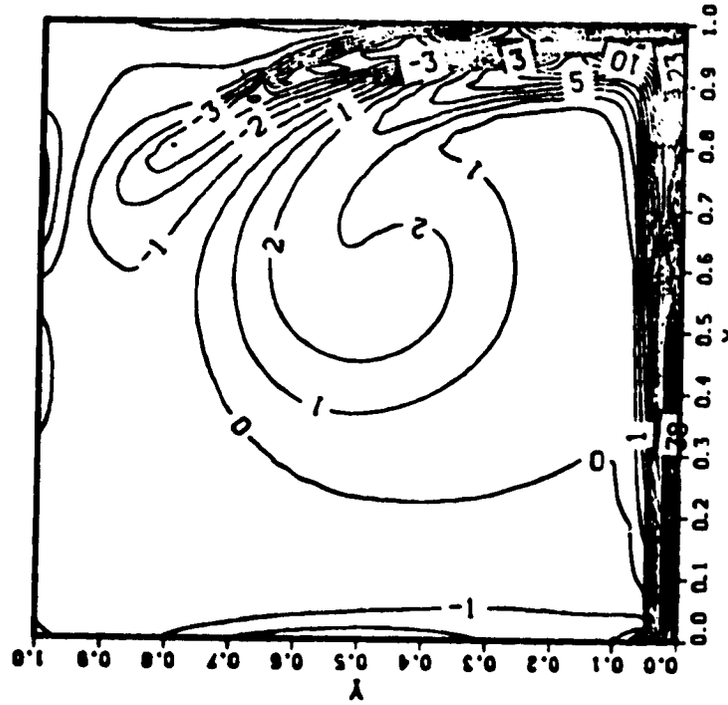

(e) t = 10

Figure 17 (cont'd)

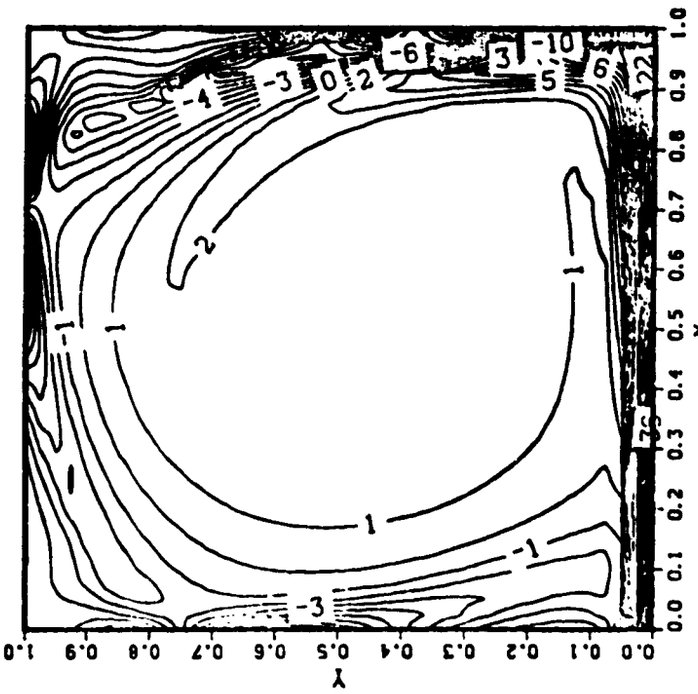

(h) t = 60

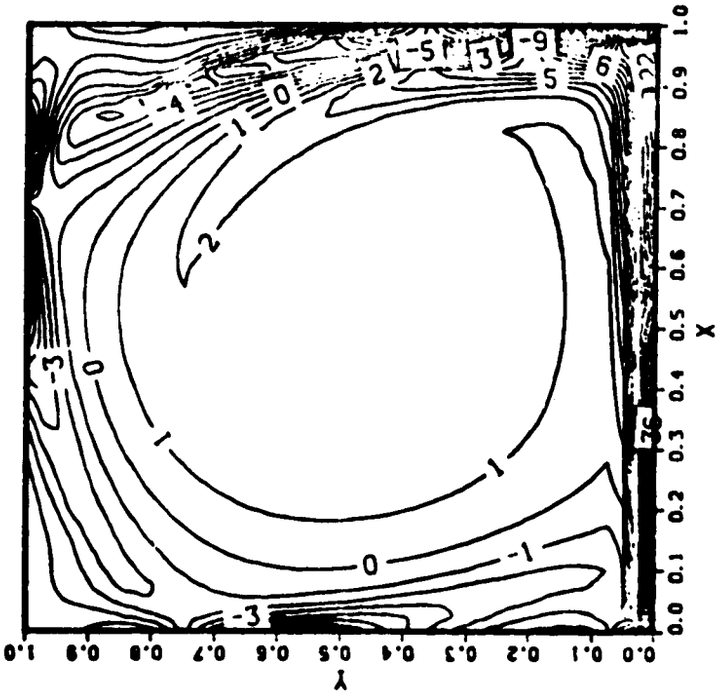

(g) t = 26

Figure 17 (cont'd)

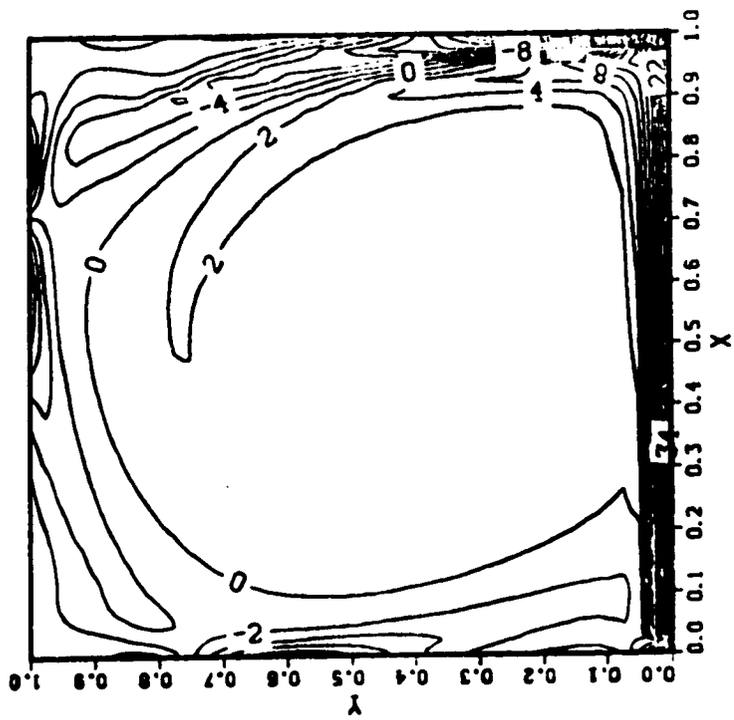

(i) t = 65

Second-order vorticity boundary conditions

Figure 17 (cont'd)

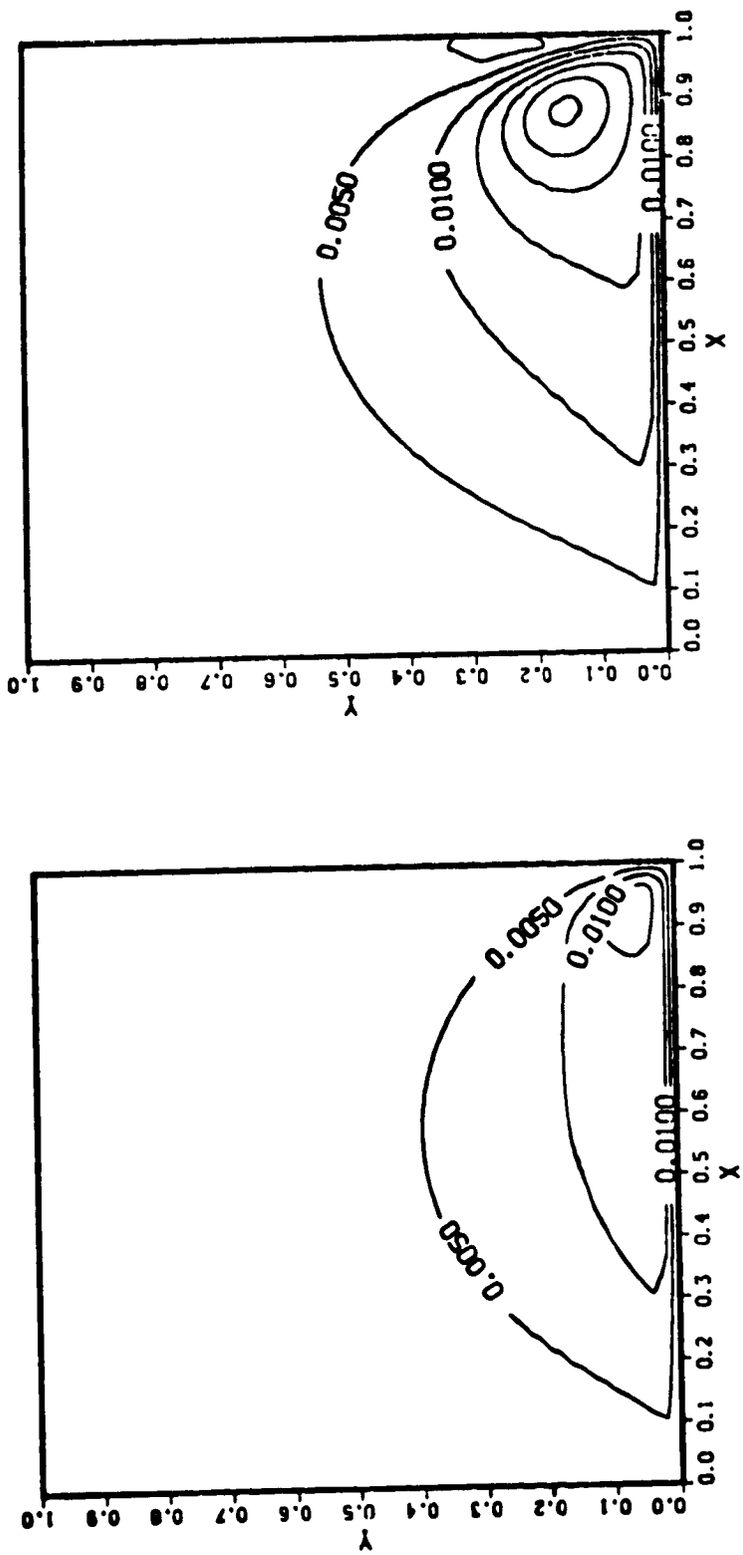

(a) t = 1

(b) t = 2

Figure 18 : Streamlines for 2D starting cavity flow of Re = 5000, 51 x 51 nonuniform grid.

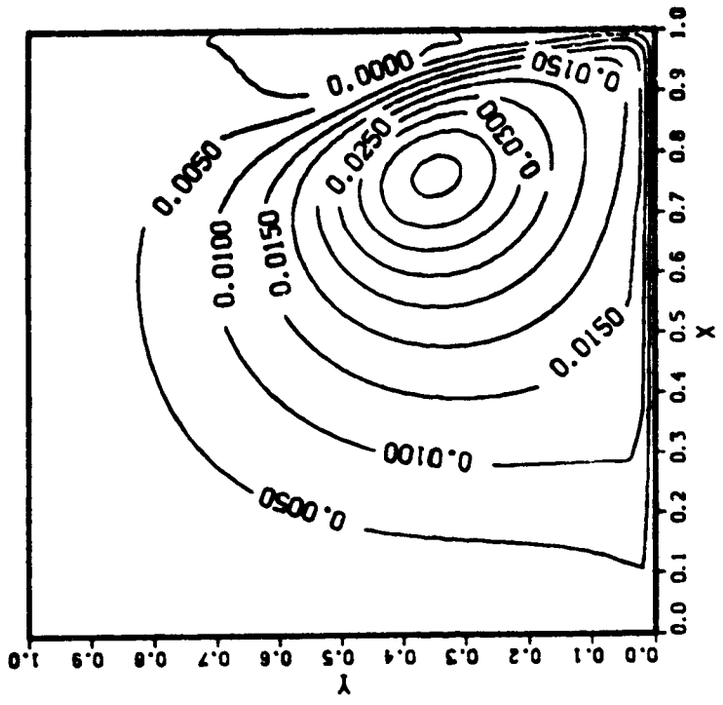

(d) t = 5

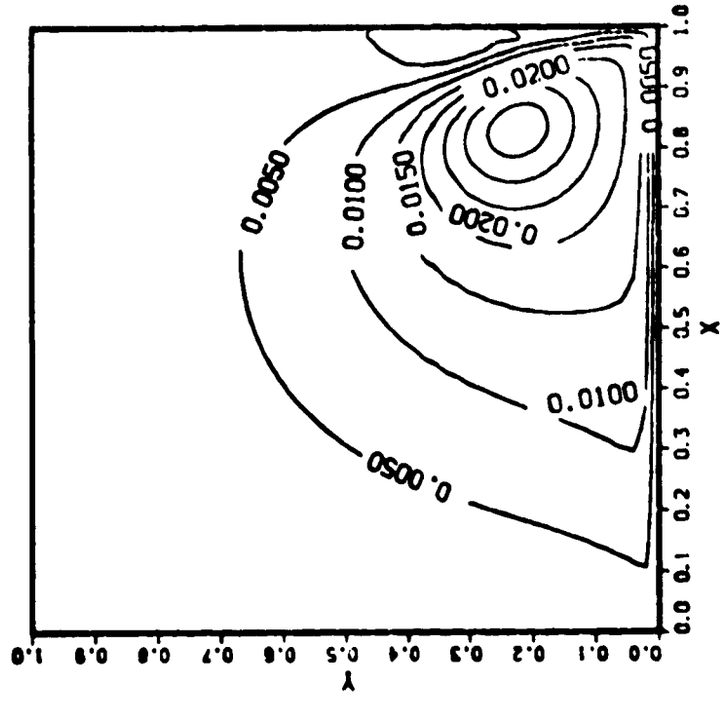

(c) t = 3

Figure 18 (cont'd)

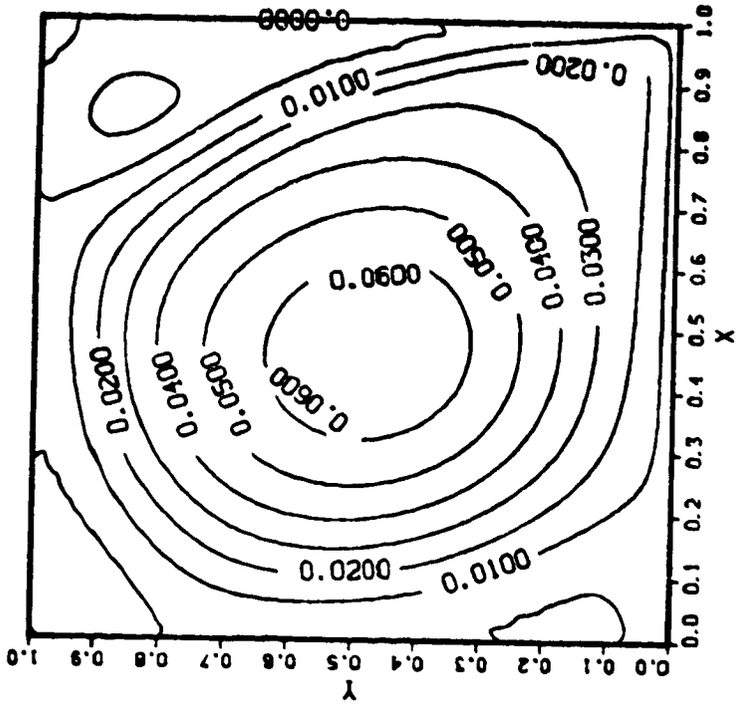

(f) t = 20

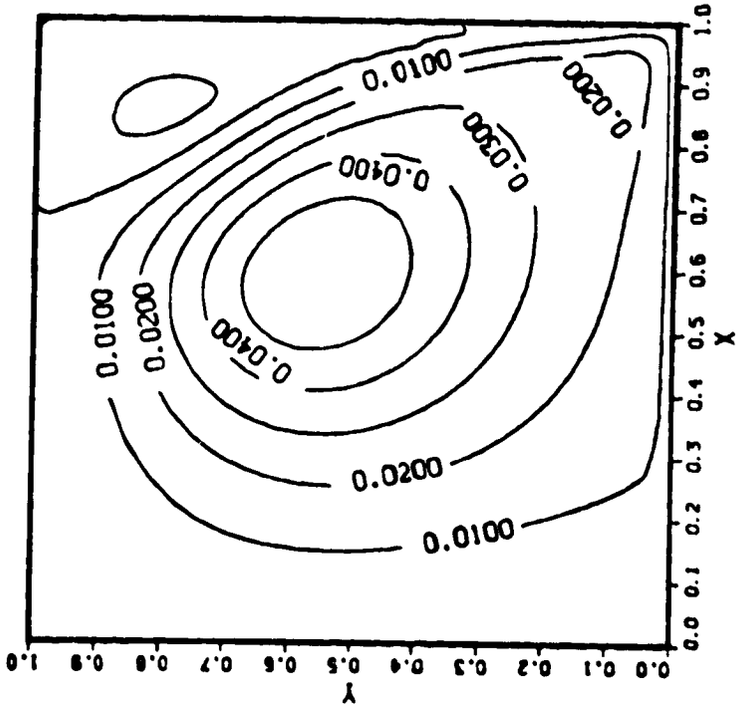

(e) t = 10

Figure 18 (cont'd)

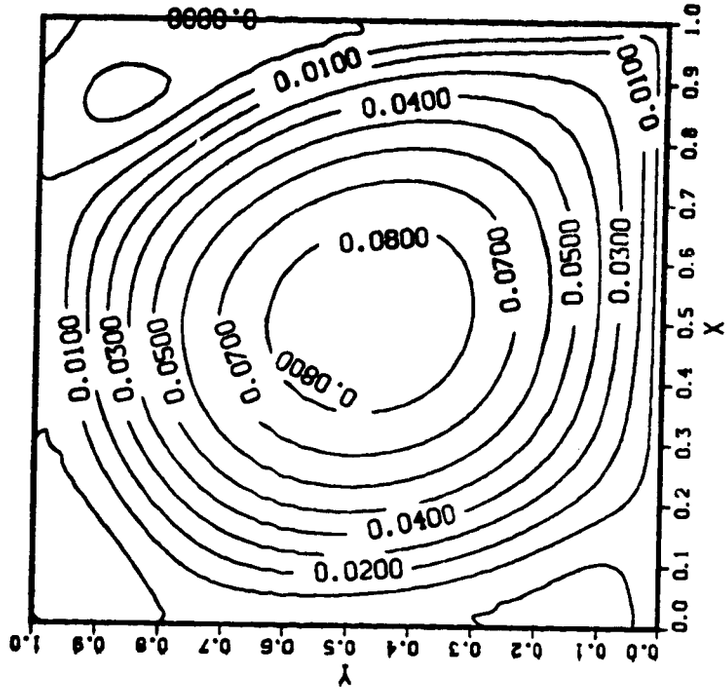

(h) t = 52

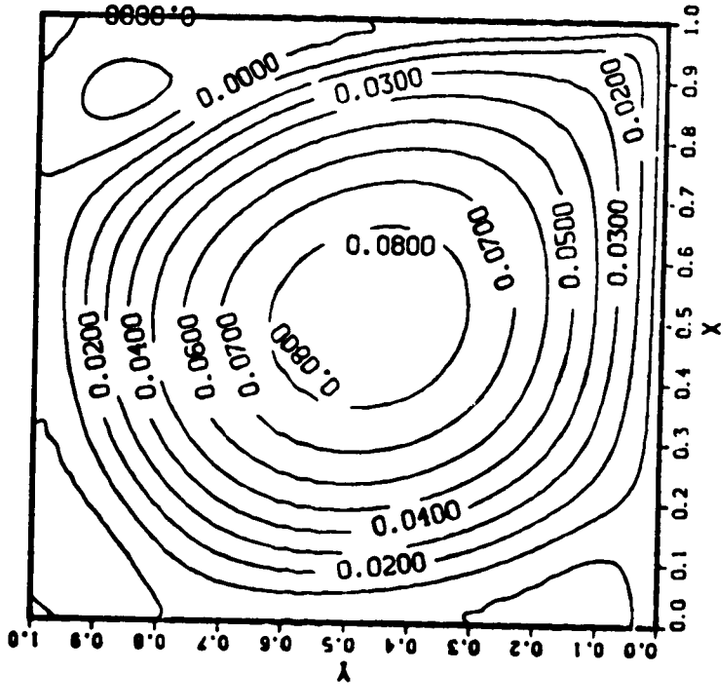

(g) t = 47

Second-order vorticity
boundary conditions

Figure 18 (cont'd)

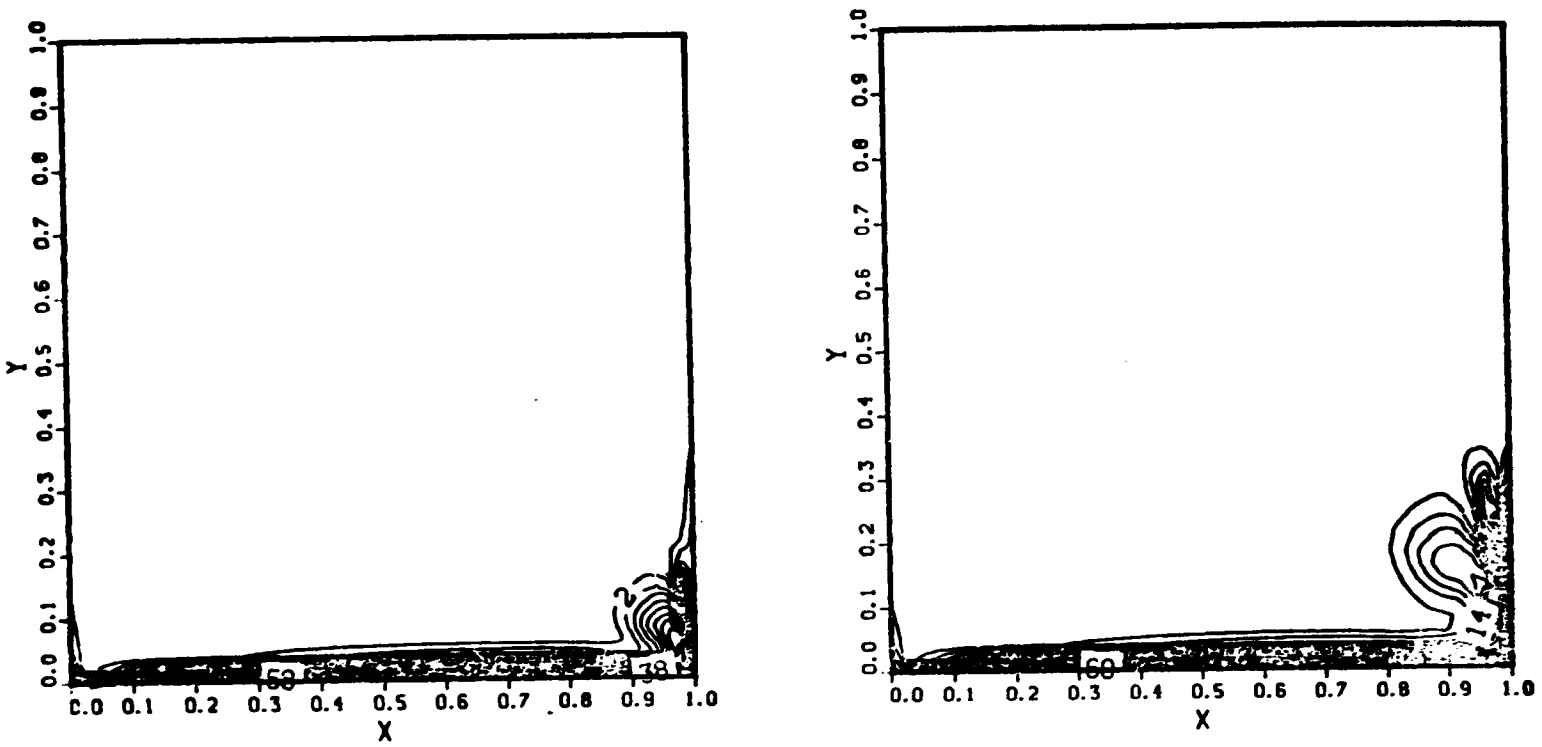

(a) t = 1

(b) t = 2

Figure 19 : Vorticity contours for 2D starting cavity flow of Re = 5000, 51 × 51 nonuniform grid.

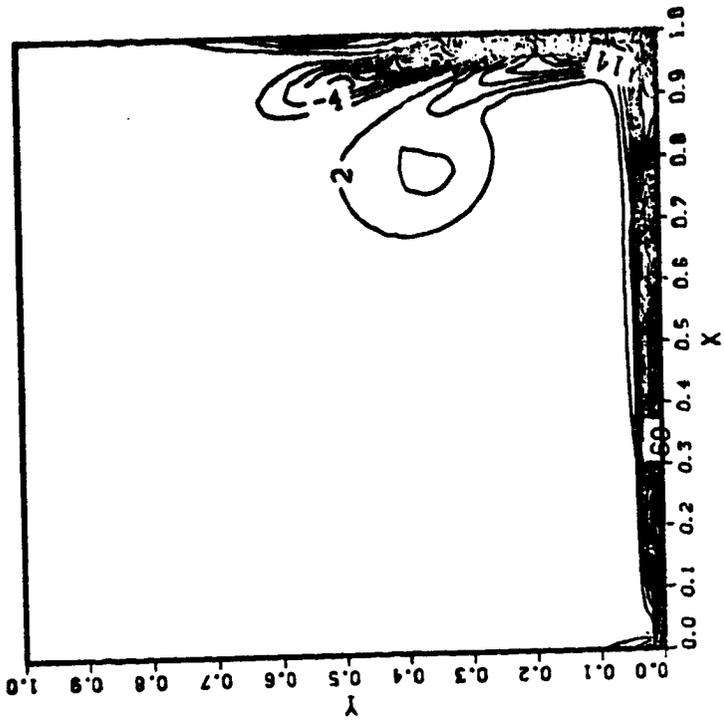

(d) t = 5

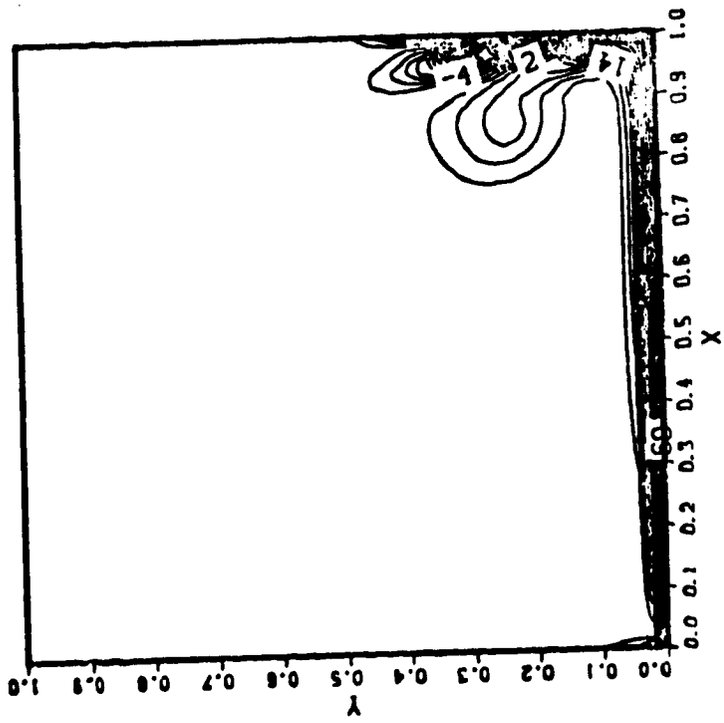

(c) t = 3

Figure 19 (cont'd)

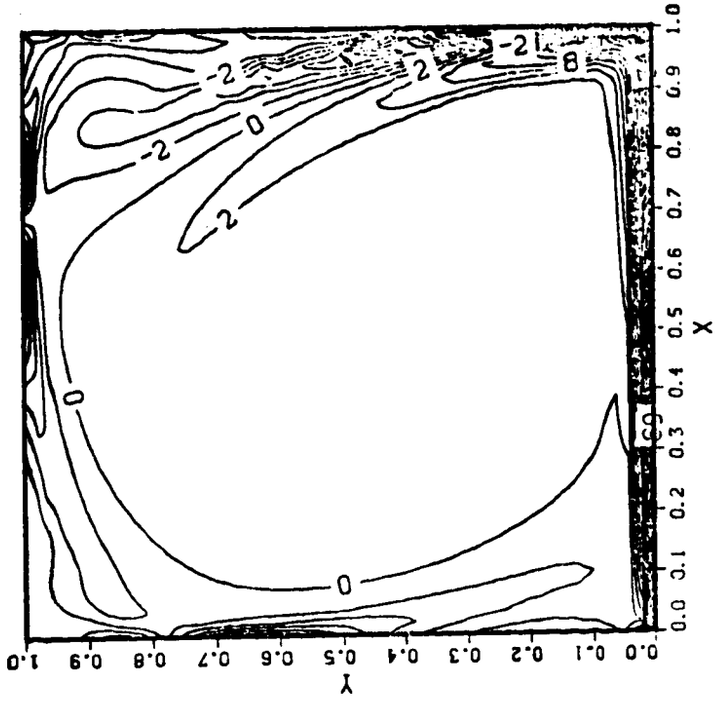

(f) t = 20

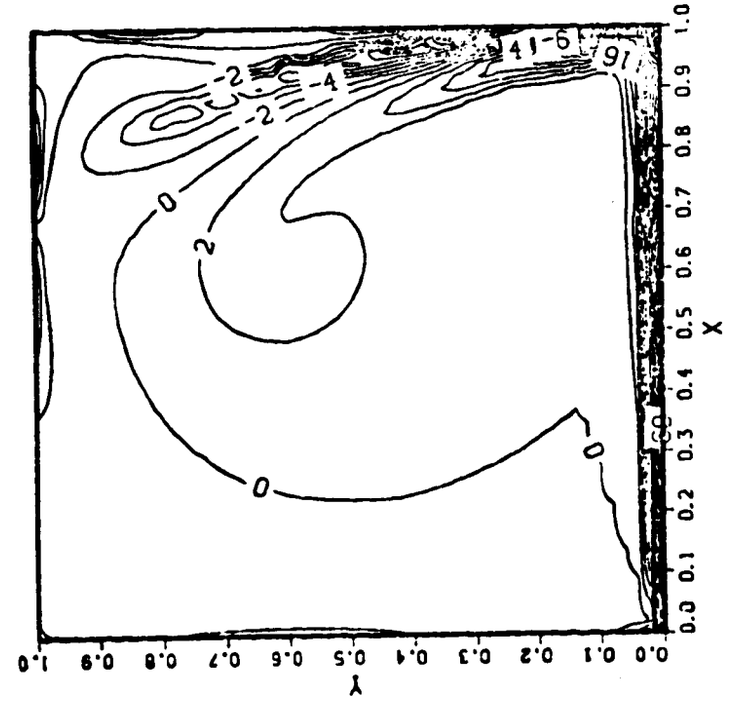

(e) t = 10

Figure 19 (cont'd)

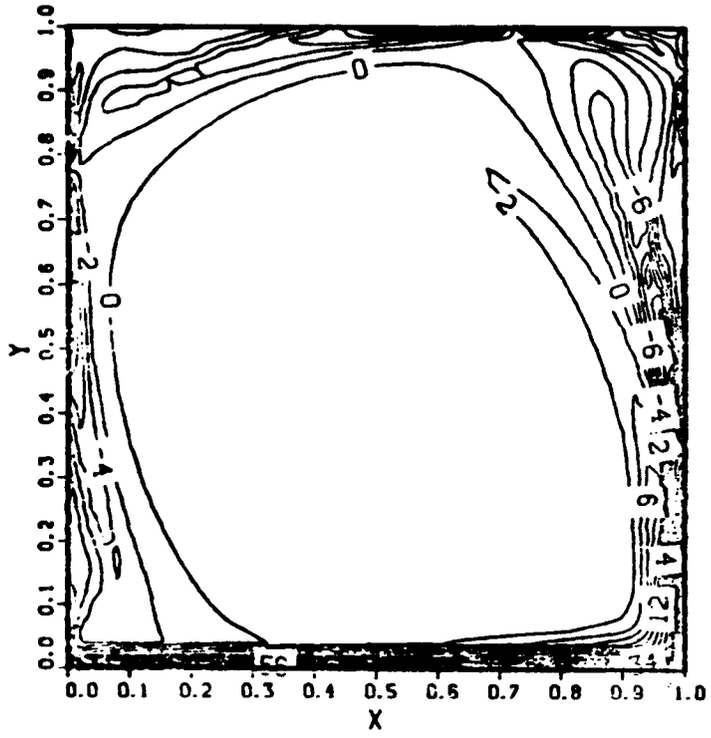

(g) t = 47

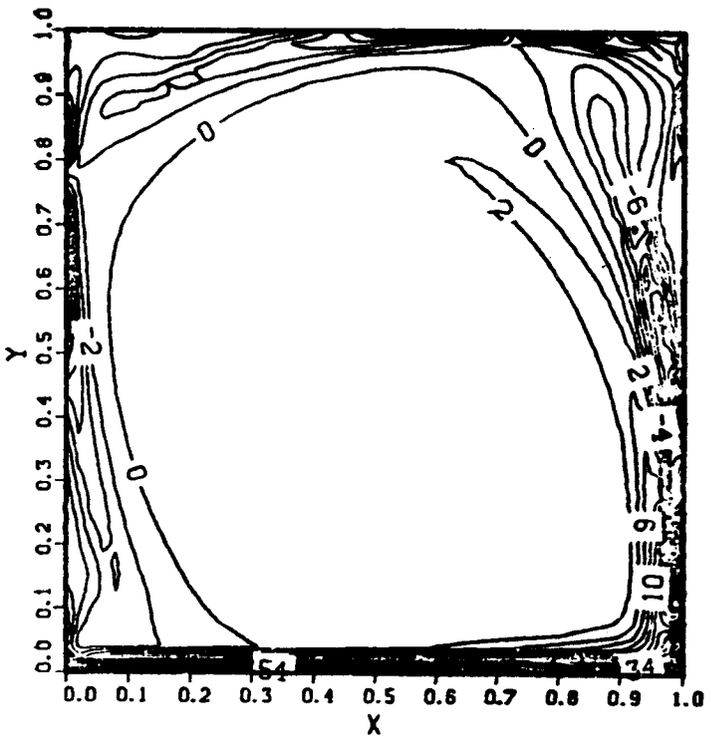

(h) t = 52

Second-order vorticity
boundary conditions

Figure 19 (cont'd)

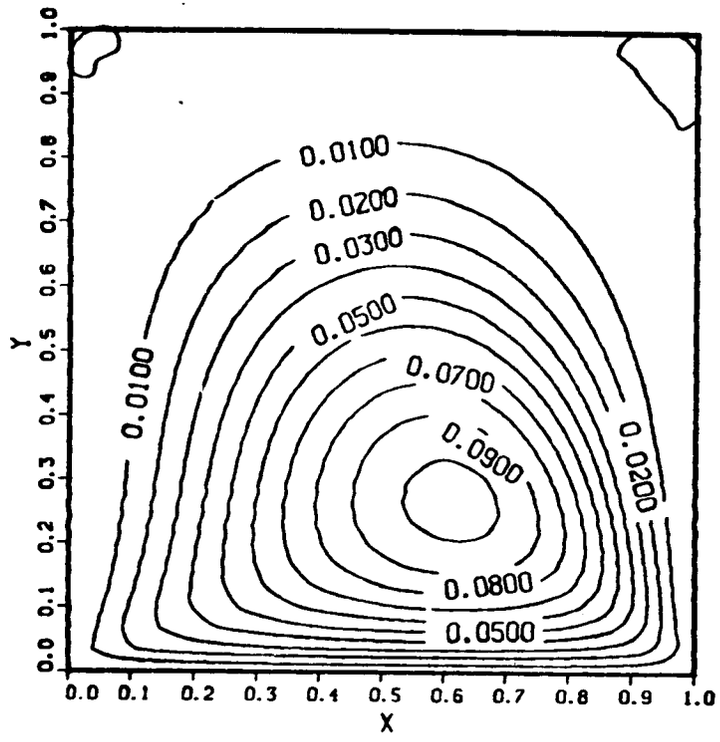

(a) Streamlines

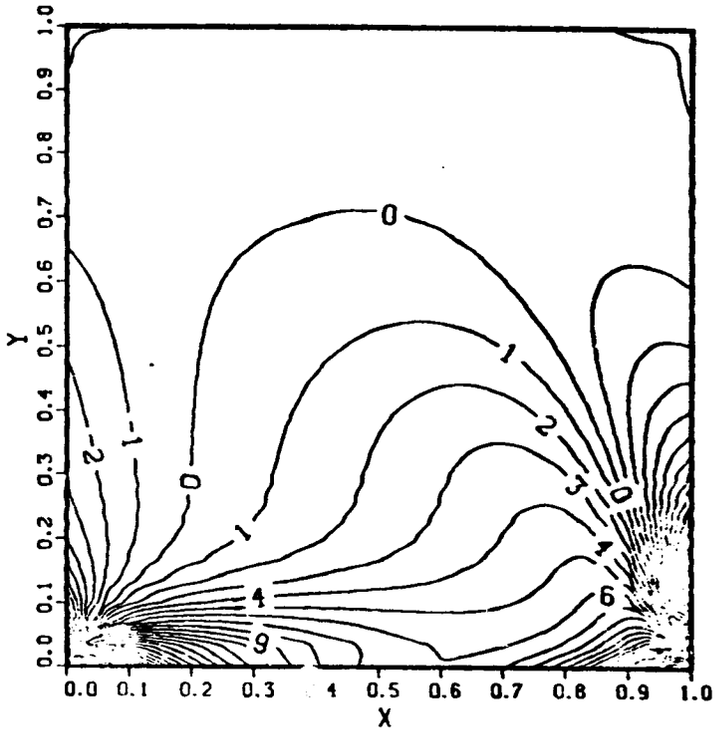

(b) Vorticity contours

Figure 20 : Steady streamlines and vorticity contours for 2D starting cavity flow of Re = 100, 31 × 31 uniform grid (non-conservative higher order correction term).

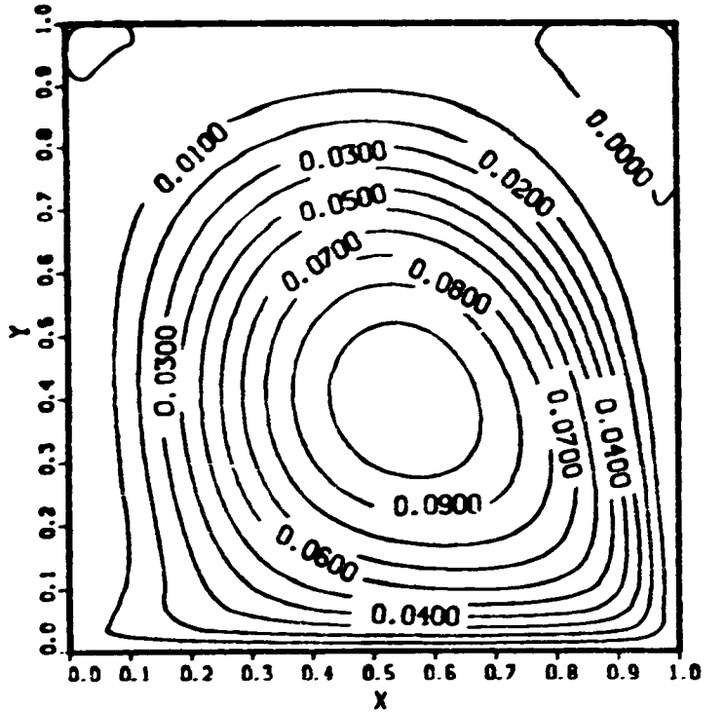

(a) Streamlines

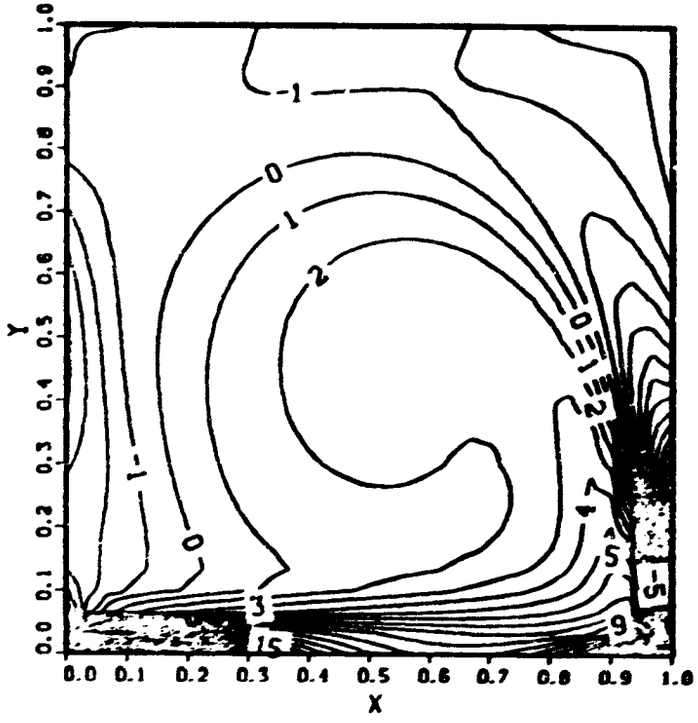

(b) Vorticity contours

Figure 21 : Steady streamlines and vorticity contours for 2D starting cavity flow of Re = 400, 31 × 31 uniform grid (non-conservative higher order correction term).

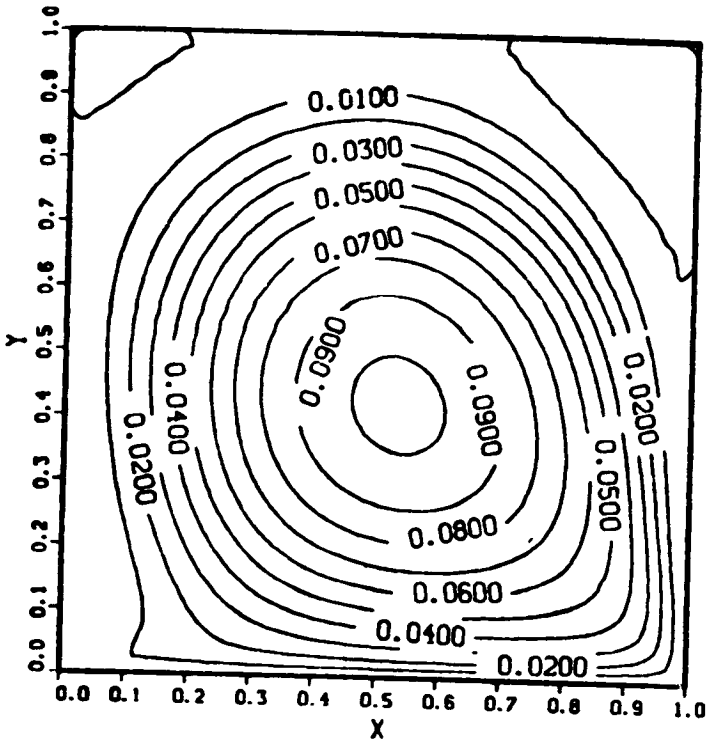

(a) Streamlines

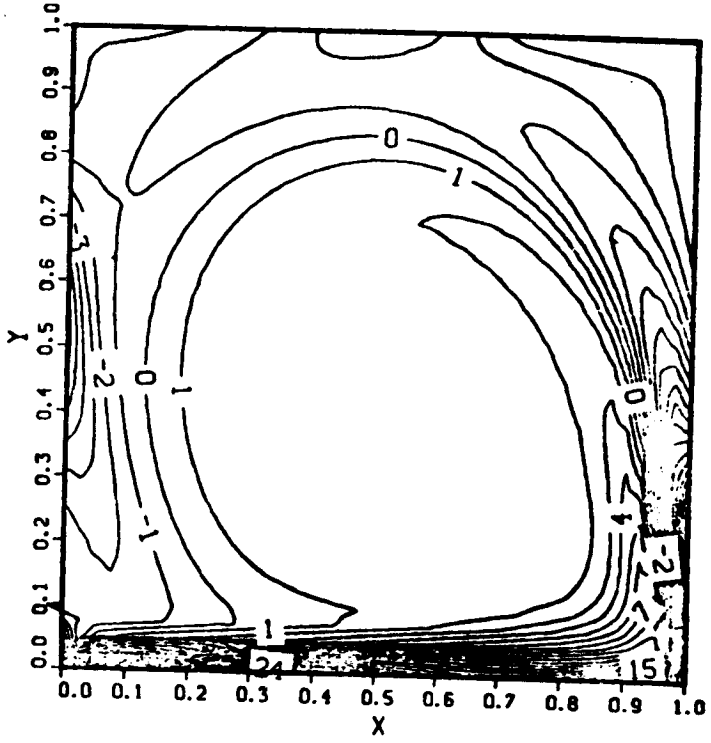

(b) Vorticity contours

Figure 22 : Steady streamlines and vorticity contours for 2D starting cavity flow of Re = 1000, 41 × 41 uniform grid (non-conservative higher order correction term).

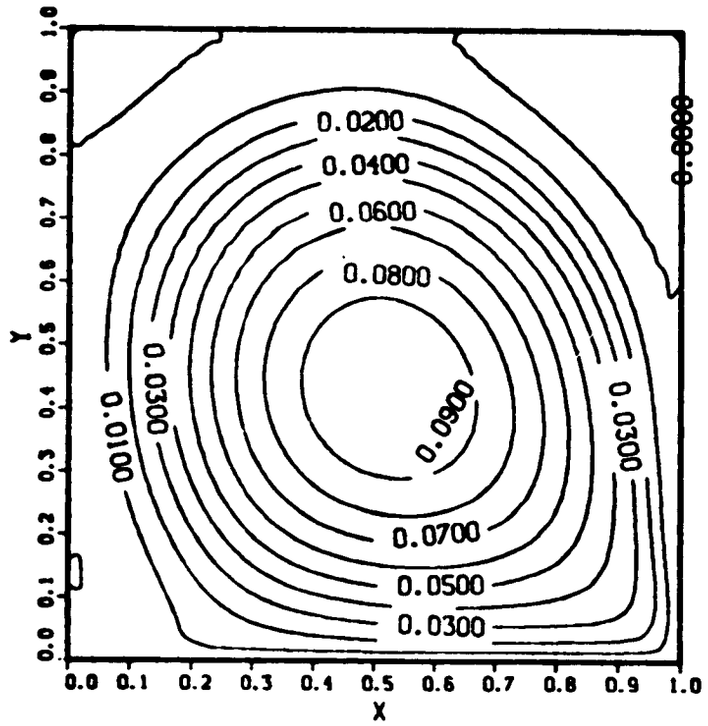

(a) Streamlines

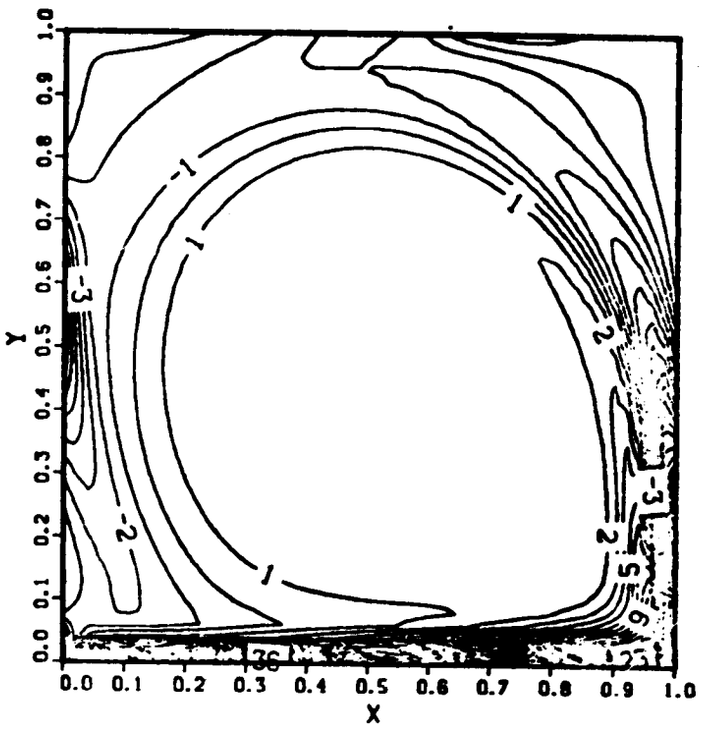

(b) Vorticity contours

Figure 23 : Steady streamlines and vorticity contours for 2D starting cavity flow of Re = 2000, 51 × 51 uniform grid (non-conservative higher order correction term).

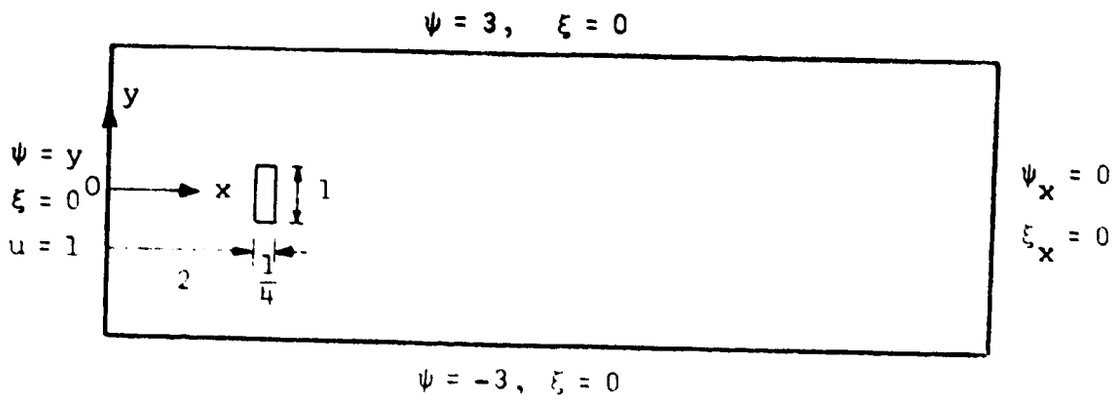

Figure 24 : Coordinate and boundary conditions for vortex street development problem.

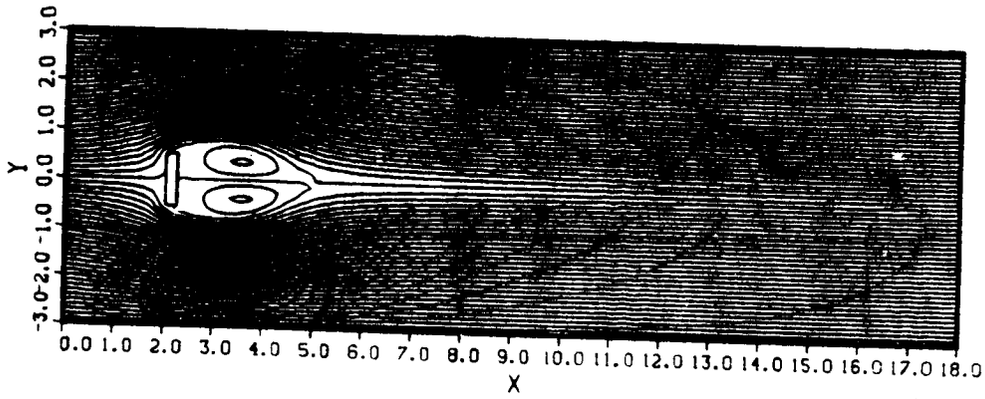

(a) Streamlines at t = 10

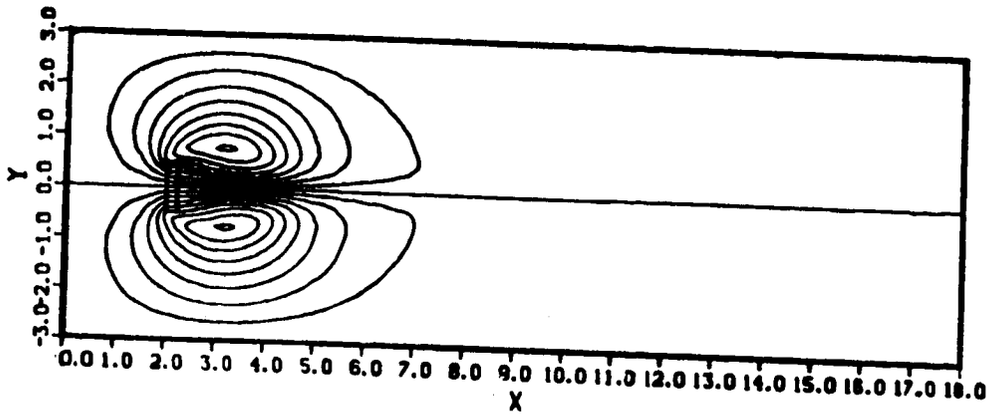

(b) Rest streamlines at t = 10

Figure 25 : Streamlines and rest streamlines for vortex street development process of Re = 500. $\Delta\psi = 0.1$.

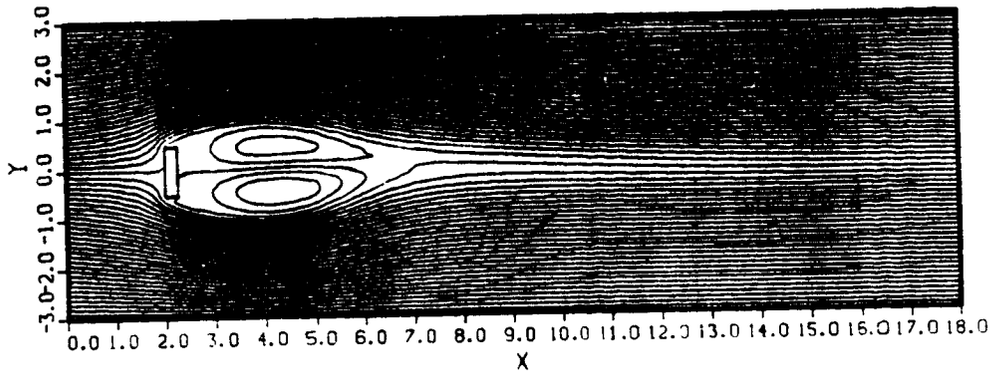

(c) Streamlines at t = 20

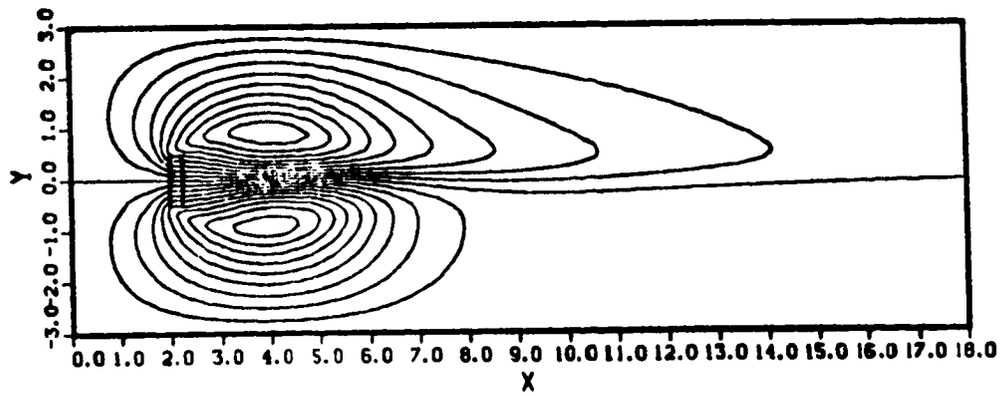

(d) Rest streamlines at t = 20

Figure 25 (cont'd)

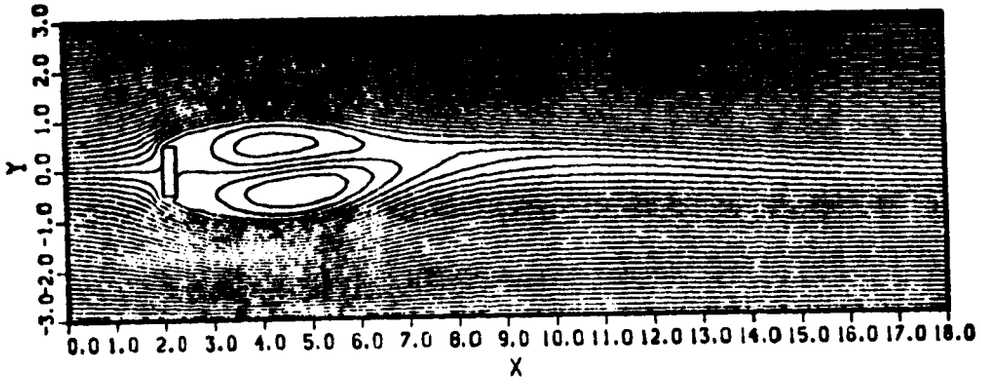

(a) With artificial perturbation

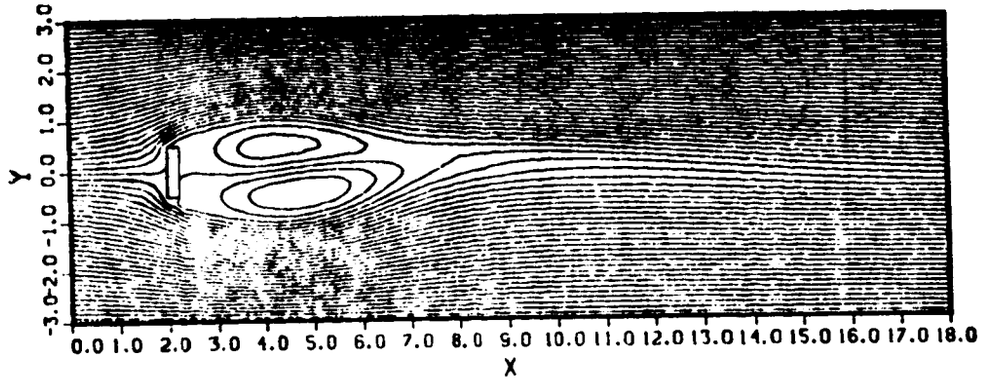

(b) Without artificial perturbation

Figure 26 : Comparison of streamlines at t = 24 for vortex street development process of Re = 500. $\Delta\psi = 0.1$.

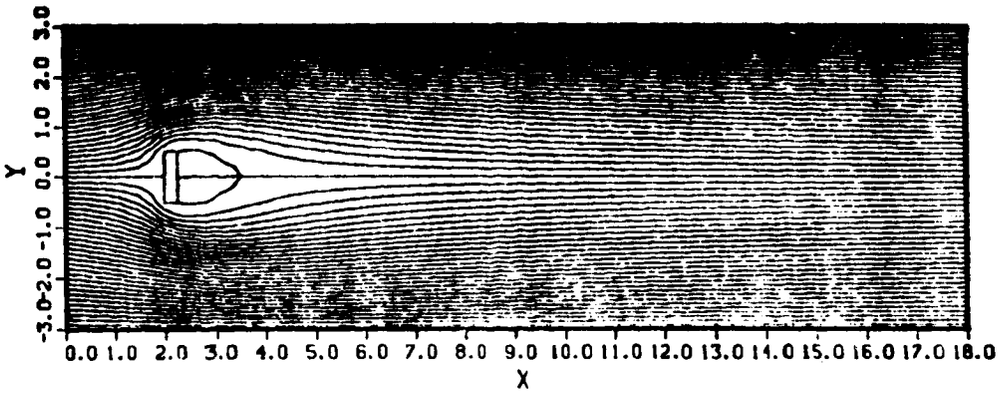

(a) Steady streamlines at t = 30

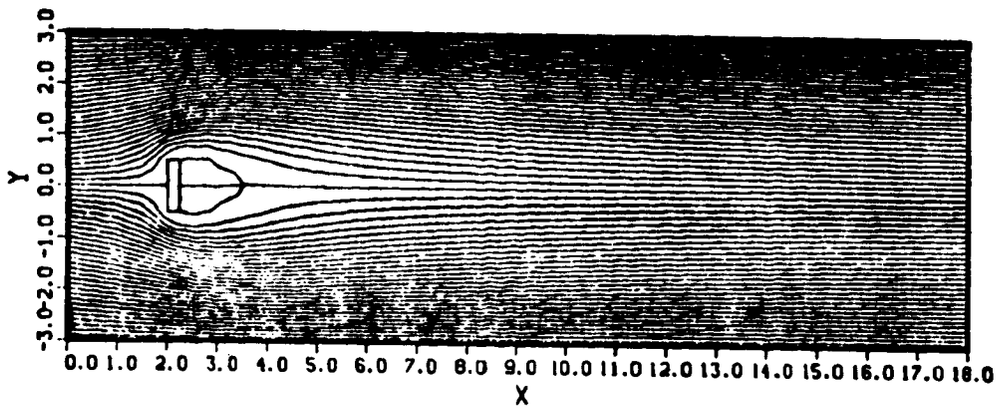

(b) Streamlines at t = 35
(after perturbation)

Figure 27 : Comparison of streamlines for vortex street development process of Re = 10. $\Delta\psi = 0.1$.

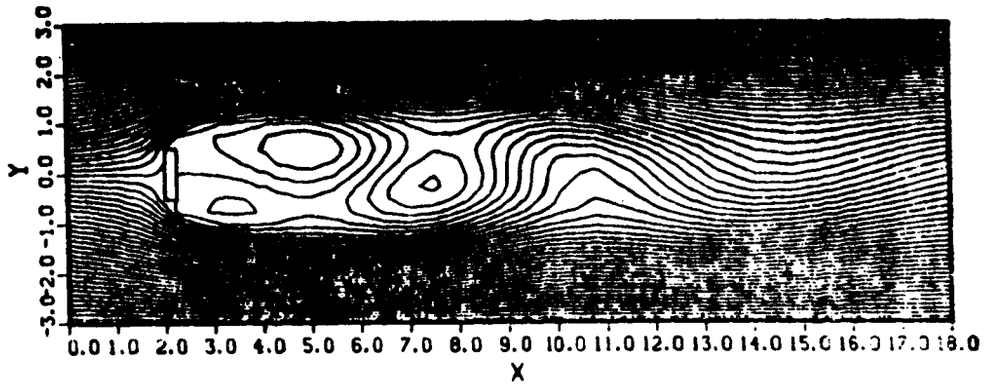

(a) t = 43.6

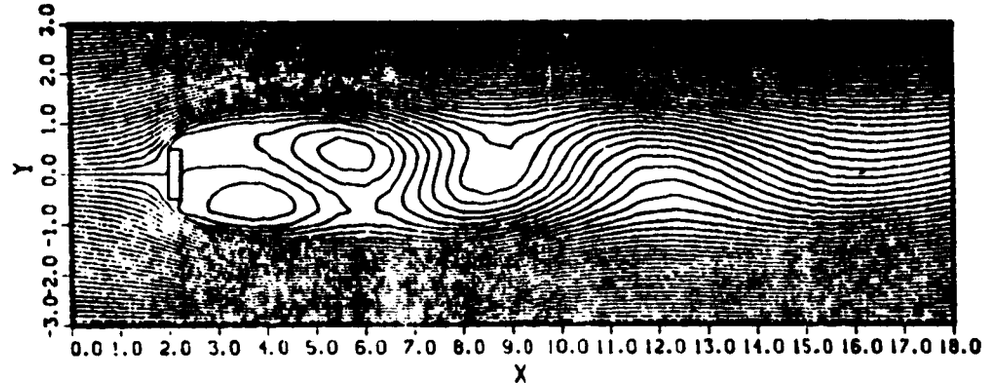

(b) t = 45.2

Figure 28 : Streamlines for vortex street development process of Re = 100. $\Delta\psi = 0.1$.

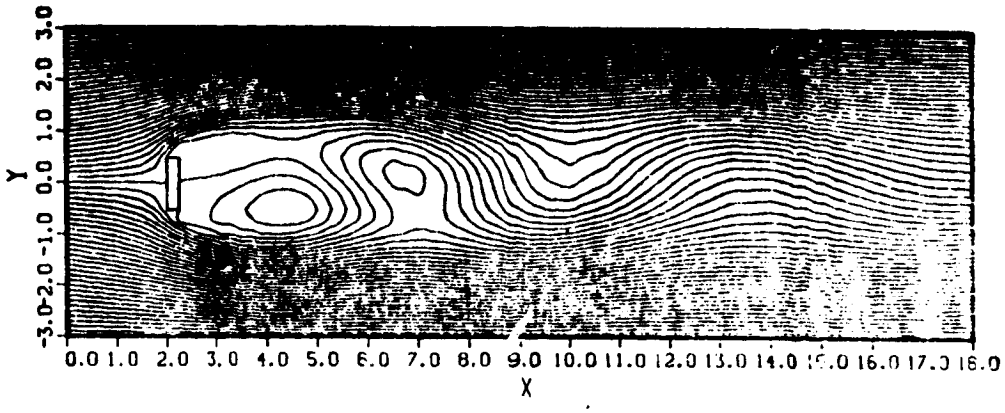

(c) t = 46.8

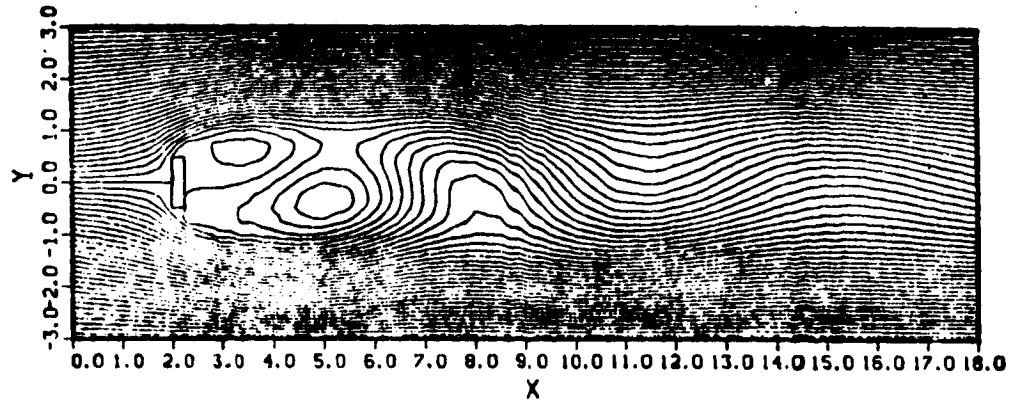

(d) t = 48.4

Figure 28 (cont'd)

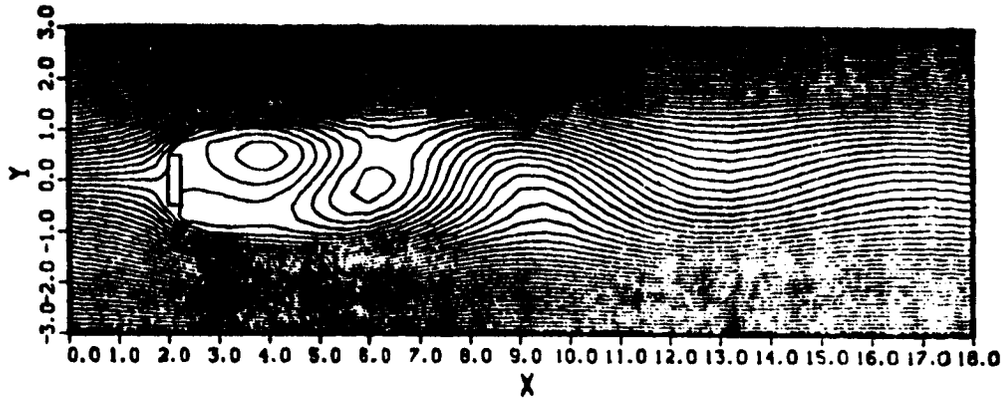

(e) t = 50.0

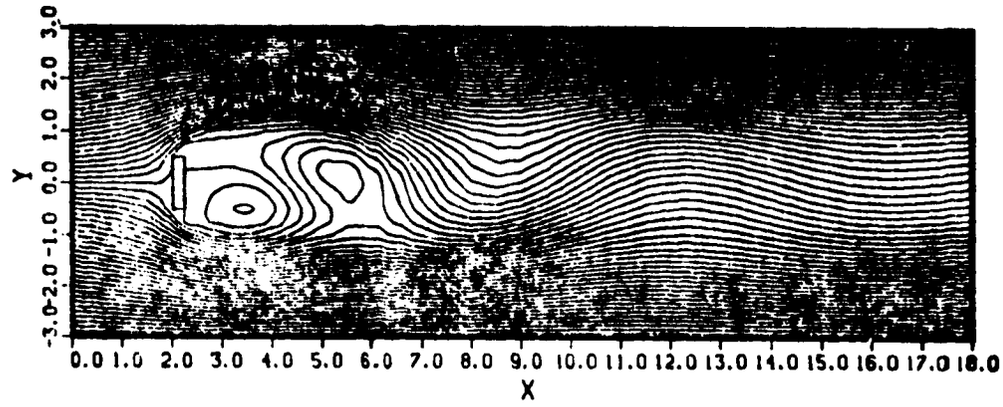

(f) t = 53.2

Figure 28 (cont'd)

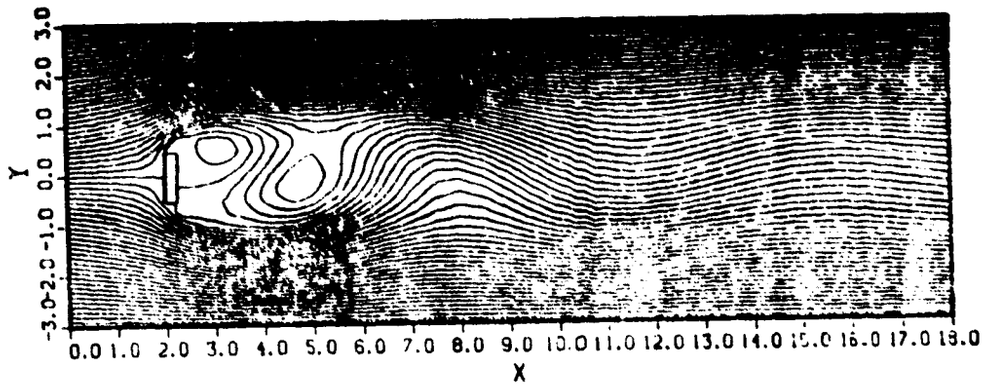

(g) t = 56.4

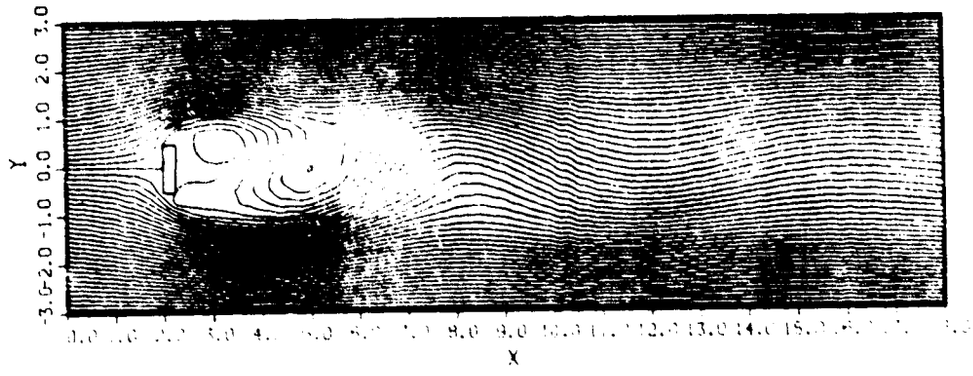

(h) t = 56.8

Figure 28 (cont'd)

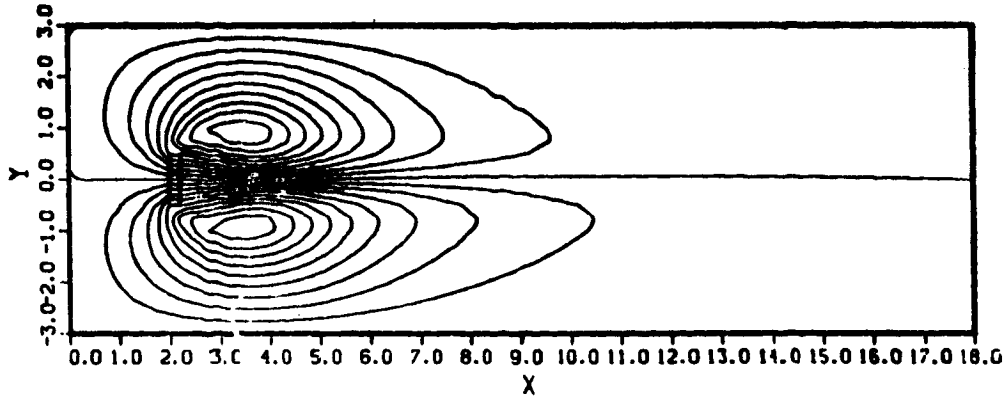

(a) Rest streamlines at t = 10

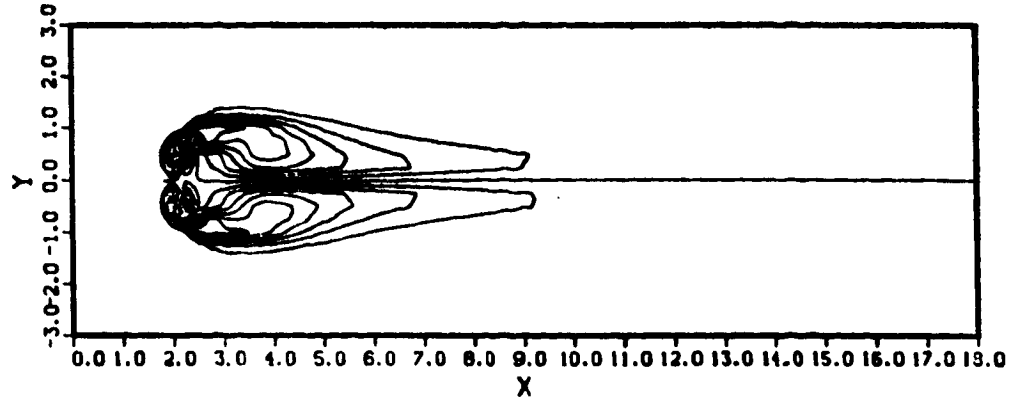

(b) Vorticity contours at t = 10

Figure 29 : Rest streamlines and vorticity contours for vortex street development process of Re = 100. $\Delta\psi = 0.1$, $\Delta\xi = 0.5$.

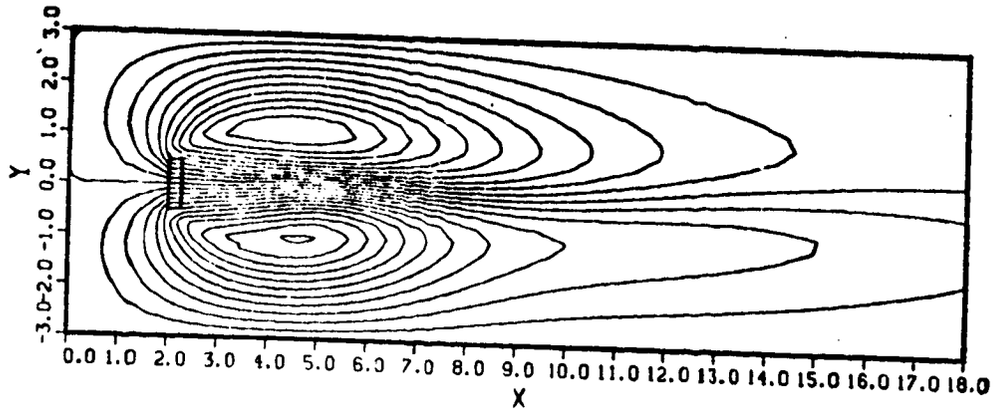

(c) Rest streamlines at t = 20

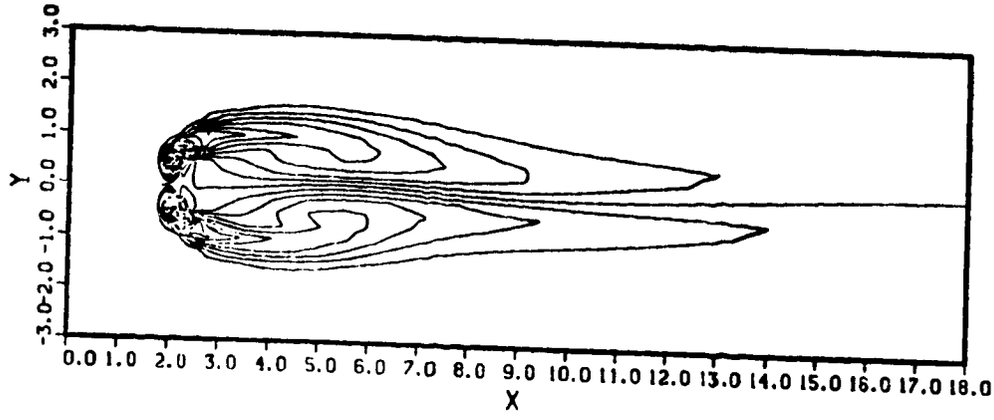

(d) Vorticity contours at t = 20

Figure 29 (cont'd)

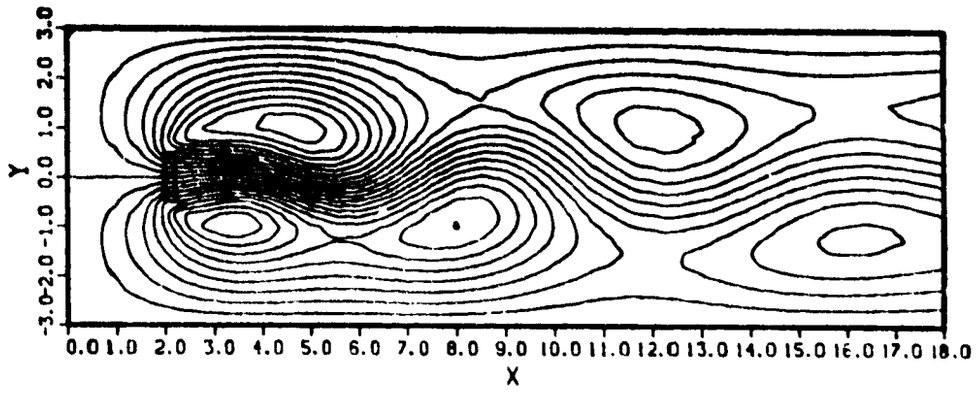

(e) Rest streamlines at t = 53.2

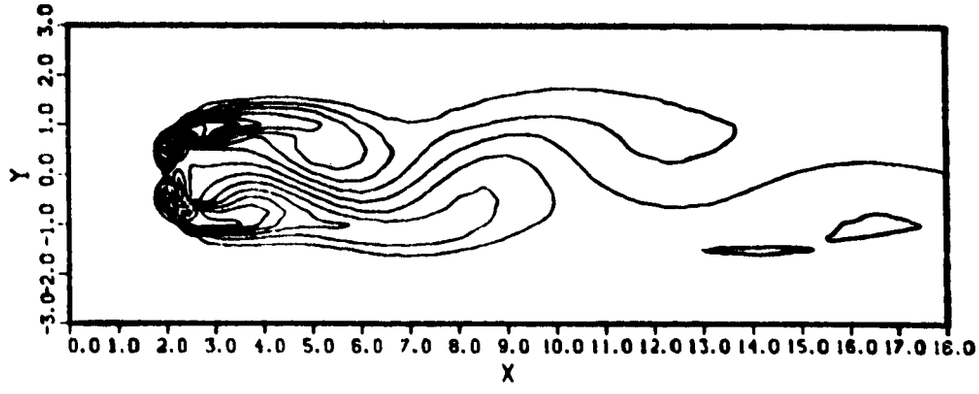

(f) Vorticity contours at t = 53.2

Figure 29 (cont'd)

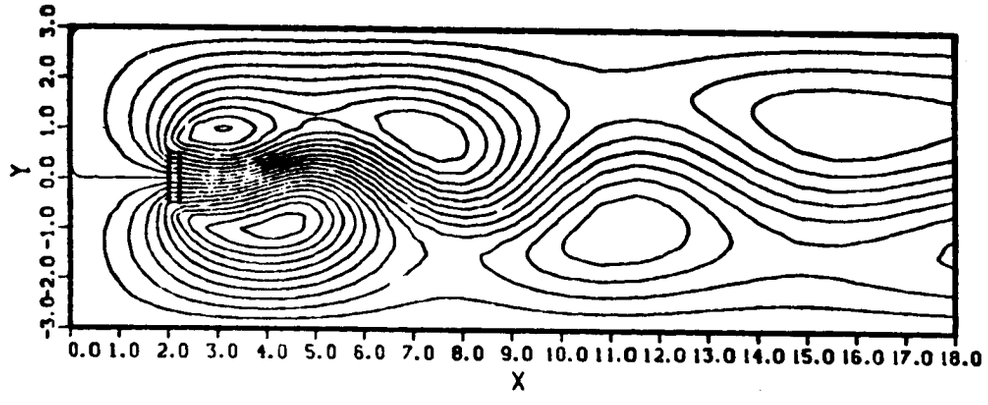

(g) Rest streamlines at t = 56.4

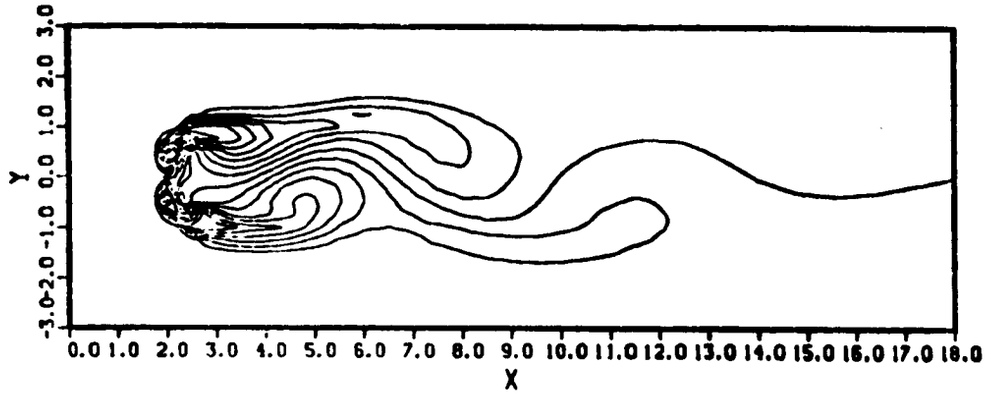

(h) Vorticity contours at t = 56.4

Figure 29 (cont'd)

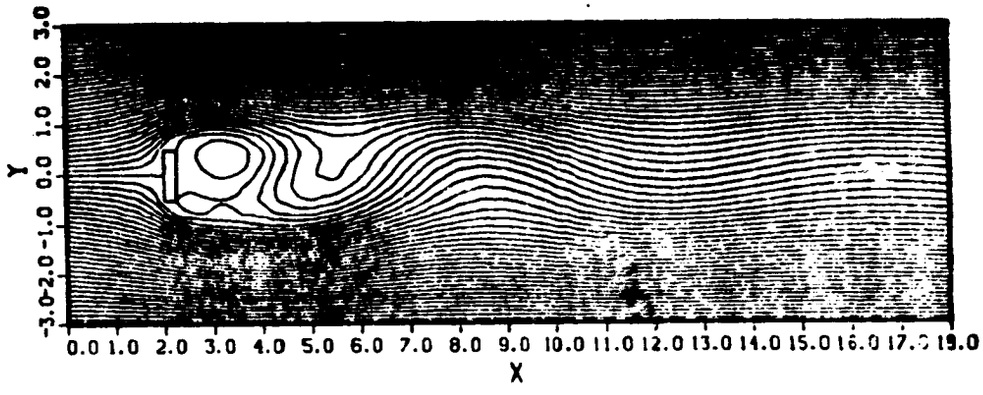

(a) Streamlines at t = 54.4

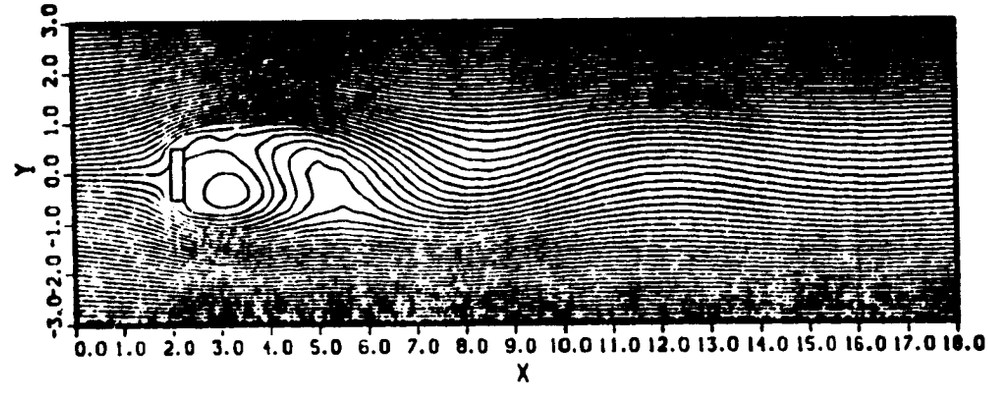

(b) Streamlines at t = 58.0

Figure 30 : Streamlines, rest streamlines and vorticity contours for vortex street development process of Re = 50. $\Delta\psi = 0.1$, $\Delta\xi = 0.5$.

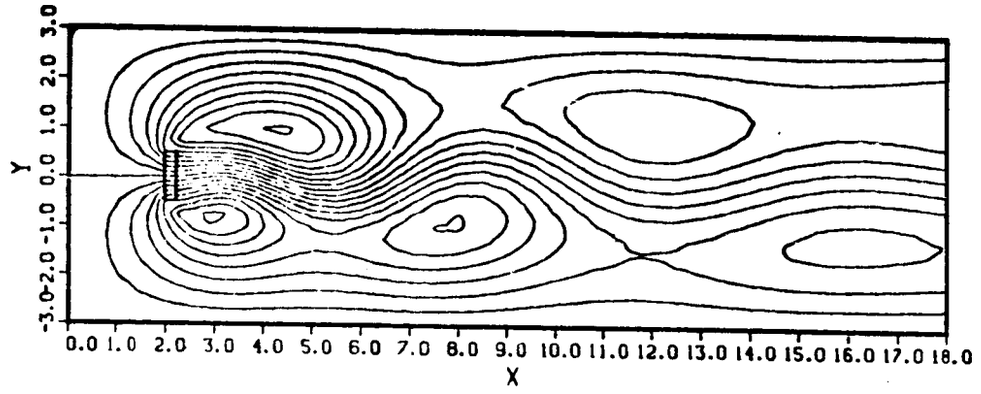

(c) Rest streamlines at t = 54.4

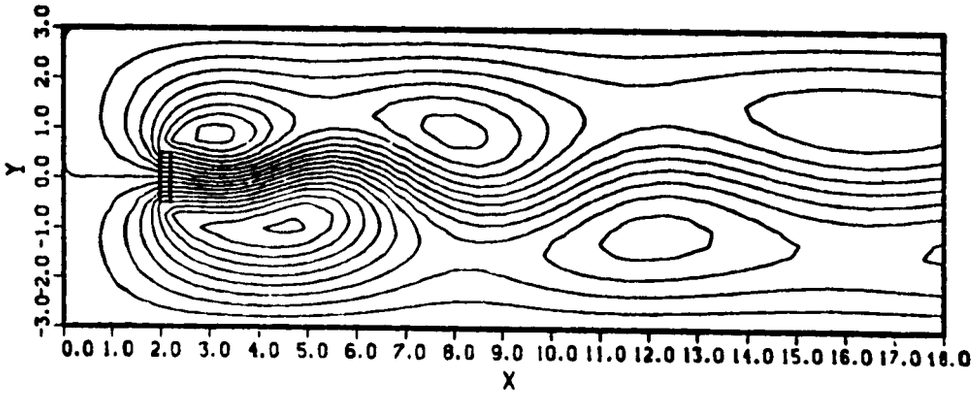

(d) Rest streamlines at t = 58.0

Figure 30 (cont'd)

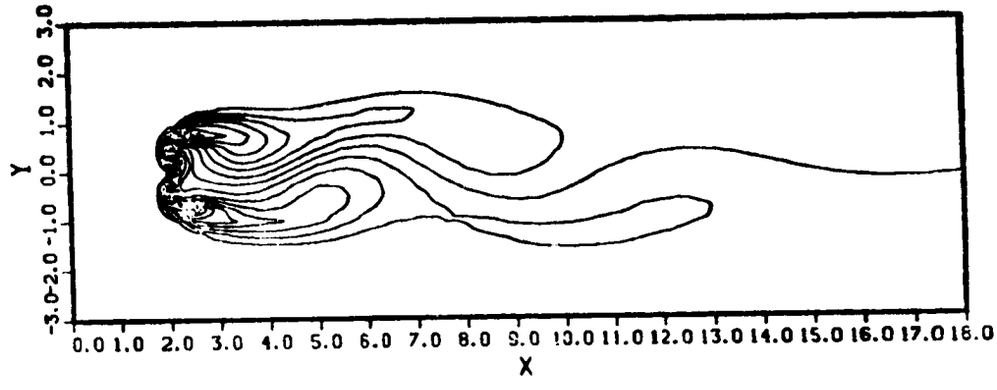

(e) Vorticity contours at t = 54.4

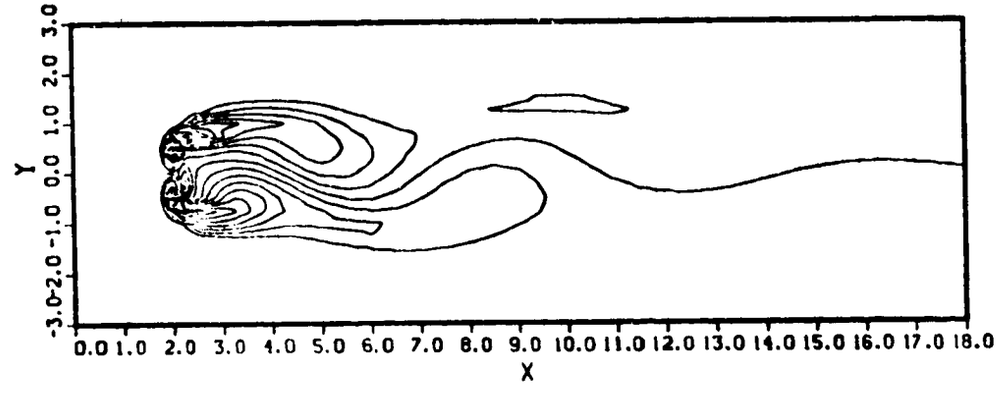

(f) Vorticity contours at t = 58.0

Figure 30 (cont'd)

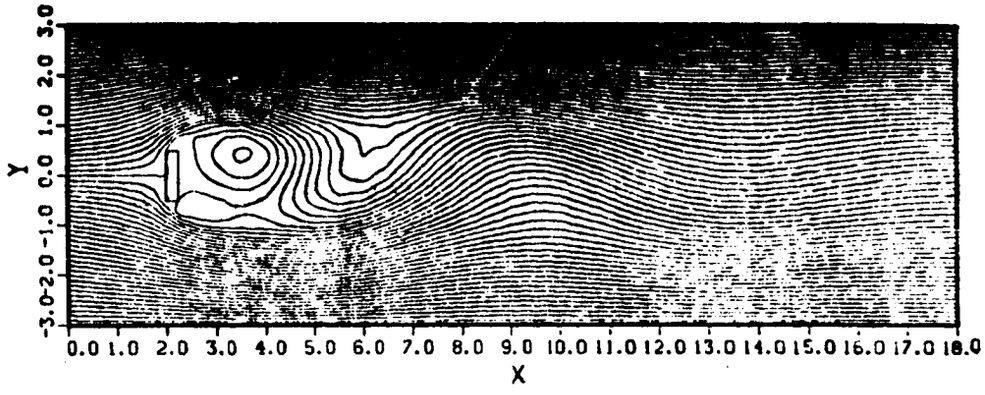

(a) Streamlines at t = 42.8

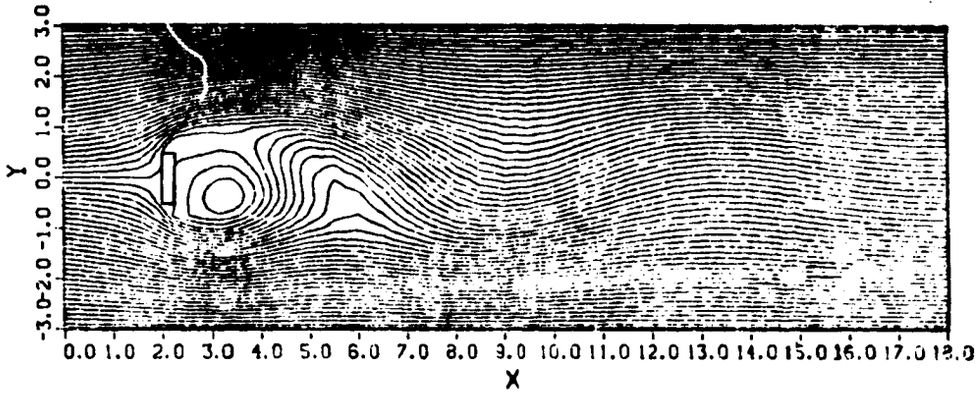

(b) Streamlines at t = 46.6

Figure 31 : Streamlines, rest streamlines and vorticity contours for vortex street development process of Re = 200. $\Delta\psi = 0.1$, $\Delta\xi = 0.5$.

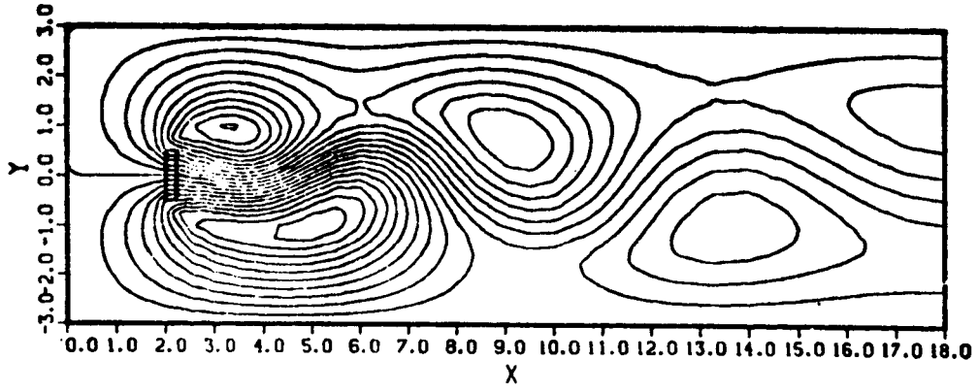

(c) Rest streamlines at t = 42.8

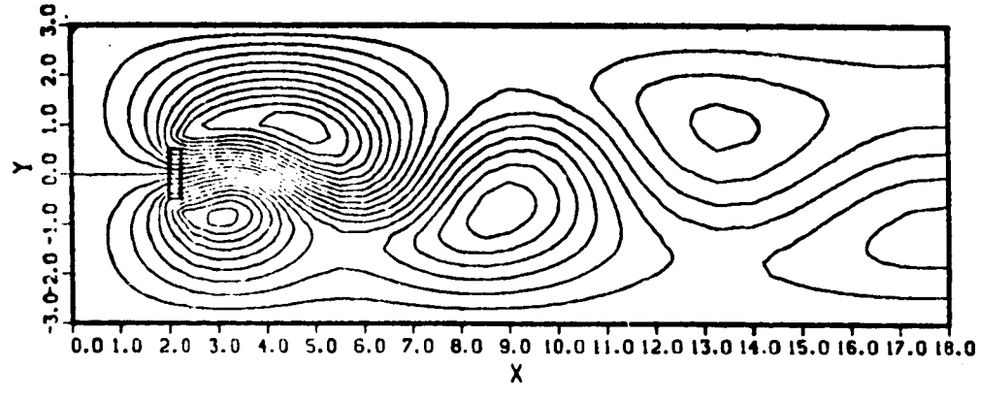

(d) Rest streamlines at t = 46.6

Figure 31 (cont'd)

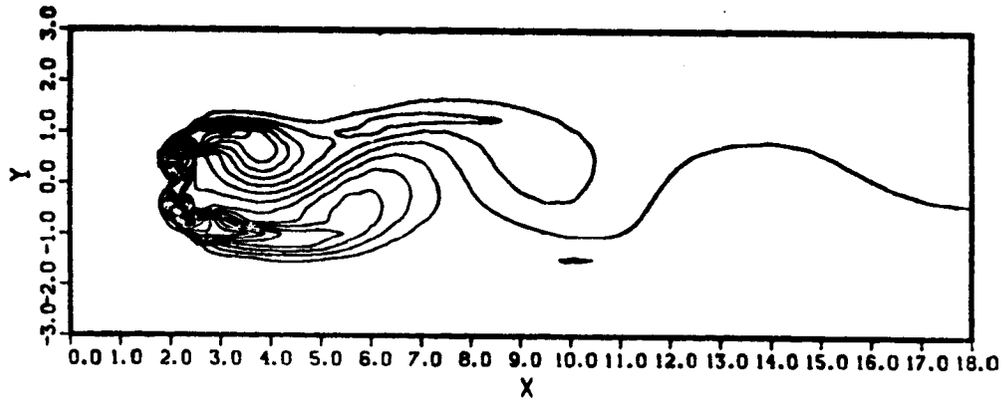

(e) Vorticity contours at t = 42.8

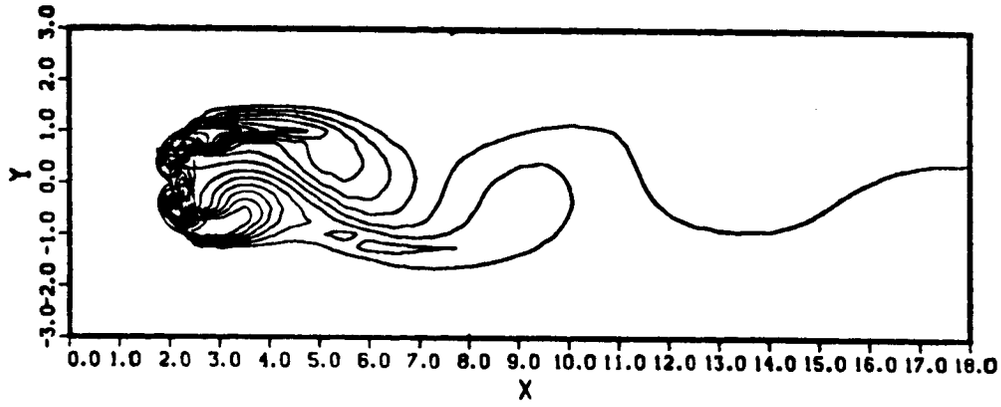

(f) Vorticity contours at t = 46.6

Figure 31 (cont'd)

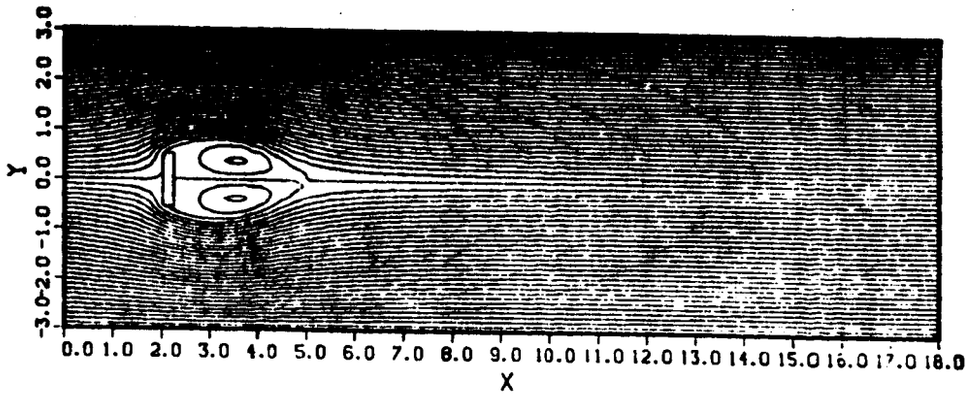

(a) t = 10

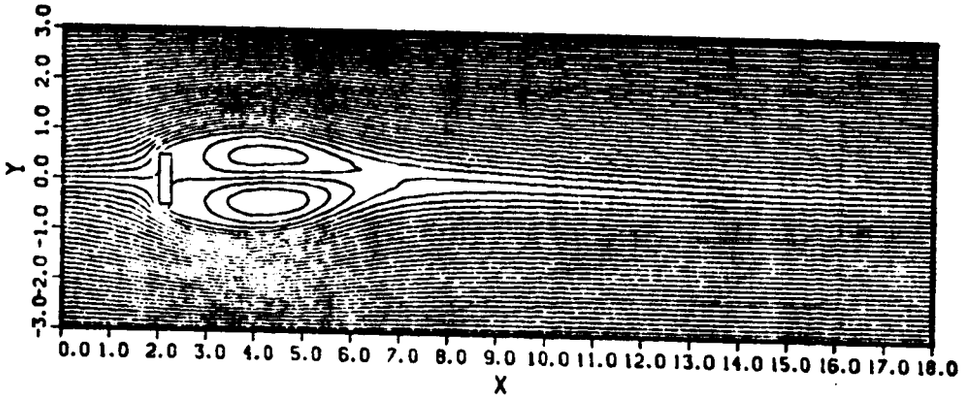

(b) t = 20

Figure 32 : Streamlines for vortex street development process of Re = 500. $\Delta\psi = 0.1$.

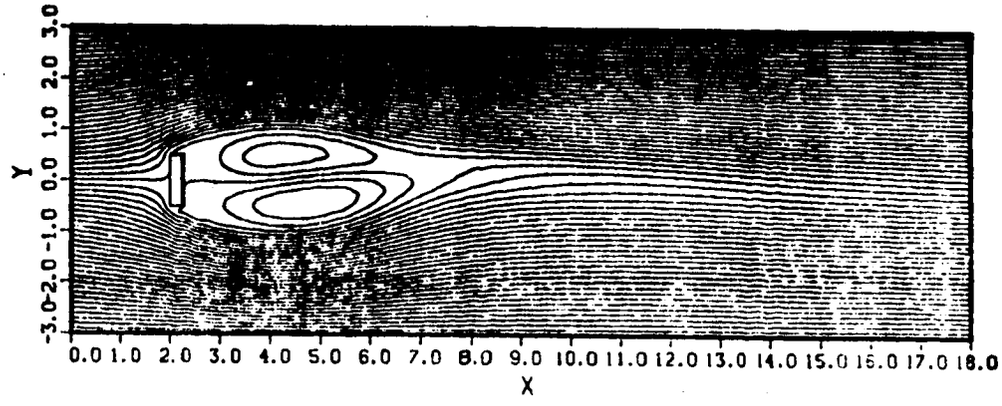

(c) t = 24

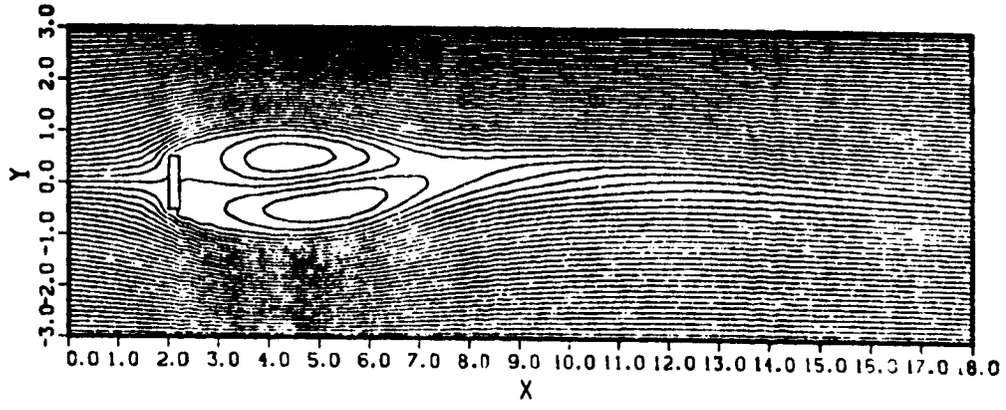

(d) t = 26

Figure 32 (cont'd)

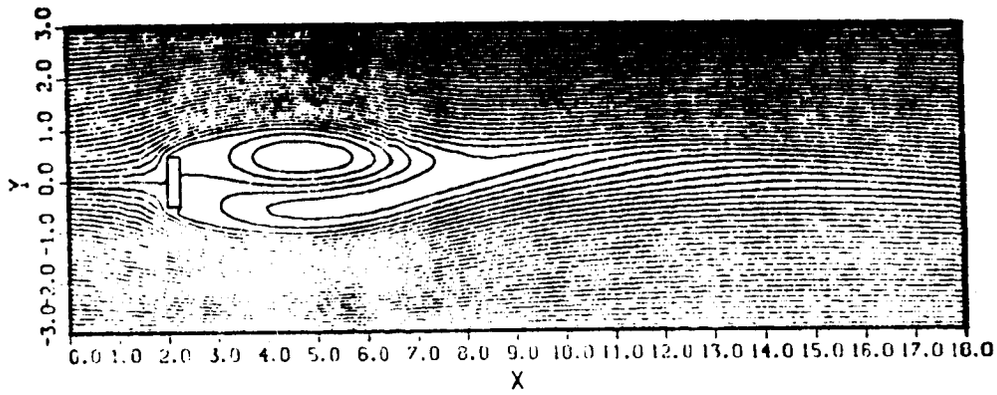

(e) t = 28

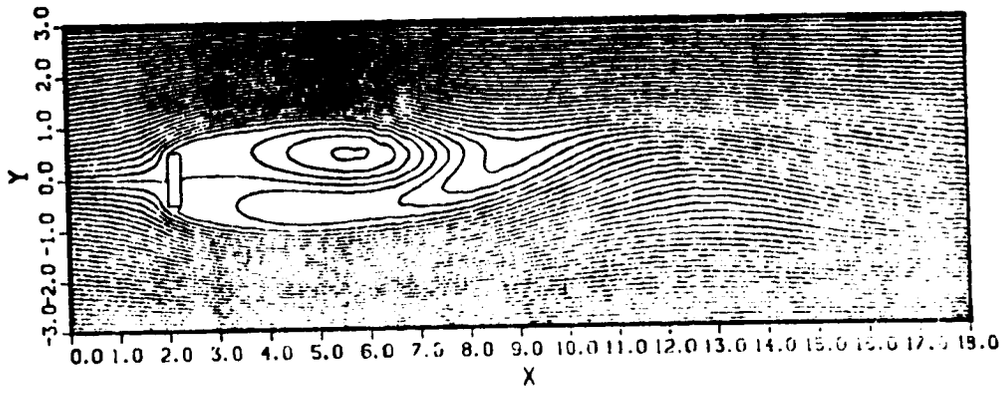

(f) t = 40

Figure 32 (cont'd)

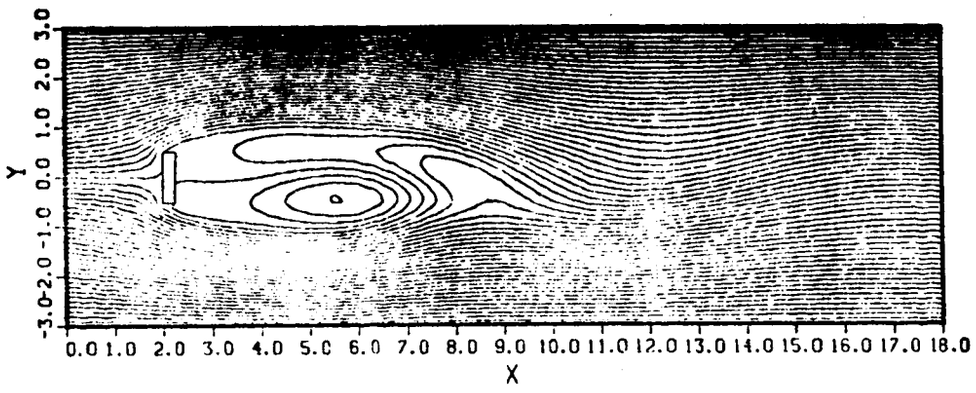

(g) t = 44.4

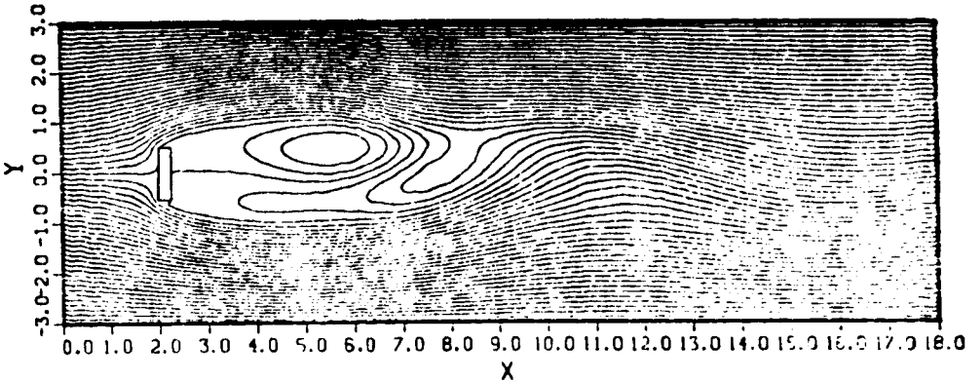

(h) t = 48.4

Figure 32 (cont'd)

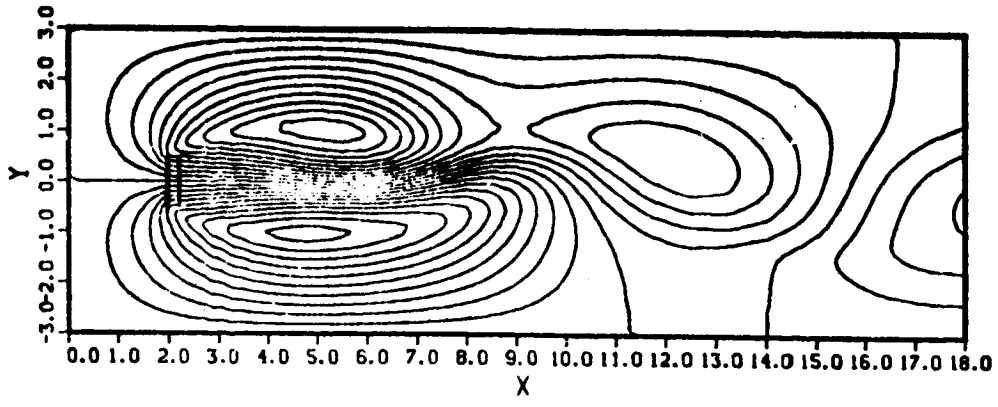

(a) t = 40.0

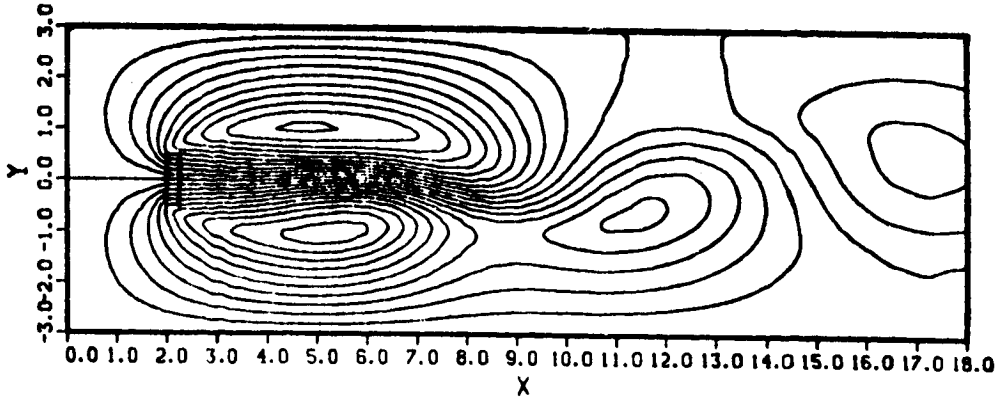

(b) t = 44.4

Figure 33 : Rest streamlines for vortex street development process of Re = 500. $\Delta\psi = 0.1$.

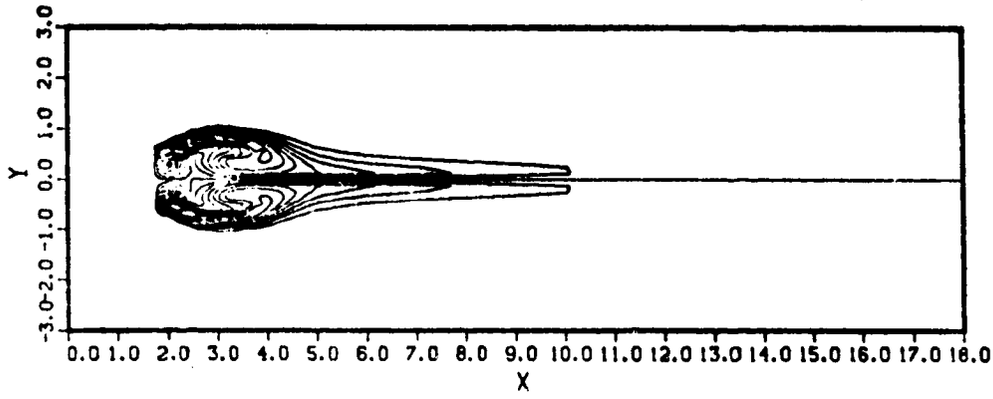

(a) t = 10

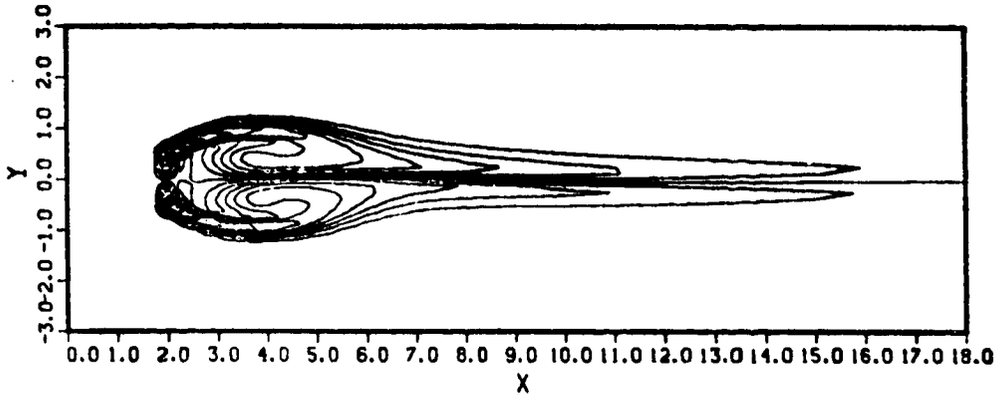

(b) t = 20

Figure 34 : Vorticity contours for vortex street development process of Re = 500. $\Delta\xi = 0.5$.

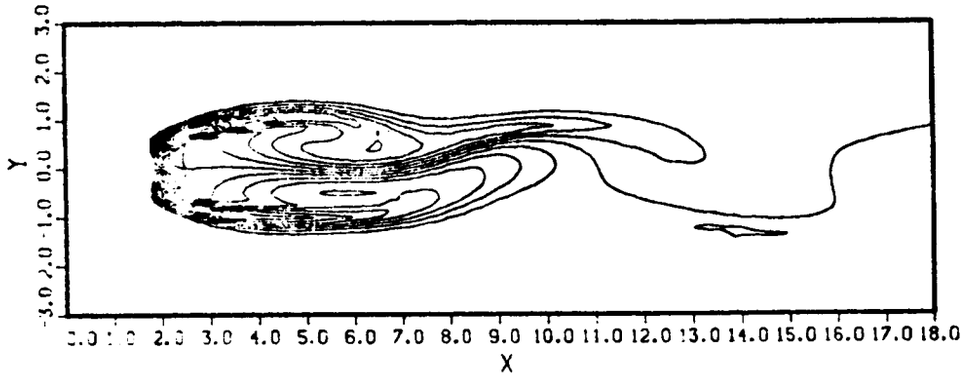

(c) t = 40

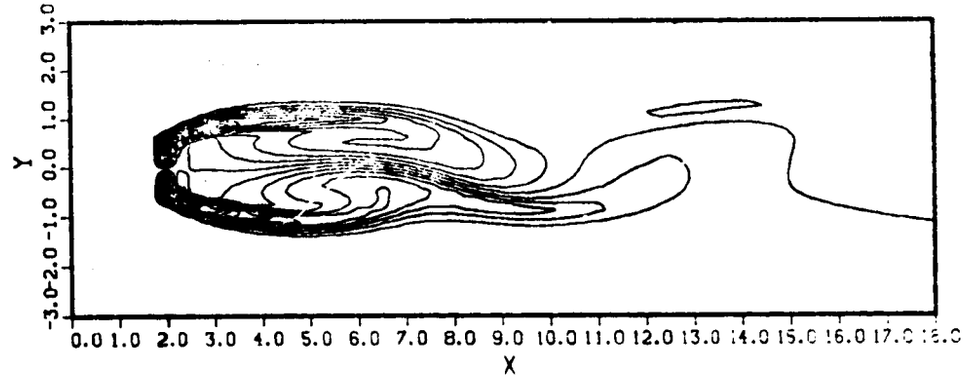

(d) t = 44.4

Figure 34 (cont'd)

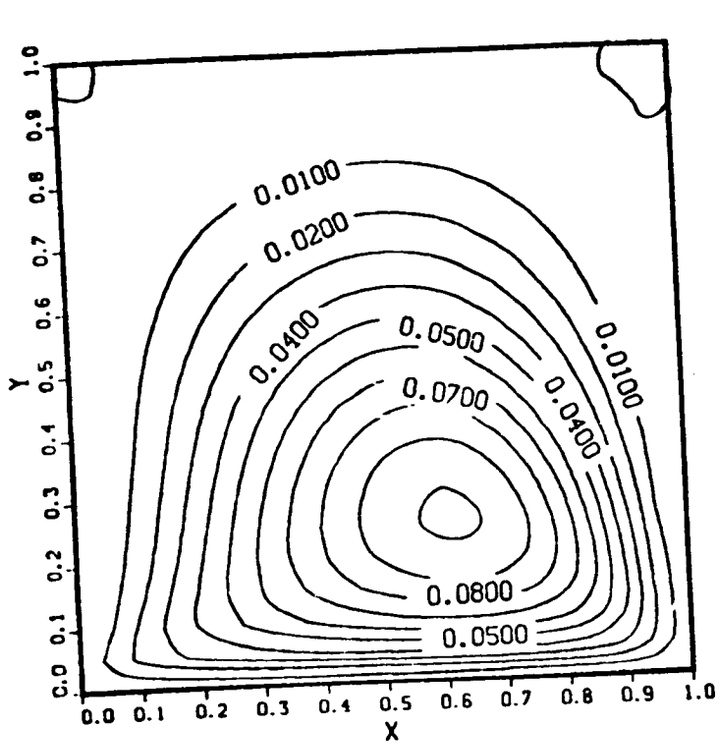

(a) Re = 100 (21 × 21)

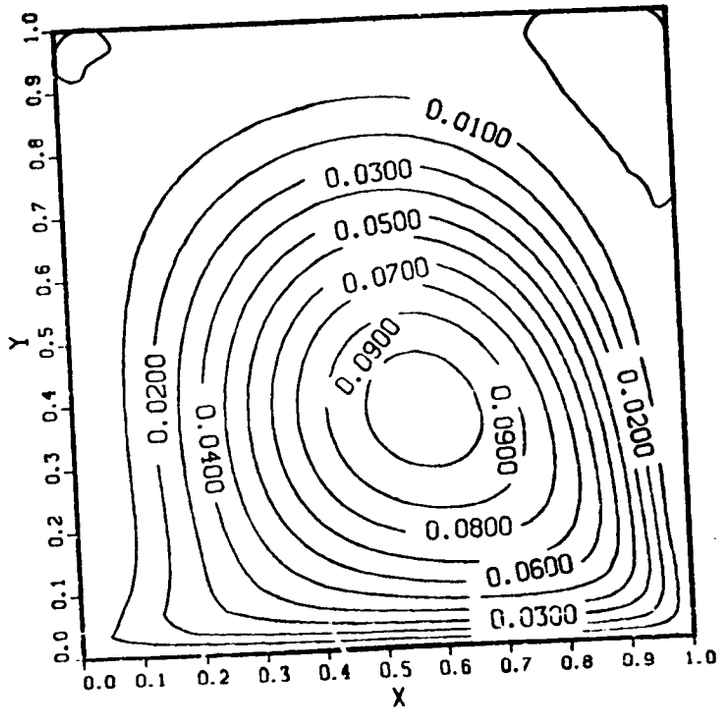

(b) Re = 400 (31 × 31)

Figure 35 : Steady streamlines for 2D starting cavity flow of Re = 100, 400 and 1000 in primitive variable formulation.

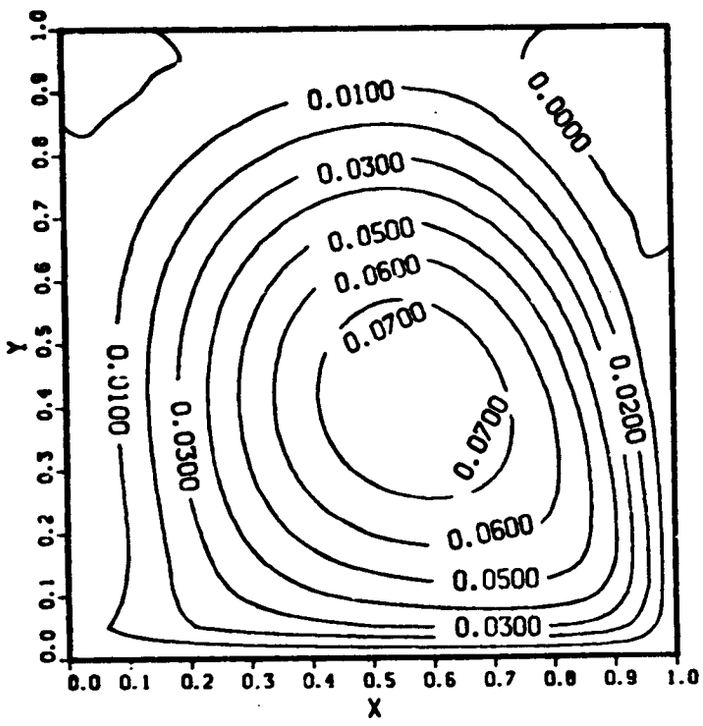

(c) Re = 1000 (21 × 21)

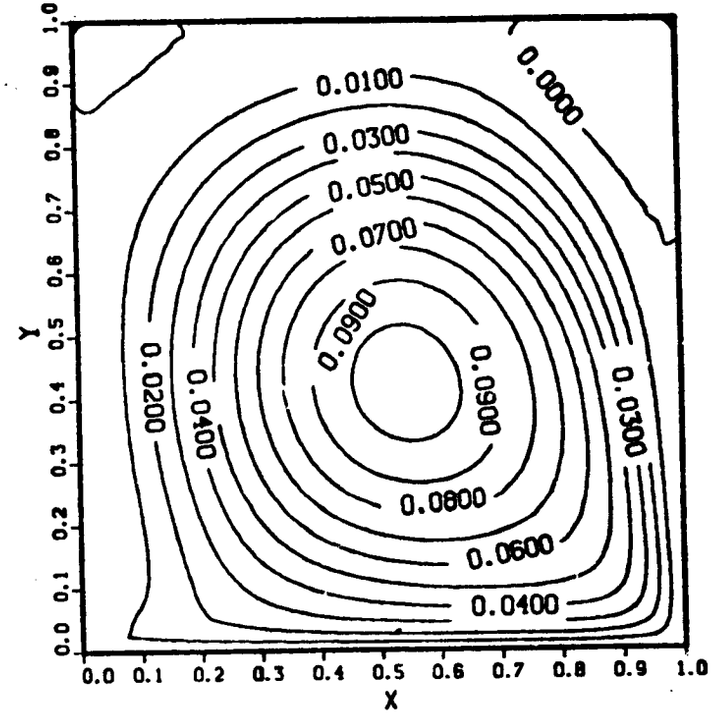

(d) Re = 1000 (41 × 41)

Figure 35 (cont'd)

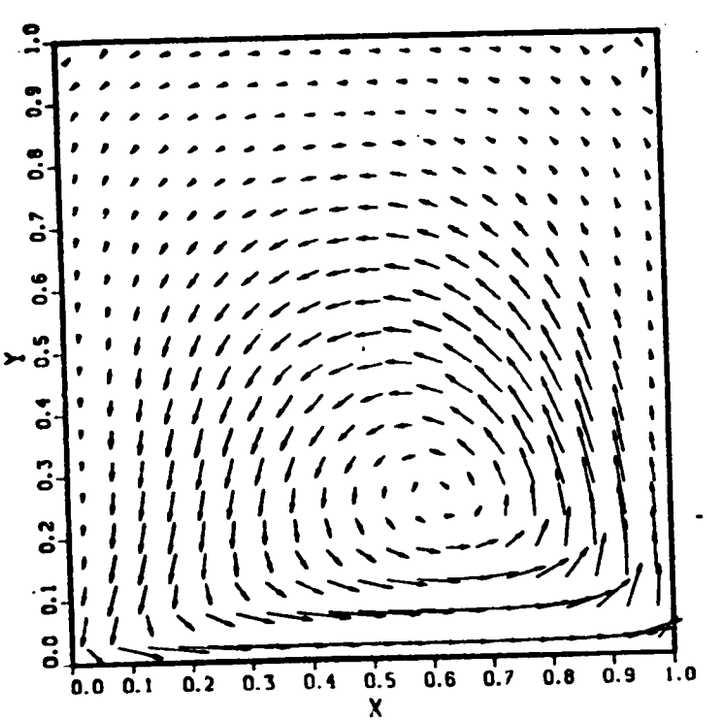

(a) Re = 100 (21 × 21)
scale for U_0 = 0.2

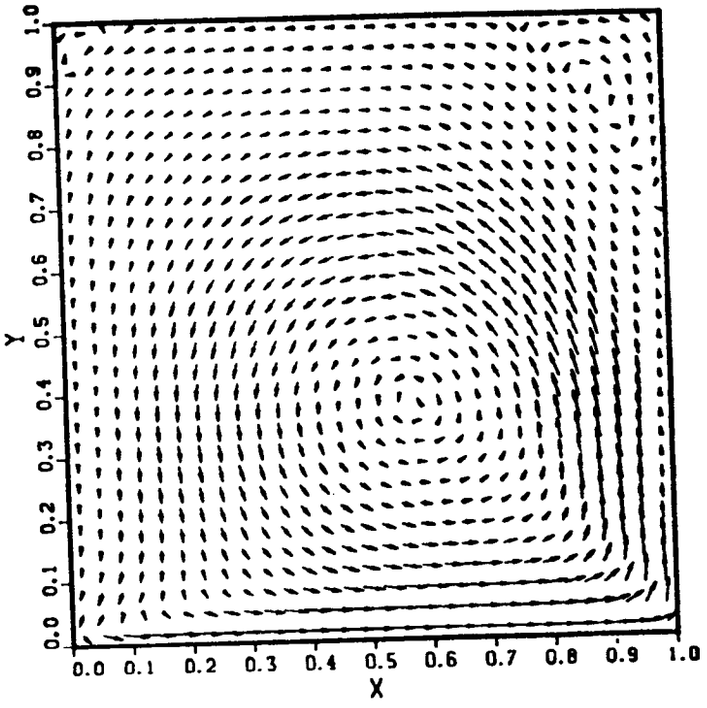

(b) Re = 400 (31 × 31)
scale for U_0 = 0.1

Figure 36 : Steady flow vector profiles for 2D starting cavity flow of Re = 100, 400 and 1000 in primitive variable formulation.

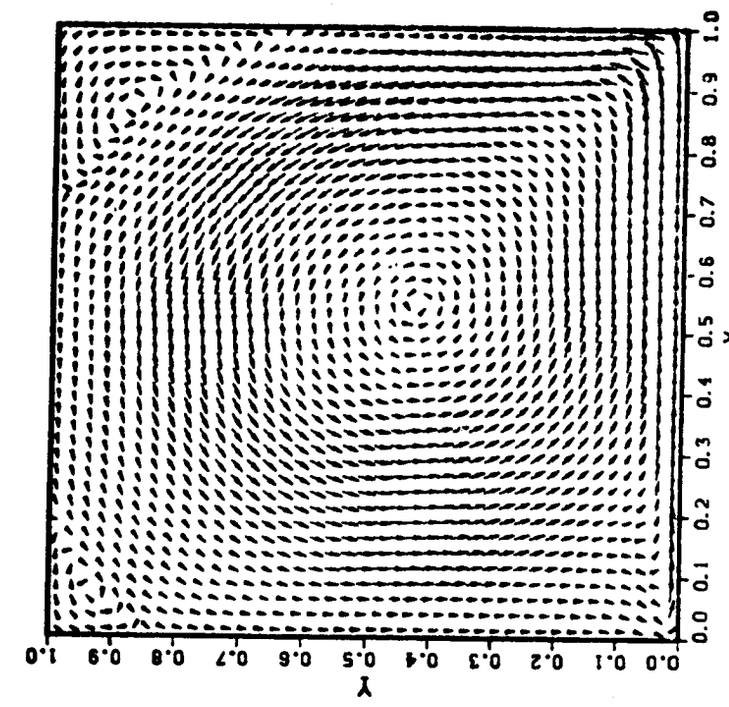

(d) Re = 1000 (41 × 41)
scale for $U_0 = 0.1$

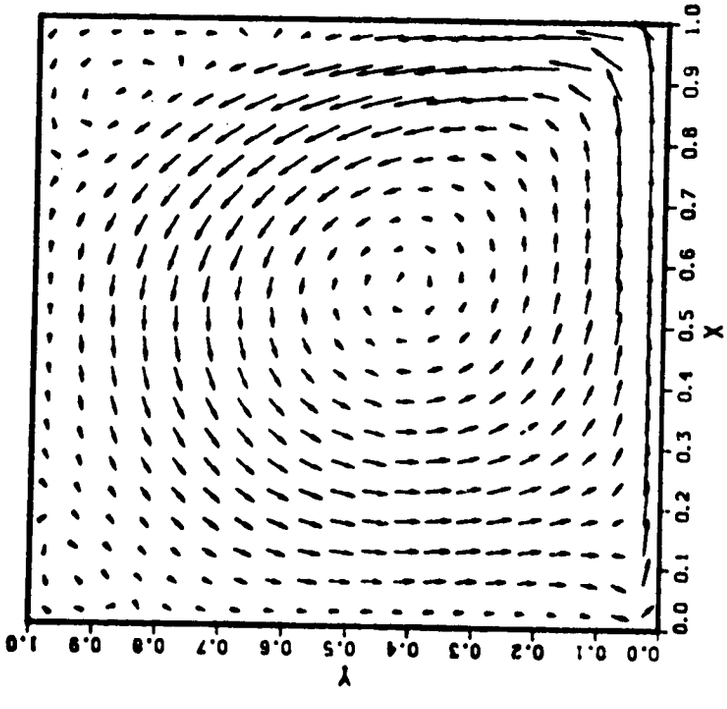

(c) Re = 1000 (21 × 21)
scale for $U_0 = 0.2$

Figure 36 (cont'd)

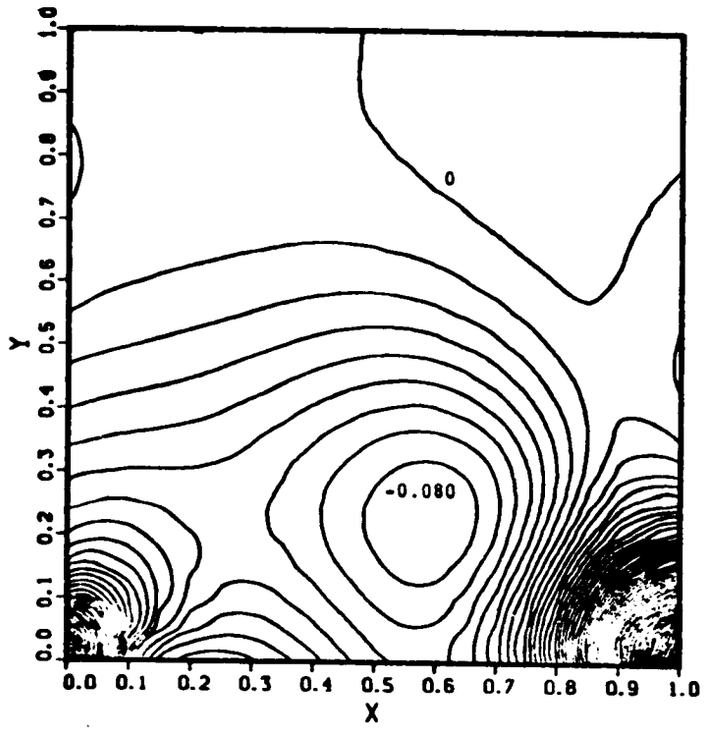

(a) Re = 100

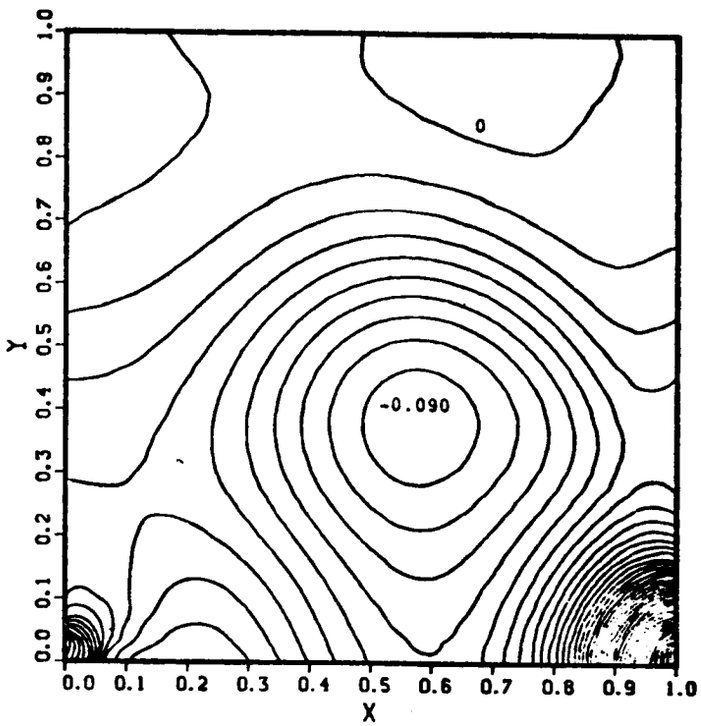

(b) Re = 400

Figure 37 : Steady pressure contours for 2D starting cavity flow of Re = 100, 400 and 1000.

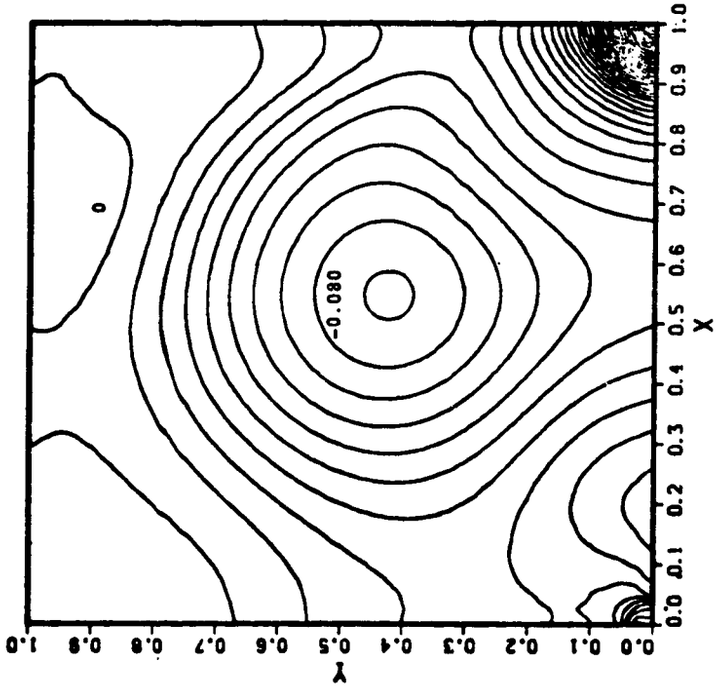

(c) Re = 1000 (41 x 41)

Figure 37 (cont'd)

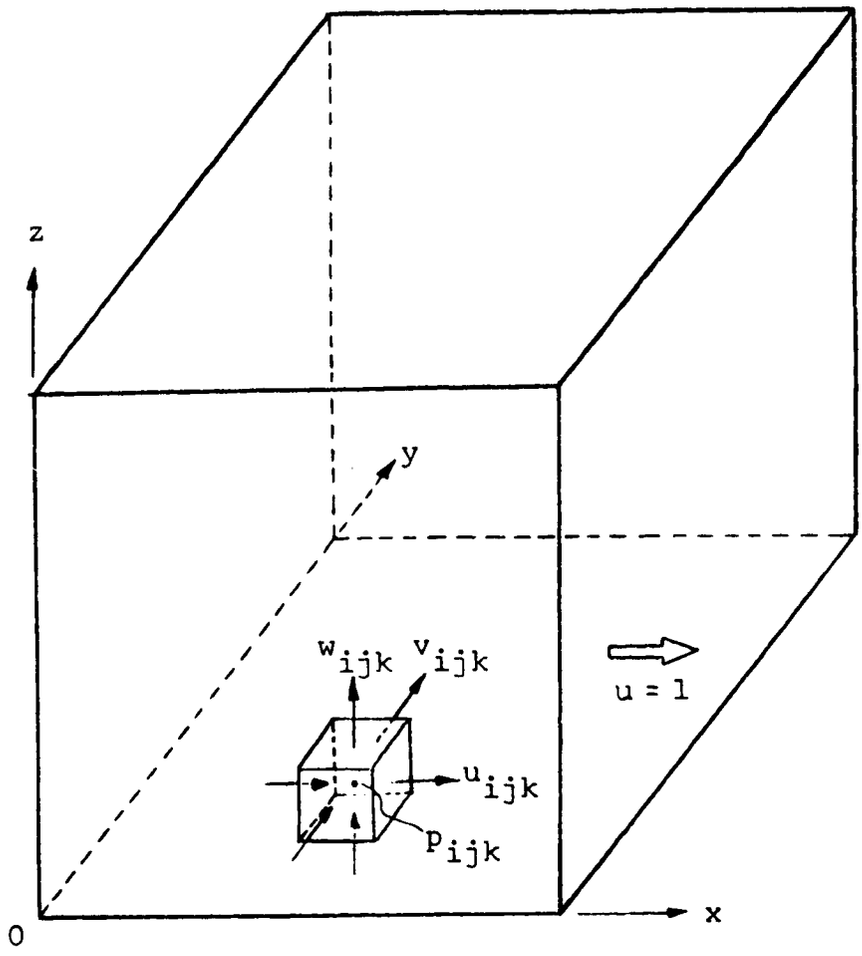

Figure 38 : Domain and control volume of cubic cavity flow.

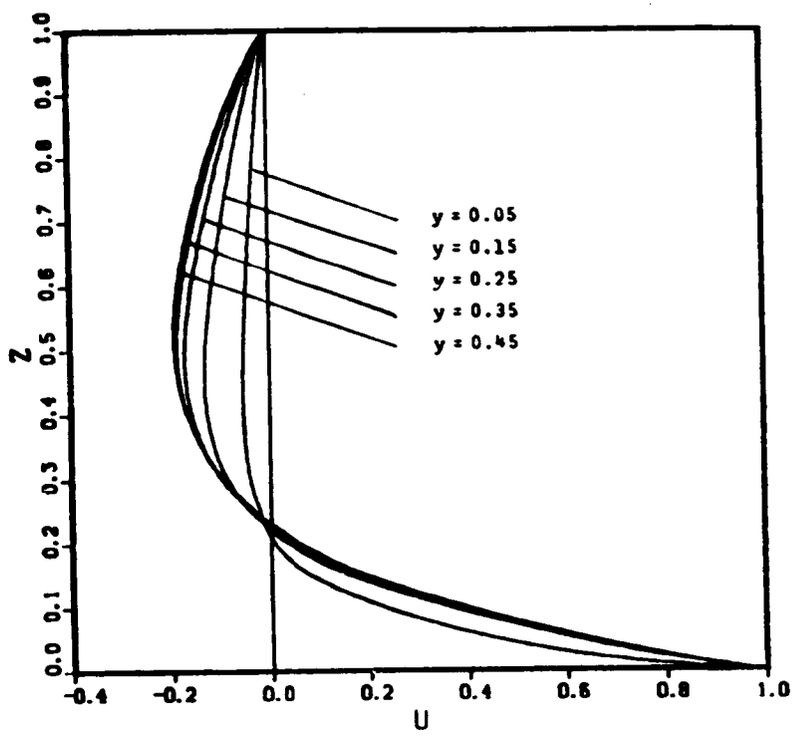

(a) Re = 100

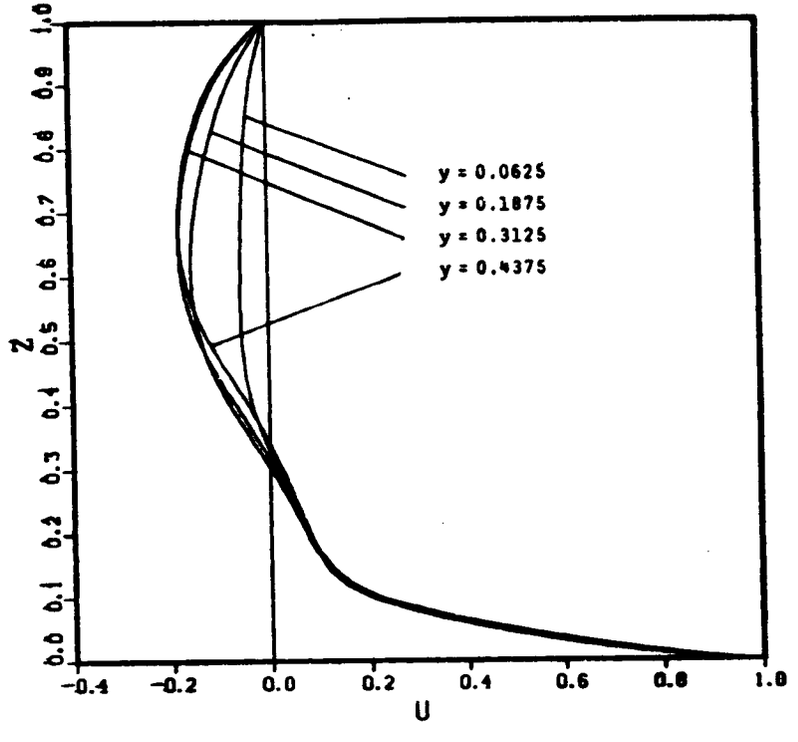

(b) Re = 400

Figure 39 : Velocity u at the plane x = 0.5 for cubic cavity flow of Re = 100 and 400.

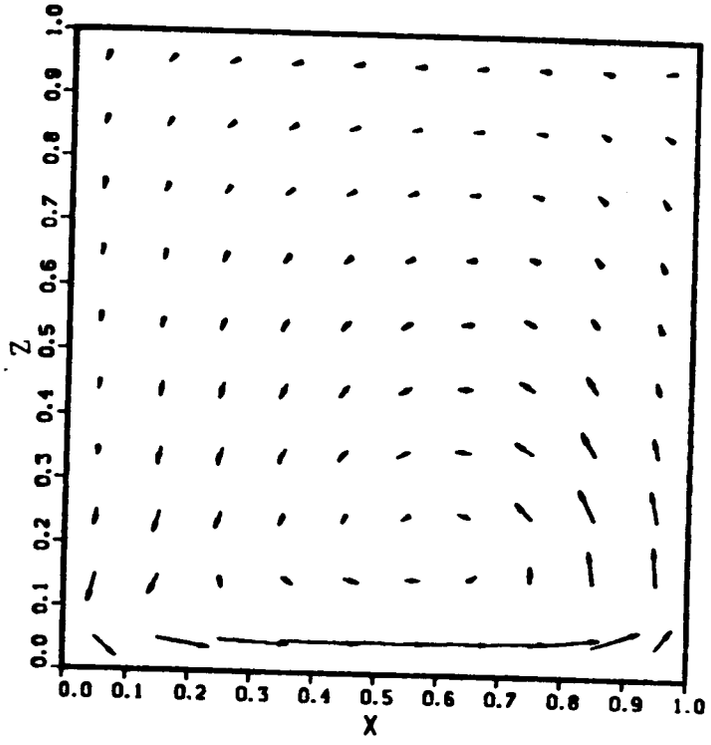

(a) y = 0.05

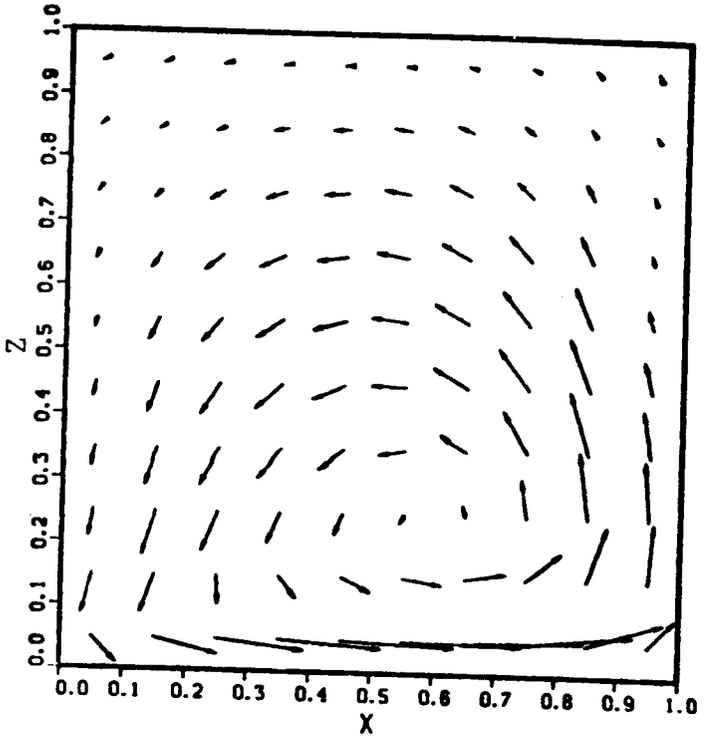

(b) y = 0.45

Figure 40 : Steady flow vector profiles at y = 0.05 and 0.45 for cubic cavity flow of Re = 100. Scale of U_0 = 0.3.

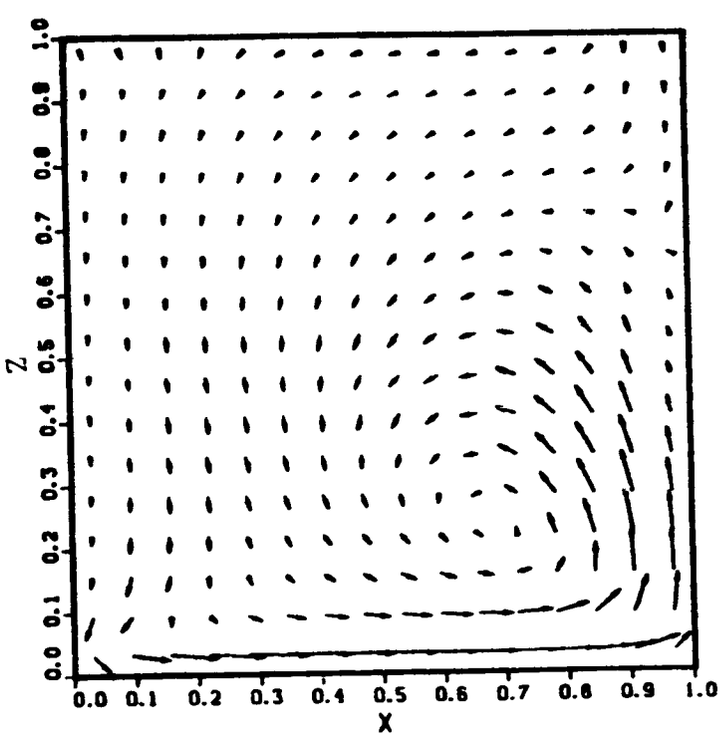

(a) y = 0.0625

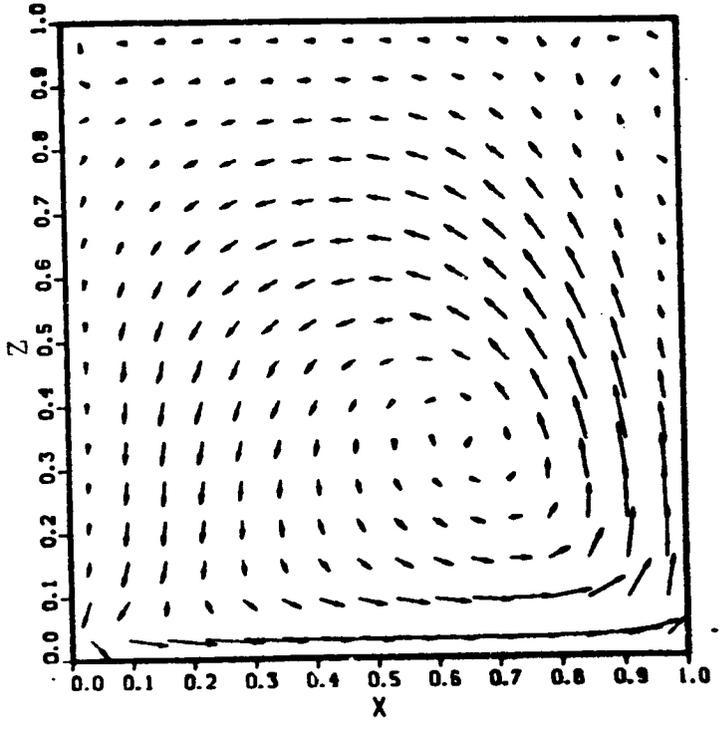

(b) y = 0.4375

Figure 41 : Steady flow vector profiles at y = 0.0625 and 0.4375 for cubic cavity flow of Re = 400. Scale of U_0 = 0.2.

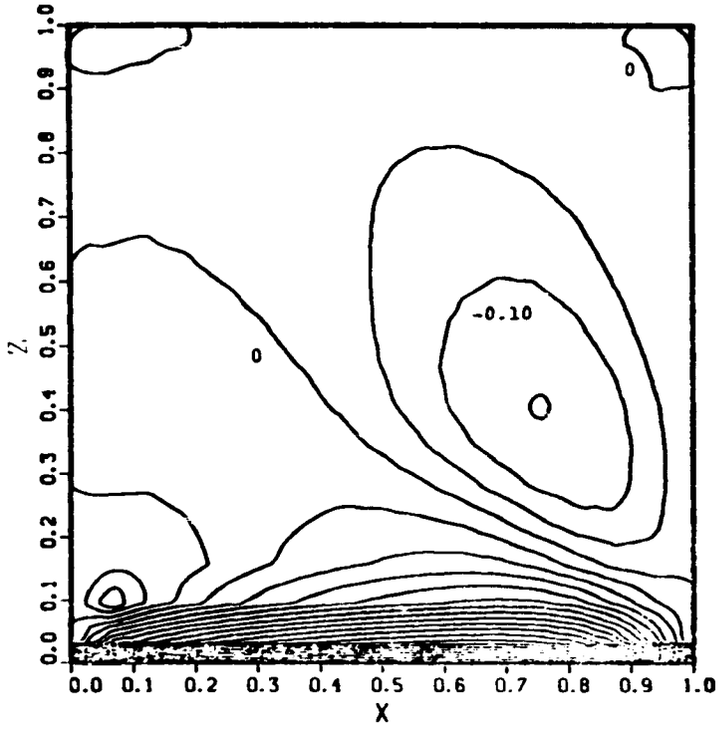

(a) y = 0.0625

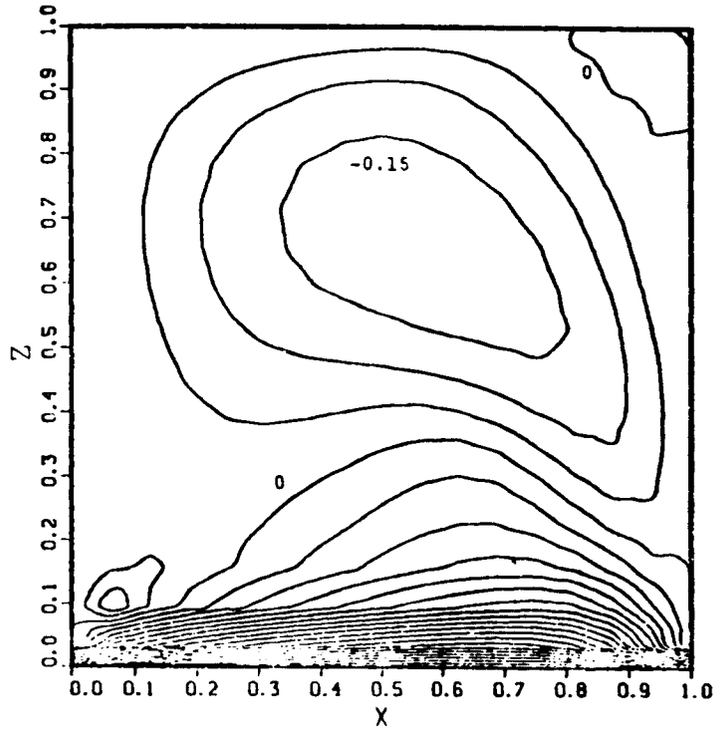

(b) y = 0.4375

Figure 42 : Contours of velocity u at y = 0.0625 and 0.4375 for cubic cavity flow of Re = 400.

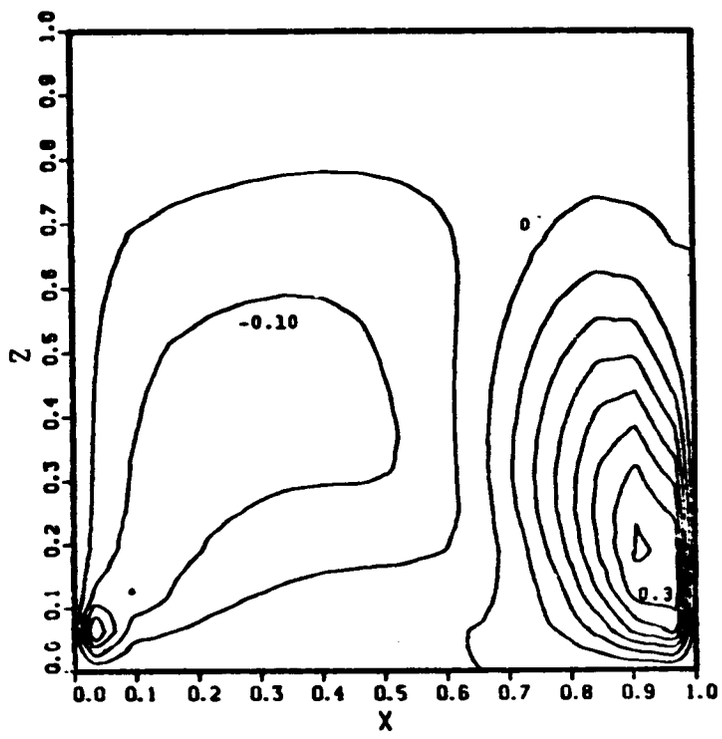

(a) y = 0.0625

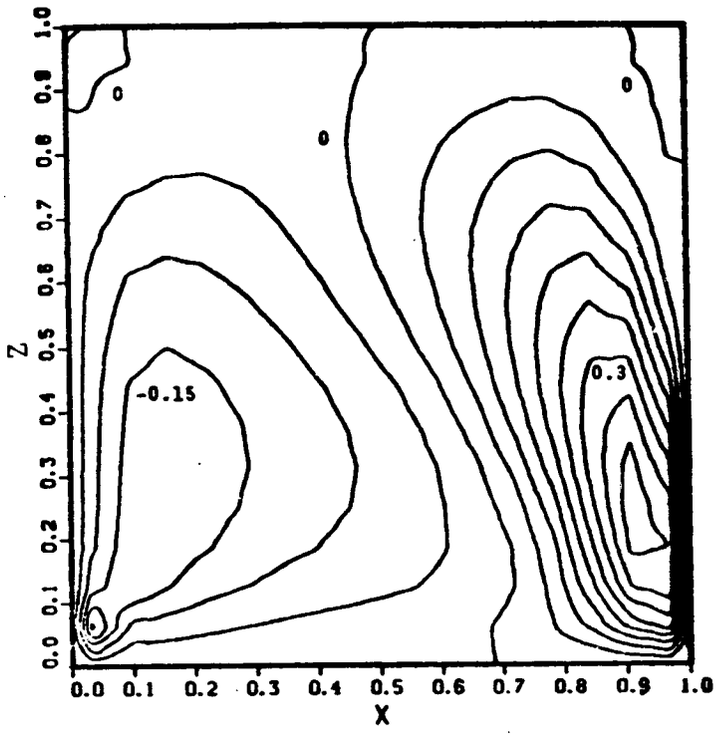

(b) y = 0.4375

Figure 43 : Contours of velocity w at y = 0.0625 and 0.4375 for cubic cavity flow of Re = 400.

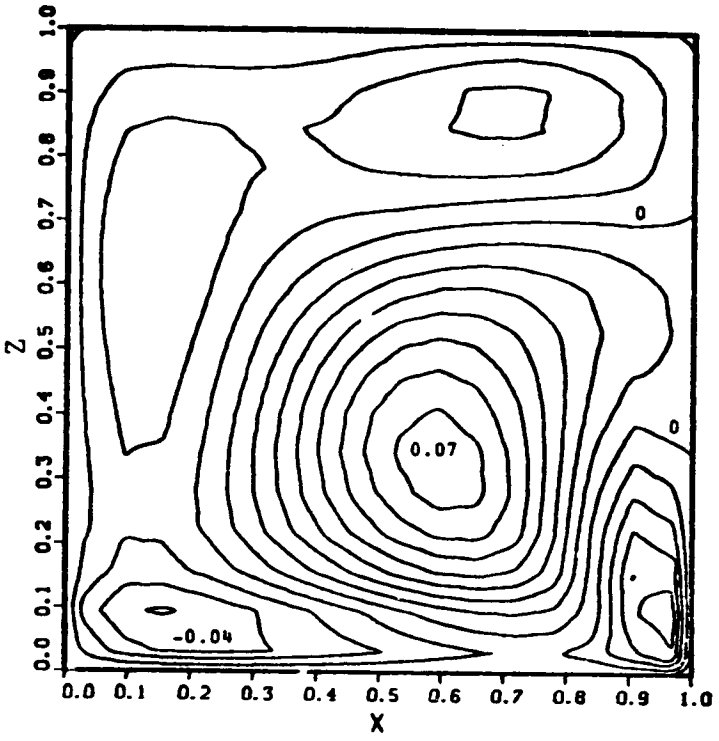

(a) y = 0.125

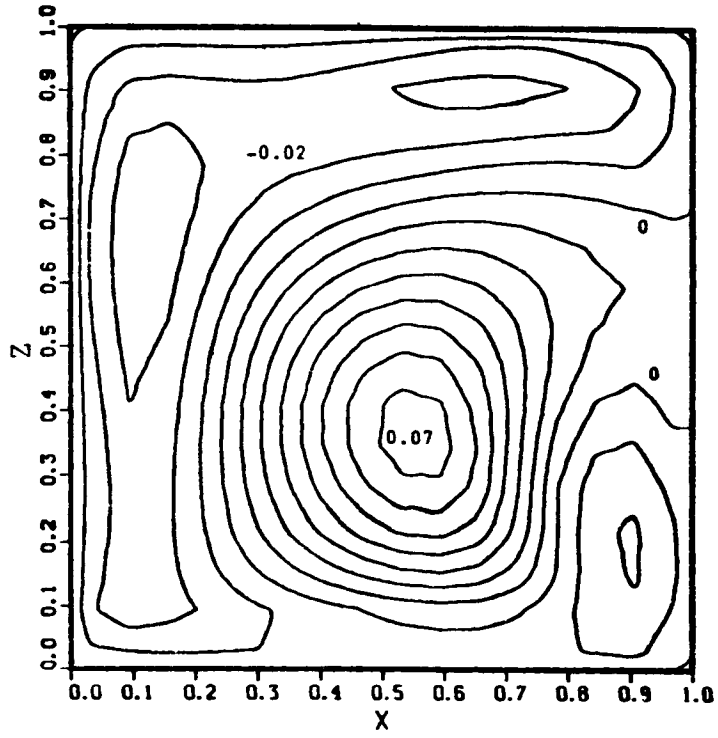

(b) y = 0.25

Figure 44 : Contours of secondary flow v at y = 0.125, 0.25 and 0.375 for cubic cavity flow of Re = 400.

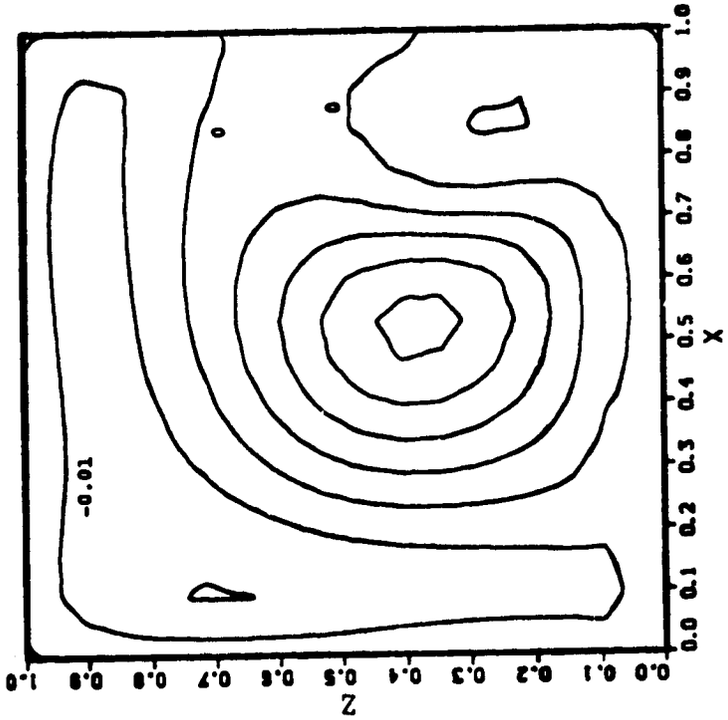

(c) y = 0.375

Figure 44 (cont'd)

APPENDIX A

FINITE ANALYTIC FORMULATION OF UNSTEADY ONE-DIMENSIONAL CONVECTIVE TRANSPORT EQUATION

Depending on boundary and initial functions selected to approximate the boundary and initial conditions for the chosen local element, several local analytic solutions of the unsteady linear or linearized one-dimensional convective transport equation

$$\phi_{xx} = 2A\phi_x + B\phi_t \qquad \text{(A-1)}$$

can be obtained. In this appendix, three FA solutions are derived in detail to illustrate the basic idea of the FA method. Three solutions of eq(A-1) are distinguished by the following formulations

(1) Eq(A-1) is solved with second-order polynomial approximation for both initial and boundary functions

$$\phi(x,0) = a_S + b_S x + c_s x^2$$

$$\phi(-h,t) = a_W + b_W t + c_W t^2$$

$$\phi(h,t) = a_E + b_E t + c_E t^2$$

(2) Eq(A-1) is solved with exponential and linear approximation for initial function, and linear approximation for boundary functions.

$$\phi(x,0) = a_S(e^{2Ax}-1) + b_S x + c_S$$

$$\phi(-h,t) = a_W + b_W t$$

$$\phi(h,t) = a_E + b_E t$$

(3) Eq(A-1) is solved with the unsteady term approximated by finite difference formula. This is a hybrid FA-FD formula.

Details of three solutions are given below:

A-1 Second-Order Polynomial Approximation for Initial and Boundary Functions

In this case, the linear or linearized convective transport equation (A-1) is solved in the local element shown in Fig. 2(b).

For the convective transport equation (A-1) to be well-posed, an initial and two boundary conditions must be specified along the south, west and east boundaries respectively. In terms of the nodal points available on each boundary, second-order polynomials are employed to approximate both the initial and boundary conditions, i.e.,

$$\phi(x,0) = a_S + b_S x + c_S x^2 \qquad \text{(A-1a)}$$

$$\phi(-h,t) = a_W + b_W t + c_W t^2 \qquad \text{(A-1b)}$$

$$\phi(h,t) = a_E + b_E t + c_E t^2 \qquad \text{(A-1c)}$$

where

$$a_S = \phi_{SC}, \quad b_S = \frac{1}{2h}(\phi_{SE} - \phi_{SW})$$

$$c_S = \frac{1}{2h^2}(\phi_{SE} + \phi_{SW} - 2\phi_{SC})$$

$$a_W = \phi_{SW}, \quad b_W = \frac{1}{2\tau}(4\phi_{WC} - 3\phi_{SW} - \phi_{NW})$$

$$c_W = \frac{1}{2\tau^2}(\phi_{SW} + \phi_{NW} - 2\phi_{WC})$$

$$a_E = \phi_{SE}, \quad b_E = \frac{1}{2\tau}(4\phi_{EC} - 3\phi_{SE} - \phi_{NE})$$

$$c_E = \frac{1}{2\tau^2}(\phi_{SE} + \phi_{NE} - 2\phi_{EC})$$

With the introuction of a change of variable

$$\phi = w\, e^{Ax - \frac{A^2}{B} t} \qquad \text{(A-2)}$$

The convective transport equation(A-1), initial condition (A-1a) and boundary conditions (A-1b) and (A-1c) are transformed to

$$w_{xx} = B\, w_t \qquad \text{(A-3)}$$

$$w(x,0) = e^{-Ax}(a_S + b_S x + c_S x^2) = \phi_I(x) \qquad \text{(A-3a)}$$

$$w(-h,t) = e^{Ah + \frac{A^2}{B}t}(a_W + b_W t + c_W t^2) = \phi_W(t) \quad \text{(A-3b)}$$

$$w(h,t) = e^{-Ah + \frac{A^2}{B}t}(a_E + b_E t + c_E t^2) = \phi_E(t) \quad \text{(A-3c)}$$

Under the method of superposition for linear equation (A-2), this problem can be solved analytically by further dividing it into two simpler problems

$$w = w_1 + w_2 \quad \text{(A-4)}$$

with w_1 satisfies the homogeneous boundary conditions and w_2 satisfies the zero initial condtion in the following manner

$$w_{1_{xx}} = B\, w_{1_t} \quad \text{(A-5)}$$

$$w_1(x,0) = \phi_I(x) \quad \text{(A-5a)}$$

$$w_1(-h,t) = 0 \quad \text{(A-5b)}$$

$$w_1(h,t) = 0 \quad \text{(A-5c)}$$

and

$$w_{2_{xx}} = B\, w_{2_t} \quad \text{(A-6)}$$

$$w_2(x,0) = 0 \quad \text{(A-6a)}$$

$$w_2(-h,t) = \phi_W(t) \quad \text{(A-6b)}$$

$$w_2(h,t) = \phi_E(t) \quad \text{(A-6c)}$$

The solution for w_1 can be easily obtained by the method of separation of variables. Assuming $w_1 = X(x)T(t)$, and substituting w_1 into eq(A-5), the variables are separated.

$$\frac{X''}{X} = B\frac{T'}{T} = \text{constant} = -\lambda^2$$

The two resulting ordinary differential equations are

$$X'' + \lambda^2 X = 0 \qquad \text{(A-7)}$$

$$T' + \frac{\lambda^2}{B} T = 0 \qquad \text{(A-8)}$$

and the boundary conditions (A-5b) and (A-5c) are transformed to

$$\begin{aligned} X(-h) &= 0 \\ X(h) &= 0 \end{aligned} \qquad \text{(A-9)}$$

The two boundary conditions (A-9) can be used to find the eigenvalues λ_n. i.e.,

$$X = a_n \sin\lambda_n(x+h)$$

where $\lambda_n = \frac{n\pi}{2h}$, $\quad n = 1, 2, 3, \ldots\ldots$

and the corresponding solution for eq(A-8) will be

$$T = b_n e^{-\frac{\lambda_n^2}{B} t}$$

By the method of superposition, the general solution for w_1 can thus be written as

$$w_1(x,t) = \sum_{n=1}^{\infty} a_n e^{-\frac{\lambda_n^2}{B} t} \sin\lambda_n(x+h)$$

where the coefficients a_n, n = 1, 2, 3,..... can be determined by applying the initial condition (A-5)

$$w_1(x,0) = \Phi_I(x) = \sum_{n=1}^{\infty} a_n \sin\lambda_n(x+h)$$

Invoking the orthogonality condition for sine series, the initial condition (A-5) gives

$$a_n = \frac{1}{h} \int_{-h}^{h} \Phi_I(x) \sin\lambda_n(x+h)\, dx$$

$$= a_S E_{0n} + b_S h\, E_{1n} + c_S h^2 E_{2n} \qquad \text{(A-10)}$$

where

$$E_{0n} = \frac{1}{h} \int_{-h}^{h} e^{-Ax} \sin\lambda_n(x+h)\, dx$$

$$= \frac{\lambda_n h}{(Ah)^2 + (\lambda_n h)^2} \left[e^{Ah} - (-1)^n e^{-Ah} \right] \qquad \text{(A-10a)}$$

$$E_{1n} = \frac{1}{h^2} \int_{-h}^{h} x e^{-Ax} \sin\lambda_n(x+h)\, dx$$

$$= \frac{2(Ah)(\lambda_n h)}{[(Ah)^2 + (\lambda_n h)^2]^2}[e^{Ah} - (-1)^n e^{Ah}]$$

$$- \frac{\lambda_n h}{(Ah)^2 + (\lambda_n h)^2}[e^{Ah} + (-1)^n e^{-Ah}] \qquad \text{(A-10b)}$$

$$E_{2n} = \frac{1}{h^3}\int_{-h}^{h} x^2 e^{-Ax} \sin\lambda_n(x+h)\, dx$$

$$= \{\frac{\lambda_n h}{(Ah)^2+(\lambda_n h)^2} - \frac{2\lambda_n h}{[(Ah)^2+(\lambda_n h)^2]^2} +$$

$$\frac{8(Ah)^2(\lambda_n h)}{[(Ah)^2+(\lambda_n h)^2]^3}\}[e^{Ah} - (-1)^n e^{-Ah}]$$

$$- \frac{4(Ah)(\lambda_n h)}{[(Ah)^2+(\lambda_n h)^2]^2}[e^{Ah} + (-1)^n e^{-Ah}] \qquad \text{(A-10c)}$$

To solve (A-6), one note that the boundary conditions (A-6b) and (A-6c) are prescribed functions of time. The solution for the problem (A-6) can be deduced from the similar constant boundary conditions by the use of Duhamel's theorem, namely,

$$w_2 = \int_0^t \frac{\partial \tilde{w}_2}{\partial t}(x,\mu,t-\mu)\, d\mu \qquad \text{(A-11)}$$

where $\tilde{w}_2$ satisfies the zero initial condition and constant boundary conditions

$$\tilde{w}_{2_{xx}} = B\,\tilde{w}_{2_t} \tag{A-12}$$

$$\tilde{w}_2 = 0 \qquad \text{at } t=0 \tag{A-12a}$$

$$\tilde{w}_2 = \Phi_W(\mu) \qquad \text{at } x=-h \tag{A-12b}$$

$$\tilde{w}_2 = \Phi_E(\mu) \qquad \text{at } x=h \tag{A-12c}$$

The solution for $\tilde{w}_2$ can be obtained by the superposition of steady-state solution Φ and a transient solution v which satisfies homogeneous boundary conditions, i.e.,

$$\tilde{w}_2 = \Phi(x,\mu) + v(x,\mu,t-\mu) \tag{A-13}$$

where

$$\frac{d^2\Phi}{dx^2} = 0 \tag{A-14}$$

$$\Phi = \Phi_W(\mu) \qquad \text{at } x=-h \tag{A-14a}$$

$$\Phi = \Phi_E(\mu) \qquad \text{at } x=h \tag{A-14b}$$

and

$$v_{xx} = B\,v_t \tag{A-15}$$

$$v = -\Phi(x,\mu) \qquad \text{at } t=0 \tag{A-15a}$$

$$v = 0 \qquad \text{at } x=\pm h \tag{A-15b}$$

The steady-state solution $\Phi(x,\mu)$ for the ordinary differential equation (A-14) is known to be

$$\Phi(x,\mu) = \frac{x}{2h}\left[\Phi_E(\mu) - \Phi_W(\mu)\right] + \frac{1}{2}\left[\Phi_E(\mu) + \Phi_W(\mu)\right] \tag{A-16}$$

which, in turn, is the initial condition for equation (A-12).

The solution for v is similar to that for w_1, except that the initial condition $\Phi_I(x)$ is replaced by $-\Phi(x,\mu)$. Thus,

$$v = \sum_{n=1}^{\infty} b_n \, e^{-\frac{\lambda_n^2}{B} t} \sin\lambda_n(x+h)$$

where b_n can be obtained from the initial condition (A-12), i.e.,

$$b_n = \int_{-h}^{h} -\Phi(x,\mu) \sin\lambda_n(x+h) \, dx$$

$$= \frac{\Phi_W(\mu) - \Phi_E(\mu)}{2h^2} \int_{-h}^{h} x \sin\lambda_n(x+h) \, dx$$

$$- \frac{\Phi_W(\mu) + \Phi_E(\mu)}{2h} \int_{-h}^{h} \sin\lambda_n(x+h) \, dx$$

$$= \frac{1}{\lambda_n h} [(-1)^n \Phi_E(\mu) - \Phi_W(\mu)]$$

Thus, $\tilde{w}_2 = v + \Phi$

$$= \sum_{n=1}^{\infty} \frac{1}{\lambda_n h} [(-1)^n \Phi_E(\mu) - \Phi_W(\mu)] e^{-\frac{\lambda_n^2}{B} t} \sin\lambda_n(x+h)$$

$$+ \frac{\Phi_E(\mu) - \Phi_W(\mu)}{2h} x + \frac{\Phi_E(\mu) + \Phi_W(\mu)}{2} \qquad \text{(A-17)}$$

After knowing $\tilde{w}_2$, w_2 can be obtained from Duhamel's theorem by substituting $\tilde{w}_2$ into eq(A-11)

$$w_2 = \int_0^t \frac{\partial \tilde{w}_2}{\partial t}(x,\mu,t-\mu)\, d\mu$$

$$= -\sum_{n=1}^{\infty} \frac{\lambda_n}{hB} \int_0^t [(-1)^n \Phi_E(\mu) - \Phi_W(\mu)]\, e^{-\frac{\lambda_n^2}{B}(t-\mu)} \sin\lambda_n(x+h)\, d\mu$$

$$= \sum_{n=1}^{\infty} \frac{\lambda_n}{hB} e^{-\frac{\lambda_n^2}{B}t} \sin\lambda_n(x+h) \int_0^t e^{\frac{\lambda_n^2}{B}\mu} [\Phi_W - (-1)^n \Phi_E]\, d\mu$$

Hence, the analytic solution ϕ for the linear or linearized convective transport equation(A-1) will be

$$\phi = w\, e^{Ax - \frac{A^2}{B}t} = (w_1 + w_2)\, e^{Ax - \frac{A^2}{B}t}$$

$$= \sum_{n=1}^{\infty} e^{Ax - \frac{A^2 + \lambda_n^2}{B}t} \sin\lambda_n(x+h)\, \{a_n +$$

$$\frac{\lambda_n}{hB} \int_0^t e^{\frac{\lambda_n^2}{B}\mu} [\Phi_W(\mu) - (-1)^n \Phi_E(\mu)]\, d\mu\} \qquad \text{(A-18)}$$

Evaluating the local analytic solution (A-18) at the interior node NC(0,2τ) in Fig. 2(b) will give an algebraic relationship between the nodal point NC and the seven neighboring nodal points, i.e.,

$$\phi_{NC} = \phi(0,2\tau)$$

$$= \sum_{n=1}^{\infty} e^{-2\frac{A^2+\lambda_n^2}{B}\tau} \sin\frac{n\pi}{2}\{a_n + \frac{\lambda_n}{hB}\int_0^{2\tau} e^{\frac{\lambda_n^2}{B}\mu}[\phi_W(\mu) - (-1)^n\phi_E(\mu)]\,d\mu\} \quad \text{(A-19)}$$

where $\sin\frac{n\pi}{2} = \begin{cases} -(-1)^{\frac{n+1}{2}}, & n \text{ is odd} \\ 0, & n \text{ is even} \end{cases}$

Equation (A-19) can be further simplified by letting $n = 2m-1$, $m = 1, 2, 3, \ldots\ldots$, so that

$$\phi_{NC} = \sum_{m=1}^{\infty} -(-1)^m e^{-\frac{A^2+\lambda_m^2}{B}\tau}\{a_m + \frac{\lambda_m}{hB}\int_0^{2\tau} e^{\frac{\lambda_m^2}{B}\mu}[\phi_W(\mu) + \phi_E(\mu)]\,d\mu\} \quad \text{(A-20)}$$

where

$$\lambda_m = \frac{(2m-1)\pi}{2h}$$

$$a_m = a_S E_{0m} + b_S h\, E_{1m} + c_S h^2 E_{2m}$$

and

$$\int_0^{2\tau} e^{\frac{\lambda_m^2}{B}\mu}[\phi_W(\mu) + \phi_E(\mu)]\,d\mu$$

$$= \int_0^{2\tau} e^{\frac{A^2+\lambda_m^2}{B}\mu} \left[e^{Ah}(a_W + b_W\mu + c_W\mu^2) + e^{-Ah}(a_E + b_E\mu + c_E\mu^2)\right] d\mu$$

$$= (e^{Ah}a_W + e^{-Ah}a_E)e_{0m} + (e^{Ah}b_W + e^{-Ah}b_E)\tau e_{1m}$$

$$+ (e^{Ah}c_W + e^{-Ah}c_E)\tau^2 e_{2m}$$

where

$$e_{0m} = \int_0^{2\tau} e^{F_m\mu}\, d\mu = \frac{1}{F_m}\left(e^{2F_m\tau} - 1\right)$$

$$e_{1m} = \frac{1}{\tau}\int_0^{2\tau} \mu e^{F_m\mu}\, d\mu = \frac{1}{F_m}\left(2e^{2F_m\tau} - \frac{e^{2F_m\tau}}{F_m\tau} + \frac{1}{F_m\tau}\right)$$

$$e_{2m} = \frac{1}{\tau^2}\int_0^{2\tau} \mu^2 e^{F_m\mu}\, d\mu = \frac{1}{F_m}\left[4e^{2F_m\tau} - \frac{4e^{2F_m\tau}}{F_m\tau} + \right.$$

$$\left. \frac{2e^{2F_m\tau}}{(F_m\tau)^2} - \frac{1}{(F_m\tau)^3}\right]$$

and $F_m = \dfrac{A^2 + \lambda_m^2}{B}$

Thus,

$$\phi_{NC} = \sum_{m=1}^{\infty} -(-1)^m e^{-2F_m\tau}\left\{a_S E_{0m} + b_S h\, E_{1m} + c_S h^2 E_{2m}\right.$$

$$+ \frac{\lambda_m}{hB}\left[(e^{Ah}a_W + e^{-Ah}a_E)e_{0m} + (e^{Ah}b_W + e^{-Ah}b_E)\tau e_{1m}\right.$$

$$\left.\left. + (e^{Ah}c_W + e^{-Ah}c_E)\tau^2 e_{2m}\right\}\right. \qquad \text{(A-21)}$$

Define

$$P_i = \sum_{m=1}^{\infty} \frac{-(-1)^m \lambda_m h \, e^{-2F_m\tau}}{[(Ah)^2 + (\lambda_m h)^2]^i} \quad , \qquad i = 1, 2, 3$$

$$Q_i = \sum_{m=1}^{\infty} \frac{-(-1)^m \lambda_m h}{[(Ah)^2 + (\lambda_m h)^2]^i} \quad , \qquad i = 1, 2, 3$$

then

$$\sum_{m=1}^{\infty} -(-1)^m E_{0m} e^{-2F_m\tau} = (e^{Ah} + e^{-Ah}) \sum_{m=1}^{\infty} \frac{-(-1)^m \lambda_m h \, e^{-2F_m\tau}}{(Ah)^2 + (\lambda_m h)^2}$$

$$= (e^{Ah} + e^{-Ah}) \, P_1$$

$$\sum_{m=1}^{\infty} -(-1)^m E_{1m} e^{-2F_m\tau} = -(e^{Ah} - e^{Ah}) \sum_{m=1}^{\infty} \frac{-(-1)^m \lambda_m h \, e^{-2F_m\tau}}{(Ah)^2 + (\lambda_m h)^2}$$

$$+ 2(Ah)(e^{Ah} + e^{-Ah}) \sum_{m=1}^{\infty} \frac{-(-1)^m \lambda_m h \, e^{-2F_m\tau}}{[(Ah)^2 + (\lambda_m h)^2]^2}$$

$$= 2(Ah)(e^{Ah} + e^{-Ah}) \, P_2 - (e^{Ah} - e^{-Ah}) \, P_1$$

$$\sum_{m=1}^{\infty} -(-1)^m E_{2m} e^{-2F_m\tau} = (e^{Ah} + e^{-Ah}) \sum_{m=1}^{\infty} \frac{-(-1)^m \lambda_m h \, e^{-2F_m\tau}}{(Ah)^2 + (\lambda_m h)^2}$$

$$- 2 \sum_{m=1}^{\infty} \frac{-(-1)^m \lambda_m h e^{-2F_m\tau}}{[(Ah)^2 + (\lambda_m h)^2]^2} + 8(Ah)^2 \sum_{m=1}^{\infty} \frac{-(-1)^m \lambda_m h \, e^{-2F_m\tau}}{[(Ah)^2 + (\lambda_m h)^2]^3}$$

$$- 4Ah(e^{Ah} - e^{-Ah}) \sum_{m=1}^{\infty} \frac{-(-1)^m \lambda_m h \, e^{-2F_m\tau}}{[(Ah)^2 + (\lambda_m h)^2]^2}$$

$$= (e^{Ah} + e^{-Ah}) \, [P_1 - 2P_2 + 8(Ah)^2 P_3] - 4Ah(e^{Ah} - e^{-Ah}) P_2$$

$$\sum_{m=1}^{\infty} -(-1)^m \frac{\lambda_m}{hB} e_{0m} e^{-2F_m\tau} = \sum_{m=1}^{\infty} -(-1)^m \frac{\lambda_m}{hBF_m} (1 - e^{-2F_m\tau})$$

$$= \sum_{m=1}^{\infty} \frac{-(-1)^m \lambda_m h}{(Ah)^2 + (\lambda_m h)^2} (1 - e^{-2F_m\tau}) = Q_1 - P_1$$

$$\sum_{m=1}^{\infty} -(-1)^m \frac{\lambda_m}{hB} e_{1m} e^{-2F_m\tau}$$

$$= \sum_{m=1}^{\infty} -(-1)^m \frac{\lambda_m}{hBF_m} (2 - \frac{1}{F_m\tau} + \frac{e^{-2F_m\tau}}{F_m\tau})$$

$$= 2 \sum_{m=1}^{\infty} \frac{-(-1)^m \lambda_m h}{(Ah)^2 + (\lambda_m h)^2} - \frac{Bh^2}{\tau} \sum_{m=1}^{\infty} \frac{-(-1)^m \lambda_m h (1 - e^{-2F_m\tau})}{[(Ah)^2 + (\lambda_m h)^2]^2}$$

$$= 2Q_1 - \frac{Bh^2}{\tau} (Q_2 - P_2)$$

$$\sum_{m=1}^{\infty} -(-1)^m \frac{\lambda_m}{hB} e_{2m} e^{-2F_m\tau}$$

$$= \sum_{m=1}^{\infty} -(-1)^m \frac{\lambda_m}{hBF_m} [4 - \frac{4}{F_m\tau} + \frac{2}{(F_m\tau)^2} (1 - e^{-2F_m\tau})]$$

$$= 4 \sum_{m=1}^{\infty} \frac{-(-1)^m \lambda_m h}{(Ah)^2 + (\lambda_m h)^2} - 4 \frac{Bh^2}{\tau} \sum_{m=1}^{\infty} \frac{-(-1)^m \lambda_m h}{[(Ah)^2 + (\lambda_m h)^2]^2}$$

$$+ 2(\frac{Bh^2}{\tau})^2 \sum_{m=1}^{\infty} \frac{-(-1)^m \lambda_m h}{[(Ah)^2 + (\lambda_m h)^2]^3} (1 - e^{-2F_m\tau})$$

$$= 4Q_1 - 4\frac{Bh^2}{\tau}Q_2 + 2(\frac{Bh^2}{\tau})^2(Q_3 - P_3)$$

Substituting a_S, b_S etc. into eq(A-21), the 8-point FA formula becomes

$$\phi_{NC} = (e^{Ah} + e^{-Ah})P_1\ \phi_{SC} + [Ah(e^{Ah} + e^{-Ah})P_2 - \frac{1}{2}(e^{Ah} - e^{-Ah})P_1]\ (\phi_{SE} - \phi_{SW}) + \{(e^{Ah}+e^{-Ah})\ [\frac{1}{2}P_1 - P_2 + 4(Ah)^2P_3] - 2Ah(e^{Ah} - e^{-Ah})P_2\}\ (\phi_{SE} + \phi_{SW} - 2\phi_{SC}) + (e^{Ah}\phi_{SW} + e^{-Ah}\phi_{SE})\ (Q_1 - P_1) + [e^{Ah}(4\phi_{WC} - 3\phi_{SW} - \phi_{NW}) + e^{-Ah}(4\phi_{EC} - 3\phi_{SE} - \phi_{NE})]\ [Q_1 - (\frac{Bh^2}{2\tau})(Q_2 - P_2)] + [e^{Ah}(\phi_{SW} + \phi_{NW} - 2\phi_{WC}) + e^{-Ah}(\phi_{SE} + \phi_{NE} - 2\phi_{EC})]\ [2Q_1 - 4(\frac{Bh^2}{2\tau})Q_2 + 4(\frac{Bh^2}{2\tau})^2(Q_3 - P_3)]$$

$$= (e^{Ah}\phi_{NW} + e^{-Ah}\phi_{NE})\ \{\frac{Bh^2}{2\tau}\ (Q_2 - P_2) - Q_1 + 2Q_1 - 4\frac{Bh^2}{2\tau}\ Q_2 + 4(\frac{Bh^2}{2\tau})(Q_3 - P_3)\} + (e^{Ah}\phi_{WC} + e^{-Ah}\phi_{EC})\ \{4Q_1 - 4\frac{Bh^2}{2\tau}(Q_2 - P_2) - 4Q_1 + 8(\frac{Bh^2}{2\tau})Q_2 - 8(\frac{Bh^2}{2\tau})(Q_3 - P_3)\} + \phi_{SW}\ \{e^{Ah}[\frac{1}{2}P_1 - AhP_2 + \frac{1}{2}P_1 - P_2 + 4(Ah)^2P_3 - 2AhP_2 + Q_1 - P_1 - 3Q_1 + 3(\frac{Bh^2}{2\tau})(Q_2 - P_2) + 2Q_1 -$$

$$4\left(\frac{Bh^2}{2\tau}\right)Q_2 + 4\left(\frac{Bh^2}{2\tau}\right)^2(Q_3 - P_3)] + e^{-Ah}[-\tfrac{1}{2}P_1 - AhP_2 +$$

$$\tfrac{1}{2}P_1 - P_2 + 4(Ah)^2P_3 + 2AhP_2]\} + \phi_{SE}\{e^{-Ah}[\tfrac{1}{2}P_1 +$$

$$AhP_2 + \tfrac{1}{2}P_1 - P_2 + 4(Ah)^2P_3 + 2AhP_2 + Q_1 - P_1 - 3Q_1 +$$

$$3\left(\frac{Bh^2}{2\tau}\right)(Q_2 - P_2) + 2Q_1 - 4\left(\frac{Bh^2}{2\tau}\right)Q_2 + 4\left(\frac{Bh^2}{2\tau}\right)^2(Q_3 - P_3)]$$

$$+ e^{Ah}[-\tfrac{1}{2}P_1 + AhP_2 + \tfrac{1}{2}P_1 - P_2 + 4(Ah)^2P_3 - 2AhP_2]\}$$

$$+ \phi_{SC}\{(e^{Ah} + e^{-Ah})[P_1 - P_1 + 2P_2 - 8(Ah)^2P_3] +$$

$$4Ah(e^{Ah} - e^{-Ah})P_2\} \qquad \text{(A-22)}$$

or

$$\phi_{NC} = C_{NW}\phi_{NW} + C_{NE}\phi_{NE} + C_{WC}\phi_{WC} + C_{EC}\phi_{EC} + C_{SW}\phi_{SW}$$

$$+ C_{SE}\phi_{SE} + C_{SC}\phi_{SC} \qquad \text{(A-23)}$$

where

$$C_{NW} = e^{Ah}\left[Q_1 - \frac{Bh^2}{2\tau}(P_2 + 3Q_2) + 4\left(\frac{Bh^2}{2\tau}\right)^2(Q_3 - P_3)\right]$$

$$C_{NE} = e^{-2Ah}C_{NW}$$

$$C_{WC} = e^{Ah}\left[4\left(\frac{Bh^2}{2\tau}\right)(P_2 + Q_2) - 8\left(\frac{Bh^2}{2\tau}\right)^2(Q_3 - P_3)\right]$$

$$C_{EC} = e^{-2Ah}C_{WC}$$

$$C_{SW} = e^{Ah}\left[-P_2 - 3AhP_2 + 4(Ah)^2P_3 - \left(\frac{Bh^2}{2\tau}\right)(3P_2 + Q_2) +\right.$$

$$\left. 4\left(\frac{Bh^2}{2\tau}\right)(Q_3 - P_3)\right] + e^{-Ah}[-P_2 + AhP_2 + 4(Ah)^2P_3]$$

$$C_{SE} = e^{-Ah}\left[-P_2 + 3AhP_2 + 4(Ah)^2P_3 - \left(\frac{Bh^2}{2\tau}\right)(3P_2 + Q_2) + 4\left(\frac{Bh^2}{2\tau}\right)^2(Q_3 - P_3)\right] + e^{Ah}\left[-P_2 - AhP_2 + 4(Ah)^2P_3\right]$$

$$C_{SC} = e^{Ah}\left[2P_2 + 4AhP_2 - 8(Ah)^2P_3\right] + e^{-Ah}\left[2P_2 - 4AhP_2 - 8(Ah)^2P_2\right]$$

It is noted that there are five series summation terms P_2, P_3, Q_1, Q_2 and Q_3 need to be calculated. After some investigation, it is found that three of them can be expressed in closed form as

$$Q_1 = \frac{1}{e^{Ah} + e^{-Ah}} \qquad \text{(A-24a)}$$

$$Q_2 = \frac{e^{Ah} - e^{-Ah}}{2Ah(e^{Ah} + e^{-Ah})^2} \qquad \text{(A-24b)}$$

$$Q_3 = \frac{1}{8(Ah)^2(e^{Ah} + e^{-Ah})} + \frac{e^{Ah} - e^{-Ah}}{8(Ah)^3(e^{Ah} + e^{-Ah})^2} - \frac{1}{(Ah)^2(e^{Ah} + e^{-Ah})^3} \qquad \text{(A-24c)}$$

Hence, numerical summation is need for P_2 and P_3 only. There are several ways in obtaining the analytic expressions (A-24a) to (A-24c). One of them will be outlined in the following.

Consider

$$e^{-Ax} = \sum_{n=1}^{\infty} a_n \sin\lambda_n(x+h) \qquad \text{(A-25)}$$

where

$$a_n = \frac{1}{h} \int_{-h}^{h} e^{-Ax} \sin\lambda_n(x+h)\, dx$$

$$= \frac{\lambda_n h}{(Ah)^2 + (\lambda_n h)^2} \left[e^{Ah} - (-1)^n e^{-Ah}\right]$$

Evaluating eq(A-25) at x=0 gives

$$1 = \sum_{n=1}^{\infty} a_n \sin\frac{n\pi}{2} = \sum_{m=1}^{\infty} -(-1)^m a_m \quad \text{with } n = 2m-1$$

thus

$$1 = (e^{Ah} + e^{-Ah}) \sum_{m=1}^{\infty} \frac{-(-1)^m \lambda_m h}{(Ah)^2 + (\lambda_m h)^2}$$

$$\text{or} \quad Q_1 = \sum_{m=1}^{\infty} \frac{-(-1)^m \lambda_m h}{(Ah)^2 + (\lambda_m h)^2} = \frac{1}{e^{Ah} + e^{-Ah}} \qquad \text{(A-25a)}$$

After obtaining the closed form of Q_1, the analytic expression for Q_2 can be easily obtained by differentiating both sides of eq(A-25a) with respect to Ah, i.e.,

$$\frac{dQ_1}{d(Ah)} = -2Ah \sum_{m=1}^{\infty} \frac{-(-1)^m \lambda_m h}{[(Ah)^2 + (\lambda_m h)^2]^2} = -\frac{e^{Ah} - e^{-Ah}}{(e^{Ah} + e^{-Ah})^2}$$

$$\text{or} \quad Q_2 = \sum_{m=1}^{\infty} \frac{-(-1)^m \lambda_m h}{[(Ah)^2 + (\lambda_m h)^2]^2} = \frac{e^{Ah} - e^{-Ah}}{2Ah(e^{Ah} + e^{-Ah})^2} \qquad \text{(A-26)}$$

Similarly, the analytic expression for Q_3 can be obtained by differentiating eq(A-26) with respect to Ah as follows

$$\frac{dQ_2}{d(Ah)} = -4Ah \sum_{m=1}^{\infty} \frac{-(-1)^m \lambda_m h}{[(Ah)^2 + (\lambda_m h)^2]^2}$$

$$= -2 \frac{(e^{Ah} - e^{-Ah})^2}{2Ah(e^{Ah} + e^{-Ah})^3} - \frac{e^{Ah} - e^{-Ah}}{2(Ah)^2(e^{Ah} + e^{-Ah})^3}$$

$$+ \frac{1}{2(Ah)(e^{Ah} + e^{-Ah})}$$

thus

$$Q_3 = \sum_{m=1}^{\infty} \frac{-(-1)^m \lambda_m h}{[(Ah)^2 + (\lambda_m h)^2]^3}$$

$$= \frac{(e^{Ah} - e^{-Ah})^2}{4(Ah)^2(e^{Ah}+e^{-Ah})^3} + \frac{e^{Ah}-e^{-Ah}}{8(Ah)^3(e^{Ah}+e^{-Ah})^2} -$$

$$\frac{1}{8(Ah)^2(e^{Ah} + e^{-Ah})}$$

$$= \frac{1}{8(Ah)^2(e^{Ah}+e^{-Ah})} + \frac{e^{Ah} - e^{-Ah}}{8(Ah)^3(e^{Ah}+e^{-Ah})^2}$$

$$\frac{1}{(Ah)^2(e^{Ah} + e^{-Ah})^3} \qquad \text{(A-27)}$$

A-2 Exponential and Linear Approximation for Initial Function, and Linear Approximation for Boundary Functions

In this case, the linear convective transport equation (A-1) is solved in the local element shown in Fig. 2(c).

In order to avoid the unrealistic negative FA coefficients appeared in Sec. A-1, an exponential and linear function based on the natural solution of governing equation (A-1) is employed to approximate the initial condition. As to the boundary conditions, linear functions are used to approximate the boundary conditions in terms of the two nodal points available on each boundary, i.e.,

$$\phi(x,0) = a_S (e^{2Ax} - 1) + b_S x + c_S \qquad \text{(A-28a)}$$

$$\phi(-h,t) = a_W + b_W t \qquad \text{(A-28b)}$$

$$\phi(h,t) = a_E + b_E t \qquad \text{(A-28c)}$$

where

$$a_S = \frac{\phi_{SE} + \phi_{SW} - 2\phi_{SC}}{4 \sinh^2 Ah}$$

$$b_S = \frac{\phi_{SE} - \phi_{SW} - \coth Ah (\phi_{SE} + \phi_{SW} - 2\phi_{SC})}{2h}, \qquad c_S = \phi_{SC},$$

$$a_W = \phi_{SW}, \qquad b_W = \frac{\phi_{WC} - \phi_{SW}}{\tau}$$

$$a_E = \phi_{SE}, \qquad b_E = \frac{\phi_{EC} - \phi_{SE}}{\tau}$$

With the introduction of a change of variable

$$\phi = w\, e^{Ax - \frac{A^2}{B}t}$$

the convective transport equation (A-1), initial condition (A-28a) and boundary conditions (A-28b) and (A-28c) can be transformed to

$$w_{xx} = B\, w_t \tag{A-29}$$

$$w(x,0) = a_S e^{Ax} + b_S x e^{-Ax} + (c_S - a_S) e^{-Ax} = \Phi_I(x) \tag{A-29a}$$

$$w(-h,t) = e^{Ah + \frac{A^2}{B}t}\,(a_W + b_W t) = \Phi_W(t) \tag{A-29b}$$

$$w(h,t) = e^{-Ah + \frac{A^2}{B}t}\,(a_E + b_E t) = \Phi_E(t) \tag{A-29c}$$

The solution of eq(A-29) for w can be obtained by superposition of two simpler problems

$$w = w_1 + w_2 \tag{A-30}$$

Where w_1 satisfies the homogeneous boundary conditions, and w_2 satisfies the zero initial condition as follows

$$w_{1_{xx}} = B\, w_{1_t} \tag{A-31}$$

$$w_1(x,0) = \Phi_I(x) \tag{A-31a}$$

$$w_1(-h,t) = 0 \tag{A-31b}$$

$$w_1(h,t) = 0 \tag{A-31c}$$

$$w_{2_{xx}} = B\, w_{2_t} \tag{A-32}$$

$$w_2(x,0) = 0 \tag{A-32a}$$

$$w_2(-h,t) = \phi_W(t) \tag{A-32b}$$

$$w_2(h,t) = \phi_E(t) \tag{A-32c}$$

The solution w_1 can be obtained by the method of separation of variables as that described in Sec. A-1. It gives

$$w_1 = \sum_{n=1}^{\infty} a_n\, e^{-\frac{\lambda_n^2}{B}t} \sin\lambda_n(x+h)$$

Which satisfies the governing equation (A-31) and boundary conditions (A-31b) and (A-31c). The coefficients a_n can be determined by the initial condition (A-31a)

$$a_n = \frac{1}{h}\int_{-h}^{h} \phi_I(x)\, \sin\lambda_n(x+h)\, dx$$

$$= a_S E_{0n} + b_S h\, E_{1n} + (c_S - a_S)E_{2n} \tag{A-33}$$

where

$$E_{0n} = \frac{1}{h}\int_{-h}^{h} e^{Ax}\, \sin\lambda_n(x+h)\, dx$$

$$= \frac{\lambda_n h}{(Ah)^2+(\lambda_n h)^2}\left[e^{-Ah} - (-1)^n e^{Ah}\right] \tag{A-33a}$$

$$E_{1n} = \frac{1}{h^2}\int_{-h}^{h} xe^{-Ax}\, \sin\lambda_n(x+h)\, dx$$

$$= \frac{2(Ah)(\lambda_n h)}{[(Ah)^2+(\lambda_n h)^2]^2}\,[e^{Ah}-(-1)^n e^{-Ah}] -$$

$$\frac{\lambda_n h}{(Ah)^2+(\lambda_n h)^2}\,[e^{Ah}+(-1)^n e^{-Ah}] \qquad \text{(A-33b)}$$

$$E_{2n} = \frac{1}{h}\int_{-h}^{h} e^{-Ax}\sin\lambda_n(x+h)\,dx$$

$$= \frac{\lambda_n h}{(Ah)^2+(\lambda_n h)^2}\,[e^{Ah}-(-1)^n e^{-Ah}] \qquad \text{(A-33c)}$$

The solution w_2 for eq(A-32) can be derived from Duhamel's theorem in the same way as that shown in Sec. A-1 also, i.e.,

$$w_2 = \sum_{n=1}^{\infty} \frac{\lambda_n}{hB}\, e^{-\frac{\lambda_n^2}{B}t}\sin\lambda_n(x+h)\int_0^t e^{\frac{\lambda_n^2}{B}\mu}\,[\Phi_W-(-1)^n\Phi_E]\,d\mu \qquad \text{(A-34)}$$

Thus, the local analytic solution will be

$$\phi = w\, e^{Ax-\frac{A^2}{B}t} = (w_1+w_2)e^{Ax-\frac{A^2}{B}t}$$

$$= \sum_{n=1}^{\infty} e^{Ax-\frac{A^2}{B}t}\sin\lambda_n(x+h)\,\{a_n +$$

$$\frac{\lambda_n}{hB}\int_0^t e^{\frac{\lambda_n^2}{B}\mu}\,[\Phi_W(\mu)-(-1)^n\Phi_E(\mu)]\,d\mu\,\} \qquad \text{(A-35)}$$

When evaluating the local analytic solution (A-35) at an interior node $P(0,\tau)$, a 6-point algebraic FA formula is obtained.

$$\phi_P = \phi(0,\tau)$$

$$= \sum_{n=1}^{\infty} e^{-\frac{A^2+\lambda_n^2}{B}\tau} \sin\frac{n\pi}{2}\{a_n +$$

$$\frac{\lambda_n}{hB}\int_0^{\tau} e^{\frac{\lambda_n^2}{B}\mu}[\phi_W(\mu) - (-1)^n\phi_E(\mu)]\,d\mu\} \quad \text{(A-36)}$$

Because $\sin\frac{n\pi}{2} = 0$ for even number of n, equation (A-36) can be further simplified by letting $n=2m-1$, so that

$$\phi_P = \sum_{m=1}^{\infty} -(-1)^m e^{-\frac{A^2+\lambda_m^2}{B}\tau}\{a_n +$$

$$\frac{\lambda_m}{hB}\int_0^{\tau} e^{\frac{\lambda_m^2}{B}\mu}[\phi_W(\mu) + \phi_E(\mu)]\,d\mu\} \quad \text{(A-37)}$$

where

$$\int_0^{\tau} e^{\frac{\lambda_m^2}{B}\mu}[\phi_W(\mu) + \phi_E(\mu)]\,d\mu$$

$$= (e^{Ah}a_W + e^{-Ah}a_E)\int_0^{\tau} e^{F_m\mu}\,d\mu +$$

$$(e^{Ah}b_W + e^{-Ah}b_E)\int_0^{\tau} \mu e^{F_m\mu}\,d\mu$$

$$= (e^{Ah}a_W + e^{-Ah}a_E)\frac{1}{F_m}(e^{F_m\tau} - 1) + (e^{Ah}b_W + e^{-Ah}b_E)\tau *$$

$$\frac{1}{F_m}(e^{F_m\tau} - \frac{e^{F_m\tau}}{F_m\tau} + \frac{1}{F_m\tau})$$

and

$$F_m = \frac{A^2 + \lambda_m^2}{B}$$

Thus,

$$\phi_P = \sum_{m=1}^{\infty} -(-1)^m e^{-F_m\tau}\{a_S E_{0m} + b_S h\, E_{1m} + (c_S - a_S)E_{2m}$$

$$+ \frac{\lambda_m}{hBF_m}[(e^{Ah}a_W + e^{-Ah}a_E)(e^{F_m\tau} - 1) + (e^{Ah}b_W +$$

$$e^{-Ah}b_E)\tau(e^{F_m\tau} - \frac{e^{F_m\tau}}{F_m\tau} + \frac{1}{F_m\tau})]\} \qquad \text{(A-38)}$$

Define

$$P_i = \sum_{m=1}^{\infty} \frac{-(-1)^m\lambda_m h\, e^{-F_m\tau}}{[(Ah)^2 + (\lambda_m h)^2]^i}, \qquad i = 1, 2$$

$$Q_i = \sum_{m=1}^{\infty} \frac{-(-1)^m\lambda_m h}{[(Ah)^2 + (\lambda_m h)^2]^i}, \qquad i = 1, 2$$

then

$$\sum_{m=1}^{\infty} -(-1)^m e^{F_m\tau} E_{0m} = (e^{Ah} + e^{-Ah})P_1$$

$$\sum_{m=1}^{\infty} -(-1)^m e^{F_m\tau} E_{1m} = 2Ah(e^{Ah} + e^{-Ah})P_2 - (e^{Ah} - e^{-Ah})P_1$$

$$\sum_{m=1}^{\infty} -(-1)^m e^{F_m\tau} E_{2m} = (e^{Ah} + e^{-Ah})P_1$$

$$\sum_{m=1}^{\infty} -(-1)^m e^{-F_m\tau} \frac{\lambda_m}{hBF_m} (e^{F_m\tau} - 1)$$

$$= \sum_{m=1}^{\infty} \frac{-(-1)^m \lambda_m h}{(Ah)^2 + (\lambda_m h)^2} (1 - e^{-F_m\tau}) = Q_1 - P_1$$

$$\sum_{m=1}^{\infty} -(-1)^m e^{-F_m\tau} \frac{\lambda_m}{hBF_m} (e^{F_m\tau} - \frac{e^{F_m\tau}}{F_m\tau} + \frac{1}{F_m\tau})$$

$$= \sum_{m=1}^{\infty} \frac{-(-1)^m \lambda_m h}{(Ah)^2+(\lambda_m h)^2} - \frac{Bh^2}{\tau} \sum_{m=1}^{\infty} \frac{-(-1)^m \lambda_m h(1-e^{-F_m\tau})}{[(Ah)^2+(\lambda_m h)^2]^2}$$

$$= Q_1 - \frac{Bh^2}{\tau} (Q_2 - P_2)$$

Hence,

$$\phi_P = a_S(e^{Ah} + e^{-Ah})P_1 + b_S h[2Ah(e^{Ah} + e^{-Ah})P_2 - (e^{Ah} - e^{-Ah})P_1] + (c_S - a_S)(e^{Ah} + e^{-Ah})P_1 + (e^{Ah}a_W + e^{-Ah}a_E)(Q_1 - P_1) + (e^{Ah}b_W + e^{-Ah}b_E)\tau[Q_1 + \frac{Bh^2}{\tau}(P_2 - Q_2)]$$

$$= \frac{1}{2}[\phi_{SE} - \phi_{SW} - \coth Ah\ (\phi_{SE} + \phi_{SW} - 2\phi_{SC})](4Ah \cosh Ah\ P_2 - 2\sinh Ah\ P_1) + \phi_{SC}(e^{Ah} + e^{-Ah})P_1 + (e^{Ah}\phi_{SW} + e^{-Ah}\phi_{SE})(Q_1 - P_1) + [e^{Ah}(\phi_{WC} - \phi_{SW}) + e^{-Ah}(\phi_{EC} -$$

$$\phi_{SE})][Q_1 + \frac{Bh^2}{\tau}(P_2 - Q_2)]$$

$$= (2\cosh Ah\ \phi_{SC} - e^{Ah}\phi_{SW} - e^{-Ah}\phi_{SE})(2Ah\ \coth Ah\ P_2 - P_1) + 2\cosh Ah\ P_1\phi_{SC} + (e^{Ah}\phi_{SW} + e^{-Ah}\phi_{SE})(Q_1 - P_1) + [(e^{Ah}\phi_{WC} + e^{-Ah}\phi_{EC}) - (e^{Ah}\phi_{SW} + e^{-Ah}\phi_{SE})[Q_1 + \frac{Bh^2}{\tau}(P_2 - Q_2)]$$

$$= (e^{Ah}\phi_{SW} + e^{-Ah}\phi_{SE})\{P_1 - 2Ah\ \coth Ah\ P_2 + Q_1 - P_1 - Q_1 - \frac{Bh^2}{\tau}(P_2 - Q_2)\} + (e^{Ah}\phi_{WC} + e^{-Ah}\phi_{EC})\{Q_1 + \frac{Bh^2}{\tau}(P_2 - Q_2)\} + \phi_{SC}\{2\cosh Ah\,(2Ah\coth Ah\ P_2 - P_1 + P_1)\}$$

or

$$\phi_P = C_{WC}\phi_{WC} + C_{EC}\phi_{EC} + C_{SW}\phi_{SW} + C_{SE}\phi_{SE} + C_{SC}\phi_{SC} \qquad \text{(A-39)}$$

where

$$C_{WC} = e^{Ah}\left[Q_1 + \frac{Bh^2}{\tau}(P_2 - Q_2)\right] \qquad \text{(A-39a)}$$

$$C_{EC} = e^{-2Ah}C_{WC} \qquad \text{(A-39b)}$$

$$C_{SW} = e^{Ah}\left[\frac{Bh^2}{\tau}(Q_2 - P_2) - 2Ah\ \coth Ah\ P_2\right] \qquad \text{(A-39c)}$$

$$C_{SE} = e^{-2Ah}C_{SW} \qquad \text{(A-39d)}$$

$$C_{SC} = 4Ah\ \cosh Ah\ \coth Ah\ P_2 \qquad \text{(A-39e)}$$

Because Q_1, Q_2 can be expressed in closed form as shown in eq(A-24a) & (A-24b), there is only one series summation P_2 need to be calculated numerically.

A-3 Hybrid Finite Analytic Formula for One-Dimensional Convective Transport Equation

In this formulation, the unsteady term in the convective transport equation (A-1) is approximated by a simple finite difference formula of the form of

$$B\phi_t = B\,\frac{\phi_P - \phi_{SC}}{\tau} = \text{constant} = g \qquad \text{(A-40)}$$

Thus, eq(A-1) becomes

$$\phi_{xx} = 2A\phi_x + g \qquad \text{(A-41)}$$

The analytic solution for eq(A-41) can be easily found to be

$$\phi = a(e^{2Ax} - 1) + b - \frac{g}{2A}x \qquad \text{(A-42)}$$

where a and b can be determined by the boundary conditions at x = ±h respectively.

$$\phi = \phi_{EC} = a(e^{2Ah} - 1) + b - \frac{g}{2A}h \qquad \text{at } x = h$$

$$\phi = \phi_{WC} = a(e^{-2Ah} - 1) + b + \frac{g}{2A}h \qquad \text{at } x = -h$$

Evaluating the analytic solution (A-42) at x = 0, a 4-point FA formula can be obtained as follows

$$\phi_P = \frac{(e^{2Ah}-1)\phi_{WC} + (e^{-2Ah}-1)\phi_{EC} - \frac{gh}{2A}(e^{2Ah} + e^{-2Ah} - 2)}{e^{2Ah} - e^{-2Ah}}$$

$$= \frac{e^{Ah}\phi_{WC} + e^{-Ah}\phi_{EC}}{e^{Ah} + e^{-Ah}} - \frac{\tanh Ah}{2Ah} gh^2 \qquad \text{(A-43)}$$

Substituting g into eq(A-43) results in

$$\phi_P = \frac{e^{Ah}\phi_{WC} + e^{-Ah}\phi_{EC}}{e^{Ah} + e^{-Ah}} - \frac{Bh^2}{2\tau} \frac{\tanh Ah}{Ah} (\phi_P - \phi_{SC})$$

or

$$\phi_P = \frac{1}{1 + C_{SC}} (C_{WC}\phi_{WC} + C_{EC}\phi_{EC} + C_{SC}\phi_{SC}) \qquad \text{(A-44)}$$

where

$$C_{SC} = \frac{Bh^2}{2\tau} \frac{\tanh Ah}{Ah} \qquad \text{(A-44a)}$$

$$C_{WC} = \frac{e^{Ah}}{e^{Ah} + e^{-Ah}} \qquad \text{(A-44b)}$$

$$C_{EC} = \frac{e^{-Ah}}{e^{Ah} + e^{-Ah}} \qquad \text{(A-44c)}$$

APPENDIX B

FINITE ANALYTIC FORMULATION OF UNSTEADY TWO-DIMENSIONAL CONVECTIVE TRANSPORT EQUATION

In this appendix, the analytic solution for unsteady two-simensional convective transport equation is derived for a local element as shown in Fig. 3.

Consider a dimensionless unsteady two-dimensional convective transport equation of the form of

$$\phi_{xx} + \phi_{yy} = R\left[\phi_t + (u\phi)_x + (v\phi)_y\right] + F \qquad \text{(B-1)}$$

where ϕ may represent any one of convective transport quantities, ϕ_j, such as vorticity, velocity, concentration or temperature. The coefficients u, v and F may be functions of independent variables x, y and t, and dependent variables ϕ_j. R is a dimensionless parameter, and is Reynolds number when ϕ represents vorticity or velocity. Since, in general, an analytic solution of equation (B-1) in the local element is not available due to variable coefficients and/or nonlinearity, the finite analytic numerical method is used to obtain the local analytic solution.

In order to solve the convective transport equation (B-1) analytically in the local element, eq(B-1) is first

rearranged to be

$$\phi_{xx} + \phi_{yy} = R(\phi_t + U\phi_x + V\phi_y) + F + R[(u'\phi)_x + (v'\phi)_y] \tag{B-2}$$

with

$$u(x,y,t,\phi_j) = U + u'(x,y,t,\phi_j) \tag{B-2a}$$

$$v(x,y,t,\phi_j) = V + v'(x,y,t,\phi_j) \tag{B-2b}$$

where U and V are representative constant values in the local element, for example, the velocities at the interior point P or the area-averaged velocities over the small element.

When the local element is small enough, the deviations u' and v' from U and V should be small also, therefore the term $R[(u'\phi)_x + (v'\phi)_y]$ may be considered as a higher order correction term. Denoting two time steps t_{n-1} and t_n, one may locally linearized the convective transport equation (B-1) by approximating the inhomogeneous and the higher order correction term as a function known from previous time step t_{n-1}, i.e.,

$$(\phi_{xx} + \phi_{yy})^n = R(\phi_t + U\phi_x + V\phi_y)^n + f^{n-1}(x,y,\phi_j) \tag{B-3}$$

where

$$f(x,y,t,\phi_j) = F(x,y,t,\phi_j) + R[(u'\phi)_x + (v'\phi)_y]$$

Equation (B-3) is a linearized PDE with constant soefficients at n^{th} time step, various solution methods

as those described in Appendix A can thus be employed to obtain the analytic solution for this linear partial differential equation.

In order to reduce the complexity of the derivation and to save the computational time, a hybrid FA method as that outlined in Sec. A-3 will be employed in this appendix to approximate the unsteady term as follows

$$R\phi_t = R\,\frac{\phi_P^{n} - \phi_P^{n-1}}{\tau} = \text{constant} \qquad \text{(B-4)}$$

Furthermore, the nonhomogeneous part $f^{n-1}(x,y,\phi_j)$ can also be approximated by a representative constant value f_P in the local element to further reduce the manipulation effort and computational time needed. Under these approximations, the unsteady 2D convective transport equation (B-1) is simplified to be

$$\phi_{xx} + \phi_{yy} = 2A\phi_x + 2B\phi_y + g \qquad \text{(B-5)}$$

with $A = \frac{1}{2}\,RU$, $B = \frac{1}{2}\,RV$

and $$g = R\,\frac{\phi_P^{n} - \phi_P^{n-1}}{\tau} + f_P \qquad \text{(B-5a)}$$

The constant inhomogenecus term in eq(B-5) can be taken care by introducing a new variable

$$\tilde{\phi} = \phi + \frac{g}{2(A^2 + B^2)}\,(Ax + By) \qquad \text{(B-6)}$$

such that the new variable $\tilde{\phi}$ satisfies the homogeneous governing equation

$$\tilde{\phi}_{xx} + \tilde{\phi}_{yy} = 2A\tilde{\phi}_x + 2B\tilde{\phi}_y \qquad \text{(B-7)}$$

in the local element.

For the problem to be well-posed, four boundary conditions are specified on the east, west, south and north boundaries in terms of the 8 boundary nodes of the local element. Depending on the local element and boundary functions chosen, several local analytic solutions will be derived in the following

(1) Uniform grid spacing local element ($h_E=h_W=h$, $h_N=h_S=k$) with exponential and linear boundary approximation. (see Fig. 4(a))

(2) Nonuniform grid spacing local element ($h_E \neq h_W$, $h_N \neq h_S$) with exponential and linear boundary approximation. (see Fig. 4(b))

(3) Uniform grid spacing local element ($h_E=h_W=h$, $h_N=h_S=k$) with piecewise-linear boundary approximation.

B-1 Finite Analytic Formulation of Two-Dimensional Convective Transport Equation for Uniform Grid Local Element with Exponential and Linear Boundary Approximations

In this case, the local analytic solution for steady or unsteady 2D convective transport equation is derived in

a rectangular local element of uniform grid spacing shown in Fig. 4(a).

For the linear homogeneous partial differential equation (B-7) to be well-posed in the local element shown, an exponential and linear boundary function based on the natural solution of equation (B-7) is specified on all of the four boundaries in terms of the 8 boundary nodes of the local element. For example, the boundary condition at north side can be approximated by

$$\tilde{\phi}_N(x) = a_N (e^{2Ax} - 1) + b_N x + c_N \qquad \text{(B-8a)}$$

where

$$a_N = \frac{\tilde{\phi}_{NE} + \tilde{\phi}_{NW} - 2\tilde{\phi}_{NC}}{4\sinh^2 Ah}$$

$$b_N = \frac{\tilde{\phi}_{NE} - \tilde{\phi}_{NW} - \coth Ah(\tilde{\phi}_{NE} + \tilde{\phi}_{NW} - 2\tilde{\phi}_{NC})}{2h} , \quad c_N = \tilde{\phi}_{NC}$$

and the other three boundary conditions for south, east and west sides, i.e., $\tilde{\phi}_S(x)$, $\tilde{\phi}_E(y)$ and $\tilde{\phi}_W(y)$ can be similarly approximated.

$$\tilde{\phi}_S(x) = a_S (e^{2Ax} - 1) + b_S x + c_S \qquad \text{(B-8b)}$$

$$\tilde{\phi}_E(y) = a_E (e^{2By} - 1) + b_E y + c_E \qquad \text{(B-8c)}$$

$$\tilde{\phi}_W(y) = a_W (e^{2By} - 1) + b_W y + c_W \qquad \text{(B-8d)}$$

With the introduction of a change of variable

$$\tilde{\phi} = w\, e^{Ax + By} \tag{B-9}$$

Equation (B-7) and boundary conditions (B-8a) to (B-8d) are transformed to

$$w_{xx} + w_{yy} = (A^2 + B^2)\, w \tag{B-10}$$

$$w(x,k) = e^{-Bk}\,[\, a_N e^{Ax} + b_N x e^{-Ax} + (c_N - a_N) e^{-Ax}] = w_1(x) \tag{B-10a}$$

$$w(x,-k) = e^{Bk}\,[\, a_S e^{Ax} + b_S x e^{-Ax} + (c_S - a_S) e^{-Ax}] = w_2(x) \tag{B-10b}$$

$$w(h,y) = e^{-Ah}\,[\, a_E e^{By} + b_E y e^{-By} + (c_E - a_E) e^{-By}] = w_3(y) \tag{B-10c}$$

$$w(-h,y) = e^{Ah}\,[\, a_W e^{By} + b_W y e^{-By} + (c_W - a_W) e^{-By}] = w_4(y) \tag{B-10d}$$

Under the method of superposition for linear equation (B-10), this problem can be solved analytically by further dividing it into foun simpler problems with each of them contains one inhomogeneous and three homogeneous boundary conditions, i.e.,

$$w = w^E + w^W + w^N + w^S \tag{B-11}$$

Problem (I)

$$w^N_{xx} + w^N_{yy} = (A^2 + B^2)\, w^N \tag{B-12}$$

$$w^N(x,k) = w_1(x) \tag{B-12a}$$

$$w^N(x,-k) = w^N(h,y) = w^N(-h,y) = 0 \tag{B-12b}$$

Problem (II)

$$w^S_{xx} + w^S_{yy} = (A^2 + B^2)\, w^S \qquad \text{(B-13)}$$

$$w^S(x,-k) = w_2(x) \qquad \text{(B-13a)}$$

$$w^S(x,k) = w^S(h,y) = w^S(-h,y) = 0 \qquad \text{(B-13b)}$$

Problem (III)

$$w^E_{xx} + w^E_{yy} = (A^2 + B^2)\, w^E \qquad \text{(B-14)}$$

$$w^E(h,y) = w_3(y) \qquad \text{(B-14a)}$$

$$w^E(-h,y) = w^E(x,k) = w^E(x,-k) = 0 \qquad \text{(B-14b)}$$

Problem (IV)

$$w^W_{xx} + w^W_{yy} = (A^2 + B^2)\, w^W \qquad \text{(B-15)}$$

$$w^W(-h,y) = w_4(y) \qquad \text{(B-15a)}$$

$$w^W(h,y) = w^W(x,k) = w^W(x,-k) = 0 \qquad \text{(B-15b)}$$

Problem (I) - (IV) can be solved analytically by the method of separation of variables. For example, let $w^N = X(x)Y(y)$ and substituting it into eq(B-12), the linear PDE is then separated into two ordinary differential equations.

$$X'' + \lambda^2 X = 0 \qquad \text{(B-16)}$$

$$X(-h) = X(h) = 0 \qquad \text{(B-16a)}$$

$$Y'' - (A^2 + B^2 + \lambda^2)Y = 0 \qquad \text{(B-17)}$$

$$Y(-k) = 0 \qquad \text{(B-17a)}$$

The two boundary conditions in the x-direction, $x = \pm h$, in this case can be used to find the eigenvalues λ_n. And the series solution w^N can be written as

$$w^N(x,y) = \sum_{n=1}^{\infty} A_n \sinh\mu_n(y+k) \sin\lambda_n(x+h) \qquad \text{(B-18)}$$

with $\lambda_n = \frac{n\pi}{2h}$, $\mu_n = \sqrt{A^2 + B^2 + \lambda_n^2}$, $n = 1, 2, 3, \ldots$

The coefficients A_n in eq(B-18) can be easily obtained by applying the nonhomogeneous boundary condition (B-12a), i.e.,

$$w^N(x,k) = w_1(x) = \sum_{n=1}^{\infty} A_n \sinh 2\mu_n k \sin\lambda_n(x+h) \qquad \text{(B-19)}$$

where

$$A_n = \frac{1}{h} \int_{-h}^{h} w_1(x) \sin\lambda_n(x+h)\, dx$$

$$= \frac{e^{-Bk}}{\sinh 2\mu_n k} \left[a_N e_{0n} + b_N h\, e_{1n} + (c_N - a_N) e_{2n} \right] \qquad \text{(B-20)}$$

and

$$e_{0n} = \frac{1}{h} \int_{-h}^{h} e^{Ax} \sin\lambda_n(x+h)\, dx$$

$$= \frac{\lambda_n h}{(Ah)^2 + (\lambda_n h)^2} \left[e^{-Ah} - (-1)^n e^{Ah} \right] \qquad \text{(B-20a)}$$

$$e_{1n} = \frac{1}{h^2} \int_{-h}^{h} xe^{-Ax} \sin\lambda_n(x+h)\, dx$$

$$= \frac{2(Ah)(\lambda_n h)}{[(Ah)^2+(\lambda_n h)^2]^2}\left[e^{Ah} - (-1)^n e^{-Ah}\right] -$$

$$\frac{\lambda_n h}{(Ah)^2+(\lambda_n h)^2}\left[e^{Ah} - (-1)^n e^{-Ah}\right] \qquad \text{(B-20b)}$$

$$e_{2n} = \frac{1}{h} \int_{-h}^{h} e^{-Ax} \sin\lambda_n(x+h)\, dx$$

$$= \frac{\lambda_n h}{(Ah)^2 + (\lambda_n h)^2}\left[e^{Ah} - (-1)^n e^{-Ah}\right] \qquad \text{(B-20c)}$$

The local analytic solution (B-19) when evaluated at the interior node P of the local element located at (0,0) gives the finite analytic algebraic equation relating the interior nodal value to the 8 boundary nodal values as

$$w_P^N = w^N(0,0) = \sum_{n=1}^{\infty} A_n \sinh\mu_n k \sin\lambda_n h \qquad \text{(B-21)}$$

Since $\sin\lambda_n h = \sin\frac{n\pi}{2} = \begin{cases} 0, & n=2m \\ -(-1)^m, & n=2m-1 \end{cases}$ $m=1, 2, 3, \ldots$

eq(B-21) can be further simplified to be

$$w_P^N = \sum_{m=1}^{\infty} \frac{-(-1)^m e^{-Bk} \sinh\lambda_m k}{\sinh 2\mu_m k}\left[a_N e_{0m} + b_N h\, e_{1m} + (c_N - a_N) e_{2m}\right]$$

$$= e^{-Bk} \sum_{m=1}^{\infty} \frac{-(-1)^m}{2\cosh\mu_m k} [\, a_N e_{0m} + b_N h\, e_{1m} + (c_N - a_N) e_{2m}] \qquad \text{(B-22)}$$

Define

$$E_i = \sum_{m=1}^{\infty} \frac{-(-1)^m \lambda_m h}{[(Ah)^2 + (\lambda_m h)^2]^i \cosh\mu_m k} \quad , \quad i = 1,2 \qquad \text{(B-22a)}$$

then

$$\sum_{m=1}^{\infty} \frac{-(-1)^m}{\cosh\mu_m k} e_{0m} = (e^{Ah} + e^{-Ah}) \sum_{m=1}^{\infty} \frac{-(-1)^m \lambda_m h}{[(Ah)^2 + (\lambda_m h)^2]\cosh\mu_m k}$$

$$= 2\cosh Ah\ E_1 \qquad \text{(B-22b)}$$

$$\sum_{m=1}^{\infty} \frac{-(-1)^m}{\cosh\mu_m k} e_{1m} = -(e^{Ah} - e^{-Ah}) \sum_{m=1}^{\infty} \frac{-(-1)^m \lambda_m h}{[(Ah)^2 + (\lambda_m h)^2]\cosh\mu_m k}$$

$$+ 2(Ah)(e^{Ah} + e^{-Ah}) \sum_{m=1}^{\infty} \frac{-(-1)^m \lambda_m h}{[(Ah)^2 + (\lambda_m h)^2]^2 \cosh\mu_m k}$$

$$= 4Ah\ \cosh Ah\ E_2 - 2\sinh Ah\ E_1 \qquad \text{(B-22c)}$$

$$\sum_{m=1}^{\infty} \frac{-(-1)^m}{\cosh\mu_m k} e_{2m} = (e^{Ah} + e^{-Ah}) \sum_{m=1}^{\infty} \frac{-(-1)^m \lambda_m h}{[(Ah)^2 + (\lambda_m h)^2]\cosh\mu_m k}$$

$$= 2\cosh Ah\ E_1 \qquad \text{(B-22d)}$$

Substituting a_N, b_N and c_N into eq(B-22), the local analytic solution becomes

$$\tilde{\phi}_P^N = w_P^N = \frac{1}{2}e^{-Bk}\{\frac{1}{2}[\tilde{\phi}_{NE} - \tilde{\phi}_{NW} - \coth Ah(\tilde{\phi}_{NE} + \tilde{\phi}_{NW} - 2\tilde{\phi}_{NC})]$$

$$(4Ah\ \cosh Ah\ E_2 - 2\sinh Ah\ E_1) + \tilde{\phi}_{NC}(2\cosh Ah\ E_2)\}$$

$$= e^{-Bk}\{(2\cosh Ah\ \tilde{\phi}_{NC} - e^{Ah}\tilde{\phi}_{NW} - e^{-Ah}\tilde{\phi}_{NE})(Ah\ \coth Ah\ E_2$$

$$- \frac{1}{2}E_1) + (\cosh Ah\ E_1)\tilde{\phi}_{NC}\}$$

$$= e^{-Bk}[(\frac{1}{2}E_1 - Ah\coth Ah\ E_2)(e^{-Ah}\tilde{\phi}_{NE} + e^{Ah}\tilde{\phi}_{NW}) +$$

$$(2Ah\ \cosh Ah\ \coth Ah\ E_2)\tilde{\phi}_{NC}] \qquad \text{(B-23a)}$$

Similarly, $\tilde{\phi}_P^S$, $\tilde{\phi}_P^E$ and $\tilde{\phi}_P^W$ can be solved in terms of the nodal values at the south, east and west boundary respectively.

$$\tilde{\phi}_P^S = e^{Bk}[(\frac{1}{2}E_1 - Ah\ \coth Ah\ E_2)(e^{-Ah}\tilde{\phi}_{SE} + e^{Ah}\tilde{\phi}_{SW}) +$$

$$(2Ah\ \cosh Ah\ \coth Ah\ E_2)\tilde{\phi}_{SC}] \qquad \text{(B-23b)}$$

$$\tilde{\phi}_P^E = e^{-Ah}[(\frac{1}{2}E_1' - Bk\ \coth Bk\ E_2')(e^{-Bk}\tilde{\phi}_{NE} + e^{Bk}\tilde{\phi}_{SE}) +$$

$$(2Bk\ \cosh Bk\ \coth Bk\ E_2')\tilde{\phi}_{EC}] \qquad \text{(B-23c)}$$

$$\tilde{\phi}_P^W = e^{Ah}[(\frac{1}{2}E_1' - Bk\ \coth Bk\ E_2')(e^{-Bk}\tilde{\phi}_{NW} + e^{Bk}\tilde{\phi}_{SW}) +$$

$$(2Bk\ \cosh Bk\ \coth Bk\ E_2')\tilde{\phi}_{WC}] \qquad \text{(B-23d)}$$

where

$$E_i' = \sum_{m=1}^{\infty} \frac{-(-1)^m(\lambda_m'k)}{[(Bk)^2 + (\lambda_m'k)^2]^i \cosh\mu_m'h}, \quad i = 1, 2$$

and

$$\lambda'_m = \frac{(2m-1)\pi}{2k} \quad , \qquad \mu'_m = \sqrt{A^2 + B^2 + \lambda'^2_m}$$

The 9-point FA formula relating the center nodal value $\tilde{\phi}_P$ and its neighboring nodal values can thus be obtained by superimposed the four solutions of the linear problems (I) - (IV), or

$$\tilde{\phi}_P = \tilde{\phi}_P^N + \tilde{\phi}_P^S + \tilde{\phi}_P^E + \tilde{\phi}_P^W$$

$$= (e^{-Ah-Bk}\tilde{\phi}_{NE} + e^{Ah-Bk}\tilde{\phi}_{NW} + e^{-Ah+Bk}\tilde{\phi}_{SE} +$$

$$e^{Ah+Bk}\tilde{\phi}_{SW})[\tfrac{1}{2}(E_1 + E'_1) - Ah\ \text{coth}Ah\ E_2 - Bk\ \text{coth}Bk\ E'_2]$$

$$+2Ah\ \text{cosh}Ah\ \text{coth}Ah\ E_2\ (e^{-Bk}\tilde{\phi}_{NC} + e^{Bk}\tilde{\phi}_{SC}) +$$

$$2Bk\ \text{cosh}Bk\ \text{coth}Bk\ E'_2\ (e^{-Ah}\tilde{\phi}_{EC} + e^{Ah}\tilde{\phi}_{WC}) \qquad (B-24)$$

Since $\tilde{\phi} = 1$ and $\tilde{\phi} = -Bx+Ay$ are two particular solutions of convective transport equation(B-7), and both of them can be represented by the exponential and linear boundary functions (B-10), it is instructive to utilized these exact solutions to obtain the analytic expressions between series summation terms E_1, E'_1, E_2 and E'_2 as follows

(a) $\tilde{\phi} = 1$

Since $\tilde{\phi} = 1$ is an analytic solution of eq(B-7) and can be represented by boundary functions (B-10), it should

satisfies the FA formula (B-24) also. By substituting

$$\tilde{\phi}_P = \tilde{\phi}_{EC} = \tilde{\phi}_{WC} = \tilde{\phi}_{NC} = \tilde{\phi}_{SC} = \tilde{\phi}_{NE} = \tilde{\phi}_{NW} = \tilde{\phi}_{SE} = \tilde{\phi}_{SW} = 1$$

into eq(B-24), an analytic relation between E_1 and E_1' can be obtained

$$\tilde{\phi}_P = 1 = (e^{-Ah}+e^{Ah})(e^{-Bk}+e^{Bk})\left[\frac{1}{2}(E_1+E_1') - Ah\ \coth Ah\ E_2 - Bk\ \coth Bk\ E_2'\right] + 2Ah\ \cosh Ah\ \coth Ah\ E_2(e^{-Bk}+e^{Bk}) + 2Bk\ \cosh Bk\ \coth Bk\ E_2'(e^{-Ah}+e^{Ah})$$

$$= 2\cosh Ah\ \cosh Bk(E_1+E_1')$$

or

$$E_1 + E_1' = \frac{1}{2\cosh Ah\ \cosh Bk} \qquad \text{(B-25)}$$

(b) $\tilde{\phi} = -Bx+Ay$

Similarly, $\tilde{\phi} = -Bx+Ay$ satisfies the FA formula (B-24) also. It gives $\tilde{\phi}_P = 0$, $\tilde{\phi}_{EC} = -Bh$, $\tilde{\phi}_{NC} = Ak$ etc. By substituting these values into eq(B-24), an analytic expression between between E_2 and E_2' is obtained.

$$\tilde{\phi}_P = 0 = [Ak(e^{-Ah-Bk}+e^{Ah-Bk}-e^{-Ah+Bk}-e^{Ah+Bk}) + Bh(e^{Ah-Bk}+e^{Ah+Bk}-e^{-Ah-Bk}-e^{-Ah+Bk})]\left[\frac{1}{2}(E_1+E_1')-Ah\ \coth Ah\ E_2 - Bk\ \coth Bk\ E_2'\right] + 2Ah\ \cosh Ah\ \coth Ah\ E_2\ Ak\ (e^{-Bk}-e^{Bk}) + 2Bk\ \cosh Bk\ \coth Bk\ E_2'\ Bk(e^{Ah}-e^{-Ah})$$

$$= \frac{1}{\cosh Ah \cosh Bk}\,(Bh \sinh Ah \cosh Bk - Ak \cosh Ah \sinh Bk)$$

$$+ 4(Ak)(Bk)\cosh Ah \sinh Bk \coth Bk\, E_3'$$

$$- 4(Ah)(Bh)\cosh Bk \sinh Ah \coth Ah\, E_3$$

or

$$E_3' = \left(\frac{B}{K}\right)^2 E_3 + \frac{Ak \tanh Bk - Bh \tanh Ah}{4AK\,BK \cosh Ah \cosh Bk} \qquad (B\text{-}26a)$$

the same analytic expression (B-26a) may also be obtained by differentiating (B-25) with respect to A and B, i.e.,

$$\frac{1}{2A}\frac{\partial}{\partial A}(E_1 + E_1') - \frac{1}{2B}\frac{\partial}{\partial B}(E_1 + E_1')$$

$$= h^2 E_3 - k^2 E_3' = \frac{Bh \tanh Ah - Ak \tanh Bk}{4AB \cosh Ah \cosh Bk} \qquad (B\text{-}26b)$$

Define

$$E = \frac{1}{2}(E_1 + E_1') - Ah \coth Ah\, E_3 - Bk \coth Bk\, E_3' \qquad (B\text{-}26c)$$

$$EA = 2Ah \cosh Ah \coth Ah\, E_3 \qquad (B\text{-}26d)$$

$$EB = 2Bk \cosh Bk \coth Bk\, E_3' \qquad (B\text{-}26e)$$

Then the 9-point finite analytic solution (B-24) can be summarized as

$$\phi_P = C_{NE}\phi_{NE} + C_{NW}\phi_{NW} + C_{SE}\phi_{SE} + C_{EC}\phi_{EC} + C_{WC}\phi_{WC} +$$

$$C_{EC}\phi_{EC} + C_{SC}\phi_{SC} + C_{NC}\phi_{NC} \qquad (B\text{-}27)$$

where

$$C_{NE} = e^{-Ah-Bk}\,E \quad , \qquad C_{NW} = e^{Ah-Bk}\,E$$

$$C_{SE} = e^{-Ah+Bk}\,E \quad , \qquad C_{SW} = e^{Ah+Bk}\,E$$

$$C_{NC} = e^{-Bk(EA)} \quad , \qquad C_{SC} = e^{Bk(EA)}$$

$$C_{EC} = e^{-Ah(EB)} \quad , \qquad C_{WC} = e^{Ah(EB)}$$

After applying the analytic expressions (B-25) and (B-26), there is only one series summation term E_2 need to be evaluated numerically. In most of the applications, 10 terms of summation for E_2 are enough to achieve an accuracy of 10^{-6}.

For the unsteady, inhomogeneous convective transport equation (B-5) with higher order correction term, i.e., $g \neq 0$, the local analytic solution can be obtained by substituting $\tilde{\phi}$ of eq(B-6) into eq(B-24) for ϕ , which gives

$$\phi_P = C_{NE}\phi_{NE} + C_{NW}\phi_{NW} + C_{SE}\phi_{SE} + C_{SW}\phi_{SW} + C_{EC}\phi_{EC} + C_{WC}\phi_{WC} + C_{NC}\phi_{NC} + C_{SC}\phi_{SC} - C_P\, g \qquad \text{(B-28)}$$

where

$$C_P = \frac{1}{2(A^2+B^2)}\,[\,Ah(C_{NW} + C_{SW} + C_{WC} - C_{NE} - C_{SE} - C_{EC}) + Bk(C_{SE} + C_{SW} + C_{SC} - C_{NE} - C_{NW} - C_{NC})] \qquad \text{(B-28a)}$$

or

$$C_P = \frac{1}{2(A^2+B^2)}\,\{\,Ah\,\tanh Ah + Bk\,\tanh Bk - 4\cosh Ah\,\cosh Bk\,[\,(Ah)^2E_2 + (Bk)^2E_2'\,]\,\} \qquad \text{(B-28b)}$$

By substituting g of eq(B-5a) into eq(B-28), a 10-point FA formula for unsteady inhomogeneous convective transport equation with higher order correction term can be obtained

$$\phi_P = \frac{1}{1+\frac{R}{\tau}C_P}\left(C_{NE}\phi_{NE} + C_{NW}\phi_{NW} + C_{SE}\phi_{SE} + C_{SW}\phi_{SW} + C_{EC}\phi_{EC} + C_{WC}\phi_{WC} + C_{NC}\phi_{NC} + C_{SC}\phi_{SC} + \frac{R}{\tau}C_P\phi_P^{n-1} - C_P f_P\right) \quad \text{(B-29)}$$

where

$$f_P = f^{n-1}(x,y,\phi_j)\big|_{P(0,0)}$$

and the nodal values without superscript denote those values evaluated at n^{th} time step, while ϕ_P^{n-1} denotes the nodal value of interior point P at $(n-1)^{th}$ step.

B-2 Finite Analytic Formulation of Unsteady Two-Dimensional Convective Transport Equation for Nonuniform Grid Spacing Local Element with Exponential and Linear Boundary Approximation

In previous formulation, the local analytic solution is derived in terms of the eight boundary nodes which are equally spaced on the boundary of the rectangular local element with grid spacing h and k respectively. A 9-point FA formula is then obtained by evaluating the local analytic solution at the center of the local element. The resulting 9-point FA formula is applicable to problems

with uniform rectangular or square elements over the whole domain of calculation. However, in many engineering applications, the use of nonuniform grid spacing local element as that shown in Fig. 4(b) is often desirable, because it enables us to obtain physically meaningful solutions more effectively.

It is possible to derive a local analytic solution for the local element of nonuniform grid spacing (see Fig. 3 or Fig. 4(b)) in a way similar to that outlined in B-1. For example, an exponential and linear boundary function can be employed to approximate the north boundary condition in terms of the three unequally spaced nodal values $\tilde{\phi}_{NE}$, $\tilde{\phi}_{NW}$ and $\tilde{\phi}_{NC}$ as follows

$$\tilde{\phi}_N(x) = a_N (e^{2Ax} - 1) + b_N x + c_N \qquad \text{(B-30)}$$

where

$$a_N = \begin{vmatrix} \tilde{\phi}_{NW} - \tilde{\phi}_{NC} & -h_W \\ \tilde{\phi}_{NE} - \tilde{\phi}_{NC} & h_E \end{vmatrix} = \frac{1}{D} [h_W \tilde{\phi}_{NE} + h_E \tilde{\phi}_{NW} - (h_E + h_W) \tilde{\phi}_{NC}] \qquad \text{(B-30a)}$$

$$b_N = \begin{vmatrix} e^{-2Ah_W} - 1 & \tilde{\phi}_{NW} - \tilde{\phi}_{NC} \\ e^{2Ah_E} - 1 & \tilde{\phi}_{NE} - \tilde{\phi}_{NC} \end{vmatrix}$$

$$= \frac{1}{D} [(e^{-2Ah_W} - 1)(\tilde{\phi}_{NE} - \tilde{\phi}_{NC}) - (e^{2Ah_E} - 1)(\tilde{\phi}_{NW} - \tilde{\phi}_{NC}) \qquad \text{(B-30b)}$$

$$c_N = \tilde{\phi}_{NC} \qquad \text{(B-30c)}$$

and

$$D = \begin{vmatrix} e^{-2Ah_W} - 1 & -h_W \\ e^{2Ah_E} - 1 & h_E \end{vmatrix} = h_W(e^{2Ah_E} - 1) + h_E(e^{-2Ah_W} - 1)$$

With homogeneous boundary conditions assigned for three other boundaries, the corresponding analytic solution $w^N(x,y)$ for eq(B-12) will be of the form of

$$w^N(x,y) = \sum_{m=1}^{\infty} A_n \cosh\mu_n(y + h_S) \sin\lambda_n(x + h_W) \qquad (B-31)$$

where

$$\lambda_n = \frac{n\pi}{h_E + h_W} \quad , \qquad \mu_n = \sqrt{A^2 + B^2 + \lambda_n^2}$$

and the coefficients A_n for the series solution (B-31) can be obtained by performing the similar integrations as e_{0n}, e_{1n} and e_{2n} in Sec. B-1. Similar solution procedures can also be applied to obtain other analytic solutions $w^S(x,y)$, $w^E(x,y)$ and $w^W(x,y)$. The 9-point FA formula for nonuniform grid spacing local element is then obtained by evaluating the local analytic solution $w(x,y)$ at the origin $P(0,0)$ of the local element, i.e.,

$$\tilde{\phi}_P = w(0,0) = w_P^E + w_P^W + w_P^N + w_P^S$$

with

$$w_P^N = \sum_{n=1}^{\infty} A_n \cosh\mu_n h_S \sin\lambda_n h_W \qquad \text{etc.}$$

However, because of the unequal upper and lower limits, the evaluation of A_n is more complicate. Furthermore, 12 more summation terms in additional to E_1, E_2, E_1' and E_2' will be encountered in obtaining the local analytic solution. These additional difficulties may toally offset the advantages gained from the use of nonuniform grid. Thus, in present study, instead of using this general formulation, a simpler approximation method utilizing the local analytic solution (B-28) or (B-29) for uniform grid rectangular element will be employed to derive the finite analytic solution for the case of nonuniform grid spacing formulation.

Consider the case $h_E < h_W$ and $h_N < h_S$ shown in Fig. 4(b) as an example. A smaller rectangular element of width $2h_E$, height $2h_N$ and with the interior point P located at the center can be drawn as shown. If suitable interpolation functions are employed to approximate the unknown nodal values ϕ^*_{NW}, ϕ^*_{WC} etc. on smaller rectangular element in terms of the known values ϕ_{NW}, ϕ_{NC}, ϕ_P etc. at 9 nodes which are unequally spaced on the larger element, then the FA formula (B-28) or (B-29) derived previously for ϕ_P can be applied to this smaller rectangular element directly. After some simple manipulation, a FA formulation for nonuniform grid case can be obtained.

Although there are several interpolation functions

may be used to approximate the nodal values ϕ^*_{NW}, ϕ^*_{WC} etc., the same exponential and linear boundary function will be employed as the interpolation function to obtain the unknown nodal values on smaller rectangular element, so that the error introduced by interpolation will be minimized. For example, the north boundary condition can be approximated by the boundary function

$$\phi_N(x) = a_N (e^{2Ax} - 1) + b_N x + c_N \qquad \text{(B-32)}$$

where a_N, b_N and c_N are defined in eq(B-30a) thru (B-30c).

Evaluating the boundary function (B-32) at $x = -h_E$ will give the interpolated nodal value ϕ^*_{NW}

$$\phi^*_{NW} = \phi_N(-h_E) = a_N (e^{-2Ah_E} - 1) - b_N h_E + c_N$$

$$= (s-1)\phi_{NE} + \bar{s}\phi_{NW} + (2-s-\bar{s})\phi_{NC} \qquad \text{(B-33a)}$$

where

$$s = \frac{h_W(e^{2Ah_E} + e^{-2Ah_E} - 2)}{h_W(e^{2Ah_E} - 1) + h_E(e^{-2Ah_W} - 1)} \quad , \text{ and } \quad \bar{s} = s\,\frac{h_E}{h_W}$$

Similar exponential and linear boundary functions can be employed to obtained other nodal values ϕ^*_{WC}, ϕ^*_{SW} etc.

$$\phi^*_{WC} = (s-1)\phi_{EC} + \bar{s}\phi_{WC} + (2-s-\bar{s})\phi_P \qquad \text{(B-33b)}$$

$$\phi^*_{SC} = (t-1)\phi_{NC} + \bar{t}\phi_{SC} + (2-t-\bar{t})\phi_P \qquad \text{(B-33c)}$$

$$\phi^*_{SE} = (t-1)\phi_{NE} + \bar{t}\phi_{SE} + (2-t-\bar{t})\phi_{EC} \qquad \text{(B-33d)}$$

$$\phi_1 = (t-1)\phi_{NW} + \bar{t}\phi_{SW} + (2-t-\bar{t})\phi_{WC}$$

and

$$\phi^*_{SW} = (s-1)\phi_{SE} + \bar{s}\phi_1 + (2-t-\bar{t})\phi^*_{SC}$$

$$= (s-1)(t-1)\phi_{NE} + \bar{t}(s-1)\phi_{SE} + (s-1)(2-t-\bar{t})\phi_{EC} +$$

$$\bar{s}(t-1)\phi_{NW} + \bar{s}\bar{t}\phi_{SW} + \bar{s}(2-t-\bar{t})\phi_{WC} + (2-s-\bar{s})(t-1)\phi_{NC}$$

$$+ \bar{t}(2-s-\bar{s})\phi_{SC} + (2-s-\bar{s})(2-t-\bar{t})\phi_P \qquad \text{(B-33e)}$$

where

$$t = \frac{h_S(e^{2Bh_N} + e^{-2Bh_N} - 2)}{h_S(e^{2Bh_N} - 1) + h_N(e^{-2Bh_S} - 1)}, \text{ and } \bar{t} = t\,\frac{h_N}{h_S}$$

After knowing all 9 nodal values on the smaller rectangular local element, the 9-point FA formula (B-28) derived previously can be applied to this smaller element, i.e.,

$$\phi^*_P = C_{NE}\phi_{NE} + C_{NW}\phi^*_{NW} + C_{SE}\phi^*_{SE} + C_{SW}\phi^*_{SW} + C_{EC}\phi_{EC} +$$

$$C_{WC}\phi^*_{WC} + C_{NC}\phi_{NC} + C_{SC}\phi^*_{SC} - C_P\,g \qquad \text{(B-34)}$$

Substituting the interpolated nodal values (B-33a) - (B-33e) into eq(B-34) will give a 9-point FA formula for local element of nonuniform grid spacing as follows

$$\phi_P = \frac{1}{G} (b_{NE}\phi_{NE} + b_{NW}\phi_{NW} + b_{SE}\phi_{SE} + b_{SW}\phi_{SW} + b_{EC}\phi_{EC} + b_{WC}\phi_{WC} + b_{NC}\phi_{NC} + b_{SC}\phi_{SC} - b_P g) \qquad (B\text{-}35)$$

with

$$G = 1 - (2-s-\bar{s})C_{WC} - (2-t-\bar{t})C_{SC} - (2-s-\bar{s})(2-t-\bar{t})C_{SW}$$

and

$$b_{NE} = C_{NE} + (s-1)C_{NW} + (t-1)C_{SE} + (s-1)(t-1)C_{SW}$$

$$b_{NW} = \bar{s}C_{NW} + \bar{s}(t-1)C_{SW}$$

$$b_{SE} = \bar{t}C_{SE} + \bar{t}(s-1)C_{SW}$$

$$b_{SW} = \bar{s}\bar{t}C_{SW}$$

$$b_{EC} = C_{EC} + (s-1)C_{WC} + (2-t-\bar{t})C_{SE} + (s-1)(2-t-\bar{t})C_{SW}$$

$$b_{WC} = \bar{s}C_{WC} + \bar{s}(2-t-\bar{t})C_{SW}$$

$$b_{NC} = C_{NC} + (t-1)C_{SC} + (2-s-\bar{s})C_{NW} + (t-1)(2-s-\bar{s})C_{SW}$$

$$b_{SC} = \bar{t}C_{SC} + \bar{t}(2-s-\bar{s})C_{SW}$$

$$b_P = C_P$$

where all of the FA coefficients C_{NE}, C_{NW} etc. are defined previously in eq(B-27) and (B-28) with $h = h_E$ and $k = h_N$.

A 10-point FA formula for unsteady 2D convective transport equation can also be obtained by further substitution of g in eq(B-5a) into eq(B-35).

$$\phi_P = \frac{1}{G + \frac{R}{\tau} b_P} (b_{NE}\phi_{NE} + b_{NW}\phi_{NW} + b_{SE}\phi_{SE} + b_{SW}\phi_{SW} + b_{EC}\phi_{EC} + b_{WC}\phi_{WC} + b_{NC}\phi_{NC} + b_{SC}\phi_{SC} + \frac{R}{\tau} b_P \phi_P^{n-1} - b_P f_P) \quad \text{(B-36)}$$

where the nodal values without superscript denote those values evaluated at n^{th} time step while ϕ_P^{n-1} denotes the nodal value of interior point P at $(n-1)^{th}$ time step.

For the cases $h_E > h_W$ and/or $h_N > h_S$, the finite analytic formula (B-36) can still be applied by simply opposite the flow direction and rename the nodal points. These procedures can be carried out easily in the numerical calculation, details can be found in the subroutine of attached computer program shown in Appendix D.

B-3 Finite Analytic Formulation of Unsteady Two-Dimensional Convective Transport Equation for Uniform Grid Spacing Local Element with Piecewise-linear Boundary Approximation

In this case, the unsteady 2D convective transport equation is solved in the rectangular local element shown in Fig. 4(a) using the same solution method given in Sec. B-1, except that the exponential and linear boundary function is replaced by the piecewise-linear boundary condition. Following exactly the same procedures as those described in Sec. B-1, the unsteady convective transport

equation is simplified to be an equivalent elliptic PDE (B-5) with constant inhomogeneous term, and the solution for (B-5) can be further separated into a homogeneous solution $\tilde{\phi}$ and a particular solution shown in eq(B-6), such that $\tilde{\phi}$ satisfies the linearized homogeneous convective transport equation (B-7) in the rectangular local element.

Instead of using exponential and linear boundary approximation, a piecewise-linear profile is employed to approximate the boundary conditions for all of the four boundaries of the local element. For example, the north boundary condition $\tilde{\phi}_N(x)$ is approximated by

$$\tilde{\phi}_N(x) = \begin{cases} \tilde{\phi}_{NC} + \dfrac{\tilde{\phi}_{NE} - \tilde{\phi}_{NC}}{h} x , & 0 < x < h \\ \tilde{\phi}_{NC} - \dfrac{\tilde{\phi}_{NW} - \tilde{\phi}_{NC}}{h} x , & -h < x < 0 \end{cases} \qquad \text{(B-37)}$$

The boundary conditions for the south, east and west sides, i.e., $\tilde{\phi}_S(x)$, $\tilde{\phi}_E(y)$ and $\tilde{\phi}_W(y)$ can be similarly approximated by piecewise-linear boundary functions. With the transformation $w = \tilde{\phi} e^{-(Ax+By)}$, the linear convective transport eq(B-7) with piecewise linear boundary conditions can be transformed to

$$w_{xx} + w_{yy} = (A^2+B^2)w \qquad \text{(B-38)}$$

$$w(x,k)=w_1(x)=\begin{cases} e^{-Bk}\left[\tilde{\phi}_{NC}e^{-Ax}+(\tilde{\phi}_{NC}-\tilde{\phi}_{NE})\frac{x}{h}e^{-Ax}\right], & 0\le x\le h \\ e^{-Bk}\left[\tilde{\phi}_{NC}e^{-Ax}+(\tilde{\phi}_{NC}-\tilde{\phi}_{NW})\frac{x}{h}e^{-Ax}\right], & -h\le x\le 0 \end{cases}$$

$$w(x,-k)=w_2(x)=\begin{cases} e^{Bk}\left[\tilde{\phi}_{SC}e^{-Ax}+(\tilde{\phi}_{SC}-\tilde{\phi}_{SE})\frac{x}{h}e^{-Ax}\right], & 0\le x\le h \\ e^{Bk}\left[\tilde{\phi}_{SC}e^{-Ax}+(\tilde{\phi}_{SC}-\tilde{\phi}_{SW})\frac{x}{h}e^{-Ax}\right], & -h\le x\le 0 \end{cases}$$

$$w(h,y)=w_3(y)=\begin{cases} e^{-Ah}\left[\tilde{\phi}_{EC}e^{-By}+(\tilde{\phi}_{EC}-\tilde{\phi}_{NE})\frac{y}{k}e^{-By}\right], & 0\le y\le k \\ e^{-Ah}\left[\tilde{\phi}_{EC}e^{-By}+(\tilde{\phi}_{EC}-\tilde{\phi}_{SE})\frac{y}{k}e^{-By}\right], & -k\le y\le 0 \end{cases}$$

$$w(-h,y)=w_4(y)=\begin{cases} e^{Ah}\left[\tilde{\phi}_{WC}e^{-By}+(\tilde{\phi}_{WC}-\tilde{\phi}_{NW})\frac{y}{k}e^{-By}\right], & 0\le y\le k \\ e^{Ah}\left[\tilde{\phi}_{WC}e^{-By}+(\tilde{\phi}_{WC}-\tilde{\phi}_{SW})\frac{y}{k}e^{-By}\right], & -k\le y\le 0 \end{cases}$$

Equation (B-38) can be solved by the method of separation of variables as those used in solving equation (B-10), i.e.,

$$w(x,y) = w^N + w^S + w^E + w^W \qquad \text{(B-39)}$$

where w^N, w^S, w^E and w^W satisfy the same equations and boundary conditions for problem (I) - (IV) in Sec. B-1. Thus, the analytic solution for $w^N(x,y)$, for example, will be

$$w^N(x,y) = \sum_{n=1}^{\infty} A_n \sinh\mu_n(y+k) \sin\lambda_n(x+h) \qquad (B\text{-}40)$$

where

$$A_n = \frac{1}{h}\int_{-h}^{h} w_1(x) \sin\lambda_n(x+h)\, dx$$

$$= \frac{e^{-Bk}}{\sinh 2\mu_n k}\{\tilde{\phi}_{NC}\left[\frac{1}{h}\int_{-h}^{h} e^{-Ax}\sin\lambda_n(x+h)\, dx\right] +$$

$$(\tilde{\phi}_{NE} - \tilde{\phi}_{NC})\left[\frac{1}{h^2}\int_{0}^{h} xe^{-Ax}\sin\lambda_n(x+h)\, dx\right] +$$

$$(\tilde{\phi}_{NW} - \tilde{\phi}_{NC})\left[\frac{1}{h^2}\int_{-h}^{0} xe^{-Ax}\sin\lambda_n(x+h)\, dx\right]\}$$

$$= \frac{e^{-Bk}}{\sinh 2\mu_n k}\{\frac{\lambda_n h}{(Ah)^2+(\lambda_n h)^2}\left[e^{Ah} - (-1)^n e^{-Ah}\right]\tilde{\phi}_{NC} +$$

$$(\tilde{\phi}_{NE} - \tilde{\phi}_{NC})\left[-\frac{(-1)^n e^{-Ah}}{(Ah)^2+(\lambda_n h)^2}\left(\lambda_n h + \frac{2(Ah)(\lambda_n h)}{(Ah)^2+(\lambda_n h)^2}\right) +\right.$$

$$\left.\frac{2(Ah)(\lambda_n h)}{[(Ah)^2+(\lambda_n h)^2]^2}\cos\frac{n\pi}{2} + \frac{(Ah)^2-(\lambda_n h)^2}{[(Ah)^2+(\lambda_n h)^2]^2}\sin\frac{n\pi}{2}\right]$$

$$-(\tilde{\phi}_{NW} - \tilde{\phi}_{NC})\left[-\frac{(Ah)^2-(\lambda_n h)^2}{[(Ah)^2+(\lambda_n h)^2]^2}\sin\frac{n\pi}{2} -\right.$$

$$\left.\frac{2(Ah)(\lambda_n h)}{(Ah)^2+(\lambda_n h)^2}\cos\frac{n\pi}{2} + \frac{e^{Ah}}{(Ah)^2+(\lambda_n h)^2}\left(-\lambda_n h + \frac{2(Ah)(\lambda_n h)}{(Ah)^2+(\lambda_n h)^2}\right)\right]\} \qquad (B\text{-}41)$$

The local analytic solution (B-40) when evaluated at the interior node P of the local element gives the finite analytic algebraic relation between interior nodal value w_P^N and three neighboring nodal values at north boundary

$$w_P^N = \sum_{n=1}^{\infty} A_n \sinh\mu_n k \sin\lambda_n h$$

$$= \sum_{m=1}^{\infty} -(-1)^m A_m \sinh\mu_m k , \qquad n = 2m-1 \qquad \text{(B-42)}$$

Substituting A_m in eq(B-41) with n = 2m-1 into eq(B-42) results in

$$w_P^N = e^{-Bk}\{ \sum_{m=1}^{\infty} \frac{1}{2\cosh\mu_m k} \frac{-(-1)^m\lambda_m h}{(Ah)^2+(\lambda_m h)^2} (e^{Ah}-e^{-Ah})\tilde{\phi}_{NC} +$$

$$(\tilde{\phi}_{NE} - \tilde{\phi}_{NC}) [e^{-Ah} \frac{-(-1)^m\lambda_m h}{(Ah)^2+(\lambda_m h)^2} + \frac{(Ah)^2-(\lambda_m h)^2}{[(Ah)^2+(\lambda_m h)^2]^2}$$

$$+ 2(Ah)e^{-Ah} \frac{-(-1)^m\lambda_m h}{[(Ah)^2+(\lambda_m h)^2]^2}] - (\tilde{\phi}_{NW} - \tilde{\phi}_{NC}) [$$

$$- \frac{(Ah)^2-(\lambda_m h)^2}{[(Ah)^2+(\lambda_m h)^2]^2} - e^{Ah} \frac{-(-1)^m\lambda_m h}{(Ah)^2+(\lambda_m h)^2} +$$

$$2(Ah)e^{Ah} \frac{-(-1)^m\lambda_m h}{[(Ah)^2+(\lambda_m h)^2]^2}] \}$$

Define

$$E_i = \sum_{m=1}^{\infty} \frac{-(-1)^m \lambda_m h}{[(Ah)^2 + (\lambda_m h)^2]^i \cosh \mu_m k}, \quad i = 1, 2$$

$$F_2 = \sum_{m=1}^{\infty} \frac{(Ah)^2 - (\lambda_m h)^2}{[(Ah)^2 + (\lambda_m h)^2]^2 \cosh \mu_m k}$$

where

$$\lambda_m h = (m - \tfrac{1}{2})\pi, \qquad \mu_m = \sqrt{A^2 + B^2 + \lambda_m^2}$$

then

$$\tilde{\phi}_P^N = w_P^N = e^{-Bk}\{\tilde{\phi}_{NC}[(Ah)(e^{Ah} - e^{-Ah})E_2 - F_2] + \tilde{\phi}_{NE}[\tfrac{1}{2}(F_2 + e^{-Ah}E_1) + (Ah)e^{-Ah}E_2] + \tilde{\phi}_{NW}[\tfrac{1}{2}(F_2 + e^{Ah}E_1) - (Ah)e^{Ah}E_2]\} \qquad \text{(B-43a)}$$

Similarly, $\tilde{\phi}_P^S$, $\tilde{\phi}_P^E$ and $\tilde{\phi}_P^W$ can be solved in terms of the nodal values at south, east and west boundary respectively

$$\tilde{\phi}_P^S = e^{Bk}\{\tilde{\phi}_{SC}[Ah(e^{Ah} - e^{-Ah})E_2 - F_2] + \tilde{\phi}_{SE}[\tfrac{1}{2}(F_2 + e^{-Ah}E_1) + (Ah)e^{-Ah}E_2] + \tilde{\phi}_{SW}[\tfrac{1}{2}(F_2 + e^{Ah}E_1) - (Ah)e^{Ah}E_2]\} \qquad \text{(B-43b)}$$

$$\tilde{\phi}_P^E = e^{-Ah}\{\tilde{\phi}_{EC}[(Bk)(e^{Bk} - e^{-Bk})E_2' - F_2'] + \tilde{\phi}_{NE}[\tfrac{1}{2}(F_2' + e^{-Bk}E_1') + (Bk)e^{-Bk}E_2'] + \tilde{\phi}_{SE}[\tfrac{1}{2}(F_2' + e^{Bk}E_1') - (Bk)e^{Bk}E_2']\} \qquad \text{(B-43c)}$$

$$\tilde{\phi}_P^W = e^{Ah}\{\tilde{\phi}_{WC}[(Bk)(e^{Bk}-e^{-Bk})E_2'-F_2'] + \tilde{\phi}_{NW}[\tfrac{1}{2}(F_2'+e^{-Bk}E_1') + (Bk)e^{-Bk}E_2'] + \tilde{\phi}_{SW}[\tfrac{1}{2}(F_2'+e^{Bk}E_1') - (Bk)e^{Bk}E_2']\} \quad \text{(B-43d)}$$

where

$$E_i' = \sum_{m=1}^{\infty} \frac{-(-1)^m \lambda_m' k}{[(Bk)^2 + (\lambda_m' k)^2]^i \cosh \mu_m' h}, \quad i = 1, 2$$

$$F_2' = \sum_{m=1}^{\infty} \frac{(Bk)^2 - (\lambda_m' k)^2}{[(Bk)^2 + (\lambda_m' k)^2]^2 \cosh \mu_m' h}$$

and $\lambda_m' k = (k - \frac{1}{2})\pi$, $\quad \mu_m' = \sqrt{A^2 + B^2 + \lambda_m'^2}$

The 9-point FA formula can then be obtanied by superimposed the four solutions (B-43a) - (B-43d).

$$\tilde{\phi}_P = \tilde{\phi}_P^N + \tilde{\phi}_P^S + \tilde{\phi}_P^E + \tilde{\phi}_P^W$$

or

$$\tilde{\phi}_P = C_{NE}\tilde{\phi}_{NE} + C_{NW}\tilde{\phi}_{NW} + C_{SE}\tilde{\phi}_{SE} + C_{SW}\tilde{\phi}_{SW} + C_{EC}\tilde{\phi}_{EC} + C_{WC}\tilde{\phi}_{WC} + C_{NC}\tilde{\phi}_{NC} + C_{SC}\tilde{\phi}_{SC} \quad \text{(B-44)}$$

where

$$C_{NE} = \tfrac{1}{2}(e^{-Bk}F_2 + e^{-Ah}F_2') + e^{-Ah-Bk}[\frac{E_1+E_1'}{2} + Ah\,E_2 + Bk\,E_2']$$

$$C_{NW} = \tfrac{1}{2}(e^{-Bk}F_2 + e^{Ah}F_2') + e^{Ah-Bk}[\frac{E_1+E_1'}{2} - Ah\,E_2 + Bk\,E_2']$$

$$C_{SE} = \tfrac{1}{2}(e^{Bk}F_2 + e^{-Ah}F_2') + e^{-Ah+Bk}[\frac{E_1+E_1'}{2} + Ah\,E_2 - Bk\,E_2']$$

$$C_{SW} = \tfrac{1}{2}(e^{Bk}F_2 + e^{Ah}F_2') + e^{Ah+Bk}[\tfrac{1}{2}(E_1+E_1') - Ah\,E_2 - Bk\,E_2']$$

$$C_{EC} = -e^{-Ah}F_2' + (e^{-Ah+Bk} - e^{-Ah-Bk})(Bk)E_2'$$

$$C_{WC} = -e^{Ah}F_2' + (e^{Ah+Bk} - e^{Ah-Bk})(Bk)E_2'$$

$$C_{NC} = -e^{-Bk}F_2 + (e^{Ah-Bk} - e^{-Ah-Bk})(Ah)E_2$$

$$C_{SC} = -e^{Bk}F_2 + (e^{Ah+Bk} - e^{-Ah+Bk})(Ah)E_2$$

It is noted that there are 5 series summation terms (E_1+E_1'), E_2, E_2', F_2 and F_2' need to be evaluated, after utilizing the analytic expressions (B-25a) and (B-26), there are still three series summations E_2, F_2 and F_2' needed to be calculated numerically.

For unsteady two-dimensional convective transport equation with higher order correction term, a 10-point FA formula can be derived by substituting eq(B-5a) and (B-6) into eq(B-40)

$$\phi_P = \frac{1}{1 + \frac{R}{\tau}C_P}\,(C_{NE}\phi_{NE} + C_{NW}\phi_{NW} + C_{SE}\phi_{SE} + C_{SW}\phi_{SW} + C_{EC}\phi_{EC} + C_{WC}\phi_{WC} + C_{NC}\phi_{NC} + C_{SC}\phi_{SC} + \frac{R}{\tau}C_P\phi_P^{n-1} - C_P f_P) \qquad \text{(B-45)}$$

where

$$C_P = \frac{1}{2(A^2+B^2)}\,[Ah(C_{NW} + C_{SW} + C_{WC} - C_{NE} - C_{SE} - C_{EC}) + Bk(C_{SE} + C_{SW} + C_{SC} - C_{NE} - C_{NW} - C_{NC})]$$

APPENDIX C

FINITE ANALYTIC FORMULATION OF UNSTEADY THREE-DIMENSIONAL CONVECTIVE TRANSPORT EQUATION

In this appendix, the unsteady three-dimensional convective transport equation is solved in a local element shown in Fig. 1.

Considered an unsteady three-dimensional convective transport equation of the form of

$$\phi_{xx} + \phi_{yy} + \phi_{zz} = R\left[\phi_t + (u\phi)_x + (v\phi)_y + (w\phi)_z\right] + F \quad \text{(C-1)}$$

where ϕ may represent any one of convective transport quantities, ϕ_j, such as velocities, vorticities, temperature or concentration. The coefficients u, v, w and the source function F, in general, are functions of independent variables x, y, z, t and dependent variables ϕ_j. R is a constant parameter such as Reynolds or Peclet number. Since in most of the engineering applications, the analytic solution of eq(C-1) is not available due to variable coefficients and/or nonlinearity, the finite analytic numerical method is employed to derive the local analytic solution.

In order to solve the convective transport equation

(C-1) analytically in the local element shown in Fig. 6(a), eq(C-1) is first rearranged to be

$$\phi_{xx} + \phi_{yy} + \phi_{zz} = R(\phi_t + U\phi_x + V\phi_y + W\phi_z) + F + R[(u'\phi)_x + (v'\phi)_y + (w'\phi)_z] \qquad (C-2)$$

with

$$u(x,y,z,t,\phi_j) = U + u'(x,y,z,t,\phi_j)$$

$$v(x,y,z,t,\phi_j) = V + v'(x,y,z,t,\phi_j)$$

$$w(x,y,z,t,\phi_j) = W + w'(x,y,z,t,\phi_j)$$

where U, V and W are representative constant values in the local element, for example, the velocities at the interior point P or the area-averaged velocities over the local element. u', v' and w' denote velocity components in the local element that deviate from U, V and W and are sufficiently small when compared with U, V and W. Therefore, the term $R[(u'\phi)_x + (v'\phi)_y + (w'\phi)_z]$ may be considered as a higher order correction term.

Denoting two time steps t_{n-1} and t_n, one may approximately write eq(C-2) as

$$(\phi_{xx} + \phi_{yy} + \phi_{zz})^n = R(\phi_t + U\phi_x + V\phi_y + W\phi_z)^n + f^{n-1}(x,y,z,\phi_j) \qquad (C-3)$$

where

$$f(x,y,z,t,\phi_j) = F(x,y,z,t,\phi_j) + R[(u'\phi)_x + (v'\phi)_y + (w'\phi)_z] \qquad (C-3a)$$

Eq(C-3) can then be written as a linear or linearized partial differential equation with constant coefficients of the form of

$$\phi_{xx} + \phi_{yy} + \phi_{zz} = R\phi_t + 2A\phi_x + 2B\phi_y + 2C\phi_z + f^{n-1}(x,y,z,\phi_j) \qquad (C-4)$$

where $A = \frac{1}{2}RU$, $B = \frac{1}{2}RV$ and $C = \frac{1}{2}RW$ are constants in the local element.

It is noted that these constants may differ from one element to another, so that the overall nonlinear behavior is approximately preserved.

The linear or linearized partial differential equation (C-4) can be solved analytically by similar solution methods outlined in Appendix A and B. In this study, the hybrid FA method is employed to approximate the unsteady term, so that the manipulation effort and computational time can be greatly reduced. i.e.,

$$R\phi_t = R\,\frac{\phi_P^n - \phi_P^{n-1}}{\tau} \qquad (C-5)$$

Moreover, the nonhomogeneous term f^{n-1} in eq(C-4) will be approximated by a representative constant f_P $(=f^{n-1}\big|_{P(0,0,0)}$, for example) in the local element to simplify the solution procedures further. The linear or linearized PDE (C-4) can thus be written as

$$\phi_{xx} + \phi_{yy} + \phi_{zz} = 2A\phi_x + 2B\phi_y + 2C\phi_z + g \qquad (C\text{-}6)$$

with

$$g = \frac{R}{\tau}(\phi_P^n - \phi_P^{n-1}) + f_P = \text{constant} \qquad (C\text{-}6a)$$

The constant nonhomegeneous term in eq(C-6) can be easily taken care of by introducing a new variable

$$\tilde{\phi} = \phi + \frac{g}{2(A^2 + B^2 + C^2)}(Ax + By + Cz) \qquad (C\text{-}7)$$

such that $\tilde{\phi}$ satisfies the homogeneous convective transport equation

$$\tilde{\phi}_{xx} + \tilde{\phi}_{yy} + \tilde{\phi}_{zz} = 2A\tilde{\phi}_x + 2B\tilde{\phi}_y + 2C\tilde{\phi}_z \qquad (C\text{-}8)$$

in the local element.

Equation (C-8) with suitable boundary conditions can be solved analytically by the method of separation of variables. In this study, the problem is first solved for a rectangular local element of $h_E = h_W = h$, $h_N = h_S = k$, $h_T = h_B = 1$, (see Fig. 6(a)) and is then extended to that for the local element of nonuniform grid spacing of $h_E \neq h_W$, $h_N \neq h_S$ and $h_T \neq h_B$.

C-1 Finite Analytic Formulation of Unsteady 3D Convective Transport Equation in a Local Element of Uniform Grid Spacing

In previous formulations, the unsteady 3D convective transport equation is simplified to be an equivalent

elliptic PDE (C-6) with a constant inhomogeneous term g as the source term representing higher order correction term and unsteady term in the small local element. By further subtraction of the particular solution given in eq(C-7) from ϕ, a homogeneous convective transport equation (C-8) is resulted. For the homogeneous convective transport equation (C-8) to be well-posed in a rectangular local element of $h_E = h_W = h$, $h_N = h_S = k$ and $h_T = h_B = l$, boundary conditions must be specified on six boundary surfaces at $x = \pm h$, $y = \pm k$ and $z = \pm l$ respectively. In this appendix, the exponential and linear boundary functions based on the natural solutions of eq(C-8) is employed to approximate the boundary conditions in terms of the 26 boundary nodes available. For example, the boundary condition at top surface can be approximated by

$$\tilde{\phi}_T(x,y) = a_{T1} + a_{T2}(e^{2Ax}-1)(e^{2By}-1) + a_{T3}(e^{2Ax}-1)y + a_{T4}(e^{2By}-1)x + a_{T5}(e^{2Ax}-1) + a_{T6}(e^{2By}-1) + a_{T7}x + a_{T8}y + a_{T9}xy \qquad (C-9)$$

where

$$a_{T1} = \tilde{\phi}_{TC}$$

$$a_{T2} = \frac{1}{16 \sinh^2 Ah \sinh^2 Bk}[\tilde{\phi}_{NET} + \tilde{\phi}_{NWT} + \tilde{\phi}_{SET} + \tilde{\phi}_{SWT} + 4\tilde{\phi}_{TC} - 2(\tilde{\phi}_{ECT} + \tilde{\phi}_{WCT} + \tilde{\phi}_{NCT} + \tilde{\phi}_{SCT})]$$

$$a_{T3} = \frac{1}{8k \sinh^2 Ah \sinh Bk}[\,2\cosh Bk\,(\tilde{\phi}_{ECT} + \tilde{\phi}_{WCT} - 2\tilde{\phi}_{TC}) - e^{Bk}(\tilde{\phi}_{SET} + \tilde{\phi}_{SWT} - 2\tilde{\phi}_{SCT}) - e^{-Bk}(\tilde{\phi}_{NWT} + \tilde{\phi}_{NET} - 2\tilde{\phi}_{NCT})\,]$$

$$a_{T4} = \frac{1}{8h \sinh^2 Bk \sinh Ah}[\,2\cosh Ah\,(\tilde{\phi}_{NCT} + \tilde{\phi}_{SCT} - 2\tilde{\phi}_{TC}) - e^{Ah}(\tilde{\phi}_{NWT} + \tilde{\phi}_{SWT} - 2\tilde{\phi}_{WCT}) - e^{-Ah}(\tilde{\phi}_{NET} + \tilde{\phi}_{SET} - 2\tilde{\phi}_{ECT})\,]$$

$$a_{T5} = \frac{1}{4 \sinh^2 Ah}\,(\tilde{\phi}_{ECT} + \tilde{\phi}_{WCT} - 2\tilde{\phi}_{TC})$$

$$a_{T6} = \frac{1}{4 \sinh^2 Bk}\,(\tilde{\phi}_{NCT} + \tilde{\phi}_{SCT} - 2\tilde{\phi}_{TC})$$

$$a_{T7} = \frac{1}{2h}[\,\tilde{\phi}_{ECT} - \tilde{\phi}_{WCT} - \coth Ah(\tilde{\phi}_{ECT} + \tilde{\phi}_{WCT} - 2\tilde{\phi}_{TC})\,]$$

$$= \frac{1}{2h \sinh Ah}[\,2\cosh Ah\ \tilde{\phi}_{TC} - (e^{-Ah}\tilde{\phi}_{ECT} + e^{Ah}\tilde{\phi}_{WCT})\,]$$

$$a_{T8} = \frac{1}{2k}[\,\tilde{\phi}_{NCT} - \tilde{\phi}_{SCT} - \coth Bk(\tilde{\phi}_{NCT} + \tilde{\phi}_{SCT} - 2\tilde{\phi}_{TC})\,]$$

$$= \frac{1}{2k \sinh Bk}[\,2\cosh Bk\ \tilde{\phi}_{TC} - (e^{-Bk}\tilde{\phi}_{NCT} + e^{Bk}\tilde{\phi}_{SCT})\,]$$

$$a_{T9} = \frac{1}{4hk \sinh Ah \sinh Bk}[\,e^{-Ah-Bk}\tilde{\phi}_{NET} + e^{Ah-Bk}\tilde{\phi}_{NWT} + e^{-Ah+Bk}\tilde{\phi}_{SET} + e^{Ah+Bk}\tilde{\phi}_{SWT} + 4\cosh Ah \cosh Bk\ \tilde{\phi}_{TC} - 2\cosh Ah\,(e^{Bk}\tilde{\phi}_{SCT} + e^{-Bk}\tilde{\phi}_{NCT}) - 2\cosh Bk\,(e^{Ah}\tilde{\phi}_{WCT} + e^{-Ah}\tilde{\phi}_{ECT})\,]$$

The boundary conditions for bottom, east, west, north and south sides, i.e., $\tilde{\phi}_B(x,y)$, $\tilde{\phi}_E(y,z)$, $\tilde{\phi}_W(y,z)$, $\tilde{\phi}_N(x,z)$ and $\tilde{\phi}_S(x,z)$, can be similarly approximated by exponential and linear boundary functions in terms of the 9 nodal values available on each boundary.

With the introduction of a change variable

$$\tilde{\phi} = w\, e^{Ax+By+Cz} \tag{C-10}$$

the convective transport equation (C-8) and boundary conditions (C-9) etc. are transformed to

$$w_{xx} + w_{yy} + w_{zz} = (A^2+B^2+C^2)\, w \tag{C-11}$$

and

$$w(x,y,1) = w_1(x,y)$$

$$= e^{-cl}\,[\, a_{T1}e^{-Ax-By} + a_{T2}(e^{Ax}-e^{-Ax})(e^{By}-e^{-By}) + a_{T3}(e^{Ax} - e^{-Ax})ye^{-By} + a_{T4}(e^{By}-e^{-By})xe^{-Ax} + a_{T5}e^{-By}(e^{Ax}-e^{-Ax}) + a_{T6}e^{-Ax}(e^{By}-e^{-By}) + a_{T7}e^{-By}(xe^{-Ax}) + a_{T8}e^{-Ax}(ye^{-By}) + a_{T9}(xe^{-Ax})(ye^{-By})\,] \tag{C-11a}$$

$$w(x,y,-1) = w_2(x,y)$$

$$= e^{cl}\,[\, a_{B1}e^{-Ax-By} + a_{B2}(e^{Ax}-e^{-Ax})(e^{By}-e^{-By}) + a_{B3}(e^{Ax} - e^{-Ax})ye^{-By} + a_{B4}(e^{By}-e^{-By})xe^{-Ax} + a_{B5}e^{-By}(e^{Ax}-e^{-Ax})$$

$$+ a_{B6}e^{-Ax}(e^{By}-e^{-By}) + a_{B7}e^{-By}(xe^{-Ax}) + a_{B8}e^{-Ax}(ye^{-By}) + a_{B9}(xe^{-Ax})(ye^{-By})] \quad \text{(C-11b)}$$

$$w(h,y,z) = w_3(y,z)$$

$$= e^{-Ah}[a_{E1}e^{-By-Cz} + a_{E2}(e^{By}-e^{-By})(e^{Cz}-e^{-Cz}) + a_{E3}(e^{By} - e^{-By})ze^{-Cz} + a_{E4}(e^{Cz}-e^{-Cz})ye^{-By} + a_{E5}e^{-Cz}(e^{By}-e^{-By}) + a_{E6}e^{-By}(e^{Cz}-e^{-Cz}) + a_{E7}e^{-Cz}(ye^{-By}) + a_{E8}e^{-By}(ze^{-Cz}) + a_{E9}(ye^{-By})(ze^{-Cz})] \quad \text{(C-11c)}$$

$$w(-h,y,z) = w_4(y,z)$$

$$= e^{Ah}[a_{W1}e^{-By-Cz} + a_{W2}(e^{By}-e^{-By})(e^{Cz}-e^{-Cz}) + a_{W3}(e^{By} - e^{-By})ze^{-Cz} + a_{W4}(e^{Cz}-e^{-Cz})ye^{-By} + a_{W5}e^{-Cz}(e^{By}-e^{-By}) + a_{W6}e^{-By}(e^{Cz}-e^{-Cz}) + a_{W7}e^{-Cz}(ye^{-By}) + a_{W8}e^{-By}(ze^{-Cz}) + a_{W9}(ye^{-By})(ze^{-Cz})] \quad \text{(C-11d)}$$

$$w(x,k,z) = w_5(x,z)$$

$$= e^{-Bk}[a_{N1}e^{-Ax-Cz} + a_{N2}(e^{Ax}-e^{-Ax})(e^{Cz}-e^{-Cz}) + a_{N3}(e^{Ax} - e^{-Ax})ze^{-Cz} + a_{N4}(e^{Cz}-e^{-Cz})xe^{-Ax} + a_{N5}e^{-Cz}(e^{Ax}-e^{-Ax}) + a_{N6}e^{-Ax}(e^{Cz}-e^{-Cz}) + a_{N7}e^{-Cz}(xe^{-Ax}) + a_{N8}e^{-Ax}(ze^{-Cz}) + a_{N9}(xe^{-Ax})(ze^{-Cz})] \quad \text{(C-11e)}$$

$$w(x,-k,z) = w_6(x,z)$$

$$= e^{Bk}\,[\,a_{S1}e^{-Ax-Cz} + a_{S2}(e^{Ax}-e^{-Ax})(e^{Cz}-e^{-Cz}) + a_{S3}(e^{Ax} - e^{-Ax})ze^{-Cz} + a_{S4}(e^{Cz}-e^{-Cz})xe^{-Ax} + a_{S5}e^{-Cz}(e^{Ax}-e^{-Ax}) + a_{S6}e^{-Ax}(e^{Cz}-e^{-Cz}) + a_{S7}e^{-Cz}(xe^{-Ax}) + a_{S8}e^{-Ax}(ze^{-Cz}) + a_{S9}(xe^{-Ax})(ze^{-Cz})] \qquad \text{(C-11f)}$$

Applying the method of superposition for linear equation, this problem can be solved analytically by further dividing it into six simpler problems with each of them having only one nonhomogeneous boundary condition. i.e., $w = w^T + w^B + w^E + w^W + w^N + w^S$ and

Problem (I)

$$w^T_{xx} + w^T_{yy} + w^T_{zz} = (A^2+B^2+C^2)\,w^T \qquad \text{(C-12)}$$

$$w^T(x,y,1) = w_1(x,y) \qquad \text{(C-12a)}$$

$$w^T = 0 \quad \text{at } x = \pm h,\ y = \pm k \text{ and } z = -1 \qquad \text{(C-12b)}$$

Problem (II)

$$w^B_{xx} + w^B_{yy} + w^B_{zz} = (A^2+B^2+C^2)\,w^B \qquad \text{(C-13)}$$

$$w^B(x,y,-1) = w_2(x,y) \qquad \text{(C-13a)}$$

$$w^B = 0 \quad \text{at } x = \pm h,\ y = \pm k \text{ and } z = 1 \qquad \text{(C-13b)}$$

Problem (III)

$$w^E_{xx} + w^E_{yy} + w^E_{zz} = (A^2+B^2+C^2)\, w^E \qquad \text{(C-14)}$$

$$w^E(h,y,z) = w_3(y,z) \qquad \text{(C-14a)}$$

$$w^E = 0 \quad \text{at } x = -h,\ y = \pm k \text{ and } z = \pm l \qquad \text{(C-14b)}$$

Problem (IV)

$$w^W_{xx} + w^W_{yy} + w^W_{zz} = (A^2+B^2+C^2)\, w^W \qquad \text{(C-15)}$$

$$w^W(-h,y,z) = w_4(y,z) \qquad \text{(C-15a)}$$

$$w^W = 0 \quad \text{at } x = h,\ y = \pm k \text{ and } z = \pm l \qquad \text{(C-15b)}$$

Problem (V)

$$w^N_{xx} + w^N_{yy} + w^N_{zz} = (A^2+B^2+C^2)\, w^N \qquad \text{(C-16)}$$

$$w^N(x,k,z) = w_5(x,z) \qquad \text{(C-16a)}$$

$$w^N = 0 \quad \text{at } x = \pm h,\ y = -k \text{ and } z = \pm l \qquad \text{(C-16b)}$$

Problem (VI)

$$w^S_{xx} + w^S_{yy} + w^S_{zz} = (A^2+B^2+C^2)\, w^S \qquad \text{(C-17)}$$

$$w^S(x,-k,z) = w_6(x,z) \qquad \text{(C-17a)}$$

$$w^S = 0 \quad \text{at } x = \pm h,\ y = k \text{ and } z = \pm l \qquad \text{(C-17b)}$$

Problem (I) - (VI) can be solved analytically by the method of separation of variables. For example, by assuming $w^T(x,y,z) = X(x)Y(y)Z(z)$ and substituting it into eq(C-12) of Problem (I), the variables are separated

$$\frac{X''}{X} + \frac{Y''}{Y} + \frac{Z''}{Z} = (A^2+B^2+C^2) \qquad \text{(C-18)}$$

The solution for equation (C-18) with homogeneous boundary conditions (C-12b) is known to be

$$w^T(x,y,z) = \sum_{m=1}^{\infty} \sum_{n=1}^{\infty} A_{mn} \sin\lambda_m(x+h) \sin\mu_n(y+k) * \sinh\gamma_{mn}(z+1) \qquad \text{(C-19)}$$

with

$$\lambda_m = \frac{m\pi}{2h}, \quad \mu_n = \frac{n\pi}{2k} \quad \text{and} \quad \gamma_{mn} = \sqrt{A^2+B^2+C^2+\lambda_m^2+\mu_n^2}$$

$$m, n = 1, 2, 3, \ldots\ldots$$

where eigenvalues are obtained by applying the four homogeneous boundary conditions at $x = \pm h$ and $y = \pm k$ in eq(C-12b). Applying the boundary condition (C-12a) at top boundary

$$w^T(x,y,1) = w_1(x,y)$$

$$= \sum_{m=1}^{\infty} \sum_{n=1}^{\infty} A_{mn} \sinh 2\gamma_{mn} 1 \sin\lambda_m(x+h) \sin\mu_n(y+k) \qquad \text{(C-20)}$$

The coefficients A_{mn} can then be obtained by invoking

the orthogonality condition of sine series, i.e.,

$$A_{mn} = \frac{1}{hk\ \sinh 2\gamma_{mn}l} \int_{-k}^{k}\int_{-h}^{h} w_1(x,y)\sin\lambda_m(x+h)\sin\mu_n(y+k)dxdy$$

$$= \frac{e^{-cl}}{\sinh 2\gamma_{mn}l}\left(a_{T1}e_{mn1} + a_{T2}e_{mn2} + a_{T3}h\, e_{mn3} + \right.$$

$$a_{T4}h\, e_{mn4} + a_{T5}e_{mn5} + a_{T6}e_{mn6} + a_{T7}h\, e_{mn7} +$$

$$\left. a_{T8}k\, e_{mn8} + a_{T9}hk\, e_{mn9}\right) \qquad \text{(C-21)}$$

where

$$e_{mn1} = \frac{1}{hk} \int_{-k}^{k}\int_{-h}^{h} e^{-Ax-By}\sin\lambda_m(x+h)\sin\mu_n(y+k)\ dxdy$$

$$e_{mn2} = \frac{1}{hk} \int_{-k}^{k}\int_{-h}^{h} (e^{Ax}-e^{-Ax})(e^{By}-e^{-By})\sin\lambda_m(x+h)*$$

$$\sin\mu_n(y+k)\ dxdy$$

$$e_{mn3} = \frac{1}{hk^2} \int_{-k}^{k}\int_{-h}^{h} (e^{Ax}-e^{-Ax})ye^{-By}\sin\lambda_m(x+h)\sin\mu_n(y+k)dxdy$$

$$e_{mn4} = \frac{1}{h^2k} \int_{-k}^{k}\int_{-h}^{h} (e^{By}-e^{-By})xe^{-Ax}\sin\lambda_m(x+h)\sin\mu_n(y+k)dxdy$$

$$e_{mn5} = \frac{1}{hk} \int_{-k}^{k}\int_{-h}^{h} e^{-By}(e^{Ax}-e^{-Ax})\sin\lambda_m(x+h)\sin\mu_n(y+k)\ dxdy$$

$$e_{mn6} = \frac{1}{hk} \int_{-k}^{k}\int_{-h}^{h} e^{-Ax}(e^{By}-e^{-By})\sin\lambda_m(x+h)\sin\mu_n(y+k)\ dxdy$$

$$e_{mn7} = \frac{1}{h^2k} \int_{-k}^{k}\int_{-h}^{h} e^{-By}(xe^{-Ax})\sin\lambda_m(x+h)\sin\mu_n(y+k)\ dxdy$$

$$e_{mn8} = \frac{1}{hk^2} \int_{-k}^{k} \int_{-h}^{h} e^{-Ax}(ye^{-By})\sin\lambda_m(x+h)\sin\mu_n(y+k)\,dxdy$$

$$e_{mn9} = \frac{1}{h^2k^2} \int_{-k}^{k} \int_{-h}^{h} (xe^{-Ax})(ye^{-By})\sin\lambda_m(x+h)\sin\mu_n(y+k)dxdy$$

When the local analytic solution (C-20) is evaluated at an interior node P located at the center of the rectangular local element, it gives an algebraic equation relating the interior nodal value to its neighboring nodal values at top boundary surface as

$$w_P^T = w^T(0,0,0)$$

$$= \sum_{m=1}^{\infty} \sum_{n=1}^{\infty} A_{mn} \sinh\gamma_{mn}l \sin\lambda_m h \sin\mu_n k \qquad \text{(C-22)}$$

Since

$$\sin\lambda_m h = \sin\frac{m\pi}{2} = \begin{cases} 0, & m = 2p \\ -(-1)^p, & m = 2p-1 \end{cases} \qquad p = 1, 2, 3, \ldots$$

$$\sin\mu_n k = \sin\frac{n\pi}{2} = \begin{cases} 0, & n = 2q \\ -(-1)^q, & n = 2q-1 \end{cases} \qquad q = 1, 2, 3, \ldots$$

Eq(C-22) can be further simplified by letting $m = 2p-1$ and $n = 2q-1$, such that

$$\tilde{\phi}_P^T = w_P^T = \sum_{p=1}^{\infty} \sum_{q=1}^{\infty} (-1)^{p+q} A_{pq} \sinh\gamma_{pq}l \qquad \text{(C-23)}$$

where

$$A_{pq} = \frac{e^{-Cl}}{\sinh 2\gamma_{pq} l} \left(a_{T1} e_{pq1} + a_{T2} e_{pq2} + a_{T3}^{k} e_{pq3} + a_{T4}^{h} e_{pq4} + a_{T5} e_{pq5} + a_{T6} e_{pq6} + a_{T7}^{h} e_{pq7} + a_{T8}^{k} e_{pq8} + a_{T9}^{hk} e_{pq9} \right) \quad \text{(C-23a)}$$

By performing a set of integrations similar to e_{0m}, e_{1m} and e_{2m} shown in Appendix B as follows

$$e_{0xp} = \frac{1}{h} \int_{-h}^{h} e^{Ax} \sin\lambda_p(x+h)\, dx$$

$$= \frac{\lambda_p h}{(Ah)^2+(\lambda_p h)^2} \left(e^{Ah}+e^{-Ah}\right) \quad \text{(C-24a)}$$

$$e_{1xp} = \frac{1}{h^2} \int_{-h}^{h} x e^{-Ax} \sin\lambda_p(x+h)\, dx$$

$$= \frac{2Ah\lambda_p h}{[(Ah)^2+(\lambda_p h)^2]^2} \left(e^{Ah}+e^{-Ah}\right) - \frac{\lambda_p h\left(e^{Ah}-e^{-Ah}\right)}{(Ah)^2+(\lambda_p h)^2} \quad \text{(C-24b)}$$

$$e_{2xp} = \frac{1}{h} \int_{-h}^{h} e^{-Ax} \sin\lambda_p(x+h)\, dx$$

$$= \frac{\lambda_p h}{(Ah)^2+(\lambda_p h)^2} \left(e^{Ah}+e^{-Ah}\right) = e_{0xp} \quad \text{(C-24c)}$$

$$e_{0yq} = \frac{1}{k} \int_{-k}^{k} e^{By} \sin\mu_q(y+k)\, dy$$

$$= \frac{\mu_q k}{(Bk)^2+(\mu_q k)^2} \left(e^{Bk}+e^{-Bk}\right) \quad \text{(C-24d)}$$

$$e_{1yq} = \frac{1}{k^2}\int_{-k}^{k} ye^{-By}\sin\mu_q(y+k)\,dy$$

$$= \frac{2Bk\,\mu_q k}{[(Bk)^2+(\mu_q k)^2]^2}(e^{Bk}+e^{-Bk}) + \frac{\mu_q k(e^{Bk}-e^{-Bk})}{(Bk)^2+(\mu_q k)^2} \qquad \text{(C-24e)}$$

$$e_{2yq} = \frac{1}{k}\int_{-k}^{k} e^{-By}\sin\mu_q(y+k)\,dy = e_{0yq} \qquad \text{(C-24f)}$$

where

$$\lambda_p h = (p-\tfrac{1}{2})\pi\ , \quad \mu_q k = (q-\tfrac{1}{2})\pi$$

The double integrations e_{pq1}, e_{pq2} etc. can then be expressed in terms of the products of e_0, e_1 and e_2 in x and y direction respectively. i.e.,

$$e_{pq1} = e_{2xp}e_{2yq} = \frac{(e^{Ah}+e^{-Ah})(e^{Bk}\ e^{-Bk})(\lambda_p h)(\mu_q k)}{[(Ah)^2+(\lambda_p h)^2][(Bk)^2+(\mu_q k)^2]}$$

$$e_{pq2} = (e_{2xp}-e_{0xp})(e_{2yq}-e_{0yq}) = 0$$

$$e_{pq3} = (e_{2xp}-e_{0xp})\ e_{1yq} = 0$$

$$e_{pq4} = (e_{2yq}-e_{0yq})\ e_{1xp} = 0$$

$$e_{pq5} = (e_{2xp}-e_{0xp})\ e_{2yq} = 0$$

$$e_{pg6} = (e_{2yq}-e_{0yq})\ e_{2xp} = 0$$

$$e_{pq7} = \frac{2Ah(e^{Ah}+e^{-Ah})(e^{Bk}+e^{-Bk})(\lambda_p h)(\mu_q k)}{[(Ah)^2+(\lambda_p h)^2]^2[(Bk)^2+(\mu_q k)^2]} -$$

$$\frac{(e^{Ah}-e^{-Ah})(e^{Bk}+e^{-Bk})(\lambda_p h)(\mu_q k)}{[(Ah)^2+(\lambda_p h)^2][(Bk)^2+(\mu_q k)^2]} = e_{1xp}e_{2yq}$$

$$e_{pq8} = \frac{2Bk(e^{Ah}+e^{-Ah})(e^{Bk}+e^{-Bk})(\lambda_p h)(\mu_q k)}{[(Ah)^2+(\lambda_p h)^2][(Bk)^2+(\mu_q k)^2]^2} -$$

$$\frac{(e^{Ah}+e^{-Ah})(e^{Bk}-e^{-Bk})(\lambda_p h)(\mu_q k)}{[(Ah)^2+(\lambda_p h)^2][(Bk)^2+(\mu_q k)^2]} = e_{1yq}e_{2xp}$$

$$e_{Pq9} = \frac{4AhBk(e^{Ah}+e^{-Ah})(e^{Bk}+e^{-Bk})(\lambda_p h)(\mu_q k)}{[(Ah)^2+(\lambda_p h)^2]^2[(Bk)^2+(\mu_q k)^2]^2} -$$

$$\frac{2Ah(e^{Ah}+e^{-Ah})(e^{Bk}-e^{-Bk})(\lambda_p h)(\mu_q k)}{[(Ah)^2+(\lambda_p h)^2]^2[(Bk)^2+(\mu_q k)^2]} -$$

$$\frac{2Bk(e^{Ah}-e^{-Ah})(e^{Bk}+e^{-Bk})(\lambda_p h)(\mu_q k)}{[(Ah)^2+(\lambda_p h)^2][(Bk)^2+(\mu_q k)^2]^2} +$$

$$\frac{(e^{Ah}-e^{-Ah})(e^{Bk}-e^{-Bk})(\lambda_p h)(\mu_q k)}{[(Ah)^2+(\lambda_p h)^2][(Bk)^2+(\mu_q k)^2]} = e_{1xp}e_{1yq}$$

The local analytic algebraic equation (C-23) can hence be simplified as

$$\check{\phi}_P^T = e^{-Cl} \sum_{p=1}^{\infty}\sum_{q=1}^{\infty} \frac{(-1)^{p+q}}{2\cosh\gamma_{pq}l} (a_{T1}e_{pq1} + a_{T7}h\, e_{pq7} +$$

$$a_{T8}k\, e_{pq8} + a_{T9}hk\, e_{pq9})$$

$$= e^{-Cl}\{a_{T1}(e^{Ah}+e^{-Ah})(e^{Bk}+e^{-Bk})E^z_{11} + (a_{T7}h)[2Ah(e^{Ah}+e^{-Ah})(e^{Bk}+e^{-Bk})E^z_{21} - (e^{Ah}-e^{-Ah})(e^{Bk}+e^{-Bk})E^z_{11}] + (a_{T8}k)[2Bk(e^{Ah}+e^{-Ah})(e^{Bk}+e^{-Bk})E^z_{12} - (e^{Ah}+e^{-Ah})*(e^{Bk}-e^{-Bk})E^z_{11}] + (a_{T9}hk)[4AhBk(e^{Ah}+e^{-Ah})(e^{Bk}+e^{-Bk})E^z_{22} - 2Ah(e^{Ah}+e^{-Ah})(e^{Bk}-e^{-Bk})E^z_{21} - 2Bk(e^{Bk}+e^{-Bk})(e^{Ah}-e^{-Ah})E^z_{12} + (e^{Ah}-e^{-Ah})(e^{Bk}-e^{-Bk})E^z_{11}]\} \quad (C\text{-}25)$$

where

$$E^z_{ij} = \sum_{p=1}^{\infty}\sum_{q=1}^{\infty} \frac{(-1)^{p+q}(\lambda_p h)(\mu_q k)}{2[(Ah)^2+(\lambda_p h)^2]^i[(Bk)^2+(\mu_q k)^2]^j \cosh\gamma_{pq} l} \qquad i, j = 1,2 \quad (C\text{-}25a)$$

Substituting a_{T1}, a_{T7}, a_{T8} and a_{T9} obtained from eq(C-9) into eq(C-25), the finite analytic algebraic equation becomes

$$\tilde{\phi}^T_p = e^{-Cl}\{(4\cosh Ah \cosh Bk\, E^z_{11})\tilde{\phi}_{TC} + [2\cosh Ah\, \tilde{\phi}_{TC} - (e^{-Ah}\tilde{\phi}_{ECT}+e^{Ah}\tilde{\phi}_{WCT})](4Ah \coth Ah \cosh Bk\, E^z_{21} - 2\cosh Bk\, E^z_{11}) + [2\cosh Bk\tilde{\phi}_{TC} - (e^{-Bk}\tilde{\phi}_{NCT}+e^{Bk}\tilde{\phi}_{SCT})]*(4Bk \coth Bk \cosh Ah\, E^z_{12} - 2\cosh Ah\, E^z_{11}) + [e^{-Ah-Bk}\tilde{\phi}_{NET}+e^{Ah-Bk}\tilde{\phi}_{NWT}+e^{-Ah+Bk}\tilde{\phi}_{SET}+e^{Ah+Bk}\tilde{\phi}_{SWT}+$$

$$4\text{coshAh coshBk}\ \tilde{\phi}_{TC} - 2\text{coshAh}(e^{-Bk}\tilde{\phi}_{NCT}+e^{Bk}\tilde{\phi}_{SCT}) -$$

$$2\text{coshBk}(e^{-Ah}\tilde{\phi}_{ECT}+e^{Ah}\tilde{\phi}_{WCT})]\,(\,4\text{AhBk cothAh cothBk} *$$

$$E^z_{22} - 2\text{Ah cothAh}\ E^z_{21} - 2\text{Bk cothBk}\ E^z_{12} + E^z_{11})\}$$

$$= (E^z_{11} - 2\text{Ah cothAh}\ E^z_{21} - 2\text{Bk cothBk}\ E^z_{12} +$$

$$4\text{AhBk cothAh cothBk}\ E^z_{22})(e^{-Ah-Bk-Cl}\tilde{\phi}_{NET} +$$

$$e^{Ah-Bk-Cl}\tilde{\phi}_{NWT} + e^{-Ah+Bk-Cl}\tilde{\phi}_{SET} + e^{Ah+Bk-Cl}\tilde{\phi}_{SWT})$$

$$+ 4\text{Ah coshAh cothAh}(E^z_{21}-2\text{Bk cothBk}\ E^z_{22}) *$$

$$(e^{-Bk-Cl}\tilde{\phi}_{NCT}+e^{Bk-Cl}\tilde{\phi}_{SCT}) + 4\text{Bk coshBk cothBk}(E^z_{12}$$

$$- 2\text{Ah cothAh}\ E^z_{22})(e^{-Ah-Cl}\tilde{\phi}_{ECT}+e^{Ah-Cl}\tilde{\phi}_{WCT}) +$$

$$(16\text{AhBk coshAh coshBk cothAh cothBk}\ E^z_{22})e^{-Cl}\tilde{\phi}_{TC}$$

(C-26a)

Similarly, the finite analytic solutions $\tilde{\phi}^B_P$, $\tilde{\phi}^E_P$, $\tilde{\phi}^W_P$, $\tilde{\phi}^N_P$ and $\tilde{\phi}^S_P$ of Problem (II)-(VI) can be obtained in terms of the nodal values on the bottom, east, west, north and south boundary respectively.

$$\tilde{\phi}^B_P = (E^z_{11}-2\text{Ah cothAh}\ E^z_{21}-2\text{Bk cothBk}\ E^z_{12}+4\text{AhBk cothAh} *$$

$$\text{cothBk}\ E^z_{22})(e^{-Ah-Bk+Cl}\tilde{\phi}_{NEB}+e^{Ah-Bk+Cl}\tilde{\phi}_{NWB}+$$

$$e^{-Ah+Bk+Cl}\tilde{\phi}_{SEB}+e^{Ah+Bk+Cl}\tilde{\phi}_{SWB}) + 4\text{Ah coshAh cothAh}*$$

$$(E^z_{21}-2Bk\ \text{cothBk}\ E^z_{22})(e^{-Bk+Cl}\tilde{\phi}_{NCB}+e^{Bk+Cl}\tilde{\phi}_{SCT}) +$$

$$4Bk\ \text{coshBk}\ \text{cothBk}(E^z_{12}-2Ah\ \text{cothAh}\ E^z_{22})(e^{-Ah+Cl}\tilde{\phi}_{ECB}$$

$$+e^{Ah+Cl}\tilde{\phi}_{WCB}) + (16AhBk\ \text{coshAh}\ \text{coshBk}\ \text{cothAh}\ \text{cothBk}$$

$$E^z_{22})e^{Cl}\tilde{\phi}_{BC} \qquad \text{(C-26b)}$$

$$\tilde{\phi}^E_P = (E^x_{11}-2Bk\ \text{cothBk}\ E^x_{21}-2Cl\ \text{cothCl}\ E^x_{12}+4BkCl\ \text{cothBk}\ *$$

$$\text{cothCl}\ E^x_{22})(e^{-Ah-Bk-Cl}\tilde{\phi}_{NET}+e^{-Ah+Bk+Cl}\tilde{\phi}_{SET}+$$

$$e^{-Ah-Bk+Cl}\tilde{\phi}_{NEB}+e^{-Ah+Bk+Cl}\tilde{\phi}_{SEB}) + 4Bk\ \text{coshBk}\ \text{cothBk}$$

$$(E^x_{21}-2Cl\ \text{cothCl}\ E^x_{22})(e^{-Ah-Cl}\tilde{\phi}_{ECT}+e^{-Ah+Cl}\tilde{\phi}_{ECB}) +$$

$$4Cl\ \text{coshCl}\ \text{cothCl}(E^x_{12}-2Bk\ \text{cothBk}\ E^x_{22})(e^{-Ah-Bk}\tilde{\phi}_{NEC}$$

$$+e^{-Ah+Bk}\tilde{\phi}_{SEC}) + (16BkCl\ \text{coshBk}\ \text{coshCl}\ \text{cothBk}\ \text{cothCl}$$

$$E^x_{22})e^{-Ah}\tilde{\phi}_{EC} \qquad \text{(C-26c)}$$

$$\tilde{\phi}^W_P = (E^x_{11}-2Bk\ \text{cothBk}\ E^x_{21}-2Cl\ \text{cothCl}\ E^x_{12}+4BkCl\ \text{cothBk}*$$

$$\text{cothCl}\ E^x_{22})(e^{Ah-Bk-Cl}\tilde{\phi}_{NWT}+e^{Ah+Bk-Cl}\tilde{\phi}_{SWT} +$$

$$e^{Ah-Bk+Cl}\tilde{\phi}_{NWB}+e^{Ah+Bk+Cl}\tilde{\phi}_{SWB}) + 4Bk\ \text{coshBk}\ \text{cothBk}\ *$$

$$(E^x_{21}-2Cl\ \text{cothCl}\ E^x_{22})(e^{Ah-Cl}\tilde{\phi}_{WCT}+e^{Ah+Cl}\tilde{\phi}_{WCB}) +$$

$$4Cl\ \text{coshCl}\ \text{cothCl}(E^x_{12}-2Bk\ \text{cothBk}\ E^x_{22})(e^{Ah-Bk}\tilde{\phi}_{NWC}+$$

$$e^{Ah+Bk}\tilde{\phi}_{SWC}) + (16BkCl\ coshBk\ coshCl\ cothBk\ cothCl\ E^x_{22})\ e^{Ah}\tilde{\phi}_{WC} \qquad \text{(C-26d)}$$

$$\tilde{\phi}^N_P = (E^y_{11}-2Ah\ cothAh\ E^y_{12}-2Cl\ cothCl\ E^y_{21}+4AhCl\ cothAh*\ cothCl\ E^y_{22})(e^{-Ah-Bk-Cl}\tilde{\phi}_{NET} + e^{Ah-Bk-Cl}\tilde{\phi}_{NWT} + e^{-Ah-Bk+Cl}\tilde{\phi}_{NEB}+e^{Ah-Bk+Cl}\tilde{\phi}_{NWB}) + 4Ah\ coshAh\ cothAh\ (E^y_{12}-2Cl\ cothCl\ E^y_{22})(e^{-Bk-Cl}\tilde{\phi}_{NCT} + e^{-Bk+Cl}\tilde{\phi}_{NCB}) + 4Cl\ coshCl\ cothCl(E^y_{21}-2Ah\ cothAh\ E^y_{22})(e^{-Ah-Bk}\tilde{\phi}_{NEC} +e^{Ah-Bk}\tilde{\phi}_{NWC}) + (16AhCl\ coshAh\ coshCl\ cothAh\ cothCl\ E^y_{22})\ e^{-Bk}\tilde{\phi}_{NC} \qquad \text{(C-26e)}$$

$$\tilde{\phi}^S_P = (E^y_{11}-2Ah\ cothAh\ E^y_{12}\ -2Cl\ cothCl\ E^y_{21}+4AhCl\ cothAh*\ cothCl\ E^y_{22})(e^{-Ah+Bk-Cl}\tilde{\phi}_{SET} + e^{Ah+Bk-Cl}\tilde{\phi}_{SWT} + e^{-Ah+Bk+Cl}\tilde{\phi}_{SEB}+e^{Ah+Bk+Cl}\tilde{\phi}_{SWB}) + 4Ah\ coshAh\ cothAh\ (E^y_{12}-2Cl\ cothCl\ E^y_{22})(e^{Bk-Cl}\tilde{\phi}_{SCT}+e^{Bk+Cl}\tilde{\phi}_{SCB}) + 4Cl\ coshCl\ cothCl(E^y_{21}-2Ah\ cothAh\ E^y_{22})(e^{-Ah+Bk}\tilde{\phi}_{SEC} +e^{Ah+Bk}\tilde{\phi}_{SWC}) + (16AhCl\ coshAh\ coshCl\ cothAh\ cothCl\ E^y_{22})\ e^{Bk}\tilde{\phi}_{SC} \qquad \text{(C-26f)}$$

where

$$E^x_{ij} = \sum_{q=1}^{\infty}\sum_{r=1}^{\infty} \frac{(-1)^{q+r}(\mu_q k)(\delta_r l)}{2[(Bk)^2+(\mu_q k)^2]^i[(Cl)^2+(\delta_r l)^2]^j \cosh\gamma_{qr} h}$$

$$E^y_{ij} = \sum_{p=1}^{\infty}\sum_{r=1}^{\infty} \frac{(-1)^{p+r}(\lambda_p h)(\delta_r l)}{2[(Cl)^2+(\delta_r l)^2]^i[(Ah)^2+(\lambda_p h)^2]^j \cosh\gamma_{pr} k}$$

$$i, j = 1, 2$$

and

$$\delta_r l = (r - \tfrac{1}{2})\,\pi$$

$$\gamma_{qr} = \sqrt{A^2+B^2+C^2+\mu_q^2+\delta_r^2}$$

$$\gamma_{pr} = \sqrt{A^2+B^2+C^2+\lambda_p^2+\delta_r^2}$$

The finite analytic algebraic equation for the homogeneous convective transport equation (C-8) with exponential and linear boundary condition (C-9) etc. is then obtained by superimposed the six solutions (C-26a) - (C-26f) of the linear problem (I) - (VI).

$$\tilde{\phi}_P = \tilde{\phi}_P^T + \tilde{\phi}_P^B + \tilde{\phi}_P^E + \tilde{\phi}_P^W + \tilde{\phi}_P^N + \tilde{\phi}_P^S = [-2Cl\ \mathrm{coth}Cl(E^x_{12}+E^y_{21})$$

$$+(E^x_{11}+E^y_{11}+E^z_{11}) - 2Ah\ \mathrm{coth}Ah(E^y_{12}+E^z_{21}) - 2Bk\ \mathrm{coth}Bk$$

$$(E^x_{21}+E^z_{12}) + 4AhBk\ \mathrm{coth}Ah\ \mathrm{coth}Bk\ E^z_{22} + 4BkCl*$$

$$\mathrm{coth}Bk\ \mathrm{coth}Cl\ E^x_{22} + 4AhCl\ \mathrm{coth}Ah\ \mathrm{coth}Cl\ E^y_{22}] *$$

$$(e^{-Ah-Bk-Cl}\tilde{\phi}_{NET} + e^{Ah-Bk-Cl}\tilde{\phi}_{NWT} + e^{-Ah+Bk-Cl}\tilde{\phi}_{SET}$$

$$+ e^{Ah+Bk-Cl}\tilde{\phi}_{SWT} + e^{-Ah-Bk+Cl}\tilde{\phi}_{NEB} + e^{Ah-Bk+Cl}\tilde{\phi}_{NWB}$$

$$+ e^{-Ah+Bk+Cl}\tilde{\phi}_{SEB} + e^{AH+BK+CL}\tilde{\phi}_{SWB}) + 4Ah\ coshAh *$$

$$cothAh\ [\ (E^y_{12} + E^z_{21}) - 2Bk\ cothBk\ E^z_{22} -$$

$$2Cl\ cothCl\ E^y_{22}\ ]\ (e^{Bk-Cl}\tilde{\phi}_{SCT} + e^{-Bk-Cl}\tilde{\phi}_{NCT} +$$

$$e^{Bk+Cl}\tilde{\phi}_{SCB} + e^{-Bk+Cl}\tilde{\phi}_{NCB}) + 4Bk\ coshBk\ cothBk *$$

$$[(E^x_{21} + E^z_{12}) - 2Ah\ cothAh\ E^z_{22} - 2Cl\ cothCl\ E^x_{22}\ ]$$

$$(e^{Ah-Cl}\tilde{\phi}_{WCT} + e^{-Ah-Cl}\tilde{\phi}_{ECT} + e^{Ah+Cl}\tilde{\phi}_{WCB} + e^{-Ah+Cl}\tilde{\phi}_{ECB})$$

$$+ 4Cl\ coshCl\ cothCl\ [\ (E^x_{12} + E^y_{21}) - 2Ah\ cothAh\ E^y_{22}$$

$$- 2Bk\ cothBk\ E^x_{22})(e^{-Ah-Bk}\tilde{\phi}_{NEC} + e^{-Ah+Bk}\tilde{\phi}_{SEC}$$

$$+ e^{Ah-Bk}\tilde{\phi}_{NWC} + e^{Ah+Bk}\tilde{\phi}_{SWC}) + (16AhBk\ coshAh\ coshBk$$

$$cothAh\ cothBk\ E^z_{22}\ )\ (e^{-Cl}\tilde{\phi}_{TC} + e^{Cl}\tilde{\phi}_{BC}) + (16BkCl *$$

$$coshBk\ coshCl\ cothBk\ cothCl\ E^x_{22}\ )\ (e^{-Ah}\tilde{\phi}_{EC} +$$

$$e^{Ah}\tilde{\phi}_{WC}) + (16AhCl\ coshAh\ cothAh\ cothAh\ cothCl\ E^y_{22})$$

$$(e^{-Bk}\tilde{\phi}_{NC} + e^{Bk}\tilde{\phi}_{SC}) \qquad (C\text{-}27)$$

Define

$$EA = E^y_{12} + E^z_{21},\quad EB = E^x_{21} + E^z_{12},\quad EC = E^x_{12} + E^y_{21}$$

$$FA = 2Ah\ cothAh\ (\ EA),\qquad FB = 2Bk\ cothBk\ (EB)$$

$$FC = 2Cl\ cothCl\ (\ EC)$$

$$GA = 4BkCl\ cothBk\ cothCl\ E_{22}^{x}$$

$$GB = 4AhCl\ cothAh\ cothCl\ E_{22}^{y}$$

$$GC = 4AhBk\ cothAh\ cothBk\ E_{22}^{z}$$

and

$$P = (E_{11}^{x} + E_{11}^{y} + E_{11}^{z}) - FA - FB - FC + GA + GB + GC$$

$$QA = 2coshAh(FA - GB - GC)$$

$$QB = 2coshBk(FB - GA - GC)$$

$$Qc = 2coshCl(FC - GA - GB)$$

$$RA = 4coshBk\ coshCl(GA)$$

$$RB = 4coshAh\ coshCl(GB)$$

$$RC = 4coshAh\ coshBk(GC)$$

Then the 27-point finite analytic formula (C-27) can be summarized as follows

$$\tilde{\phi}_P = C_{NET}\tilde{\phi}_{NET} + C_{NWT}\tilde{\phi}_{NWT} + C_{SET}\tilde{\phi}_{SET} + C_{SWT}\tilde{\phi}_{SWT} + C_{NEB}\tilde{\phi}_{NEB} + C_{NWB}\tilde{\phi}_{NWB} + C_{SEB}\tilde{\phi}_{SEB} + C_{SWB}\tilde{\phi}_{SWB} + C_{SCT}\tilde{\phi}_{SCT} + C_{NCT}\tilde{\phi}_{NCT} + C_{SCB}\tilde{\phi}_{SCB} + C_{NCB}\tilde{\phi}_{NCB} + C_{WCT}\tilde{\phi}_{WCT} + C_{ECT}\tilde{\phi}_{ECT} + C_{WCB}\tilde{\phi}_{WCB} + C_{ECB}\tilde{\phi}_{ECB} + C_{NWC}\tilde{\phi}_{NWC} + C_{NEC}\tilde{\phi}_{NEC} + C_{SWC}\tilde{\phi}_{SWC} + C_{SEC}\tilde{\phi}_{SEC} + C_{EC}\tilde{\phi}_{EC} + C_{WC}\tilde{\phi}_{WC} + C_{NC}\tilde{\phi}_{NC} + C_{SC}\tilde{\phi}_{SC} + C_{TC}\tilde{\phi}_{TC} + C_{BC}\tilde{\phi}_{BC} \qquad (C\text{-}28)$$

$$= \sum_{1}^{26} C_{nb}\tilde{\phi}_{nb} \qquad (C\text{-}28a)$$

where the subscript "nb" denetes the neighboring nodal

points to node P, and the FA coefficients C_{nb} are given in the following

$$C_{NET} = e^{-Ah-Bk-Cl}\,P\,, \qquad C_{NWT} = e^{Ah-Bk-Cl}\,P\,,$$

$$C_{SET} = e^{-Ah+Bk-Cl}\,P\,, \qquad C_{SWT} = e^{Ah+Bk-Cl}\,P\,,$$

$$C_{NEB} = e^{-Ah-Bk+Cl}\,P\,, \qquad C_{NWB} = e^{Ah-Bk+Cl}\,P\,,$$

$$C_{SEB} = e^{-Ah+Bk+Cl}\,P\,, \qquad C_{SWB} = e^{Ah+Bk+Cl}\,P\,,$$

$$C_{SCT} = e^{Bk-Cl}\,(QA)\,, \qquad C_{NCT} = e^{-Bk-Cl}\,(QA),$$

$$C_{SCB} = e^{Bk+Cl}\,(QA)\,, \qquad C_{NCB} = e^{-Bk+Cl}\,(QA),$$

$$C_{WCT} = e^{Ah-Cl}\,(QB)\,, \qquad C_{ECT} = e^{-Ah-Cl}\,(QB),$$

$$C_{WCB} = e^{Ah+Cl}\,(QB)\,, \qquad C_{ECB} = e^{-Ah+Cl}\,(QB),$$

$$C_{NWC} = e^{Ah-Bk}\,(QC)\,, \qquad C_{NEC} = e^{-Ah-Bk}\,(QC),$$

$$C_{SWC} = e^{Ah+Bk}\,(QC)\,, \qquad C_{SEC} = e^{-Ah+Bk}\,(QC),$$

$$C_{EC} = e^{-Ah}\,(RA)\,, \qquad C_{WC} = e^{Ah}\,(RA)\,,$$

$$C_{NC} = e^{-Bk}\,(RB)\,, \qquad C_{SC} = e^{Bk}\,(RB)\,,$$

$$C_{TC} = e^{-Cl}\,(RC)\,, \qquad C_{BC} = e^{Cl}\,(RC)\,,$$

There are 12 double series summation terms E^x_{ij}, E^y_{ij} and E^z_{ij}, i, j = 1, 2 need to be evaluated in the calculation of the 27-point FA formula (C-28). However, analytic

expressions similar to those derived in Appendix B may be employed to reduce the numerical calculations needed.

It is known that $\tilde{\phi} = 1$, $\tilde{\phi} = Bx-Ay$, $\tilde{\phi} = Cx-Az$, $\tilde{\phi} = e^{2Ax}$ etc. are particular solutions of eq(C-8), and all of them can be adequately represented by the exponential and linear boundary functions on six boundary surfaces. Thus, the FA algebraic equation (C-28) should recover all these exact solutions in the following manner.

(a) $\tilde{\phi} = 1$

Since $\tilde{\phi} = 1$ satisfies the convective transport equation (C-8) and can be represented by exponential and linear boundary functions with six nonzero coefficients $a_{T1} = a_{B1} = a_{E1} = a_{W1} = a_{N1} = a_{S1} = 1$, it should satisfies the algebraic equation (C-28) also. By substituting this exact solution into eq(C-28), an analytic expression of $E^x_{11} + E^y_{11} + E^z_{11}$ can then be obtained

$$\begin{aligned}\tilde{\phi}_P = 1 &= 8\text{coshAh coshBk coshCl } P + 4\text{coshBk coshCl (QA)} + \\ &\quad 4\text{coshAh coshCl (QB)} + 4\text{coshAh coshBk (QC)} + \\ &\quad 2\text{coshAh (RA)} + 2\text{coshBk (RB)} + 2\text{coshCl (RC)} \\ &= 8\text{coshAh coshBk coshCl } \{ [(E^x_{11} + E^y_{11} + E^z_{11}) - FA - \\ &\quad FB - FC + GA + GB + GC] + (FA - GB - GC) + (FB - GA - \\ &\quad GC) + (FC - GA - GB) + GA + GB + GC \} \\ &= 8\text{coshAh coshBk coshCl } (E^x_{11} + E^y_{11} + E^z_{11})\end{aligned}$$

hence

$$E^x_{11} + E^y_{11} + E^z_{11} = \frac{1}{8\text{coshAh coshBk coshCl}} \qquad \text{(C-29)}$$

(b) $\tilde{\phi} = Bx - Ay$

Since $\tilde{\phi} = Bx - Ay$ is an exact solution of eq(C-8) and can be represented by exponential and linear boundary functions with 12 nonzero coefficients $a_{T7} = a_{B7} = a_{N7} = a_{S7} = B$, $a_{T8} = a_{B8} = a_{E8} = a_{W8} = -A$, $a_{E1} = Bh$, $a_{W1} = -Bh$, $a_{N1} = -Ak$ and $a_{S1} = Ak$, it should satisfies the 27-point FA formula (C-28) also. By evaluating this exact solution at 27 nodal points, eq(C-28) becomes

$$\begin{aligned}\tilde{\phi}_P = 0 = {} & (Bh-Ak)(C_{NET}+C_{NEC}+C_{NEB}) + (-Bh-Ak)(C_{NWT}+ \\ & C_{NWC}+C_{NWB}) + (Bh+Ak)(C_{SET}+C_{SEC}+C_{SEB}) + (-Bh \\ & +Ak)(C_{SWT}+C_{SWC}+C_{SWB}) + Bh(C_{ECT}+C_{EC}+C_{ECB}) - \\ & Bh(C_{WCT}+C_{WC}+C_{WCB}) - Ak(C_{NCT}+C_{NC}+C_{NCB}) + Ak(\\ & C_{SCT}+C_{SC}+C_{SCB}) \\ = {} & 2\text{coshCl}\{-4Bh\ \text{sinhAh coshBk}[(E^x_{11}+E^y_{11}+E^z_{11} - \\ & FA-FB-FC+GA+GB+GC) + (FC-GA-GB) + (FB \\ & -GA-GC) + GA] + 4Ak\ \text{coshAh sinhBk}[(E^x_{11}+ \\ & E^y_{11}+E^z_{11}-FA-FB-FC+GA+GB+GC) + (FC-GA- \\ & GB) + (FA-GB-GC) + GB]\}\end{aligned}$$

Applying the analytic expression (C-29), another analytic expression can then be obtained

$$k^2(EB) - h^2(EA) = \frac{Ak\ \cosh Ah\ \sinh Bk - Bh\ \sinh Ah\ \cosh Bk}{16AB\ \cosh^2 Ah\ \cosh^2 Bk\ \cosh Cl} \qquad (C\text{-}30)$$

$$\text{or} \quad EB = \left(\frac{h}{k}\right)^2 (EA) + \frac{1}{16 \cosh Ah\ \cosh Bk\ \cosh Cl} \left[\frac{\tanh Bk}{Bk} - \left(\frac{h}{k}\right)^2 \frac{\tanh Ah}{Ah} \right] \qquad (C\text{-}30a)$$

(c) $\tilde{\phi} = Cx - Az$

When the exact solution $\tilde{\phi} = Cx - Az$ is considered, an analytic expression similar to eq(C-30) can be obtained as follows

$$EC = \left(\frac{h}{l}\right)^2 (EA) + \frac{1}{16 \cosh Ah\ \cosh Bk\ \cosh Cl} \left[\frac{\tanh Cl}{Cl} - \left(\frac{h}{l}\right)^2 \frac{\tanh Ah}{Ah} \right] \qquad (C\text{-}31)$$

It is noted that there are still some exact solutions, for example, $\tilde{\phi} = Cy - Bz$, $\tilde{\phi} = e^{2Ax}$, $\tilde{\phi} = e^{2Ax+2By+2Cz}$, $\tilde{\phi} = (Bx - Ay)e^{2Cz}$ etc. may be employed, however, the results are either linearly dependent to or the same as eq(C-29) thru (C-31). Thus, there are still 4 series summations EA, E^x_{22}, E^y_{22} and E^z_{22} needed to be evaluated numerically.

When the unsteady 3D convective transport equation is considered, a 28-point FA formula will be resulted by substituting eq(C-7) into eq(C-28a), i.e.,

$$\phi_P = \tilde{\phi}_P = \sum_1^{26} C_{nb} \left[\phi_{nb} + \frac{Ax_{nb} + By_{nb} + Cz_{nb}}{2(A^2 + B^2 + C^2)} g \right] \qquad (C\text{-}32)$$

where (x_{nb}, y_{nb}, z_{nb}) is the position of each neighboring node at Cartesian coordinate, and g contains the information from previous time step ϕ_P^{n-1}.

Substituting the expression of g of eq(C-6a) into eq(C-32), the 28-point FA formula for unsteady 3D convective transport equation becomes

$$\phi_P = \frac{1}{1 + \frac{R}{\tau} C_P} \left(\sum_{1}^{26} C_{nb} \phi_{nb} + \frac{R}{\tau} C_P \phi_P^{n-1} - C_P f_P \right) \qquad (C\text{-}33)$$

with

$$C_P = - \sum_{1}^{26} \frac{(Ax_{nb} + By_{nb} + Cz_{nb}) C_{nb}}{2(A^2 + B^2 + C^2)} \qquad (C\text{-}34a)$$

$$= \frac{1}{2(A^2+B^2+C^2)} \{ Ah \tanh Ah + Bk \tanh Bk + Cl \tanh Cl$$

$$- 16 \cosh Ah \cosh Bk \cosh Cl \left[(Ah)^2 (EA) + (Bk)^2 (EB) \right.$$

$$\left. + (Cl)^2 (EC) \right] \} \qquad (C\text{-}34b)$$

C-2 Finite Analytic Formulation of Unsteady 3D Convective Transport Equation in a Local Element of Nonuniform Grid Spacing

In previous Sec. C-1 formulation, the local analytic solution is derived in terms of the 26 boundary nodes which are equally spaced on the boundary of the local element of uniform grid spacing h, k and l in x, y and z direction respectively. For local element of nonuniform grid spacing h_E, h_W, h_N, h_S, h_T and h_B, a simple

generalization based on FA solution for uniform grid can be made to obtain the finite analytic algebraic equation. Details of the procedures, which is a generalization of two-dimensional case described in Appendix B, will be outlined in the following.

Consider the case $h_E < h_W$, $h_N < h_S$ and $h_T < h_B$ shown in Fig. 6(b) as an example, a smaller rectangular parallelepiped of width $2h_E$, depth $2h_N$, height $2h_T$ and point P located at the center can be drawn. The same exponential and linear interpolation function given in Appendix B will be employed to obtain the interpolated nodal values ϕ^*_{NWT}, ϕ^*_{WCT} etc. on smaller rectangular element in terms of those known nodal values on larger local element, so that the error introduced by interpolation will be minimized. i.e.,

$$\phi^*_{NWT} = (s-1)\phi_{NET} + \bar{s}\phi_{NWT} + (2-s-\bar{s})\phi_{NCT}$$

$$\phi^*_{WCT} = (s-1)\phi_{ECT} + \bar{s}\phi_{WCT} + (2-s-\bar{s})\phi_{TC}$$

$$\phi^*_{NWC} = (s-1)\phi_{NEC} + \bar{s}\phi_{NWC} + (2-s-\bar{s})\phi_{NC}$$

$$\phi^*_{WC} = (s-1)\phi_{EC} + \bar{s}\phi_{WC} + (2-s-\bar{s})\phi_{P}$$

$$\phi^*_{SET} = (t-1)\phi_{NET} + \bar{t}\phi_{SET} + (2-t-\bar{t})\phi_{ECT}$$

$$\phi^*_{SCT} = (t-1)\phi_{NCT} + \bar{t}\phi_{SCT} + (2-t-\bar{t})\phi_{TC}$$

$$\phi^*_{SEC} = (t-1)\phi_{NEC} + \bar{t}\phi_{SEC} + (2-t-\bar{t})\phi_{EC}$$

$$\phi^*_{SC} = (t-1)\phi_{NC} + \bar{t}\phi_{SC} + (2-t-\bar{t})\phi_{P}$$

$$\phi^*_{NEB} = (r-1)\phi_{NET} + \bar{r}\phi_{NEB} + (2-r-\bar{r})\phi_{NEC}$$

$$\phi^*_{NCB} = (r-1)\phi_{NCT} + \bar{r}\phi_{NCB} + (2-r-\bar{r})\phi_{NC}$$

$$\phi^*_{ECB} = (r-1)\phi_{ECT} + \bar{r}\phi_{ECB} + (2-r-\bar{r})\phi_{EC}$$

$$\phi^*_{BC} = (r-1)\phi_{TC} + \bar{r}\phi_{BC} + (2-r-\bar{r})\phi_{P}$$

$$\phi^*_{NWB} = (s-1)(r-1)\phi_{NET} + (s-1)\bar{r}\phi_{NEB} + (s-1)(2-r-\bar{r})\phi_{NEC}$$

$$+ \bar{s}(r-1)\phi_{NWT} + \bar{s}\bar{r}\phi_{NWB} + \bar{s}(2-r-\bar{r})\phi_{NWC} + (2-s-\bar{s})$$

$$(r-1)\phi_{NCT} + (2-s-\bar{s})\bar{r}\phi_{NCB} + (2-s-\bar{s})(2-r-\bar{r})\phi_{NC}$$

$$\phi^*_{WCB} = (s-1)(r-1)\phi_{ECT} + (s-1)\bar{r}\phi_{ECB} + (s-1)(2-r-\bar{r})\phi_{EC}$$

$$+ \bar{s}(r-1)\phi_{WCT} + \bar{s}\bar{r}\phi_{WCB} + \bar{s}(2-r-\bar{r})\phi_{WC} + (2-s-\bar{s})*$$

$$(r-1)\phi_{TC} + (2-s-\bar{s})\bar{r}\phi_{BC} + (2-s-\bar{s})(2-r-\bar{r})\phi_{P}$$

$$\phi^*_{SEB} = (t-1)(r-1)\phi_{NET} + (t-1)\bar{r}\phi_{NEB} + (t-1)(2-r-\bar{r})\phi_{NEC}$$

$$+ \bar{t}(r-1)\phi_{SET} + \bar{t}\bar{r}\phi_{SEB} + \bar{t}(2-r-\bar{r})\phi_{SEC} + (2-t-\bar{t})$$

$$(r-1)\phi_{ECT} + (2-t-\bar{t})\bar{r}\phi_{ECB} + (2-t-\bar{t})(2-r-\bar{r})\phi_{EC}$$

$$\phi^*_{SCB} = (t-1)(r-1)\phi_{NCT} + (t-1)\bar{r}\phi_{NCB} + (t-1)(2-r-\bar{r})\phi_{NC}$$

$$+ \bar{t}(r-1)\phi_{SCT} + \bar{t}\bar{r}\phi_{SCB} + \bar{t}(2-r-\bar{r})\phi_{SC} + (2-t-\bar{t})*$$

$$(r-1)\phi_{TC} + (2-t-\bar{t})\bar{r}\phi_{BC} + (2-t-\bar{t})(2-r-\bar{r})\phi_{P}$$

$$\phi^*_{SWT} = (s-1)(t-1)\phi_{NET} + (s-1)\bar{t}\phi_{SET} + (s-1)(2-t-\bar{t})\phi_{ECT}$$

$$+ \bar{s}(t-1)\phi_{NWT} + \bar{s}\bar{t}\phi_{SWT} + \bar{s}(2-t-\bar{t})\phi_{WCT} + (2-s-\bar{s})$$

$$(t-1)\phi_{NCT} + (2-s-\bar{s})\bar{t}\phi_{SCT} + (2-s-\bar{s})(2-t-\bar{t})\phi_{TC}$$

$$\phi^{*}_{SWC} = (s-1)(t-1)\phi_{NEC} + (s-1)\bar{t}\phi_{SEC} + (s-1)(2-t-\bar{t})\phi_{EC}$$

$$+ \bar{s}(t-1)\phi_{NWC} + \bar{s}\bar{t}\phi_{SWC} + \bar{s}(2-t-\bar{t})\phi_{WC} + (2-s-\bar{s})$$

$$(\bar{t}-1)\phi_{NC} + (2-s-\bar{s})\bar{t}\phi_{SC} + (2-s-\bar{s})(2-t-\bar{t})\phi_{P}$$

$$\phi^{*}_{SWB} = (s-1)(t-1)(r-1)\phi_{NET} + (s-1)(t-1)\bar{r}\phi_{NEB} + (s-1)$$

$$(t-1)(2-r-\bar{r})\phi_{NEC} + (s-1)(2-t-\bar{t})(r-1)\phi_{ECT} +$$

$$(2-s-\bar{s})(t-1)\bar{r}\phi_{NCB} + (s-1)(2-t-\bar{t})(2-r-\bar{r})\phi_{EC} +$$

$$(2-s-\bar{s})(t-1)(r-1)\phi_{NCT} + (2-s-\bar{s})(t-1)\bar{r}\phi_{NCB} +$$

$$+(2-s-\bar{s})(t-1)(2-r-\bar{r})\phi_{NC} + (2-s-\bar{s})(2-t-\bar{t})(r-1)*$$

$$\phi_{TC} + (2-s-\bar{s})(2-t-\bar{t})\bar{r}\phi_{BC} + (2-s-\bar{s})(2-t-\bar{t})(2-r-$$

$$\bar{r})\phi_{P} + (s-1)\bar{t}(r-1)\phi_{SET} + (s-1)\bar{t}\bar{r}\phi_{SEB} + (s-1)t*$$

$$(2-r-\bar{r})\phi_{SEC} + \bar{s}(t-1)(r-1)\phi_{NWT} + \bar{s}(t-1)\bar{r}\phi_{NWB} +$$

$$\bar{s}(t-1)(2-r-\bar{r})\phi_{NWC} + \bar{s}\bar{t}(r-1)\phi_{SWT} + \bar{s}\bar{t}\bar{r}\phi_{SWB} +$$

$$\bar{s}(2-t-\bar{t})(r-1)\phi_{WCT} + \bar{s}(2-t-\bar{t})\bar{r}\phi_{WCB} + \bar{s}(2-t-\bar{t})(2-$$

$$r-\bar{r})\phi_{WC} + (2-s-\bar{s})\bar{t}(r-1)\phi_{SCT} + (2-s-\bar{s})\bar{t}\bar{r}\phi_{SCB} +$$

$$(2-s-\bar{s})\bar{t}(2-r-\bar{r})\phi_{SC} + \bar{s}\bar{t}(2-r-\bar{r})\phi_{SWC} \qquad (C-35)$$

where

$$s = \frac{h_W(e^{2Ah_E} + e^{-2Ah_E} - 2)}{h_W(e^{2Ah_E}-1) + h_E(e^{-2Ah_W}-1)} \quad , \qquad \bar{s} = s\,\frac{h_E}{h_W}$$

$$t = \frac{h_S(e^{2Bh_N} + e^{-2Bh_N} - 2)}{h_S(e^{2Bh_N}-1) + h_N(e^{-2Bh_S}-1)} \quad , \qquad \bar{t} = t\,\frac{h_N}{h_S}$$

$$r = \frac{h_B(e^{2Ch_T} + e^{-2Ch_T} - 2)}{h_B(e^{2Ch_T}-1) + h_T(e^{-2Ch_B}-1)} \quad , \qquad \bar{r} = r\,\frac{h_T}{h_B}$$

After the interpolated nodal values on the smaller rectangular element are found, the 28-point FA formula (C-33) for unsteady 3D convective transport equation can then be applied to this smaller element.

$$\phi_P = \phi_P^* = \frac{1}{1 + \frac{R}{\tau}C_P}\left(\sum_1^{26} C_{nb}\phi_{nb}^* + \frac{R}{\tau}C_P\,\phi_P^{n-1} - C_P f_P\right) \qquad \text{(C-36)}$$

with ϕ^*= ϕ at nodal points NET, NEC, ECT, EC, NCT, NC, TC and P.

Substituting the interpolated nodal values in eq(C-35) into eq(C-36), a FA formula relating the interior nodal value ϕ_P to its neighboring nodal values at 26 boundary nodes which are unequally spaced on the larger rectangular element can then be obtained.

$$\phi_P = \frac{1}{G + \frac{R}{\tau} b_P} \left(\sum_{1}^{26} b_{nb}\phi_{nb} + \frac{R}{\tau} b_P \phi_P^{n-1} - b_P f_P \right) \quad (C\text{-}37)$$

where

$$G = 1 - (2-s-\bar{s})C_{WC} - (2-t-\bar{t})C_{SC} - (2-r-\bar{r})C_{BC} - (2-s-\bar{s})(2-t-\bar{t})C_{SWC} - (2-s-\bar{s})(2-r-\bar{r})C_{WCB} - (2-t-\bar{t})(2-r-\bar{r})C_{SCB} - (2-s-\bar{s})(2-t-\bar{t})(2-r-\bar{r})C_{SWB}$$

$$b_{NET} = C_{NET} + (s-1)C_{NWT} + (t-1)C_{SET} + (r-1)C_{NEB} + (s-1)(t-1)C_{SWT} + (s-1)(r-1)C_{NWB} + (t-1)(r-1)* C_{SEB} + (s-1)(t-1)(r-1)C_{SWB}$$

$$b_{ECT} = C_{ECT} + (s-1)C_{WCT} + (2-t-\bar{t})C_{SET} + (r-1)C_{ECB} + (s-1)(r-1)C_{WCB} + (2-t-\bar{t})(r-1)C_{SEB} + (s-1)(2-t-\bar{t})C_{SWT} + (s-1)(2-t-\bar{t})(r-1)C_{SWB}$$

$$b_{NCT} = C_{NCT} + (2-s-\bar{s})C_{NWT} + (t-1)C_{SCT} + (r-1)C_{NCB} + (2-s-\bar{s})(t-1)C_{SWT} + (2-s-\bar{s})(r-1)C_{NWB} + (t-1)(r-1)C_{SCB} + (2-s-\bar{s})(t-1)(r-1)C_{SWB}$$

$$b_{NEC} = C_{NEC} + (s-1)C_{NWC} + (t-1)C_{SEC} + (2-r-\bar{r})C_{NEB} + (s-1)(t-1)C_{SWC} + (s-1)(2-r-\bar{r})C_{NWB} + (t-1)(2-r-\bar{r})C_{SEB} + (s-1)(t-1)(2-r-\bar{r})C_{SWB}$$

$$b_{EC} = C_{EC} + (s-1)C_{WC} + (2-t-\bar{t})C_{SEC} + (2-r-\bar{r})C_{ECB} + (s-1)(2-t-\bar{t})C_{SWC} + (s-1)(2-r-\bar{r})C_{WCB} + (2-t-\bar{t})*$$

$$(2-r-\bar{r})C_{SEB} + (s-1)(2-t-\bar{t})(2-r-\bar{r})C_{SWB}$$

$$b_{NC} = C_{NC} + (t-1)C_{SC} + (2-s-\bar{s})C_{NWC} + (2-r-\bar{r})C_{NCB} + (2-s-\bar{s})(t-1)C_{SWC} + (t-1)(2-r-\bar{r})C_{SCB} + (2-s-\bar{s})*(2-r-\bar{r})C_{NWB} + (2-s-\bar{s})(t-1)(2-r-\bar{r})C_{SWB}$$

$$b_{TC} = C_{TC} + (r-1)C_{BC} + (2-s-\bar{s})C_{WCT} + (2-t-\bar{t})C_{SCT} + (2-s-\bar{s})(r-1)C_{WCB} + (2-t-\bar{t})(r-1)C_{SCB} + (2-s-\bar{s})*(2-t-\bar{t})C_{SWT} + (2-s-\bar{s})(2-t-\bar{t})(r-1)C_{SWB}$$

$$b_{NWT} = \bar{s}\,[\,C_{NWT} + (t-1)C_{SWT} + (r-1)C_{NWB} + (t-1)(r-1)*C_{SWB}]$$

$$b_{NWC} = \bar{s}\,[\,C_{NWC} + (t-1)C_{SWC} + (2-r-\bar{r})C_{NWB} + (t-1)(2-r-\bar{r})C_{SWB}]$$

$$b_{WCT} = \bar{s}\,[\,C_{WCT} + (2-t-\bar{t})C_{SWT} + (r-1)C_{WCB} + (2-t-\bar{t})(r-1)C_{SWB}]$$

$$b_{WC} = \bar{s}\,[\,C_{WC} + (2-t-\bar{t})C_{SWC} + (2-r-\bar{r})C_{WCB} + (2-t-\bar{t})*(2-r-\bar{r})C_{SWB}]$$

$$b_{SET} = \bar{t}\,[\,C_{SET} + (s-1)C_{SWT} + (r-1)C_{SEB} + (s-1)(r-1)*C_{SWB}]$$

$$b_{SEC} = \bar{t}\,[\,C_{SEC} + (s-1)C_{SWC} + (2-r-\bar{r})C_{SEB} + (s-1)(2-r-\bar{r})C_{SWB}]$$

$$b_{SCT} = \bar{t}\,[\,C_{SCT} + (2-s-\bar{s})C_{SWT} + (r-1)C_{SCB} + (2-s-\bar{s})(r-1)C_{SWB}]$$

$$b_{SC} = \bar{t}\,[\,C_{SC} + (2-s-\bar{s})C_{SWC} + (2-r-\bar{r})C_{SCB} + (2-s-\bar{s})*(2-r-\bar{r})C_{SWB}]$$

$$b_{NEB} = \bar{r}\,[\,C_{NEB} + (s-1)C_{NWB} + (t-1)C_{SEB} + (s-1)(t-1)*C_{SWB}]$$

$$b_{ECB} = \bar{r}\,[\,C_{ECB} + (s-1)C_{WCB} + (2-t-\bar{t})C_{SEB} + (s-1)(2-t-\bar{t})C_{SWB}]$$

$$b_{NCB} = \bar{r}\,[\,C_{NCB} + (2-s-\bar{s})C_{NWB} + (t-1)C_{SCB} + (2-s-\bar{s})*(t-1)C_{SWB}]$$

$$b_{BC} = \bar{r}\,[\,C_{BC} + (2-s-\bar{s})C_{WCB} + (2-t-\bar{t})C_{SCB} + (2-s-\bar{s})*(2-t-\bar{t})C_{SWB}]$$

$$b_{SEB} = \bar{t}\bar{r}\,[\,C_{SEB} + (s-1)C_{SWB}]$$

$$b_{SCB} = \bar{t}\bar{r}\,[\,C_{SCB} + (2-s-\bar{s})C_{SWB}]$$

$$b_{NWB} = \bar{s}\bar{r}\,[\,C_{NWB} + (t-1)C_{SWB}]$$

$$b_{WCB} = \bar{s}\bar{r}\,[\,C_{WCB} + (2-t-\bar{t})C_{SWB}]$$

$$b_{SWT} = \bar{s}\bar{t}\,[\,C_{SWT} + (r-1)C_{SWB}]$$

$$b_{SWC} = \bar{s}\bar{t}\,[\,C_{SWC} + (2-r-\bar{r})C_{SWB}]$$

$$b_{SWB} = \bar{s}\bar{t}\bar{r}C_{SWB}$$

$$b_{P} = C_{P}$$

Where the FA coefficients C_{nb} are given in eq(C-28) with $h = h_E$, $k = h_N$ and $l = h_T$.

For the cases $h_E > h_W$, $h_N > h_S$ etc., the finite analytic solution (C-37) can still be used by simply opposite the flow directions and rearrange the indices of nodal points. Details can be found from computer programs given in Appendix D.

APPENDIX D

COMPUTER PROGRAMS

D-1 Computer Program For Solving Unsteady Two-Dimensional Fluid Flow Problems Using Vorticity-Streamfunction Formulation

```
C     ************************************************************
C     DEVELOPMENT OF FINITE ANALYTIC METOD FOR UNSTEADY
C     TWO-DIMENSIONAL CONVECTIVE TRANSPORT EQUATIONS
C     ************************************************************
C
C     BY CHEN,HAMN-CHING
C     UNIVERSITY OF IOWA
C     ************************************************************
C     TEST PROBLEM :  DEVELOPMENT OF VORTEX STREET BEHIND A
C                     RECTANGULAR BLOCK
C     ************************************************************
C
C
$INSERT SYSCOM>ERRD.F
$INSERT SYSCOM>KEYS.F
$INSERT SYSCOM>A$KEYS
      IMPLICIT REAL*8(A-H,O-Z)
      COMMON/ABC1/PSIN(48,37),ZETAN(48,37,2)
      COMMON/ABC2/U(48,37),V(48,37),HX(48),HY(48)
      COMMON/ABC3/F(48,37),D
      COMMON/ABC4/PSINO(48,37),ZETANO(48,37)
      COMMON/COEFA/CMP(48,37),CNP(48,37),CPP(48,37)
      COMMON/COEFB/CMN(48,37),CNN(48,37),CPN(48,37)
      COMMON/COEFC/CMM(48,37),CNM(48,37),CPM(48,37)
      COMMON/EOEFA/EMP(48,37),ENP(48,37),EPP(48,37)
      COMMON/EOEFB/EMN(48,37),ENN(48,37),EPN(48,37)
      COMMON/EOEFC/EMM(48,37),ENM(48,37),EPM(48,37)
      COMMON/COEF1/CF(3,3)
      CALL SRCH$$(K$READ,'A500',4,7,TYPE,CODE)
      CALL SRCH$$(K$WRIT,'C500',4,2,TYPE,CODE)
      IXMAX=48
      IYMAX=37
      IXM1=IXMAX-1
      IYM1=IYMAX-1
```

```
      IXF=6
      IXR=7
      IYL=15
      IYU=23
      IXFM1=IXF-1
      IXFP1=IXF+1
      IXRM1=IXR-1
      IXRP1=IXR+1
      IYLM1=IYL-1
      IYLP1=IYL+1
      IYUM1=IYU-1
      IYUP1=IYU+1
      ITERP=50
      ITERZ=20
      IEND=100
      NM=2
      EPE=0.0001
      DIFFMP=0.00001
      DIFFMZ=0.00001
      RFP=1.6
      TAU=0.2
      RE=500.
      D=RE/TAU
C     DO 30 IX=2,4
C  30 HX(IX)=0.5
C     DO 31 IX=5,18
C  31 HX(IX)=0.25
C     DO 32 IX=19,28
C  32 HX(IX)=0.5
C     DO 33 IX=29,48
C  33 HX(IX)=0.8
C     DO 34 IY=2,3
C  34 HY(IY)=0.5
C     DO 35 IY=4,35
C  35 HY(IY)=0.125
C     DO 36 IY=36,37
C  36 HY(IY)=0.5
      READ(11,50)(HX(IX),IX=2,IXMAX)
      READ(11,50)(HY(IY),IY=2,IYMAX)
      WRITE(6,50)RE,TAU
      WRITE(6,50)(HX(IX),IX=2,IXMAX)
      WRITE(6,50)(HY(IY),IY=2,IYMAX)
   50 FORMAT(//5X,6F8.4)
C
C     ***********************************************************
C     INITIAL AND BOUNDARY CONDITIONS
C     ***********************************************************
C
      DO 100 IX=1,IXMAX
      DO 100 IY=1,IYMAX
```

```
      ZETAN(IX,IY,1)=0.
      ZETAN(IX,IY,2)=0.
      U(IX,IY)=0.
      V(IX,IY)=0.
      F(IX,IY)=0.
  100 PSIN(IX,IY)=0.
      DO 102 IX=1,IXMAX
      PSIN(IX,1)=-3.
      PSIN(IX,IYMAX)=3.
      U(IX,1)=1.
  102 U(IX,IYMAX)=1.
      DO 103 IY=1,IYMAX
  103 U(1,IY)=1.
      Y=-3.
      DO 104 IY=1,IYMAX
      Y=Y+HY(IY)
  104 PSIN(1,IY)=Y
      DO 122 IY=1,IYMAX
  122 READ(11,1350)(PSIN(IX,IY),IX=1,IXMAX)
      DO 123 IY=1,IYMAX
  123 READ(11,1350)(ZETAN(IX,IY,1),IX=1,IXMAX)
      DO 125 IX=1,IXMAX
      DO 125 IY=1,IYMAX
  125 ZETAN(IX,IY,2)=ZETAN(IX,IY,1)
C
C     ********************************************************
C     CALCULATION OF FINITE ANALYTIC COEFFICIENTS
C     FOR STREAMFUNCTION
C     ********************************************************
C
      DO 150 IX=2,IXM1
      DO 150 IY=2,IYM1
C     IF(IX.GE.IXF.AND.IX.LE.IXR.AND.IY.GE.IYL.AND.IY.LE.
C    1IYU) GO TO 150
      HE=HX(IX+1)
      HW=HX(IX)
      HN=HY(IY+1)
      HS=HY(IY)
      CALL COEFF2(0.,0.,HE,HW,HN,HS)
      EMM(IX,IY)=CF(1,1)
      EMN(IX,IY)=CF(1,2)
      EMP(IX,IY)=CF(1,3)
      ENM(IX,IY)=CF(2,1)
      ENN(IX,IY)=CF(2,2)
      ENP(IX,IY)=CF(2,3)
      EPM(IX,IY)=CF(3,1)
      EPN(IX,IY)=CF(3,2)
      EPP(IX,IY)=CF(3,3)
  150 CONTINUE
      MM=0
```

```
C
CCC   ************************************************************
CCC   RETURN POINT OF MARCHING PROCESS
CCC   ************************************************************
C
      DO 1200 IT=1,IEND
      MM=MM+1
C
CCC   ************************************************************
CCC   CALCULATION OF STREAMFUNCTIONS FOR FIELD POINTS
CCC   ************************************************************
C
      DO 155 ITER=1,ITERP
      DIFFM=0.
      DO 161 IX=2,IXM1
      IF(IX.GE.IXF.AND.IX.LE.IXR)GO TO 156
      CALL PSINA(2,IYM1,IX)
      GO TO 160
  156 CALL PSINA(2,IYLM1,IX)
      CALL PSINA(IYUP1,IYM1,IX)
  160 DO 161 IY=2,IYM1
      DIFF=DABS(PSIN(IX,IY)-PSINO(IX,IY))
      IF(DIFF.GT.DIFFM) DIFFM=DIFF
      PSIN(IX,IY)=PSINO(IX,IY)+RFP*(PSIN(IX,IY)-PSINO(IX,IY))
  161 PSINO(IX,IY)=PSIN(IX,IY)
      IF(DIFFM.LT.DIFFMP) GO TO 163
  155 CONTINUE
  163 WRITE(6,166)ITER,DIFFM
  166 FORMAT(5X,'NO. OF ITERATIONS FOR PSIN=',I5,5X,
     1'DMAXP=',E12.4)
      DO 157 IY=2,IYM1
  157 PSIN(IXMAX,IY)=PSIN(IXM1,IY)
C
CCC   ************************************************************
CCC   CALCULATION OF VELOCITY FIELDS
CCC   ************************************************************
C
      DO 175 IX=2,IXM1
      DO 175 IY=2,IYM1
      IF(IX.GE.IXF.AND.IX.LE.IXR.AND.IY.GE.IYL.AND.IY.LE.
     1IYU) GO TO 175
      HE=HX(IX+1)
      HW=HX(IX)
      HN=HY(IY+1)
      HS=HY(IY)
      U(IX,IY)=(HS*HS*(PSIN(IX,IY+1)-PSIN(IX,IY))-HN*HN*
     1(PSIN(IX,IY-1)-PSIN(IX,IY)))/HN/HS/(HN+HS)
      V(IX,IY)=(HE*HE*(PSIN(IX-1,IY)-PSIN(IX,IY))-HW*HW*
     1(PSIN(IX+1,IY)-PSIN(IX,IY)))/HE/HW/(HE+HW)
  175 CONTINUE
```

```
      DO 176 IY=2,IYM1
  176 U(IXMAX,IY)=U(IXM1,IY)
C
C     ********************************************************
C     CALCULATION OF FINITE ANALYTIC COEFFICIENTS
C      FOR VORTICITY
C     ********************************************************
C
      DO 200 IX=2,IXM1
      DO 200 IY=2,IYM1
C     IF(IX.GE.IXF.AND.IX.LE.IXR.AND.IY.GE.IYL.AND.IY.LE.
C    1IYU) GO TO 200
      AR=0.5*RE*U(IX,IY)
      BR=0.5*RE*V(IX,IY)
      HE=HX(IX+1)
      HW=HX(IX)
      HN=HY(IY+1)
      HS=HY(IY)
      CALL COEFF2(AR,BR,HE,HW,HN,HS)
      CMM(IX,IY)=CF(1,1)
      CMN(IX,IY)=CF(1,2)
      CMP(IX,IY)=CF(1,3)
      CNM(IX,IY)=CF(2,1)
      CNN(IX,IY)=CF(2,2)
      CNP(IX,IY)=CF(2,3)
      CPM(IX,IY)=CF(3,1)
      CPN(IX,IY)=CF(3,2)
      CPP(IX,IY)=CF(3,3)
  200 CONTINUE
C
C     ********************************************************
C     CALCULATION OF BOUNDARY VORTICITY
C     ********************************************************
C
      DO 250 IY=IYLP1,IYUM1
      ZETAN(IXF,IY,2)=0.-2.*PSIN(IXFM1,IY)/HX(IXF)/HX(IXF)
      ZETAN(IXR,IY,2)=0.-2.*PSIN(IXRP1,IY)/HX(IXRP1)
     1/HX(IXRP1)
  250 CONTINUE
      ZETAN(IXF,IYU,2)=0.-2.*PSIN(IXFM1,IYU)/HX(IXF)/HX(IXF)
     1-2.*PSIN(IXF,IYUP1)/HY(IYUP1)/HY(IYUP1)
      ZETAN(IXR,IYU,2)=0.-2.*PSIN(IXRP1,IYU)/HX(IXRP1)/
     1HX(IXRP1)-2.*PSIN(IXR,IYUP1)/HY(IYUP1)/HY(IYUP1)
      ZETAN(IXF,IYL,2)=0.-2.*PSIN(IXFM1,IYL)/HX(IXF)/HX(IXF)
     1-2.*PSIN(IXF,IYLM1)/HY(IYL)/HY(IYL)
      ZETAN(IXR,IYL,2)=0.-2.*PSIN(IXRP1,IYL)/HX(IXRP1)/
     1HX(IXRP1)-2.*PSIN(IXR,IYLM1)/HY(IYL)/HY(IYL)
C
C     ********************************************************
C     CALCULATION OF VORTICITY FOR FIELD POINTS USING
C     VORTICITY TRANSPORT EQUATION
```

```
C     ************************************************************
C
      DO 305 ITER=1,ITERZ
      DIFFM=0.
      DO 311 IX=2,IXM1
      IF(IX.GE.IXF.AND.IX.LE.IXR)GO TO 306
      CALL ZETANA(2,IYM1,IX)
      GO TO 310
  306 CALL ZETANA(2,IYLM1,IX)
      CALL ZETANA(IYUP1,IYM1,IX)
  310 DO 311 IY=2,IYM1
      DIFF=DABS(ZETAN(IX,IY,2)-ZETANO(IX,IY))
      IF(DIFF.GT.DIFFM) DIFFM=DIFF
  311 ZETANO(IX,IY)=ZETAN(IX,IY,2)
      IF(DIFFM.LT.DIFFMZ) GO TO 313
  305 CONTINUE
  313 WRITE(6,316) ITER,DIFFM
  316 FORMAT(5X,'NO. OF ITERATIONS FOR ZETAN=',I4,5X,
     1'DMAXZ=',E12.4)
      DO 307 IY=2,IYM1
  307 ZETAN(IXMAX,IY,2)=ZETAN(IXM1,IY,2)
      DO 500 IX=1,IXMAX
      DO 500 IY=1,IYMAX
  500 ZETAN(IX,IY,1)=ZETAN(IX,IY,2)
      IF(MM.LT.NM) GO TO 999
      MM=0
      WRITE(6,600)IT
  600 FORMAT(//5X,'NO. OF TIME STEPS =',I5)
      DO 700 IY=1,IYMAX
  700 WRITE(6,1350)(PSIN(IX,IY),IX=1,IXMAX)
      DO 800 IY=1,IYMAX
  800 WRITE(6,1350)(ZETAN(IX,IY,2),IX=1,IXMAX)
C
C     ************************************************************
C     CHECK THE CIRCULATION
C     ************************************************************
C
  999 CIRCUL=0.
      DO 1000 IX=2,IXMAX
      DO 1000 IY=2,IYMAX
      IF(IX.GT.IXF.AND.IX.LE.IXR.AND.IY.GT.IYL.AND.
     1IY.LE.IYU) GO TO 1000
      CIRCUL=CIRCUL+(ZETAN(IX,IY,2)+ZETAN(IX,IY-1,2)+ZETAN
     1(IX-1,IY,2)+ZETAN(IX-1,IY-1,2))*HX(IX)*HY(IY)/4.
 1000 CONTINUE
      WRITE(6,1001)CIRCUL
 1001 FORMAT(//5X,'CIRCUL=',E15.8)
 1200 CONTINUE
      DO 1101 IY=1,IYMAX
 1101 WRITE(6,1350)(U(IX,IY),IX=1,IXMAX)
      DO 1102 IY=1,IYMAX
```

```
 1102 WRITE(6,1350)(V(IX,IY),IX=1,IXMAX)
 1350 FORMAT(7F11.6)
      CALL EXIT
      END
C
C
C     ************************************************************
C     SUBROUTINE TRIDAG TO SOLVE ALGEBRAIC EQUATIONS
C     SIMULTANEOUSLY FOR EACH ROW OR COLUMN
C     ************************************************************
C
C
      SUBROUTINE TRIDAG(IF,L,A,B,C,D,V)
      IMPLICIT REAL*8(A-H,O-Z)
      DIMENSION A(48),B(48),C(48),D(48),V(48),BETA(48),
     1GAMMA(48)
      BETA(IF)=B(IF)
      GAMMA(IF)=D(IF)/BETA(IF)
      IFP1=IF+1
      DO 1 I=IFP1,L
      BETA(I)=B(I)-A(I)*C(I-1)/BETA(I-1)
    1 GAMMA(I)=(D(I)-A(I)*GAMMA(I-1))/BETA(I)
      V(L)=GAMMA(L)
      LAST=L-IF
      DO 2 K=1,LAST
      I=L-K
    2 V(I)=GAMMA(I)-C(I)*V(I+1)/BETA(I)
      RETURN
      END
C
C
C     ************************************************************
C     SUBROUTINE COEFF TO CALCULATE FINITE ANALYTIC
C     COEFFICIENTS
C     ************************************************************
C
C
      SUBROUTINE COEFF2(AR,BR,HE,HW,HN,HS)
      IMPLICIT REAL*8(A-H,O-Z)
      COMMON/COEF1/CF(3,3)
      PI=3.1415926535897930
      EPE=0.0001
      MAX=20
      JX=1
      JY=1
      IF(HE.LT.HW) GO TO 2
      JX=-1
      AR=-AR
    2 IF(HN.LT.HS) GO TO 3
      JY=-1
      BR=-BR
```

```
    3 IF(DABS(AR).LT.EPE)AR=DSIGN(EPE,AR)
      IF(DABS(BR).LT.EPE)BR=DSIGN(EPE,BR)
      HX=DMIN1(HE,HW)
      HY=DMIN1(HN,HS)
      HX1=DMAX1(HE,HW)
      HY1=DMAX1(HN,HS)
      AH=AR*HX
      BK=BR*HY
      AH1=AR*HX1
      BK1=BR*HY1
      AB2=AR*AR+BR*BR
      SEW=HX1*(DEXP(2.*AH)-1.)+HX*(DEXP(-2.*AH1)-1.)
      TNS=HY1*(DEXP(2.*BK)-1.)+HY*(DEXP(-2.*BK1)-1.)
      EPAH=DEXP(-AH)
      EPBK=DEXP(-BK)
      COSHA=0.5*EPAH+0.5/EPAH
      COSHB=0.5*EPBK+0.5/EPBK
      COTHA=(1.+EPAH*EPAH)/(1.-EPAH*EPAH)
      COTHB=(1.+EPBK*EPBK)/(1.-EPBK*EPBK)
C     IF(DABS(HE-HW).GT.EPE) MAX=30
C     IF(DABS(HN-HS).GT.EPE) MAX=30
      IF(HX.GT.HY)GO TO 20
      EX2=0.
      DO 10 I=1,MAX
      ZA=(I-0.5)*PI
      PWR=(-1.)**I*ZA
      AB=DEXP((AB2+ZA*ZA/HX/HX)**0.5*HY)
   10 EX2=EX2-2.*PWR/(AB+1./AB)/(AH*AH+ZA*ZA)**2
      EY2=EX2*HX*HX/HY/HY+(1./BK/COTHB-HX*HX/HY/HY/AH/COTHA)
     1/4./COSHA/COSHB
      GO TO 15
   20 EY2=0.
      DO 16 I=1,MAX
      ZA=(I-0.5)*PI
      PWR=(-1.)**I*ZA
      AB=DEXP((AB2+ZA*ZA/HY/HY)**0.5*HX)
   16 EY2=EY2-2.*PWR/(AB+1./AB)/(BK*BK+ZA*ZA)**2
      EX2=EY2*HY*HY/HX/HX+(1./AH/COTHA-HY*HY/HX/HX/BK/COTHB)
     1/4./COSHA/COSHB
   15 E=0.25/COSHA/COSHB-AH*COTHA*EX2-BK*COTHB*EY2
      EA=2.*AH*COSHA*COTHA*EX2
      EB=2.*BK*COSHB*COTHB*EY2
      CNN=(AH/COTHA+BK/COTHB-4.*COSHA*COSHB*(AH*AH*EX2
     ++BK*BK*EY2))/2./AB2
      CNW=E/EPAH*EPBK
      CNE=E*EPAH*EPBK
      CSW=E/EPAH/EPBK
      CSE=E*EPAH/EPBK
      CNC=EA*EPBK
      CSC=EA/EPBK
```

```
      CWC=EB/EPAH
      CEC=EB*EPAH
      S=(EPAH*EPAH+1./EPAH/EPAH-2.)*HX1/SEW
      S1=S-1.
      SB=S*HX/HX1
      SS=1.-S1-SB
      T=(EPBK*EPBK+1./EPBK/EPBK-2.)*HY1/TNS
      T1=T-1.
      TB=T*HY/HY1
      TS=1.-T1-TB
      CP=1.-SS*CWC-TS*CSC-SS*TS*CSW
      CF(2+JX,2+JY)=(CNE+S1*CNW+T1*CSE+S1*T1*CSW)/CP
      CF(2-JX,2+JY)=SB*(CNW+T1*CSW)/CP
      CF(2+JX,2-JY)=TB*(CSE+S1*CSW)/CP
      CF(2-JX,2-JY)=SB*TB*CSW/CP
      CF(2+JX,2)=(CEC+S1*CWC+TS*CSE+S1*TS*CSW)/CP
      CF(2-JX,2)=SB*(CWC+TS*CSW)/CP
      CF(2,2+JY)=(CNC+T1*CSC+SS*CNW+T1*SS*CSW)/CP
      CF(2,2-JY)=TB*(CSC+SS*CSW)/CP
      CF(2,2)=CNN/CP
      RETURN
      END
C
C     ***************************************************************
C     SUBROUTINE TO CALCULATE THE STREAMFUNCTION
C   ***************************************************************
C
      SUBROUTINE PSINA(IL,IU,IX)
      IMPLICIT REAL*8(A-H,O-Z)
      DIMENSION AA(48),BB(48),CC(48),DD(48),T(48)
      COMMON/ABC1/PSIN(48,37),ZETAN(48,37,2)
      COMMON/EOEFA/EMP(48,37),ENP(48,37),EPP(48,37)
      COMMON/EOEFB/EMN(48,37),ENN(48,37),EPN(48,37)
      COMMON/EOEFC/EMM(48,37),ENM(48,37),EPM(48,37)
      DO 160 IY=IL,IU
      AA(IY)=-ENM(IX,IY)
      BB(IY)=1.
      CC(IY)=-ENP(IX,IY)
  160 DD(IY)=EMM(IX,IY)*PSIN(IX-1,IY-1)+EMP(IX,IY)*
     1PSIN(IX-1,IY+1)+EMN(IX,IY)*PSIN(IX-1,IY)+EPN(IX,IY)*
     2PSIN(IX+1,IY)+EPM(IX,IY)*PSIN(IX+1,IY-1)+EPP(IX,IY)*
     3PSIN(IX+1,IY+1)+ENN(IX,IY)*ZETAN(IX,IY,1)
      DD(IL)=DD(IL)-AA(IL)*PSIN(IX,IL-1)
      DD(IU)=DD(IU)-CC(IU)*PSIN(IX,IU+1)
      CALL TRIDAG(IL,IU,AA,BB,CC,DD,T)
      DO 170 IY=IL,IU
  170 PSIN(IX,IY)=T(IY)
      RETURN
      END
C
C     ***************************************************************
```

```
C     SUBROUTINE TO CALCULATE THE VORTICITY
CC    ****************************************************
C
      SUBROUTINE ZETANA(IL,IU,IX)
      IMPLICIT REAL*8(A-H,O-Z)
      DIMENSION AA(48),BB(48),CC(48),DD(48),T(48)
      COMMON/ABC1/PSIN(48,37),ZETAN(48,37,2)
      COMMON/ABC2/U(48,37),V(48,37),HX(48),HY(48)
      COMMON/ABC3/F(48,37),D
      COMMON/COEFA/CMP(48,37),CNP(48,37),CPP(48,37)
      COMMON/COEFB/CMN(48,37),CNN(48,37),CPN(48,37)
      COMMON/COEFC/CMM(48,37),CNM(48,37),CPM(48,37)
      DO 320 IY=IL,IU
      UE=0.5*(U(IX+1,IY)+U(IX,IY))
      UW=0.5*(U(IX-1,IY)+U(IX,IY))
      VN=0.5*(V(IX,IY+1)+V(IX,IY))
      VS=0.5*(V(IX,IY-1)+V(IX,IY))
      EPAHE=DEXP(0.25*RE*UE*HX(IX+1))
      EPAHW=DEXP(0.25*RE*UW*HX(IX))
      EPBHN=DEXP(0.25*RE*VN*HY(IY+1))
      EPBHS=DEXP(0.25*RE*VS*HY(IY))
C
CC    ********************************************************
CC    CALCULATION OF HIGHER ORDER CORRECTION
CC    FOR CONVECTIVE TERM
CC    ********************************************************
C
      ZE=(ZETAN(IX,IY,2)*EPAHE+ZETAN(IX+1,IY,2)/EPAHE)
     1/(EPAHE+1./EPAHE)
      ZW=(ZETAN(IX-1,IY,2)*EPAHW+ZETAN(IX,IY,2)/EPAHW)
     1/(EPAHW+1./EPAHW)
      ZN=(ZETAN(IX,IY,2)*EPBHN+ZETAN(IX,IY+1,2)/EPBHN)
     1/(EPBHN+1./EPBHN).
      ZS=(ZETAN(IX,IY-1,2)*EPBHS+ZETAN(IX,IY,2)/EPBHS)
     1/(EPBHS+1./EPBHS)
      UE=(U(IX,IY)*EPAHE+U(IX+1,IY)/EPAHE)/(EPAHE+1./EPAHE)
      UW=(U(IX-1,IY)*EPAHW+U(IX,IY)/EPAHW)/(EPAHW+1./EPAHW)
      VN=(V(IX,IY)*EPBHN+V(IX,IY+1)/EPBHN)/(EPBHN+1./EPBHN)
      VS=(V(IX,IY-1)*EPBHS+V(IX,IY)/EPBHS)/(EPBHS+1./EPBHS)
      F(IX,IY)=2.*RE*(((UE-U(IX,IY))*ZE-(UW-U(IX,IY))*ZW)
     1/(HX(IX+1)+HX(IX))+((VN-V(IX,IY))*ZN
     2-(VS-V(IX,IY))*ZS)/(HY(IY+1)+HY(IY)))
      AA(IY)=-CNM(IX,IY)
      BB(IY)=1.+D*CNN(IX,IY)
      CC(IY)=-CNP(IX,IY)
  320 DD(IY)=-CPN(IX,IY)*ZETAN(IX+1,IY,2)+CMN(IX,IY)*ZETAN
     1(IX-1,IY,2)+CPP(IX,IY)*ZETAN(IX+1,IY+1,2)+CPM(IX,IY)
     2*ZETAN(IX+1,IY-1,2)+CMP(IX,IY)*ZETAN(IX-1,IY+1,2)
     3+CMM(IX,IY)*ZETAN(IX-1,IY-1,2)+CNN(IX,IY)
     4*(D*ZETAN(IX,IY,1)-F(IX,IY))
      DD(IL)=DD(IL)-AA(IL)*ZETAN(IX,IL-1,2)
```

```
      DD(IU)=DD(IU)-CC(IU)*ZETAN(IX,IU+1,2)
      CALL TRIDAG(IL,IU,AA,BB,CC,DD,T)
      DO 330 IY=IL,IU
  330 ZETAN(IX,IY,2)=T(IY)
      RETURN
      END
```

D-2 Computer Program For Solving Unsteady Three-Dimensional Fluid Flow Problems Using Primitive Variable Formulation

```
C
C     ********************************************************
C     DEVELOPMENT OF FINITE ANALYTIC METHOD FOR UNSTEADY
C     THREE-DIMENSIONAL CONVECTIVE TRANSPORT EQUATION
C     ********************************************************
C     BY CHEN, HAMN-CHING
C     THE UNIVERSITY OF IOWA
C     ********************************************************
C     TEST PROBLEM :  CUBIC CAVITY FLOW
C                     IN PRIMITIVE VARIABLE FORMULATION
C     ********************************************************
C
$INSERT SYSCOM>ERRD.F
$INSERT SYSCOM>KEYS.F
$INSERT SYSCOM>A$KEYS
      IMPLICIT REAL*8(A-H,O-Z)
      COMMON/ABC1/U(18,6,18),V(18,6,18),W(18,6,18)
      COMMON/ABC2/U1(18,6,18),V1(18,6,18),W1(18,6,18)
      COMMON/ABC3/U2(18,6,18),V2(18,6,18),W2(18,6,18)
      COMMON/ABC4/FX(18,6,18),FY(18,6,18),FZ(18,6,18)
      COMMON/ABC5/CU(18,6,18),CV(18,6,18),CW(18,6,18)
      COMMON/ABC6/DS(18,6,18),PR(18,6,18),PP(18,6,18)
      COMMON/ABC7/AA(18),BB(18),CC(18),DD(18),T(18)
     1,HX(18),HY(18),HZ(18)
      COMMON/ABC8/UX(18,6,18),VY(18,6,18),WZ(18,6,18)
      COMMON/AAA/CF(3,3,3)
      COMMON/UC1/UMPP(18,6,18),UNPP(18,6,18),UPPP(18,6,18)
      COMMON/UC2/UMNP(18,6,18),UNNP(18,6,18),UPNP(18,6,18)
      COMMON/UC3/UMMP(18,6,18),UNMP(18,6,18),UPMP(18,6,18)
      COMMON/UC4/UMPN(18,6,18),UNPN(18,6,18),UPPN(18,6,18)
      COMMON/UC5/UMNN(18,6,18),UNNN(18,6,18),UPNN(18,6,18)
      COMMON/UC6/UMMN(18,6,18),UNMN(18,6,18),UPMN(18,6,18)
      COMMON/UC7/UMPM(18,6,18),UNPM(18,6,18),UPPM(18,6,18)
      COMMON/UC8/UMNM(18,6,18),UNNM(18,6,18),UPNM(18,6,18)
      COMMON/UC9/UMMM(18,6,18),UNMM(18,6,18),UPMM(18,6,18)
      COMMON/VC1/VMPP(18,6,18),VNPP(18,6,18),VPPP(18,6,18)
      COMMON/VC2/VMNP(18,6,18),VNNP(18,6,18),VPNP(18,6,18)
```

```
      COMMON/VC3/VMMP(18,6,18),VNMP(18,6,18),VPMP(18,6,18)
      COMMON/VC4/VMPN(18,6,18),VNPN(18,6,18),VPPN(18,6,18)
      COMMON/VC5/VMNN(18,6,18),VNNN(18,6,18),VPNN(18,6,18)
      COMMON/VC6/VMMN(18,6,18),VNMN(18,6,18),VPMN(18,6,18)
      COMMON/VC7/VMPM(18,6,18),VNPM(18,6,18),VPPM(18,6,18)
      COMMON/VC8/VMNM(18,6,18),VNNM(18,6,18),VPNM(18,6,18)
      COMMON/VC9/VMMM(18,6,18),VNMM(18,6,18),VPMM(18,6,18)
      COMMON/WC1/WMPP(18,6,18),WNPP(18,6,18),WPPP(18,6,18)
      COMMON/WC2/WMNP(18,6,18),WNNP(18,6,18),WPNP(18,6,18)
      COMMON/WC3/WMMP(18,6,18),WNMP(18,6,18),WPMP(18,6,18)
      COMMON/WC4/WMPN(18,6,18),WNPN(18,6,18),WPPN(18,6,18)
      COMMON/WC5/WMNN(18,6,18),WNNN(18,6,18),WPNN(18,6,18)
      COMMON/WC6/WMMN(18,6,18),WNMN(18,6,18),WPMN(18,6,18)
      COMMON/WC7/WMPM(18,6,18),WNPM(18,6,18),WPPM(18,6,18)
      COMMON/WC8/WMNM(18,6,18),WNNM(18,6,18),WPNM(18,6,18)
      COMMON/WC9/WMMM(18,6,18),WNMM(18,6,18),WPMM(18,6,18)
      CALL SRCH$$(K$READ,'T400',4,7,TYPE,CODE)
      CALL SRCH$$(K$WRIT,'J400',4,2,TYPE,CODE)
      IXMAX=17
      IYMAX=5
      IZMAX=17
      IXP1=IXMAX+1
      IYP1=IYMAX+1
      IZP1=IZMAX+1
      IXM1=IXMAX-1
      IYM1=IYMAX-1
      IZM1=IZMAX-1
      IXMM=(IXMAX+1)/2
      ITERP=10
      ITERU=5
      ITERV=5
      ITERW=5
      IEND=10
      NM=5
      EPE=0.0001
      HX(1)=0.
      HX(IXP1)=0.
      HY(1)=0.
      HZ(1)=0.
      HZ(IZP1)=0.
      DO 41 IX=2,IXMAX
   41 HX(IX)=1./IXM1
      DO 42 IY=2,IYP1
   42 HY(IY)=0.5/IYM1
      DO 43 IZ=2,IZMAX
   43 HZ(IZ)=1./IZM1
      TAU=0.5
      RE=400.
      D=RE/TAU
      WRITE(6,50)RE,TAU
```

```
      WRITE(6,1350)(HX(IX),IX=1,IXP1)
      WRITE(6,1350)(HY(IY),IY=1,IYP1)
      WRITE(6,1350)(HZ(IZ),IZ=1,IZP1)
   50 FORMAT(//5X,6E12.4)
      DO 90 IX=1,IXP1
      DO 90 IY=1,IYP1
      DO 90 IZ=1,IZP1
      U(IX,IY,IZ)=0.
      V(IX,IY,IZ)=0.
      W(IX,IY,IZ)=0.
      DS(IX,IY,IZ)=0.
      PP(IX,IY,IZ)=0.
      CU(IX,IY,IZ)=0.
      CV(IX,IY,IZ)=0.
      CW(IX,IY,IZ)=0.
      UX(IX,IY,IZ)=0.
      VY(IX,IY,IZ)=0.
      WZ(IX,IY,IZ)=0.
   90 PR(IX,IY,IZ)=0.
C
C     ****************************************************
C     SPECIFY THE INITIAL CONDITION
C     ****************************************************
C
      DO 123 IX=1,IXMAX
      DO 123 IY=1,IYP1
  123 READ(11,1350)(U(IX,IY,IZ),IZ=1,IZP1)
      DO 124 IY=1,IYMAX
      DO 124 IZ=1,IZP1
  124 READ(11,1350)(V(IX,IY,IZ),IX=1,IXP1)
      DO 125 IZ=1,IZMAX
      DO 125 IY=1,IYP1
  125 READ(11,1350)(W(IX,IY,IZ),IX=1,IXP1)
      DO 126 IZ=1,IZP1
      DO 126 IY=1,IYP1
  126 READ(11,1350)(PR(IX,IY,IZ),IX=1,IXP1)
      DO 127 IX=1,IXP1
      DO 127 IY=1,IYP1
  127 U(IX,IY,1)=1.
      DO 25 IZ=1,IZP1
      DO 25 IY=1,IYP1
      DO 25 IX=1,IXP1
      U1(IX,IY,IZ)=U(IX,IY,IZ)
      U2(IX,IY,IZ)=U(IX,IY,IZ)
      V1(IX,IY,IZ)=V(IX,IY,IZ)
      V2(IX,IY,IZ)=V(IX,IY,IZ)
      W1(IX,IY,IZ)=W(IX,IY,IZ)
   25 W2(IX,IY,IZ)=W(IX,IY,IZ)
      MM=0
C
C
```

```
C     ******************************************************
CC    RETURN POINT FOR MARCHING PROCESS
C     ******************************************************
CC
C
      DO 1200 IT=1,IEND
      MM=MM+1
      DO 180 IX=2,IXMAX
      DO 180 IY=2,IYMAX
      DO 180 IZ=2,IZMAX
      HEE=0.5*(HX(IX+1)+HX(IX))
      HWW=0.5*(HX(IX-1)+HX(IX))
      HNN=0.5*(HY(IY+1)+HY(IY))
      HSS=0.5*(HY(IY-1)+HY(IY))
      HTT=0.5*(HZ(IZ+1)+HZ(IZ))
      HBB=0.5*(HZ(IZ-1)+HZ(IZ))
      AUX=0.5*RE*UX(IX,IY,IZ)
      BVY=0.5*RE*VY(IX,IY,IZ)
      CWZ=0.5*RE*WZ(IX,IY,IZ)
      IF(DABS(AUX).LT.EPE)AUX=DSIGN(EPE,AUX)
      IF(DABS(BVY).LT.EPE)BVY=DSIGN(EPE,BVY)
      IF(DABS(CWZ).LT.EPE)CWZ=DSIGN(EPE,CWZ)
      EPAUX=DEXP(0.5*AUX*HX(IX))
      EPBVY=DEXP(0.5*BVY*HY(IY))
      EPCWZ=DEXP(0.5*CWZ*HZ(IZ))
      UX(IX,IY,IZ)=(U(IX-1,IY,IZ)*EPAUX+U(IX,IY,IZ)/EPAUX)
     1/(EPAUX+1./EPAUX)
      VY(IX,IY,IZ)=(V(IX,IY-1,IZ)*EPBVY+V(IX,IY,IZ)/EPBVY)
     1/(EPBVY+1./EPBVY)
      WZ(IX,IY,IZ)=(W(IX,IY,IZ-1)*EPCWZ+W(IX,IY,IZ)/EPCWZ)
     1/(EPCWZ+1./EPCWZ)
  180 CONTINUE
C
C     ******************************************************
CC    CALCULATION OF FINITE ANALYTIC  COEFFICIENTS
CC    FOR VELOCITY U IN X-DIRECTION
C     ******************************************************
CC
C
      DO 200 IX=2,IXM1
      HE=HX(IX+1)
      HW=HX(IX)
      DO 200 IY=2,IYMAX
      HN=0.5*(HY(IY+1)+HY(IY))
      HS=0.5*(HY(IY-1)+HY(IY))
      DO 200 IZ=2,IZMAX
      HT=0.5*(HZ(IZ+1)+HZ(IZ))
      HB=0.5*(HZ(IZ-1)+HZ(IZ))
      VN=(HE*V(IX,IY,IZ)+HW*V(IX+1,IY,IZ))/(HE+HW)
      VS=(HE*V(IX,IY-1,IZ)+HW*V(IX+1,IY-1,IZ))/(HE+HW)
      WT=(HE*W(IX,IY,IZ)+HW*W(IX+1,IY,IZ))/(HE+HW)
      WB=(HE*W(IX,IY,IZ-1)+HW*W(IX+1,IY,IZ-1))/(HE+HW)
```

```
      UN=(HY(IY+1)*U(IX,IY,IZ)+HY(IY)*U(IX,IY+1,IZ))/2./HN
      US=(HY(IY-1)*U(IX,IY,IZ)+HY(IY)*U(IX,IY-1,IZ))/2./HS
      UT=(HZ(IZ+1)*U(IX,IY,IZ)+HZ(IZ)*U(IX,IY,IZ+1))/2./HT
      UB=(HZ(IZ-1)*U(IX,IY,IZ)+HZ(IZ)*U(IX,IY,IZ-1))/2./HB
      VX=0.5*(VN+VS)
      WX=0.5*(WT+WB)
      AR=0.5*RE*U(IX,IY,IZ)
      BR=0.5*RE*VX
      CR=0.5*RE*WX
      CALL COEFF3(AR,BR,CR,HE,HW,HN,HS,HT,HB)
      UMMM(IX,IY,IZ)=CF(1,1,1)
      UMMN(IX,IY,IZ)=CF(1,1,2)
      UMMP(IX,IY,IZ)=CF(1,1,3)
      UMNM(IX,IY,IZ)=CF(1,2,1)
      UMNN(IX IY,IZ)=CF(1,2,2)
      UMNP(IX,IY,IZ)=CF(1,2,3)
      UMPM(IX,IY,IZ)=CF(1,3,1)
      UMPN(IX,IY,IZ)=CF(1,3,2)
      UMPP(IX,IY,IZ)=CF(1,3,3)
      UNMM(IX,IY,IZ)=CF(2,1,1)
      UNMN(IX,IY,IZ)=CF(2,1,2)
      UNMP(IX,IY,IZ)=CF(2,1,3)
      UNNM(IX,IY,IZ)=CF(2,2,1)
      UNNN(IX,IY,IZ)=CF(2,2,2)
      UNNP(IX,IY,IZ)=CF(2,2,3)
      UNPM(IX,IY,IZ)=CF(2,3,1)
      UNPN(IX,IY,IZ)=CF(2,3,2)
      UNPP(IX,IY,IZ)=CF(2,3,3)
      UPMM(IX,IY,IZ)=CF(3,1,1)
      UPMN(IX,IY,IZ)=CF(3,1,2)
      UPMP(IX,IY,IZ)=CF(3,1,3)
      UPNM(IX,IY,IZ)=CF(3,2,1)
      UPNN(IX,IY,IZ)=CF(3,2,2)
      UPNP(IX,IY,IZ)=CF(3,2,3)
      UPPM(IX,IY,IZ)=CF(3,3,1)
      UPPN(IX,IY,IZ)=CF(3,3,2)
      UPPP(IX,IY,IZ)=CF(3,3,3)
      CU(IX,IY,IZ)=UNNN(IX,IY,IZ)*RE/(1.+D*UNNN(IX,IY,IZ))
     1/0.5/(HE+HW)
C
CC    **********************************************************
C     CALCULATION OF HIGHER ORDER CORRECTION TERM
C     FOR X MOMENTUM EQUATION
C     **********************************************************
C
      FX(IX,IY,IZ)=RE*(((UX(IX+1,IY,IZ)-U(IX,IY,IZ))*UX
     1(IX+1,IY,IZ)-(UX(IX,IY,IZ)-U(IX,IY,IZ))*UX(IX,IY,IZ))
     2/0.5/(HE+HW)+((VN-VX)*UN-(VS-VX)*US)/HY(IY)+((WT-WX)
     3*UT-(WB-WX)*UB)/HZ(IZ))
```

```
C
C     ************************************************************
C     DEFINE THE PSEUDOVELOCITY COMPONENT IN X-DIRECTION
C     ************************************************************
C
      UU1=0.
      CF(2,2,2)=0.
      DO 199 JX=1,3
      DO 199 JY=1,3
      DO 199 JZ=1,3
  199 UU1=UU1+CF(JX,JY,JZ)*U(IX+JX-2,IY+JY-2,IZ+JZ-2)
  200 U1(IX,IY,IZ)=(UU1+UNNN(IX,IY,IZ)*(D*U1(IX,IY,IZ)
     1-FX(IX,IY,IZ)))/(1.+D*UNNN(IX,IY,IZ))
C
C     ************************************************************
C     CALCULATION OF FINITE ANALYTIC COEFFICIENTS
C     FOR VELOCITY V IN Y-DIRECTION
C     ************************************************************
C
      DO 205 IY=2,IYM1
      HN=HY(IY+1)
      HS=HY(IY)
      DO 205 IX=2,IXMAX
      HE=0.5*(HX(IX+1)+HX(IX))
      HW=0.5*(HX(IX-1)+HX(IX))
      DO 205 IZ=2,IZMAX
      HT=0.5*(HZ(IZ+1)+HZ(IZ))
      HB=0.5*(HZ(IZ-1)+HZ(IZ))
      UE=(HN*U(IX,IY,IZ)+HS*U(IX,IY+1,IZ))/(HN+HS)
      UW=(HN*U(IX-1,IY,IZ)+HS*U(IX-1,IY+1,IZ))/(HN+HS)
      WT=(HN*W(IX,IY,IZ)+HS*W(IX,IY+1,IZ))/(HN+HS)
      WB=(HN*W(IX,IY,IZ-1)+HS*W(IX,IY+1,IZ-1))/(HN+HS)
      VE=(HX(IX+1)*V(IX,IY,IZ)+HX(IX)*V(IX+1,IY,IZ))/2./HE
      VW=(HX(IX-1)*V(IX,IY,IZ)+HX(IX)*V(IX-1,IY,IZ))/2./HW
      VT=(HZ(IZ+1)*V(IX,IY,IZ)+HZ(IZ)*V(IX,IY,IZ+1))/2./HT
      VB=(HZ(IZ-1)*V(IX,IY,IZ)+HZ(IZ)*V(IX,IY,IZ-1))/2./HB
      UY=0.5*(UE+UW)
      WY=0.5*(WT+WB)
      AR=0.5*RE*UY
      BR=0.5*RE*V(IX,IY,IZ)
      CR=0.5*RE*WY
      CALL COEFF3(AR,BR,CR,HE,HW,HN,HS,HT,HB)
      VMMM(IX,IY,IZ)=CF(1,1,1)
      VMMN(IX,IY,IZ)=CF(1,1,2)
      VMMP(IX,IY,IZ)=CF(1,1,3)
      VMNM(IX,IY,IZ)=CF(1,2,1)
      VMNN(IX,IY,IZ)=CF(1,2,2)
      VMNP(IX,IY,IZ)=CF(1,2,3)
      VMPM(IX,IY,IZ)=CF(1,3,1)
      VMPN(IX,IY,IZ)=CF(1,3,2)
```

```
      VMPP(IX,IY,IZ)=CF(1,3,3)
      VNMM(IX,IY,IZ)=CF(2,1,1)
      VNMN(IX,IY,IZ)=CF(2,1,2)
      VNMP(IX,IY,IZ)=CF(2,1,3)
      VNNM(IX,IY,IZ)=CF(2,2,1)
      VNNN(IX,IY,IZ)=CF(2,2,2)
      VNNP(IX,IY,IZ)=CF(2,2,3)
      VNPM(IX,IY,IZ)=CF(2,3,1)
      VNPN(IX,IY,IZ)=CF(2,3,2)
      VNPP(IX,IY,IZ)=CF(2,3,3)
      VPMM(IX,IY,IZ)=CF(3,1,1)
      VPMN(IX,IY,IZ)=CF(3,1,2)
      VPMP(IX,IY,IZ)=CF(3,1,3)
      VPNM(IX,IY,IZ)=CF(3,2,1)
      VPNN(IX,IY,IZ)=CF(3,2,2)
      VPNP(IX,IY,IZ)=CF(3,2,3)
      VPPM(IX,IY,IZ)=CF(3,3,1)
      VPPN(IX,IY,IZ)=CF(3,3,2)
      VPPP(IX,IY,IZ)=CF(3,3,3)
      CV(IX,IY,IZ)=VNNN(IX,IY,IZ)*RE/(1.+D*VNNN(IX,IY,IZ))
     1/0.5/(HN+HS)
C
C     ********************************************************
C     CALCULATION OF  HIGHER ORDER CORRECTION TERM
C     FOR Y MOMENTUM EQUATION
C     ********************************************************
C
      FY(IX,IY,IZ)=RE*(((UE-UY)*VE-(UW-UY)*VW)/HX(IX)
     1+((VY(IX,IY+1,IZ)-V(IX,IY,IZ))*VY(IX,IY+1,IZ)-
     2(VY(IX,IY,IZ)-V(IX,IY,IZ))*VY(IX,IY,IZ))/0.5/(HN+HS)
     3+((WT-WY)*VT-(WB-WY)*VB)/HZ(IZ))
C
C     ********************************************************
C     DEFINE THE PSEUDOVELOCITY COMPONENT IN Y-DIRECTION
C     ********************************************************
C
      VV1=0.
      CF(2,2,2)=0.
      DO 204 JX=1,3
      DO 204 JY=1,3
      DO 204 JZ=1,3
  204 VV1=VV1+CF(JX,JY,JZ)*V(IX+JX-2,IY+JY-2,IZ+JZ-2)
  205 V1(IX,IY,IZ)=(VV1+VNNN(IX,IY,IZ)*(D*V1(IX,IY,IZ)
     1-FY(IX,IY,IZ)))/(1.+D*VNNN(IX,IY,IZ))
C
C     ********************************************************
C     CALCULATION OF FINITE ANALYTIC COEFFICIENTS
C     FOR VELOCITY W IN Z-DIRECTION
C     ********************************************************
C
```

```
DO 210 IZ=2,IZM1
HT=HZ(IZ+1)
HB=HZ(IZ)
DO 210 IY=2,IYMAX
HN=0.5*(HY(IY+1)+HY(IY))
HS=0.5*(HY(IY-1)+HY(IY))
DO 210 IX=2,IXMAX
HE=0.5*(HX(IX+1)+HX(IX))
HW=0.5*(HX(IX-1)+HX(IX))
UE=(HT*U(IX,IY,IZ)+HB*U(IX,IY,IZ+1))/(HT+HB)
UW=(HT*U(IX-1,IY,IZ)+HB*U(IX-1,IY,IZ+1))/(HT+HB)
VN=(HT*V(IX,IY,IZ)+HB*V(IX,IY,IZ+1))/(HT+HB)
VS=(HT*V(IX,IY-1,IZ)+HB*V(IX,IY-1,IZ+1))/(HT+HB)
WE=(HX(IX+1)*W(IX,IY,IZ)+HX(IX)*W(IX+1,IY,IZ))/2./HE
WW=(HX(IX-1)*W(IX,IY,IZ)+HX(IX)*W(IX-1,IY,IZ))/2./HW
WN=(HY(IY+1)*W(IX,IY,IZ)+HY(IY)*W(IX,IY+1,IZ))/2./HN
WS=(HY(IY-1)*W(IX,IY,IZ)+HY(IY)*W(IX,IY-1,IZ))/2./HS
UZ=0.5*(UE+UW)
VZ=0.5*(VN+VS)
AR=0.5*RE*UZ
BR=0.5*RE*VZ
CR=0.5*RE*W(IX,IY,IZ)
CALL COEFF3(AR,BR,CR,HE,HW,HN,HS,HT,HB)
WMMM(IX,IY,IZ)=CF(1,1,1)
WMMN(IX,IY,IZ)=CF(1,1,2)
WMMP(IX,IY,IZ)=CF(1,1,3)
WMNM(IX,IY,IZ)=CF(1,2,1)
WMNN(IX,IY,IZ)=CF(1,2,2)
WMNP(IX,IY,IZ)=CF(1,2,3)
WMPM(IX,IY,IZ)=CF(1,3,1)
WMPN(IX,IY,IZ)=CF(1,3,2)
WMPP(IX,IY,IZ)=CF(1,3,3)
WNMM(IX,IY,IZ)=CF(2,1,1)
WNMN(IX,IY,IZ)=CF(2,1,2)
WNMP(IX,IY,IZ)=CF(2,1,3)
WNNM(IX,IY,IZ)=CF(2,2,1)
WNNN(IX,IY,IZ)=CF(2,2,2)
WNNP(IX,IY,IZ)=CF(2,2,3)
WNPM(IX,IY,IZ)=CF(2,3,1)
WNPN(IX,IY,IZ)=CF(2,3,2)
WNPP(IX,IY,IZ)=CF(2,3,3)
WPMM(IX,IY,IZ)=CF(3,1,1)
WPMN(IX,IY,IZ)=CF(3,1,2)
WPMP(IX,IY,IZ)=CF(3,1,3)
WPNM(IX,IY,IZ)=CF(3,2,1)
WPNN(IX,IY,IZ)=CF(3,2,2)
WPNP(IX,IY,IZ)=CF(3,2,3)
WPPM(IX,IY,IZ)=CF(3,3,1)
WPPN(IX,IY,IZ)=CF(3,3,2)
WPPP(IX,IY,IZ)=CF(3,3,3)
CW(IX,IY,IZ)=WNNN(IX,IY,IZ)*RE/(1.+D*WNNN(IX,IY,IZ))
```

```
     1/0.5/(HT+HB)
C
C     ******************************************************
C     CALCULATION OF HIGHER ORDER CORRECTION TERM
C     FOR Z MOMENTUM EQUATION
C     ******************************************************
C
      FZ(IX,IY,IZ)=RE*(((UE-UZ)*WE-(UW-UZ)*WW)/HX(IX)
     1+((VN-VZ)*WN-(VS-VZ)*WS)/HY(IY)+((WZ(IX,IY,IZ+1)
     2-W(IX,IY,IZ))*WZ(IX,IY,IZ+1)-(WZ(IX,IY,IZ)-W(IX,
     3IY,IZ))*WZ(IX,IY,IZ))/0.5/(HT+HB))
C
C     ******************************************************
C     DEFINE THE PSEUDOVELOCITY COMPONENT IN Z-DIRECTION
C     ******************************************************
C
      WW1=0.
      CF(2,2,2)=0.
      DO 209 JX=1,3
      DO 209 JY=1,3
      DO 209 JZ=1,3
  209 WW1=WW1+CF(JX,JY,JZ)*W(IX+JX-2,IY+JY-2,IZ+JZ-2)
  210 W1(IX,IY,IZ)=(WW1+WNNN(IX,IY,IZ)*(D*W1(IX,IY,IZ)
     1-FZ(IX,IY,IZ)))/(1.+D*WNNN(IX,IY,IZ))
C
C     ******************************************************
C     CALCULATION OF MASS SOURCE FOR PSEUDOVELOCITIES
C     ******************************************************
C
      DO 480 IX=2,IXMAX
      DO 480 IY=2,IYMAX
      DO 480 IZ=2,IZMAX
  480 DS(IX,IY,IZ)=(U1(IX,IY,IZ)-U1(IX-1,IY,IZ))/HX(IX)
     1+(V1(IX,IY,IZ)-V1(IX,IY-1,IZ))/HY(IY)+(W1(IX,IY,IZ)
     2-W1(IX,IY,IZ-1))/HZ(IZ)
C
C     ******************************************************
C     UPDATE THE PRESSURE FIELD THROUGH THE DEFINITION
C     OF PSEUDOVELOCITIES
C     ******************************************************
C
      DO 151 ITER=1,ITERP
      DO 155 IY=2,IYMAX
      DO 155 IZ=2,IZMAX
      DO 160 IX=2,IXMAX
      AA(IX)=-CU(IX-1,IY,IZ)/HX(IX)
      BB(IX)=(CU(IX,IY,IZ)+CU(IX-1,IY,IZ))/HX(IX)+
     1(CV(IX,IY,IZ)+CV(IX,IY-1,IZ))/HY(IY)+
     2(CW(IX,IY,IZ)+CW(IX,IY,IZ-1))/HZ(IZ)
      CC(IX)=-CU(IX,IY,IZ)/HX(IX)
```

```
  160 DD(IX)=(CV(IX,IY-1,IZ)*PR(IX,IY-1,IZ)+CV(IX,IY,IZ)
     1*PR(IX,IY+1,IZ))/HY(IY)+(CW(IX,IY,IZ-1)*PR(IX,IY,IZ-1)
     2+CW(IX,IY,IZ)*PR(IX,IY,IZ+1))/HZ(IZ)-DS(IX,IY,IZ)
      CALL TRIDAG(2,IXMAX,AA,BB,CC,DD,T)
      DO 171 IX=2,IXMAX
  171 PR(IX,IY,IZ)=T(IX)
  155 CONTINUE
      PRO=PR(IXMM,IYMAX,IZMAX)
      DO 159 IX=2,IXMAX
      DO 159 IY=2,IYMAX
      DO 159 IZ=2,IZMAX
  159 PR(IX,IY,IZ)=PR(IX,IY,IZ)-PRO
  151 CONTINUE
C
C     ************************************************************
C     CALCULATION OF PRESSURE BOUNDARY CONDITIONS :
C     FOR CONTOUR PLOT OF PRESSURE FIELD
C     ************************************************************
C
      DO 156 IX=2,IXMAX
      DO 156 IY=2,IYMAX
      PR(IX,IY,1)=(9.*PR(IX,IY,2)-PR(IX,IY,3))/8.-(8.*
     1W(IX,IY,2)-W(IX,IY,3))*3./16./RE/HZ(2)
  156 PR(IX,IY,IZP1)=(9.*PR(IX,IY,IZMAX)-PR(IX,IY,IZM1))/8.+
     1(8.*W(IX,IY,IZM1)-W(IX,IY,IZM1-1))*3./16./RE/HZ(IZMAX)
      DO 157 IY=2,IYMAX
      DO 157 IZ=2,IZMAX
      PR(1,IY,IZ)=(9.*PR(2,IY,IZ)-PR(3,IY,IZ))/8.-(8.*U(2,IY,
     1IZ)-U(3,IY,IZ))*3./16./RE/HX(2)
  157 PR(IXP1,IY,IZ)=(9.*PR(IXMAX,IY,IZ)-PR(IXM1,IY,IZ))/8.+
     1(8.*U(IXM1,IY,IZ)-U(IXM1-1,IY,IZ))*3./16./RE/HX(IXMAX)
      DO 158 IX=2,IXMAX
      DO 158 IZ=2,IZMAX
      PR(IX,1,IZ)=(9.*PR(IX,2,IZ)-PR(IX,3,IZ))/8.-(8.*V(IX,2,
     1IZ)-V(IX,3,IZ))*3./16./RE/HY(2)
  158 PR(IX,IYP1,IZ)=PR(IX,IYMAX,IZ)
C
C     ************************************************************
C     CALCULATE THE SOURCE TERMS OF MOMENTUM EUATIONS
C     USING UPDATED PRESSURE GRADIENT TERMS
C     ************************************************************
C
      DO 301 IX=2,IXM1
      DO 301 IY=2,IYMAX
      DO 301 IZ=2,IZMAX
  301 FX(IX,IY,IZ)=FX(IX,IY,IZ)+RE*(PR(IX+1,IY,IZ)-PR(IX,IY,
     1IZ))/0.5/(HX(IX)+HX(IX+1))
      DO 302 IY=2,IYM1
      DO 302 IX=2,IXMAX
      DO 302 IZ=2,IZMAX
  302 FY(IX,IY,IZ)=FY(IX,IY,IZ)+RE*(PR(IX,IY+1,IZ)-PR(IX,IY,
```

```
     1IZ))/0.5/(HY(IY)+HY(IY+1))
      DO 303 IZ=2,IZM1
      DO 303 IX=2,IXMAX
      DO 303 IY=2,IYMAX
  303 FZ(IX,IY,IZ)=FZ(IX,IY,IZ)+RE*(PR(IX,IY,IZ+1)-PR(IX,IY,
     1IZ))/0.5/(HZ(IZ)+HZ(IZ+1))
C
C     ****************************************************
C     CALCULATION OF VELOCITY FIELD USING THE 28-POINT
C     FA FORMULA FOR UNSTEADY THREE-DIMENSIONAL
C     CONVECTIVE TRANSPORT EQUATION
C     ****************************************************
C
      DO 305 ITER=1,ITERU
      DO 330 IY=2,IYMAX
      DO 330 IZ=2,IZMAX
      DO 320 IX=2,IXM1
      AA(IX)=-UMNN(IX,IY,IZ)
      BB(IX)=1.+D*UNNN(IX,IY,IZ)
      CC(IX)=-UPNN(IX,IY,IZ)
      DDIX=UMPP(IX,IY,IZ)*U2(IX-1,IY+1,IZ+1)+UNPP(IX,IY,IZ)
     1*U2(IX,IY+1,IZ+1)+UPPP(IX,IY,IZ)*U2(IX+1,IY+1,IZ+1)
     2+UMNP(IX,IY,IZ)*U2(IX-1,IY,IZ+1)+UNNP(IX,IY,IZ)*U2
     3(IX,IY,IZ+1)+UPNP(IX,IY,IZ)*U2(IX+1,IY,IZ+1)+UMMP
     4(IX,IY,IZ)*U2(IX-1,IY-1,IZ+1)+UNMP(IX,IY,IZ)*U2(IX,
     5IY-1,IZ+1)+UPMP(IX,IY,IZ)*U2(IX+1,IY-1,IZ+1)+UMPN(IX,
     6IY,IZ)*U2(IX-1,IY+1,IZ)+UNPN(IX,IY,IZ)*U2(IX,IY+1,
     7IZ)+UPPN(IX,IY,IZ)*U2(IX+1,IY,IZ)
  320 DD(IX)=DDIX+UMMN(IX,IY,IZ)*U2(IX-1,IY-1,IZ)+UNMN
     1(IX,IY,IZ)*U2(IX,IY-1,IZ)+UPMN(IX,IY,IZ)*U2(IX+1,
     2IY-1,IZ)+UMPM(IX,IY,IZ)*U2(IX-1,IY+1,IZ-1)+UNPM
     3(IX,IY,IZ)*U2(IX,IY+1,IZ-1)+UPPM(IX,IY,IZ)*U(IX+1,
     4IY+1,IZ)+UMNM(IX,IY,IZ)*U2(IX-1,IY,IZ-1)+UNNM(IX,
     5IY,IZ)*U2(IX,IY,IZ-1)+UPNM(IX,IY,IZ)*U2(IX+1,IY,
     6IZ-1)+UMMM(IX,IY,IZ)*U2(IX-1,IY-1,IZ-1)+UNMM(IX,
     7IY,IZ)*U2(IX,IY-1,IZ-1)+UPMM(IX,IY,IZ)*U(IX+1,IY-1,
     8IZ-1)+UNNN(IX,IY,IZ)*(D*U(IX,IY,IZ)-FX(IX,IY,IZ))
      DD(2)=DD(2)-AA(2)*U2(1,IY,IZ)
      DD(IXM1)=DD(IXM1)-CC(IXM1)*U2(IXMAX,IY,IZ)
      CALL TRIDAG(2,IXM1,AA,BB,CC,DD,T)
      DO 330 IX=2,IXM1
  330 U2(IX,IY,IZ)=T(IX)
      DO 306 IX=1,IXMAX
      DO 306 IZ=1,IZP1
  306 U2(IX,IYP1,IZ)=U2(IX,IYMAX,IZ)
  305 CONTINUE
      DO 405 ITER=1,ITERV
      DO 430 IX=2,IXMAX
      DO 430 IZ=2,IZMAX
      DO 420 IY=2,IYM1
      AA(IY)=-VNMN(IX,IY,IZ)
```

```
      BB(IY)=1.+D*VNNN(IX,IY,IZ)
      CC(IY)=-VNPN(IX,IY,IZ)
      DDIY=VMPP(IX,IY,IZ)*V2(IX-1,IY+1,IZ+1)+VNPP(IX,IY,IZ)
     1*V2(IX,IY+1,IZ+1)+VPPP(IX,IY,IZ)*V2(IX+1,IY+1,IZ+1)
     2+VMNP(IX,IY,IZ)*V2(IX-1,IY,IZ+1)+VNNP(IX,IY,IZ)*V2(IX,
     3IY,IZ+1)+VPNP(IX,IY,IZ)*V2(IX+1,IY,IZ+1)+VMMP(IX,IY,IZ)
     4*V2(IX-1,IY-1,IZ+1)+VNMP(IX,IY,IZ)*V2(IX,IY-1,IZ+1)
     5+VPMP(IX,IY,IZ)*V2(IX+1,IY-1,IZ+1)+VMPN(IX,IY,IZ)
     6*V2(IX-1,IY+1,IZ)+VPNN(IX,IY,IZ)*V2(IX+1,IY,IZ)+VPPN
     7(IX,IY,IZ)*V2(IX+1,IY+1,IZ)
  420 DD(IY)=DDIY+VMMN(IX,IY,IZ)*V2(IX-1,IY-1,IZ)+VMNN
     1(IX,IY,IZ)*V2(IX-1,IY,IZ)+VPMN(IX,IY,IZ)*V2(IX+1,
     2IY-1,IZ)+VMPM(IX,IY,IZ)*V2(IX-1,IY+1,IZ-1)+VNPM
     3(IX,IY,IZ)*V2(IX,IY+1,IZ-1)+VPPM(IX,IY,IZ)*V2
     4(IX+1,IY+1,IZ-1)+VMNM(IX,IY,IZ)*V2(IX-1,IY,IZ-1)
     5+VNNM(IX,IY,IZ)*V2(IX,IY,IZ-1)+VPNM(IX,IY,IZ)*V2
     6(IX+1,IY,IZ-1)+VMMM(IX,IY,IZ)*V2(IX-1,IY-1,IZ-1)+
     7VNMM(IX,IY,IZ)*V2(IX,IY-1,IZ-1)+VPMM(IX,IY,IZ)
     8*V2(IX+1,IY-1,IZ-1)+VNNN(IX,IY,IZ)*(D*V(IX,IY,IZ)
     9-FY(IX,IY,IZ))
      DD(2)=DD(2)-AA(2)*V2(IX,1,IZ)
      DD(IYM1)=DD(IYM1)-CC(IYM1)*V2(IX,IYMAX,IZ)
      CALL TRIDAG(2,IYM1,AA,BB,CC,DD,T)
      DO 430 IY=2,IYM1
  430 V2(IX,IY,IZ)=T(IY)
  405 CONTINUE
      DO 505 ITER=1,ITERW
      DO 530 IX=2,IXMAX
      DO 530 IY=2,IYMAX
      DO 520 IZ=2,IZM1
      AA(IZ)=-WNNM(IX,IY,IZ)
      BB(IZ)=1.+D*WNNN(IX,IY,IZ)
      CC(IZ)=-WNNP(IX,IY,IZ)
      DDIZ=WMPP(IX,IY,IZ)*W2(IX-1,IY+1,IZ+1)+WNPP(IX,IY,IZ)
     1*W2(IX,IY+1,IZ+1)+WPPP(IX,IY,IZ)*W2(IX+1,IY+1,IZ+1)
     2+WMNP(IX,IY,IZ)*W2(IX-1,IY,IZ+1)+WPNN(IX,IY,IZ)*W2
     3(IX+1,IY,IZ)+WPNP(IX,IY,IZ)*W2(IX+1,IY,IZ+1)+WMMP
     4(IX,IY,IZ)*W2(IX-1,IY-1,IZ+1)+WNMP(IX,IY,IZ)*W2
     5(IX,IY-1,IZ+1)+WPMP(IX,IY,IZ)*W2(IX+1,IY-1,IZ+1)
     6+WMPN(IX,IY,IZ)*W2(IX-1,IY+1,IZ)+WNPN(IX,IY,IZ)*W2
     7(IX,IY+1,IZ)+WPPN(IX,IY,IZ)*W2(IX+1,IY+1,IZ)
  520 DD(IZ)=DDIZ+WMMN(IX,IY,IZ)*W2(IX-1,IY-1,IZ)+WNMN
     1(IX,IY,IZ)*W2(IX,IY-1,IZ)+WPMN(IX,IY,IZ)*W2(IX+1,
     2IY-1,IZ)+WMPM(IX,IY,IZ)*W2(IX-1,IY+1,IZ-1)+WNPM
     3(IX,IY,IZ)*W2(IX,IY+1,IZ-1)+WPPM(IX,IY,IZ)*W2
     4(IX+1,IY+1,IZ-1)+WMNM(IX,IY,IZ)*W2(IX-1,IY,IZ-1)
     5+WMNN(IX,IY,IZ)*W2(IX-1,IY,IZ)+WPNM(IX,IY,IZ)*
     6W2(IX+1,IY,IZ-1)+WMMM(IX,IY,IZ)*W2(IX-1,IY-1,IZ-1)
     7+WNMM(IX,IY,IZ)*W2(IX,IY-1,IZ-1)+WPMM(IX,IY,IZ)
     8*W2(IX+1,IY-1,IZ-1)+WNNN(IX,IY,IZ)*(D*W(IX,IY,IZ)
     9-FZ(IX,IY,IZ))
```

```
      DD(2)=DD(2)-AA(2)*W2(IX,IY,1)
      DD(IZM1)=DD(IZM1)-CC(IZM1)*W2(IX,IY,IZMAX)
      CALL TRIDAG(2,IZM1,AA,BB,CC,DD,T)
      DO 530 IZ=2,IZM1
  530 W2(IX,IY,IZ)=T(IZ)
      DO 506 IZ=1,IZMAX
      DO 506 IX=1,IXP1
  506 W2(IX,IYP1,IZ)=W2(IX,IYMAX,IZ)
  505 CONTINUE
C
C     ******************************************************
C     CHECK THE CONSERVATION OF MASS
C     ******************************************************
C
      DO 680 IX=2,IXMAX
      DO 680 IY=2,IYMAX
      DO 680 IZ=2,IZMAX
  680 DS(IX,IY,IZ)=(U2(IX,IY,IZ)-U2(IX-1,IY,IZ))/HX(IX)
     1+(V2(IX,IY,IZ)-V2(IX,IY-1,IZ))/HY(IY)+(W2(IX,IY,IZ)
     2-W2(IX,IY,IZ-1))/HZ(IZ)
C
C     ************************************************************
C     CALCULATION OF PRESSURE-CORRECTION IN TERMS OF
C     MASS SOURCE TERM
C     ************************************************************
C
      DO 651 ITER=1,ITERP
      DO 655 IY=2,IYMAX
      DO 655 IZ=2,IZMAX
      DO 660 IX=2,IXMAX
      AA(IX)=-CU(IX-1,IY,IZ)/HX(IX)
      BB(IX)=(CU(IX,IY,IZ)+CU(IX-1,IY,IZ))/HX(IX)+(CV
     1(IX,IY,IZ)+CV(IX,IY-1,IZ))/HY(IY)+(CW(IX,IY,IZ)
     2+CW(IX,IY,IZ-1))/HZ(IZ)
      CC(IX)=-CU(IX,IY,IZ)/HX(IX)
  660 DD(IX)=(CV(IX,IY-1,IZ)*PP(IX,IY-1,IZ)+CV(IX,IY,IZ)*
     1PP(IX,IY+1,IZ))/HY(IY)+(CW(IX,IY,IZ-1)*PP(IX,IY,IZ-1)
     2+CW(IX,IY,IZ)*PP(IX,IY,IZ+1))/HZ(IZ)-DS(IX,IY,IZ)
      CALL TRIDAG(2,IXMAX,AA,BB,CC,DD,T)
      DO 671 IX=2,IXMAX
  671 PP(IX,IY,IZ)=T(IX)
  655 CONTINUE
      PPO=PP(IXMM,IYMAX,IZMAX)
      DO 659 IX=2,IXMAX
      DO 659 IY=2,IYMAX
      DO 659 IZ=2,IZMAX
  659 PP(IX,IY,IZ)=PP(IX,IY,IZ)-PPO
  651 CONTINUE
C
C     ************************************************************
```

```
C     CORRECT THE VELOCITY FIELD USING THE
C     VELOCITY-CORRECTION FORMULA
C     ***************************************************
C
      DO 700 IX=1,IXMAX
      DO 700 IY=2,IYMAX
      DO 700 IZ=2,IZMAX
      U1(IX,IY,IZ)=U(IX,IY,IZ)
  700 U(IX,IY,IZ)=U2(IX,IY,IZ)-CU(IX,IY,IZ)*
     1(PP(IX+1,IY,IZ)-PP(IX,IY,IZ))
      DO 701 IX=1,IXMAX
      DO 701 IZ=1,IZP1
  701 U(IX,IYP1,IZ)=U(IX,IYMAX,IZ)
      DO 750 IY=1,IYMAX
      DO 750 IX=2,IXMAX
      DO 750 IZ=2,IZMAX
      V1(IX,IY,IZ)=V(IX,IY,IZ)
  750 V(IX,IY,IZ)=V2(IX,IY,IZ)-CV(IX,IY,IZ)*
     1(PP(IX,IY+1,IZ)-PP(IX,IY,IZ))
      DO 800 IX=2,IXMAX
      DO 800 IY=2,IYMAX
      DO 800 IZ=1,IZMAX
      W1(IX,IY,IZ)=W(IX,IY,IZ)
  800 W(IX,IY,IZ)=W2(IX,IY,IZ)-CW(IX,IY,IZ)*
     1(PP(IX,IY,IZ+1)-PP(IX,IY,IZ))
      DO 801 IZ=1,IZMAX
      DO 801 IX=1,IXP1
  801 W(IX,IYP1,IZ)=W(IX,IYMAX,IZ)
      IF(MM.LT.NM) GO TO 1200
      MM=0
      WRITE(6,1600)IT
 1600 FORMAT(//5X,'NO. OF TIME STEPS =',I5)
      WRITE(6,2101)
 2101 FORMAT(///5X,'VELOCITY IN X-DIRECTION U=')
      DO 1101 IX=1,IXMAX
      DO 1101 IY=1,IYP1
 1101 WRITE(6,1350)(U(IX,IY,IZ),IZ=1,IZP1)
      WRITE(6,2102)
 2102 FORMAT(///5X,'VELOCITY IN Y-DIRECTION V=')
      DO 1102 IY=1,IYMAX
      DO 1102 IZ=1,IZP1
 1102 WRITE(6,1350)(V(IX,IY,IZ),IX=1,IXP1)
      WRITE(6,2103)
 2103 FORMAT(///5X,'VELOCITY IN Z-DIRECTION  W=')
      DO 1103 IZ=1,IZMAX
      DO 1103 IY=1,IYP1
 1103 WRITE(6,1350)(W(IX,IY,IZ),IX=1,IXP1)
      WRITE(6,2104)
 2104 FORMAT(///5X,'PRESSURE FIELD PR=')
      DO 1104 IZ=1,IZP1
      DO 1104 IY=1,IYP1
```

```
 1104 WRITE(6,1350)(PR(IX,IY,IZ),IX=1,IXP1)
      WRITE(6,2105)
 2105 FORMAT(///5X,'CONSERVATION OF MASS ')
      DO 1105 IZ=2,IZMAX
      DO 1105 IY=2,IYMAX
 1105 WRITE(6,1350)(DS(IX,IY,IZ),IX=2,IXMAX)
 1350 FORMAT(7F11.6)
 1200 CONTINUE
      CALL EXIT
      END
C
C
C
C     ****************************************************
C     SUBROUTINE TRIDAG TO SOLVE THE SYSTEM OF
C     ALGEBRAIC EQUATIONS
C     ****************************************************
C
C
C
      SUBROUTINE TRIDAG(IF,L,A,B,C,D,V)
      IMPLICIT REAL*8(A-H,O-Z)
      DIMENSION A(18),B(18),C(18),D(18),V(18),BETA(18),
     1GAMMA(18)
      BETA(IF)=B(IF)
      GAMMA(IF)=D(IF)/BETA(IF)
      IFP1=IF+1
      DO 1 I=IFP1,L
      BETA(I)=B(I)-A(I)*C(I-1)/BETA(I-1)
    1 GAMMA(I)=(D(I)-A(I)*GAMMA(I-1))/BETA(I)
      V(L)=GAMMA(L)
      LAST=L-IF
      DO 2 K=1,LAST
      I=L-K
    2 V(I)=GAMMA(I)-C(I)*V(I+1)/BETA(I)
      RETURN
      END
C
C
C
C     ****************************************************
C     SUBROUTINE COEFF3 TO CALCULATE THE FINITE ANALYTIC
C     COEFFICIENTS FOR GENERAL NONUNIFORM GRID LOCAL
C     ELEMENT
C     ****************************************************
C
C
C
      SUBROUTINE COEFF3(AR,BR,CR,HE,HW,HN,HS,HT,HB)
      IMPLICIT REAL*8(A-H,O-Z)
      COMMON/AAA/CF(3,3,3)
```

```
      PI=3.141592653589793D0
      EPE=0.0001
      MAX=5
      JX=1
      JY=1
      JZ=1
      IF(HE.LT.HW) GO TO 2
      JX=-1
      AR=-AR
    2 IF(HN.LT.HS) GO TO 3
      JY=-1
      BR=-BR
    3 IF(HT.LT.HB) GO TO 4
      JZ=-1
      CR=-CR
    4 IF(DABS(AR).LT.EPE)AR=DSIGN(EPE,AR)
      IF(DABS(BR).LT.EPE)BR=DSIGN(EPE,BR)
      IF(DABS(CR).LT.EPE)CR=DSIGN(EPE,CR)
      ABC2=AR*AR+BR*BR+CR*CR
      HX=DMIN1(HE,HW)
      HY=DMIN1(HN,HS)
      HZ=DMIN1(HT,HB)
      AH=AR*HX
      BK=BR*HY
      CL=CR*HZ
      EPA=DEXP(-AH)
      EPB=DEXP(-BK)
      EPC=DEXP(-CL)
      HXY2=HX*HX/HY/HY
      HXZ2=HX*HX/HZ/HZ
      EA=0.
      EAA=0.
      EBB=0.
      ECC=0.
      DO 10 I=1,MAX
      DO 10 J=1,MAX
      ZI=(I-0.5)*PI
      ZJ=(J-0.5)*PI
      PWR=(-1.)**(I+J)*ZI*ZJ
      ABCX=DEXP((ABC2+ZI*ZI/HY/HY+ZJ*ZJ/HZ/HZ)**0.5*HX)
      ABCY=DEXP((ABC2+ZI*ZI/HZ/HZ+ZJ*ZJ/HX/HX)**0.5*HY)
      ABCZ=DEXP((ABC2+ZI*ZI/HX/HX+ZJ*ZJ/HY/HY)**0.5*HZ)
      COSHX=PWR/(ABCX+1./ABCX)
      COSHY=PWR/(ABCY+1./ABCY)
      COSHZ=PWR/(ABCZ+1./ABCZ)
      EA=EA+(COSHY/(CL*CL+ZJ*ZJ)+COSHZ/(BK*BK+ZJ*ZJ))/
     1(AH*AH+ZI*ZI)**2
      EAA=EAA+COSHX/((BK*BK+ZI*ZI)*(CL*CL+ZJ*ZJ))**2
      EBB=EBB+COSHY/((CL*CL+ZI*ZI)*(AH*AH+ZJ*ZJ))**2
   10 ECC=ECC+COSHZ/((AH*AH+ZI*ZI)*(BK*BK+ZJ*ZJ))**2
      COSHA=0.5*EPA+0.5/EPA
```

```
      COSHB=0.5*EPB+0.5/EPB
      COSHC=0.5*EPC+0.5/EPC
      COTHA=(1.+EPA*EPA)/(1.-EPA*EPA)
      COTHB=(1.+EPB*EPB)/(1.-EPB*EPB)
      COTHC=(1.+EPC*EPC)/(1.-EPC*EPC)
      F1=0.125/COSHA/COSHB/COSHC
      EB=EA*HXY2+(1./BK/COTHB-HXY2/AH/COTHA)/2.*F1
      EC=EA*HXZ2+(1./CL/COTHC-HXZ2/AH/COTHA)/2.*F1
      FA=2.*AH*COTHA*EA
      FB=2.*BK*COTHB*EB
      FC=2.*CL*COTHC*EC
      GA=4.*BK*CL*COTHB*COTHC*EAA
      GB=4.*AH*CL*COTHA*COTHC*EBB
      GC=4.*AH*BK*COTHA*COTHB*ECC
      P=F1-FA-FB-FC+GA+GB+GC
      QA=2.*COSHA*(FA-GB-GC)
      QB=2.*COSHB*(FB-GA-GC)
      QC=2.*COSHC*(FC-GA-GB)
      RA=4.*COSHB*COSHC*GA
      RB=4.*COSHA*COSHC*GB
      RC=4.*COSHA*COSHB*GC
      CNNN=((AH/COTHA+BK/COTHB+CL/COTHC)/2.-
     1(AH*AH*EA+BK*BK*EB+CL*CL*EC)/F1)/ABC2
      CNET=P*EPA*EPB*EPC
      CNWT=P/EPA*EPB*EPC
      CSET=P*EPA/EPB*EPC
      CSWT=P/EPA/EPB*EPC
      CNEB=P*EPA*EPB/EPC
      CNWB=P/EPA*EPB/EPC
      CSEB=P*EPA/EPB/EPC
      CSWB=P/EPA/EPB/EPC
      CNCT=QA*EPB*EPC
      CSCT=QA/EPB*EPC
      CNCB=QA*EPB/EPC
      CSCB=QA/EPB/EPC
      CECT=QB*EPA*EPC
      CWCT=QB/EPA*EPC
      CECB=QB*EPA/EPC
      CWCB=QB/EPA/EPC
      CNEC=QC*EPA*EPB
      CNWC=QC/EPA*EPB
      CSEC=QC*EPA/EPB
      CSWC=QC/EPA/EPB
      CEC=RA*EPA
      CWC=RA/EPA
      CNC=RB*EPB
      CSC=RB/EPB
      CTC=RC*EPC
      CBC=RC/EPC
       IF(DABS(HE-HW).LT.EPE.AND.DABS(HN-HS).LT.EPE.AND.
     1DABS(HT-HB).LT.EPE)GO TO 500
```

```
      HX1=DMAX1(HE,HW)
      HY1=DMAX1(HN,HS)
      HZ1=DMAX1(HT,HB)
      AH1=AR*HX1
      BK1=BR*HY1
      CL1=CR*HZ1
      SEW=HX1*(DEXP(2.*AH)-1.)+HX*(DEXP(-2.*AH1)-1.)
      TNS=HY1*(DEXP(2.*BK)-1.)+HY*(DEXP(-2.*BK1)-1.)
      RTB=HZ1*(DEXP(2.*CL)-1.)+HZ*(DEXP(-2.*CL1)-1.)
      S=(EPA*EPA+1./EPA/EPA-2.)*HX1/SEW
      S1=S-1.
      S2=S*HX/HX1
      S3=1.-S1-S2
      T=(EPB*EPB+1./EPB/EPB-2.)*HY1/TNS
      T1=T-1.
      T2=T*HY/HY1
      T3=1.-T1-T2
      R=(EPC*EPC+1./EPC/EPC-2.)*HZ1/RTB
      R1=R-1.
      R2=R*HZ/HZ1
      R3=1.-R1-R2
      FP=1.-S3*CWC-T3*CSC-R3*CBC-S3*T3*CSWC-S3*R3*CWCB
     1-T3*R3*CSCB-S3*T3*R3*CSWB
      CF(2+JX,2+JY,2+JZ)=(CNET+S1*CNWT+T1*CSET+R1*CNEB+
     1S1*T1*CSWT+T1*R1*CSEB+S1*R1*CNWB+S1*T1*R1*CSWB)/FP
      CF(2-JX,2+JY,2+JZ)=S2*(CNWT+T1*CSWT+R1*CNWB+T1*R1
     1*CSWB)/FP
      CF(2+JX,2-JY,2+JZ)=T2*(CSET+S1*C WT+R1*CSEB+S1*R1
     1*CSWB)/FP
      CF(2+JX,2+JY,2-JZ)=R2*(CNEB+S1*CNWB+T1*CSEB+S1*T1
     1*CSWB)/FP
      CF(2-JX,2-JY,2+JZ)=S2*T2*(CSWT+R1*CSWB)/FP
      CF(2+JX,2-JY,2-JZ)=T2*R2*(CSEB+S1*CSWB)/FP
      CF(2-JX,2+JY,2-JZ)=S2*R2*(CNWB+T1*CSWB)/FP
      CF(2-JX,2-JY,2-JZ)=S2*T2*R2*CSWB/FP
      CF(2+JX,2,2+JZ)=(CECT+S1*CWCT+T3*CSET+R1*CECB+S1*R1
     1*CWCB+T3*R1*CSEB+S1*T3*CSWT+S1*T3*R1*CSWB)/FP
      CF(2,2+JY,2+JZ)=(CNCT+S3*CNWT+T1*CSCT+R1*CNCB+S3*T1
     1*CSWT+S3*R1*CNWB+T1*R1*CSCB+S3*T1*R1*CSWB)/FP
      CF(2+JX,2+JY,2)=(CNEC+S1*CNWC+T1*CSEC+R3*CNEB+S1*T1
     1*CSWC+S1*R3*CNWB+T1*R3*CSEB+S1*T1*R3*CSWB)/FP
      CF(2-JX,2,2+JZ)=S2*(CWCT+T3*CSWT+R1*CWCB+T3*R1*CSWB)/FP
      CF(2,2-JY,2+JZ)=T2*(CSCT+S3*CSWT+R1*CSCB+S3*R1*CSWB)/FP
      CF(2,2+JY,2-JZ)=R2*(CNCB+S3*CNWB+T1*CSCB+S3*T1*CSWB)/FP
      CF(2-JX,2+JY,2)=S2*(CNWC+R3*CNWB+T1*CSWC+T1*R3*CSWB)/FP
      CF(2+JX,2-JY,2)=T2*(CSEC+R3*CSEB+S1*CSWC+S1*R3*CSWB)/FP
      CF(2+JX,2,2-JZ)=R2*(CECB+T3*CSEB+S1*CWCB+S1*T3*CSWB)/FP
      CF(2-JX,2,2-JZ)=S2*R2*(CWCB+T3*CSWB)/FP
      CF(2,2-JY,2-JZ)=T2*R2*(CSCB+S3*CSWB)/FP
      CF(2-JX,2-JY,2)=S2*T2*(CSWC+R3*CSWB)/FP
```

```
      CF(2,2,2+JZ)=(CTC+R1*CBC+S3*CWCT+T3*CSCT+S3*R1*CWCB
     1+T3*R1*CSCB+S3*T3*CSWT+S3*T3*R1*CSWB)/FP
      CF(2+JX,2,2)=(CEC+S1*CWC+T3*CSEC+R3*CECB+T3*S1*CSWC
     1+R3*S1*CWCB+T3*R3*CSEB+T3*R3*S1*CSWB)/FP
      CF(2,2+JY,2)=(CNC+T1*CSC+S3*CNWC+R3*CNCB+S3*T1*CSWC
     1+R3*T1*CSCB+S3*R3*CNWB+S3*R3*T1*CSWB)/FP
      CF(2,2,2-JZ)=R2*(CBC+S3*CWCB+T3*CSCB+S3*T3*CSWB)/FP
      CF(2-JX,2,2)=S2*(CWC+R3*CWCB+T3*CSWC+T3*R3*CSWB)/FP
      CF(2,2-JY,2)=T2*(CSC+S3*CSWC+R3*CSCB+S3*R3*CSWB)/FP
      CF(2,2,2)=CNNN/FP
      GO TO 501
  500 CF(2+JX,2+JY,2+JZ)=CNET
      CF(2+JX,2+JY,2-JZ)=CNEB
      CF(2+JX,2-JY,2+JZ)=CSET
      CF(2+JX,2-JY,2-JZ)=CSEB
      CF(2-JX,2+JY,2+JZ)=CNWT
      CF(2-JX,2+JY,2-JZ)=CNWB
      CF(2-JX,2-JY,2+JZ)=CSWT
      CF(2-JX,2-JY,2-JZ)=CSWB
      CF(2+JX,2+JY,2)=CNEC
      CF(2+JX,2-JY,2)=CSEC
      CF(2-JX,2+JY,2)=CNWC
      CF(2-JX,2-JY,2)=CSWC
      CF(2+JX,2,2+JZ)=CECT
      CF(2+JX,2,2-JZ)=CECB
      CF(2-JX,2,2+JZ)=CWCT
      CF(2-JX,2,2-JZ)=CWCB
      CF(2,2+JY,2+JZ)=CNCT
      CF(2,2+JY,2-JZ)=CNCB
      CF(2,2-JY,2+JZ)=CSCT
      CF(2,2-JY,2-JZ)=CSCB
      CF(2+JX,2,2)=CEC
      CF(2-JX,2,2)=CWC
      CF(2,2+JY,2)=CNC
      CF(2,2-JY,2)=CSC
      CF(2,2,2+JZ)=CTC
      CF(2.2,2-JZ)=CBC
      CF(2,2,2)=CNNN
  501 RETURN
      END
```

REFERENCES

1. Roache, P. J., "Computational Fluid Mechanics", Hermosa Publishers, 1972.

2. Desai, C. S., "Elementary Finite Element Method", Prentice-Hall, 1979.

3. Chen, C. J. and Li, P., "Finite Differential Method in Heat Conduction - Application of Analytic Solution Technique", ASME Paper 79-WA/HT-50, December 2-7, 1979. ASME Winter Annual Meeting, New York, N.Y.,1979.

4. Chen, C. J. and Li, P., "The Finite Analytic Method for Steady and Unsteady Heat Transfer Problems", ASME Paper 80-HT-86, July 27-30, 1980, ASME/AIChE National Heat Transfer Conference, Orlando, FL.

5. Chen, C. J., Naseri-Neshat, H. and Ho, K. S., "Finite Analytic Numerical Solution of Heat Transfer in Two-Dimensional Cavity Flow", ASME Paper, HTD, Vol. 13, ASME Winter Annual Meeting, November, 1980, Chicago, Ill. pp. 49-61. Also Journal of Numerical Heat Transfer, vol. 4, pp. 179-197, 1981.

6. Chen, C. J., Naseri-Neshat, H. and Li, P., " The finite Analytic Method - Application of Analytic Solution Techniques to the Numerical Solutions of Ordinary and Partial Differential Equations", Report ECJC-1-80, Energy Division, The University of Iowa, Iowa City, Iowa. Jan. 1980.

7. Chen, C.J. and Yoon, Y. H., "Finite Analytic Numerical Solution of Axisymmetric Navier-Stokes and Energy Equations. ASME Paper 82-HT-42, 1982.

8. Chen, C. J. and Obasih, K., "Finite Analytic Numerical Solution of Heat Transfer and Flow Past a Square Channel Cavity", 82-IHTC-43. The 7th International Heat Transfer Conference, München. Sept. 6-10, 1982.

9. Spadling, D. B., " A Novel Finite Difference Formulation for Differential Expressions Involving Both First and Second Derivatives", International Journal for Numerical Methods in Engineering, vol. 4, pp. 551-559, 1972.

10. Runchal, A. K., "Convergence and Accuracy of Three Finite Difference Schemes for a Two-Dimensional Conduction and Convection Problem", International Journal for Numerical Methods in Engineering, vol. 4, pp. 541-550, 1972.

11. Patankar, S. V., "Numerical Heat Transfer and Fluid Flow", McGraw-Hill, 1980.

12. Raithby, G. D., "Skew Upstream Differencing Schemes for Problems Involving Fluid Flow", Computer Methods in Applied Mechanics and Engineering. vol. 9, pp. 153-164, 1976.

13. Shay, W. A., "Development of a Second Order Approximation for the Navier-Stokes Equations", Computers and Fluids, vol. 9, pp279-298, 1981.

14. Heinrich, J. C., Huyakorn, P. S., Zienkiewicz, O. C. and Mitchell, A. R., "An 'Upwind' Finite Element Scheme for Two-Dimensional Convective Transport Equation", International Journal for Numerical Methods in Engineering, vol. 11, pp. 131-143, 1977.

15. Gallagher, R. H., Oden, J. T., Taylor, C. and Zienkiewicz, O. C., "Finite Element in Fluids - vol. 3" pp. 1-22, John Wiley & Sons, 1978.

16. Burgers, J. M., "A Mathematical Model Illustrating the Theory of Turbulence", Advances in Applied Mechanics, vol. 1, R. Von Mises and T. Von Karman, ed., Academic Press, New York, pp. 171-199.

17. Greenspan, D., "On a Best 9-point Differential Equation Analogue of Laplace's Equation", J. F. S., vol. 263, No. 5, pp1425-1430, 1957.

18. Raithby, G. D., "A Critical Evaluation of Upstream Differencing Applied to Problems Involving Fluid Flow", Computer Methods in Applied Mechanics and Engineering, vol. 9, pp. 75-103, 1976.

19. Stubley, G. D., Raithby, G. D. and Strong, A. B., "Proposal for a New Discrete Method Based on an Assessment of Dicretization Errors", Numerical Heat Transfer, vol. 3, pp 411-428, 1980.

20. Raithby, G. D. and Schneider, G. E., "Numerical Solution of Problems in Incompressible Fluid Flow: Treatment of the Velocity-Pressure Coupling", Numerical Heat Transfer, vol. 2, pp. 417-440, 1979.

21. Dennis, S. C. R., Ingham, D. B. and Cook, R. N., "Finite-Difference Methods for Calculating Steady Incompressible Flows in Three Dimensions", Journal of Computational Physics, vol. 33, pp. 325-339, 1979.

22. Singh, K., "Finite Analytic Numerical Solution of Two-Dimensional Navier-Stokes Equations in Primitive Variables", M. S. Thesis, Mechanical Engineering Program, 1981, University of Iowa, Iowa City, Iowa.

23. Chorin, A. J., "Numerical Solution of the Navier-Stokes Equations", Math. Comp., vol. 22, pp745-762, 1968.

24. Chorin, A. J., "On the convergence of Discrete Approximations to the Navier-Stokes Equations", Math. Comp., vol. 22, pp341-353, 1969.

25. Goda, K., "A Multistep Technique with Implicit Difference Schemes for Calculating Two- and Three-Dimensional Cavity Flow", Journal of Computational Physics, vol. 30, pp76-95, 1979.

26. Takami, H. and Kuwahara, K., "Numerical Study of Three-Dimensional Flow within a Cubic Cavity", Journal of the Physics Society of Japan, vol. 37, No. 6, pp1695-1698, 1974.

27. Harlow, F. H. and Welch, J. E., "Numerical Calculation of Time-Dependent Viscous Incompressible Flow of Fluid with Free Surface", The Physics of Fluids, vol. 8, pp. 2182-2189, 1965.

28. Patankar, S. V. and Spadling D. B., "A Calculation Procedure for Heat, Mass and Momentum Transfer in Three-Dimensional Parabolic Flows", International Journal of Heat and Mass Transfer, vol. 15, pp. 1787-1806, 1972.

29. Lighthill, M. J., "Viscosity Effects in Sound Waves of Finite Amplitude", in "Surveys in Mechanics". Batchelor, G. K. and Davis, R. M., ed., Cambridge University Press, 1956.

30. Taylor, T. D., Ndefo, E. and Masson, B. S., "A Study of Numerical Methods for Solving Viscous and Inviscid Flow Problems", Journal of Computational Physics, vol. 9, pp. 99-119, 1972.

31. Burggraf, O. D., "Analytical and Numerical Studies of the Structure of Steady Separated Flows", Journal of Fluid Mechanics, vol. 24, part 1, pp113-151, 1966.

32. deVahl Davis, G. and Mallinson, G. D., "An Evaluation of Upwind and Central Difference Approximations By a Study of Recirculating Flow", Computers and Fluids, vol. 4, pp29-43, 1976.

33. Tuann, S. Y. and Olsen, M. D., "Review of Computing Methods for Recirculating Flows", Journal of Computational Physics, vol. 29, pp. 1-19, 1978.

34. Olsen, M. D. and Tuann, S. Y., "New Finite-Element Result for the Square Cavity", Computers and Fluids, vol. 7, pp123-135, 1979.

35. Gupta, M. M. and Manohar, R. P., "Boundary Approximations and Accuracy in Viscous Flow Computations", Journal of Computational Physics. vol. 31, pp. 265-288, 1979.

36. Gupta, M. M., Manohar, R. P. and Noble, B., "Nature of Viscous Flows Near Sharp Corners", Computers and Fluids, vol. 9, No. 4, pp379-388, 1981.

37. Benjamin, A. S. and Denny, V. E., "On the Convergence of Numerical Solutions for 2-D Flows in a Cavity at Large Re", Journal of Computational Physics, vol. 33, pp. 340-358, 1979.

38. Quartapelle, L., "Vorticity Conditioning in the Computation of Two-Dimensional Viscous Flows", Journal of Computational Physics, vol. 40, pp453-477, 1981.

39. Takemitsu, N., "On a Finite-Difference Approximation for the steady-state Navier-Stokes Equations", Journal of Computational Physics, vol. 36, pp236-248, 1980.

40. Greenspan, D., "Numerical Studies of Prototype Cavity Flow Problems", Comput. J., col. 12, pp39-94, 1969.

41. Nallasamy M. and Prasad, K. K., "Numerical Studies on Quasilinear and Linear Elliptic Equations", Journal of Computational Physics, vol. 15, pp. 429-448, 1974.

42. Nallasamy, M. and Prasad, K. K., "On Cavity Flow at Higher Reynolds numbers", Journal of Fluid Mechanics, vol. 79, part 2, pp. 391-414, 1977.

43. Gosman, A. D., Pun, W. M., Runchal, A. K., Spadling, D. B. and Wolfshtein, M., "Heat and Mass Transfer in Recirculating Flows", Academic Press, 1969.

44. Bozeman, J. D. and Dalton, C., "Numerical Study of Viscous Flow in a Cavity", Journal of Computational Physics, vol. 12, pp. 348-363, 1973.

45. Pepper, D. W. and Cooper, R. E., "Numerical Solution of Recirculating Flow By a Simple Finite Element Recusion Relation", Computers and Fluids, vol. 8, pp. 213-223, 1980.

46. Oszwa, S., "Numerical Studies of Steady Flow in a Two-Dimensional Square Cavity at High Reynolds Numbers", Journal of the Physical Society of Japan, vol. 38, No. 3, pp889-895, 1975.

47. Ghia, K. N., Hankey, W. L. and Hodge, J. K., "Study of Incompressible Navier-Stokes Equations in Primitive Variables Using Implicit Numerical Technique", Paper No. 77-648, AIAA, 3rd Computational Fluid Dynamics Conference, Albuquerque, N. Mexico, pp. 156-167, 1977.

48. Bercovier, M. and Engelman, M., "A Finite Element for the Numerical Solution of Viscous Incompressible Flows", Journal of Computational Physics, Vol. 30, pp. 181-201, 1979.

49. Mills, R. D., "On the Slosed Motion Of a Fluid in a Square Cavity", Journal of the Royal Aeronautical Society, vol. 69, pp. 116-120, 1965.

50. Pan, F. and Acrivos, A., "Steady Flows in Rectangular Cavities", Journal of Fluid Mechanics, vol. 28, part 4, pp643-655, 1967.

51. Fromm, J. E. and Harlow, F. H., "Numerical Solution of the Problem of Vortex Street Development", The Physics of Fluids, vol. 6, No. 7, pp. 975-982, 1963.

52. Smith, S. L. and Brebbia, C. A., "Finite-Element Solution of Navier-Stokes Equations for Transient Two-Dimensional Incompressible Flow", Journal of Computational Physics, vol. 17, pp. 235-245, 1975.

53. Blevins, R. D., "Flow-Induced Vibration", Van Nostrand Reinhold Company, 1977.

54. Prandtl, L. and Tietjens, O. G., "Applied Hydro- and Aeromechanics", McGraw-Hill, 1934.

55. Chen, C. J. and Chen, H. C., "The Finite Analytic Method - The Finite Analytic Numerical Solution for Unsteady Two-Dimensional Navier-Stokes Equations", vol. 6, The Finite Analytic Method Technical Report, Iowa Institute of Hydraulic Research, The University of Iowa, Iowa City, Iowa, August, 1981.

56. Cheng, W. S., "Finite Analytic Numerical Solution for Two Dimensional Incompressible Flows Over an Arbitrary Body Shape", M. S. Thesis, Mechanical Engineering Program, December 1982, University of Iowa, Iowa City, Iowa.

57. Agarwal, R. K., "A Third-Order Accurate Upwind Scheme for Navier-Stokes Solution in Three Dimensions", Computers in Flow Predition and Fluid Dynamics Experiments. The Winter Annual Meeting of the American Socity of Mechanical Engineers. Washington D. C., November 15-20, 1981.

END

DATE

FILMED

JUN 29 1983